Final Report

DSE Group 24
SERUM

Alec Sterckx	5301025
Jasmijn Tromp	5071461
Jeroen van Daelen	4993780
Jokubas Mickus	5104521
Lisanne Vermaas	5239745
Łukasz Gałecki	5073545
Marte Medina León	5293022
Martijn den Hoed	5303451
Maurits de Matos Lourenco Kuipers	5001331
Willemijn van Luik	5009650

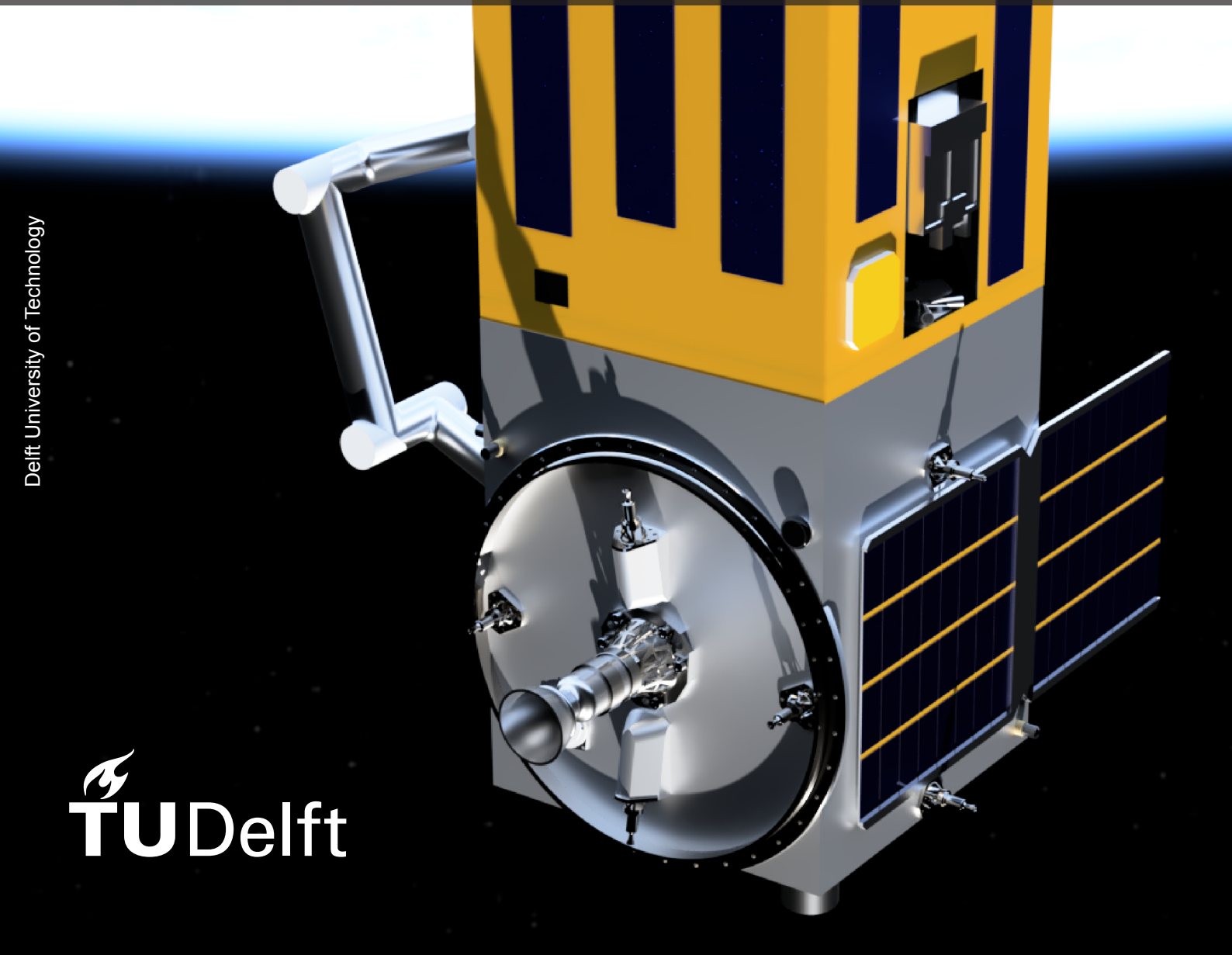

Delft University of Technology

TU Delft

Final Report

DSE Group 24
SERUM
SSETI **E**xpress **R**esc**U**e **M**ission

by

Alec Sterckx	5301025
Jasmijn Tromp	5071461
Jeroen van Daelen	4993780
Jokubas Mickus	5104521
Lisanne Vermaas	5239745
Łukasz Gałecki	5073545
Marte Medina León	5293022
Martijn den Hoed	5303451
Maurits de Matos Lourenco Kuipers	5001331
Willemijn van Luik	5009650

to obtain the degree of Bachelor of Science
at the Delft University of Technology.

Project duration:	April 24, 2023 – June 29, 2023	
Tutor:	S. Speretta PhD	TU Delft, Supervisor
Coaches:	S. Gehly PhD	TU Delft
	A.P. Pouchias PhD	TU Delft
Teaching Assistant:	A. Phillips	TU Delft

TU Delft

Executive Overview

SSETI Express (Student Space Exploration and Technology Initiative Express) - the satellite that requires repair
SERUM (SSETI Express RescUe Mission) - the name of the spacecraft under development

This report provides a comprehensive overview of the design process for the SERUM spacecraft. Which is tasked with repairing SSETI Express and de-orbiting it. The project is currently in the detailed design phase in which detailed system architecture and technology decisions are being made. Each following paragraph gives a brief summary of its corresponding section.

An introduction in Chapter 1 provides a general overview of the report and sets the context of the project. It includes the aim of the project and an overall view of the various sections covered in the document.

Besides the mission of SERUM, in-orbit satellite servicing has many other potential applications. To further explore these opportunities, a market analysis is conducted in Chapter 2. A market demand estimation and possible business model for marketability are provided. Additionally, a stakeholder analysis was performed, which resulted in a list of stakeholder requirements, that forms the basis of the design.

SSETI Express' failure analysis and possible mitigation strategies are explored in Chapter 3. After delving into the technical analysis of the failure of the electrical system on SSETI Express, two possible solutions are offered: disconnecting the failed component, or injecting power through an exposed port originally used to charge the spacecraft during launch vehicle integration and launch. The advantages and disadvantages of both solutions are outlined, with injecting power being by far the easier solution. It is therefore decided to use this as a first solution and then use the shunt disconnection as either a backup or only as a technology demonstration.

In Chapter 4, the actions performed during the mission but also in the phases prior to the launch are discussed. It contains an operations and logistic concept description, which outlines the sequence of activities of SERUM during the mission. Furthermore, the steps taken post-DSE are discussed. Finally, a Gantt chart, functional flow diagram and functional breakdown structure are presented.

The payload of SERUM is broken down into three parts, which are individually explored in their corresponding sections. For all of them, the process of choosing/developing the design is discussed first, followed up by a more detailed work out of the design, after that the cost, mass and power budgets are provided and the section is closed off with a conclusion. The following sections elaborate on the corresponding payload components:

- Chapter 5 covers SERUM's docking system. It starts with a design overview, which summarizes the choices made in the midterm report. This is followed by a first design iteration for the chosen configuration. This design consists of a robotic arm, expansion mechanism and zond. This is supported by numerous sensors, whose design and working is explained. The capture procedure can only be performed when SERUM is above a ground station, as a continuous videostream has to be send down. This leaves a 10 minute window for the entire procedure, which is further elaborated on. This chapter also entails the required torques by GNC to maintain the same rotation as SSETI Express.
- Chapter 6 treats the restoring of SSETI Express to its initial functionality. Both the repair mechanisms mentioned above and their design are explored. For the bypass strategy, power is directly feeded into the battery of SSETI Express, by means of a custom designed connector with two pogo pins on a scissor mechanism. For the shunt cutting strategy, an intercepting wiretap, which intercepts and not cuts the wires, is used. An off-the-shelf T-tap design is adjusted to fit SERUM's design. However, before the wires can be intercepted, access into SSETI Express has to be obtained. This will be done by means of piercing. To install the wiretap, an endoscope is utilized, which is also available already. Small changes will be made, such as installing the wiretap instead of the grabbing manipulator, in order to fit SERUM's goals. After performing these methods, the confirmation that SSETI Express is indeed fixed, will be done in three ways, which include the monitoring of the voltage on the battery stud and current flowing through the wiretap, as well as monitoring SSETI Express' outgoing communication signals.
  - Before deciding on the piercing, a test was performed, to confirm this method creates no debris when piercing through a honeycomb panel. This demonstration is discussed in Chapter 7. It explains the manufacturing of the aluminum honeycomb panel, the performing of the test and the result and analysis. It was found that no debris is created by piercing and that the maximal force needed is 845 N.

- Chapter 8 explains the necessities to assure that SSETI Express will de-orbit with SERUM after its operational lifetime or that SERUM de-orbits itself in case of mission failure. A secondary catching method is chosen, in case SERUM cannot dock to SSETI Express, it will use a net to try and de-orbit together anyway. Furthermore, a drag sail is chosen to de-orbit either SERUM or SERUM with SSETI Express. For the final part of de-orbiting, a final burn will be performed to ensure no inhabitant areas are hit by the remains.

The following seven chapters of the report delve deeper into the standard subsystems of the spacecraft. The chapters describe the design and corresponding considerations, chosen components, budgets (mass, power and cost), sizing and a conclusion. The following chapters elaborate on the corresponding subsystems:

- Chapter 9 looks into the communication subsystem. It performs a trade-off for the frequency band and makes the decision for three bands. It will use S- and X-band for up- and downlink communication, respectively and Ka-band for the broadcasting of a live video stream down. Different antenna types and modulation techniques are discussed. KSAT's Svalbard ground station is chosen and it is determined that SERUM will pass over approximately 12.6 times per day, with multiple passes lasting more than 10 minutes. A (closing) link budget for each frequency band is set up and off-the-shelf components are selected. Finally, a communication flow diagram is shown, which shows the steps taken by the communication subsystem throughout SERUM's lifetime.
- Chapter 10 investigates the Command and Data Handling subsystem. This section dives into the payload computer, for which the SE-2 computer with FPGA module is chosen. It also discusses the CDH computer, for which no specific component is chosen at this point. After that, an interface diagram, showing the connection of the CDH to all other subsystems, is shown. Finally, shielding of the subsystem is discussed, to mitigate the risk of failure.
- Chapter 11 delves into the propulsion system. First, a literature study on green mono-propellants is performed as no toxic propellants can be used according to the requirement MIS-008-PROP-001. A trade-off for the propellant is performed, leading to the decision for LMP-103S. The $22\,\mathrm{N}$ HPGP thruster, 12 $1\,\mathrm{N}$ HPGP thrusters and the PEPT-230 propellant tank are selected, as well as various valves, a filter and transducer.
- Chapter 12 covers the Guidance, Navigation and Control subsystem. After defining the tasks it has to execute, it recaps on the trade-offs performed in the midterm and the components selected based on this. Commercial components are selected based on size and required control authority calculations. Reaction wheels, star trackers, sun sensors, an IMU and GNSS receiver are chosen. These components are then also positioned.
- Chapter 13 reports on the electrical power system. First the choice for deployable solar panels, originating from the midterm report, is recapped on. After that, the power storage method is discussed, which is necessary because of the eclipses SERUM will experience. The choice for lithium-ion batteries in combination with a super-capacitor is made. After that, the power consumed by the payload is calculated, which is then used to set up a power budget for SERUM. To do so, different power consumption phases are identified and grouped into 6 main categories. After final sizing, the depth of discharge is evaluated.
- Chapter 14 covers the thermal control system of SERUM. From all subsystems, the most limiting components (in maximum and minimum operational temperature) are taken as design limits. This, together with the thermal environment, result in sizing and component selection of the thermal system. Passive thermal control will be used by having anodized aluminum as outer structure. For the time between expanding the drag sail and final de-orbit, a louver on the surface and flexible heaters to critical components could be attached.
- Chapter 15 describes the role of the structures subsystem. The overall design can be seen, showing the internal and external structure made from sandwich panels and monolithic panels, respectively.

The final configuration of SERUM when docked to SSETI Express can be seen in Figure 1.

In order to launch SERUM, a launch vehicle is selected and discussed in Chapter 16. The Falcon9 rideshare is chosen.

To execute the mission, an astrodynamic analysis and planning is performed in Chapter 17. This entails maneuver planning from moving from the starting orbit until docking to SSETI Express, orbit determination and determining the observation orbit. Furthermore, simulations are done for debris avoidance and the propellant required for transferring between orbits.

Chapter 18 discusses the development strategy of SERUM. As SERUM demonstrates a concept, a general production of in-orbit servicing can be deduced from it. However, to do so, sustainability of both the design and

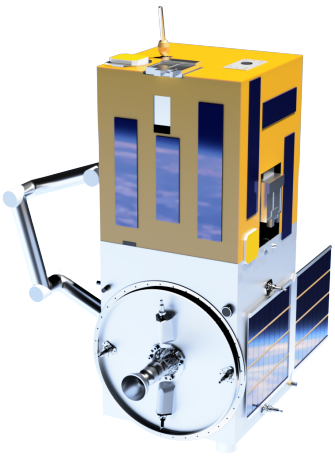

Figure 1: Annotated visualization of SERUM (below) docked to SSETI Express (above)

mission has to be taken into account. Furthermore, a manufacturing plan is set up which contains sourcing the components as well as a preliminary production plan. Finally, the potential for scaling certain parts of the production is discussed.

Chapter 19 tabulates the risks for SERUM as a whole as well as for each subsystem. The risks are further detailed and mitigation strategies are proposed. The influence of the mitigation can be seen in two risk maps, one before and one after mitigation.

Chapter 20 summarizes the cost and mass budgets for each subsystem into a total budget for SERUM. The final cost and mass are compared with the requirements to check for compliance. A total cost of $23\,507$ kEUR and total mass of 99.8 kg is found. Where the mass is well within budget, the cost is not compliant with the total cost available.

Chapter 21 details the crucial verification and validation processes in the project. All requirements are managed via Valispace, a specialized software that allows for automated requirements verification procedures and managing budgets. All 245 requirements established during the project were structured to allow people to work on consecutive subsystems in parallel. In the chapter, only a compliance matrix is shown. This shows part of the requirements, and if they are verified and compliant and if so, where it can be found in the report. After that, design observations with respect to the design requirements will be discussed. Finally, verification and future validation methods will be considered.

Chapter 22 contains the change of design from drag sail and final propulsive de-orbit to fully propulsive de-orbit, after finding out that having a long sleeping time put a high demand on the subsystems and that the mass of SERUM is way below the maximum possible mass. The chapter covers the subsystems that are affected by this choice and elaborate on the changes. Also, the budgets are updated according to the new total cost and mass.

In conclusion, this report encapsulates the rigorous planning, design, and execution involved in developing the SERUM spacecraft. The process of system architecture decision-making, comprehensive analyses of subsystems, and exploring potential solutions for challenges have all been detailed thoroughly. The critical tasks of verification and validation, which act as the backbone of the entire design process, are also illustrated, highlighting their importance in ensuring the spacecraft's alignment with stakeholder expectations and overall mission objectives. The commitment to innovation and sustainability throughout the project also embodies the evolving ethos of space exploration. As the project continues to advance, it is envisaged that the SERUM spacecraft will not only successfully fulfill its mission but also contribute to the broader field of space technology, encouraging new discoveries and pioneering future endeavors.

Contents

Nomenclature

Abbreviations

ADN Ammonium Dinitramide

ADN Ammonium dinitramide

ASK Amplitude Shift Keying

ATC Acute Toxicity Classification

BEC Bi-directional Error Correction

BPSK Binary Phase Shift Keying

CAD Computer Aiding Design

CDH Command and Data Handling

CFRP Carbon Fiber Reinforced Polymers

COTS Commercial Off-The-Shelf

DMAZ 2-Dimethylaminoethylazide

DoD Depth of Discharge

DOF Degree Of Freedom

DOT Design Option Tree

DSE Design Synthesis Exercise

DSSP Digital Solid State Propulsion

ECHA European Chemicals Agency

EDM Electrical Discharge Machining

EIL Energetic Ionic Liquid

EIRP Equivalent Isotropic Radiated Power

ELSA-d End of Life Services by Astroscale - demonstration

EOL End Of Life

EPS Electrical Power System

ESA European Space Agency

EU European Union

EUFB Ntrous Oxide Ethanol

FBD Functional Breakdown Diagram

FEC Forward Error Correction

FFD Functional Flow Diagram

FPGA Field Programmable Gate Array

FSK Frequency Shift Keying

GEM Green Electric Mono-propellant

GEO Geostationary Orbit

GHS Global Harmonized System of classification and labelling os chamicals

GNC Guidance, Navigation and Control

GNSS Global Navigation Satelite System

GPRCS Green Propellant Reaction Control System

GPU Graphics Processing Unit

HAN Hydroxylammonium Nitrate

HAN Hydroxylammonium nitrate

HNF Hydrazinium nitroformate

HPAS Hydrogen Peroxide Aqueous Solutions

HPGP High Performance Green Propulsion

HTP High-Test Peroxide

IMU Inertial Measurement Unit

ITU International Telecommunication Unit

kEUR Thousand Euros

KSAT Kongsberg Satellite Services

LDPC Low Density Partiy Check

LED Light Emitting Diode

LEO Low Earth Orbit

LiDAR LIght Detection And Ranging/Laser Imaging Detection And Ranging

LV Launch Vehicle

MEUR Million Euros

MOSFET Metal Oxide Semiconductor Field Effect Transistor

MUSD Million United States Dollars

NASA National Aeronautics and Space Administration

NOFB Nitrogen-Oxigen Fuel Blend

OBC On Board Computer

PCIe Peripheral Component Interconnect Express

PFCV Proportional Flow Control Valve

PSK Phase Shift Keying

QAM Quadrature Amplitude Modulation

QPSK Quadrature Phase Shift Keying

RCS Reaction Control System

ROS Robot Operating System

SE-2 Space Edge Two

SERUM SSETI Express RescUe Mission

SMAV Shape Memory Alloy Valve

SNR Signal to Noise Ratio

SSC Swedish Space Cooperation

SSETI Student Space Exploration & Technology Initiative

SVHC Substances of Very High Concern

T-POD Tokyo Pico-satellite Orbital Deployer

TCS Thermal Control System

TFLOPS Terra Floating Point Operations Per Second

TLE Two Line Element

TRL Technology Readiness Level

TT&C Telemetry, Tracking and Command

UHF Ultra High Frequency

UN United Nations

Software

DRAMA Orbital debris considerations

EndNote Cloud citation management software

Excel Spreadsheet creation software, used for auxiliary computations

Fusion 360 CAD software, used for models of SSETI

GMAT Orbital maneuvering calculations

Google Drive Cloud file management software

MASTER Orbital debris considerations

Overleaf Collaborative LaTex editor, used for writing the reports

TUDAT Orbital propagation

Valispace Requirements management software, used for tracking requirements and budgets

1 Introduction

With the current explosion in the amount of satellites in orbit and the ever-decreasing launch costs required for it, humanities technological presence in space is at an all-time peak. To continue to grow in a responsible and sustainable way, orbital maintenance and active de-orbiting is a field currently under high interest with the prospect of extending the life of satellites and making earth's orbit a safer place. This Design Synthesis Excercise (DSE) has the aim of servicing and de-orbiting SSETI Express, a failed and uncontrolled satellite designed and built by European students under an ESA initiative. This rescue mission, called SERUM (SETTI Express RescUe Mission), shall be a technology demonstrator, after its launch, expected in 2028, it shall maneuver to SSETI Express' $700\,\text{km}$ orbit where it will dock with the uncooperative, tumbling satellite. From there it shall demonstrate the possiblity of in-situ repair by use of a toolset custom designed for this mission. Furthermore, it shall de-orbit itself and SSETI Express within 25 years of launch, thereby reducing orbital debris and risks of collision events.

This report outlines the current state of the detailed design of the mission. The main planning of the design has been reported in the baseline report, and the conceptual design and main trade-offs are established in the midterm report. This design is the continuation of this process, such that this report can be read standalone, but does build on concepts decided on in the previous reports. Based the subsystem configurations chosen in the midterm, commercially available components are selected and integrated, resulting in the detailed design.

Chapter 2 goes in depth on the current size of the market and estimates the commercial viability of this mission. In Chapter 3, the failure mode of SSETI Express is analyzed and possible repair strategies are proposed, Chapter 4 details the steps to be taken from the start of the design process to the end of the mission. Chapter 5 - 8 describe the mission-specific payload design, required for succesful docking, repairing and de-orbiting, whereas Chapter 9 - 15 report on the generic satellite subsystems. In Chapter 16, the choice of launch vehicle, and its considerations that are taken into account are documented. Chapter 17 reports on the spacecrafts astrodynamic characteristics. Chapter 18 elaborates on the planned manufacturing, assembly and integration process. Chapter 19 outlines the expected risks, their impact and their mitigation strategies. A verification and validation strategy is established and performed in Chapter 21, and in Chapter 20, the detailed spacecraft budgets are outlined. Chapter 22 reports on the first iteration performed, where the design is simplified and made more reliable. Finally, in Chapter 23, the conclusion is stated.

2 Market Analysis

While this report outlines a mission to repair and de-orbit SSETI Express, in-orbit satellite servicing has many other potential applications beyond what the team is currently working on. To explore these opportunities, a market analysis has been conducted to identify the need for the current design and determine what other concepts could be developed with minor modifications. Section 2.1 contains an estimation for the market demand and Section 2.2 provides a possible business model to showcase marketability. Additionally, a stakeholder analysis was performed in Section 2.3, which resulted in a list of stakeholder requirements, that form the basis of the design.

2.1. Market Demand

An estimate for the market segment that can be serviced is provided in this section. In the current decade (2021-2030) the manufacturing and launch revenue of the space industry has been forecasted to be 291.80 BEUR [1]. In this forecast it is estimated that a third of the value will come from, usually larger and more expensive, GEO satellites [1]. Thus it is estimated that 50% of this market will consist of satellites that are expensive enough such that it becomes beneficial to attempt a rescue mission, instead of launching a similar model. Approximately 92.5% launches are succesfull and could thus be serviced in the event of in-orbit malfunction [1]. Of this 92.5%, approximately 10% will still experience premature failure due to unforeseen malfunctions [2]. About 30% of these malfunctions occur in the EPS subsystem [3]. Assuming that these factors are not correlated, this obtains a market segment for in-orbit servicing for an EPS malfunction of approximately 4.04 BEUR , of satellites that will have been launched between 2021 and 2030.

The previous paragraph containts the potential role of SERUM in a specific market segment. This should however, not deter the attention towards more general servicing possibilities. The repair of SSETI Express could form a reference for non-EPS related repair missions, since it can not only provide power to another spacecraft, but it can also access it without creating debris (which could increase the theoretical market to 13.47 billion dollars). Moreover, strict satellite refueling or de-orbiting missions could also be considered. These considerations increase the potential market size even more.

Furthermore, 3170 inactive satellites are currently in orbit.[2] Some of these satellites possess no functioning de-orbiting sequence, posing a threat to future space missions in those orbits. Larger objects, such as inoperative satellites, are big contributors to the Kessler syndrome, where space debris collisions cause a chain reaction resulting in even more collisions.[3] As the space sector moves to a more sustainable space environment, clear of dangerous, uncontrollable threats, SERUM could be used to de-orbit such space debris. For satellites that would not fully burn-up in the atmosphere, it is advantageous that our spacecraft has a controlled de-orbiting method (see Chapter 8), so that cleaning space up does not create possible casualties on Earth. For satellites that do not need a controlled de-orbit, operators could consider only using a drag sail. A further development could be to de-orbit a satellite constellation by being able to connect a drag sail box to each of the individual satellites without staying attached.

2.2. Marketability

From Section 2.1, it is clear that an orbital servicing and de-orbiting system is a valuable addition to the space market. In this section, the possible marketability will be investigated.

In Figure 2.1, a hypothetical business model canvas is provided to showcase the possible marketability of the eventual product. It was determined that the main customer of the servicing system would most probably be the owner/operator of a large, expensive, inoperative satellite. This satellite must be important enough for the customer to require a reproduction and launch of a similar spacecraft. A smaller servicing satellite would be a more cost-effective alternative to resume operations. A very limited, on-demand product delivery is applicable, as different customers' inoperative satellites have different needs and constraining factors. This results in a

[1] https://www.euroconsult-ec.com/press-release/new-satellite-market-forecast-anticipates-1700-satellites-to-be-launched-on-average-per-year-by-2030-as-new-entrants-and-incumbents-increase-their-investment-in-space/

[2] https://www.geospatialworld.net/prime/business-and-industry-trends/how-many-satellites-orbiting-earth/#:~:text=According%20to%20UCS%2C%20there%20are,recorded%20by%201st%20January%2C%202021

[3] https://www.nasa.gov/centers/wstf/site_tour/remote_hypervelocity_test_laboratory/micrometeoroid_and_orbital_debris.html

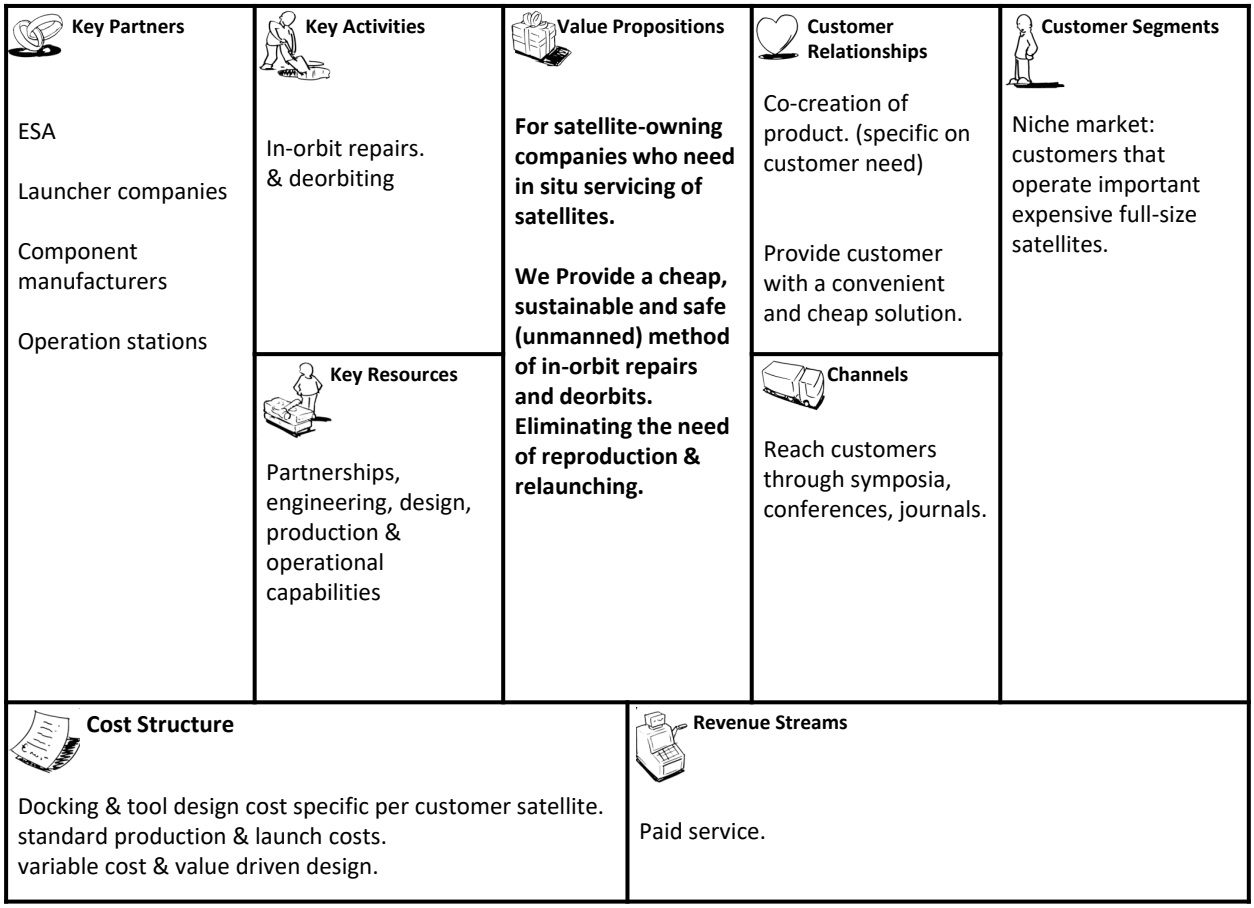

Figure 2.1: Possible business model canvas [4]

need for co-creation of the product between the hypothetical servicing company and the satellite owner. In this value driven design (as opposed to a cost-driven design), the cost structure entails variable cost (standard launch and base production costs plus customer specific docking and tool design and production cost). Our value proposition statement is:

'This product is meant for satellite-owning companies who need in-situ servicing of satellites. The to be designed spacecraft provides a cheap, sustainable and safe (unmanned) method of in-orbit repairs and de-orbits, eliminating the need of reproduction & relaunching.'

This concludes the market analysis. Servicing satellites with de-orbiting capabilities will have high demand in a big market, while also being a marketable concept. Knowing this, it is advantageous to provide a final design which takes the possibility of general EPS servicing in mind, opposed to SSETI Express specific concepts.

2.3. Stakeholder Analysis

Satellite servicing missions have exclusively been conducted as tests and proof of concept. It is merely a novel concept in development, there are no direct competitors on the market yet. However, an "indirect competitor" (general spacecraft mission trend that could jeopardize our market demand) was identified. Cubesat development is found to be an indirect competitor because it aims to build cheaper satellites at a higher frequency. For most CubeSat missions servicing mission would thus be more expensive than simply launching a replacement. Our mission therefore aims to claim the market demand for inoperative, expensive satellites.

Several stakeholders of the mission were identified. All stakeholders are mapped in the power-interest matrix seen in Figure 2.2. On the vertical axis, the power of a certain stakeholder over the project is indicated. The horizontal axis indicates the interest of a specific party in the project.

Starting from the upper left corner, one can see the European Union (EU) and the International Telecommunication Union (ITU). Both of these parties enforce regulation on the project, thereby having a lot of power. They however, have little interest in the project itself, as it does not bring them anything. The launcher company

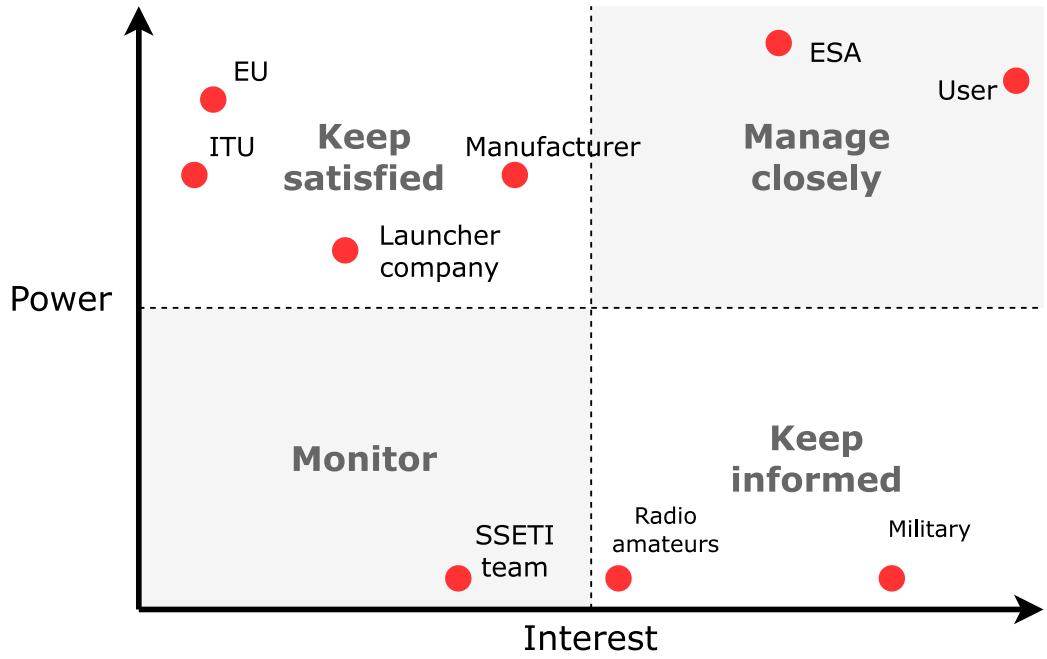

Figure 2.2: Stakeholder power interest matrix

has a little less power, as it just enforces certain boundaries to stay within. It does, however, have a bit more interest in the project, as it influences the number of spacecraft launched. The manufacturer has even more interest, as he is more involved in the development of the spacecraft.

The lower left corner only houses the SSETI Express team. The team has negligible power over the project as they do not own the spacecraft nor do they have the power to enforce any type of regulation. Their interest in the project would also be purely out of curiosity or for educational purpose.

In the lower right corner, radio amateurs and the military are positioned. They both have very limited power over the project, as they do not have the right to enforce regulations. They are, nonetheless, both very interested in the project, for different reasons. Radio amateurs are interested in the data generated by the mission. The military on the other hand, is more interested in the servicing concept. This technique could be used to either repair or destroy certain satellites.

ESA, in the upper right corner, was identified as a key stakeholder, having both a lot of power and a lot of interest. As it is the owner of SSETI Express [4] it can impose requirements and mission objectives. ESA would be most inerested in the concept of a servicing mission, rather than repairing SSETI Express. Another key stakeholder with high power & interest is the user, in this case the supervisor of our DSE project, Stefano Speretta, who determines mission and cost requirements.

Some general stakeholder requirements were found. These will be requirements of the highest level, and all upcoming requirements shall adhere to and flow down from these. They are listed in Table 2.1.

Table 2.1: Stakeholder requirements

ID	Requirement	Stakeholder
STH-001	The system shall comply with the EU space law regulations.	EU
STH-002	The system shall adhere to the communication protocols specified by the International Telecommunication Union (ITU) for space communication.	ITU
STH-003	The system shall be compatible with the launcher.	Launcher company
STH-004	The system shall be designed to prevent any damage which leads to loss of functionality of SSETI Express during operation.	ESA
STH-005	The total mission cost shall not exceed 20 million euros.	User
STH-006	The system shall aim to restore SSETI Express' functionality.	ESA & user & radio amateurs

3 SSETI Express Failure Analysis and Possible Mitigations

As the main goal of this mission is to restore functionality of SSETI Express, it is of critical importance to analyze how exactly the failure occurred and in what ways it can be repaired or circumvented. Section 3.1 describes the failure scenario that is deemed to be the most likely, and Section 3.2 additional non-critical failures. In Section 3.3, two methods of restoring functionality are proposed, with their advantages and disadvantages analyzed. Finally, Section 3.4 describes what boot sequence can be expected from SSETI Express after power is restored.

3.1. Electrical Failure

After deployment of SSETI Express, it was noticed that the voltage on the battery of the satellite was continuously decreasing, even though the solar panels were exposed to full sunlight. [5] The battery voltage decreased until it reached $14\,\mathrm{V}$, at which point the last confirmed telemetry was received during the 4th pass over the ground station. Later analysis and simulation indicates that a voltage regulating circuit, with the purpose of regulating the voltage on the main bus, failed in short circuit, thereby routing most power into a $10\,\Omega$ power resistor (shunt) and preventing the battery from charging. Figure 3.1 shows the circuit diagram of this part of SSETI Express' electrical system, where the green line indicates the shunt line, and 'Shunt 10R' the shunt power resistor.

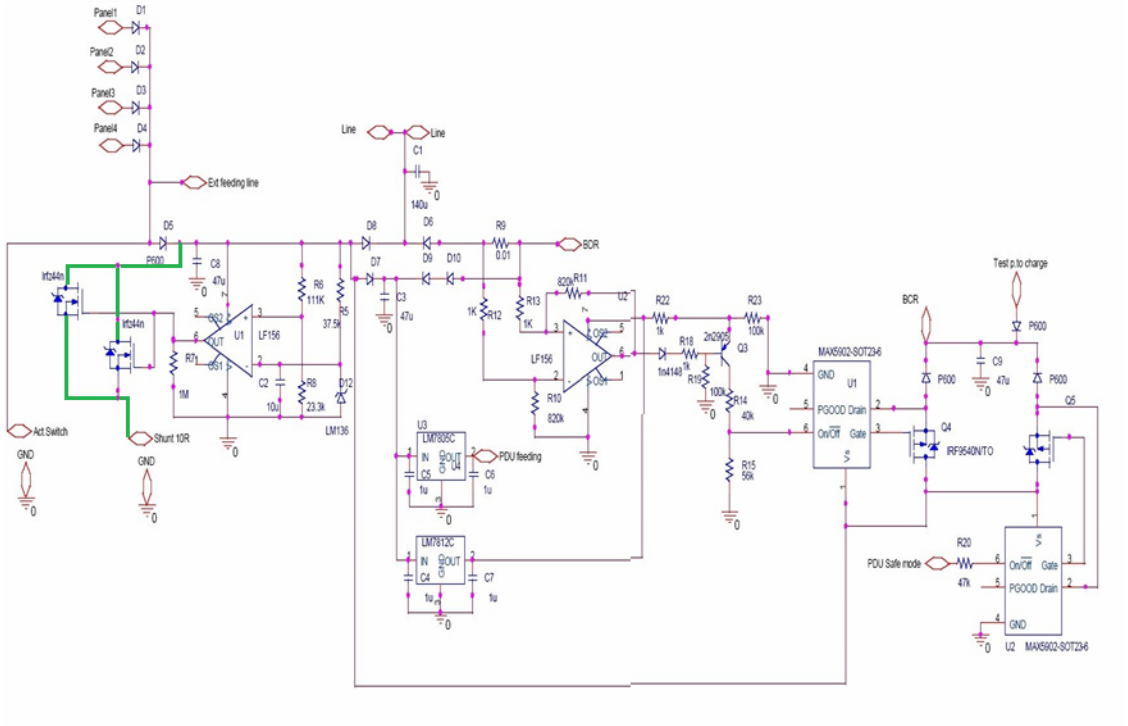

Figure 3.1: Circuit diagram of the main power bus, voltage regulator and battery charging regulator. [5]

It is visible that Op-Amp U1 drives two IRFz44n MOSFETs, which route excess power into the shunt resistor when the bus voltage exceeds $28.8\,\mathrm{V}$. However, due to failure of at least one of these MOSFETs, this connection is permanently closed, providing a low-resistance path to ground.

From this circuit diagram and the documentation of SSETI Express, two repair strategies have been identified. Both these strategies are explained in Section 3.3 and further developed in Chapter 6.

3.2. Other Failure

In addition to the power failure of SSETI Express, one of the carried cubesats failed to deploy, namely the NCUBE-2 [5]. No telemetry has been received from this module, it hasn't been detected by NORAD and SSETI Express was stabilizing on the wrong axis after deployment, leading to the conclusion that it is still contained in its respective T-POD, which is indicated to be on the -x side of SSETI Express. [6]
It is suspected that this failure is caused either by premature deployment of its antenna/gravity boom or due to failure of the T-POD to open, which is deemed less likely. As the the T-PODs are under consideration to be used as access point for the docking mechanism (Chapter 5), it is taken into account that this T-POD either hasn't opened fully or is obstructed.

3.3. Repair Strategies

In order to restore functionality of the electrical system of SSETI Express, 2 strategies are considered that can be used either individually or combined. Subsection 3.3.1 discusses the option of cutting connections to the shunt, Subsection 3.3.2 describes the strategy of injecting power externally. Section 3.4 explains how the electrical system is expected to react after being repaired, and what indications of functioning can be received.

3.3.1. Shunt Disconnection

It is expected that, by physically disconnecting the shunt line, the power is routed back to the battery and other subsystems again, restoring the functionality of the satellite.

This line is physically accessible at multiple points in the satellite, those being the connection to the MOSFETs in the Electrical Power System (EPS) box, and the wires connecting the shunt resistor to ground. Figure 3.2 shows these points, and inspection of the main structure of SSETI Express indicates that, to reach one of these components, only the outer shell needs to be breached at no more than one point.

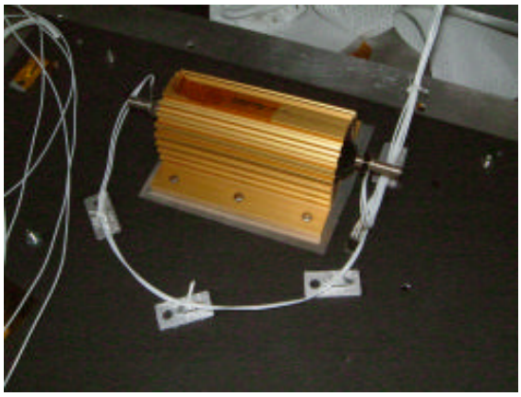

(a) The shunt resistor as mounted on the side panel, the white wire is considered the critical wire to be cut. [6]

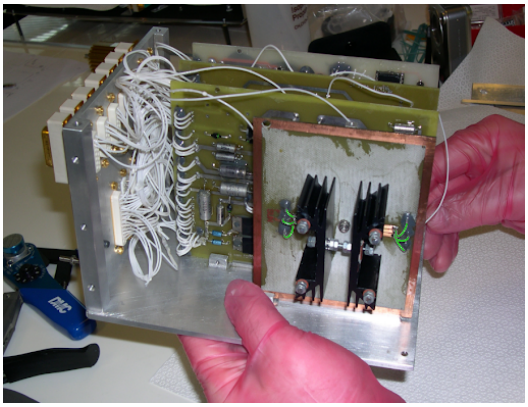

(b) The EPS box, the green wires are the critical wires which connect the power bus to the shunt resistor. [5] (green highlights added)

Figure 3.2: The two identified points where the shunt wire is accessible once inside the satellite.

Severing this connection means that the voltage on the main bus is no longer limited to its originally intended voltage. As the solar cells behave as current sources, the voltage on the bus will vary according to the load connected, and initial testing showed that the solar panel voltage can reach up to $33.8\,\mathrm{V}$ with no load connected [6]. Therefore, it needs to be verified that this higher bus voltage will not result in further component failure in SSETI Express.

Table 3.1 shows the maximum input voltage of the active semiconductor components used in this circuit. It can be concluded that a bus voltage of up to $33.8\,\mathrm{V}$ will not induce component failure in this circuit. Voltage ratings of other subsystems, including the battery charge regulator, are not specified and therefore predictions cannot be made with complete certainty. However, since the voltage increase is limited to 17%, and voltage regulators and other active components generally have a wide input voltage range, it is deemed likely that the system will not experience major issues from this. As the possibility of damaging otherwise intact subsystems by overvoltage is highly undesirable, this risk is nonetheless still deemed unacceptable.
To mitigate this, it is considered to attach an external regulator to the circuit side of the shunt line after severing it, so that the shunt resistor is selectively switched in and out of the circuit. This allows for the possibility of monitoring and regulating the voltage on the main bus externally, but relies on the condition that the failed MOSFET remains short-circuited with a significantly low resistance, unless the interception is made in the harder to reach

EPS box.

Table 3.1: Maximum voltage ratings of the active components on the circuit shown in Figure 3.1

Component	Maximum rated input voltage
LF-156	40 V [1]
LM7805C	35 V [2]
LM7812C	35 V [3]
MAX5902	72 V [4]
IRF9540N	−100 V (V_{DS})[5]

The following advantages are identified with this strategy:

- No additional power needs to be provided to SSETI Express
- A cutting tool can be multifunctional when the repair doesn't deliver the desired effects

And the following disadvantages are identified:

- The outer shell of SSETI Express needs to be physically breached
- The shunt line might be difficult to reach
- The shunt line might be difficult to sever
- SSETI Express' solar cells might be degraded to the point that they do not deliver enough power for its functioning
- The bus voltage is no longer regulated to a maximum of 28 V
- The internal battery of SSETI Express might be discharged beyond functioning

3.3.2. Power Injection

In Figure 3.1, it can be seen that diodes D8, D7, and two p600 diodes prevent current flowing from the battery circuit to the shunt line. This means that if the battery is charged from an external source, its power will not be dissipated into the shunt resistor and can be used to power the subsystems of SSETI Express, without necessarily requiring an invasive procedure.
In the bottom honeycomb panel of SSETI Express, a module with the activation switches and battery charge connector is present, visible in Figure 3.3. This battery stud is openly accessible from the outside of the satellite, and can be used to inject power into the battery of SSETI Express, thereby bypassing SSETI Express' solar cells and shunt circuit.
It is expected that in the case the battery is non-functional due to being discharged beyond its intended levels, the battery charge regulator will bypass the battery and provide the main bus with 28 V instead. The rescue spacecraft's batteries can then be used for power supply during eclipse.

The following advantages are identified with this strategy:

- The battery stud is openly exposed on the outside of SSETI Express, making it easily accessible
- Possible degradation of SSETI Express' solar cells is bypassed

And the following disadvantages are identified:

- As no documentation of the battery charge regulator is available, it cannot be predicted with complete certainty how it will handle the injected power
- SSETI Express will be powered from the rescue spacecraft, which needs to be included in the power budget

[0] https://www.strategyzer.com/canvas
[1] https://www.ti.com/product/LF156#features
[2] https://html.alldatasheet.com/html-pdf/9048/NSC/LM7805C/122/3/LM7805C.html
[3] https://html.alldatasheet.com/html-pdf/9048/NSC/LM7805C/122/3/LM7805C.html
[4] https://www.analog.com/en/products/max5902.html#product-overview
[5] https://www.infineon.com/cms/en/product/power/mosfet/p-channel/irf9540n/

(a) The battery charge stud and activation switches, as a standalone module [6]

(b) The battery charge stud and activation switches, mounted on the bottom honeycomb panel of SSETI Express [6]

Figure 3.3: Pictures of the integration process of the battery charge stud and activation switches

3.4. Boot Procedure

The electrical system of SSETI Express is setup such that after release of the activation switches, a timing circuit starts charging until, after 74 minutes, a set voltage level is reached and the satellite boots up. [6]
As it is unknown how much power is supplied by the solar cells and what fraction of that is dissipated, it is considered a possibility that the the timing circuit has discharged sufficiently to reset the timers. As a consequence, it is expected that the system will not immediately respond to the repairing operation, but will have a delay of at most 74 minutes. After this, the spacecraft is expected to boot, either into normal mode or safe mode, depending on the battery voltage, and will start transmitting beacons which indicate its state.

4 Operations & Logistics

This chapter will dive into the actions performed, not only during the mission but also in the phases prior to launch. Section 4.1 will sequentially describe the activities of SERUM during the mission. Section 4.2 will then zoom in on what happens after the DSE with respect to this mission development. Section 4.3 and Section 4.4 depict these actions in a functional flow and breakdown diagram respectively. Section 4.5 then summarizes all actions in a Gantt chart.

4.1. Operations and Logistic Concept Description

After finishing the design, SERUM will be manufactured and assembled. This is followed by verification and validation, which is the last step before the operational lifetime of SERUM begins. SERUM's operational lifetime is split into six phases: pre-deployment, coasting, transfer, approach, docked and end-of-life. These phases will be used to design SERUM according to the requirements coming from the different phases.

After being launched in the Falcon 9, the pre-deployment phase begins. During this phase SERUM has to wait without undertaking any actions for at least 120 s after deployment from the launcher, in order to prevent interfering with the launcher or other spacecraft using the same rideshare. From that moment onward, the spacecraft is allowed to perform maneuvers to stabilize and point its solar panels.

The second phase will be coasting, during which all subsystems are checked sequentially. The communication system will be started and it will try to contact the ground station. After this link is secured, SERUM can check its subsystems and report to the ground station. When this is confirmed for all subsystems, the nominal operations can be initiated.

The next phase is the transfer to SSETI Express' orbit phase. The launcher will release SERUM in a 500 km sun-synchronous orbit. In order to reach SSETI Express, which is in a (approximately) 700 km sun-synchronous orbit, a Hohmann transfer will be performed. To do so, SERUM's current position has to be determined and calculations have to be performed to update the required ΔV for each burn based on the actual insertion orbit. Subsequently, the Hohmann transfer to match SERUM's orbit to SSETI Express's will be performed, resulting in arriving at SSETI Express in 2029 in the nominal case.

During the fourth phase, SERUM will approach and dock with SSETI Express. SERUM will approach SSETI Express up to a distance of 10 m. Once it is at the right distance and SERUM is in contact with the ground station, the docking procedure can be started. During an orbit, SERUM passes over the groundstation 12.6 times on average. Multiple of these passes are more than 10 minutes and are thus considered 'good' passes. In these 'good' passes, the docking will first be practiced and finally attempted for real. There will be an up-link and down-link for the full duration of capturing. These will be used to provide a video feed to groundstation and to give possible commands to intervene in case of an emergency. Once the overpass is there and capture is initiated, SERUM will first match SSETI Express's rotation, and then decrease it's relative distance to 0.5 m. The robotic arm will close the gap between itself and the T-POD (which are cut-outs in SSETI Express's structure meant for the launch of cubesats), insert the expansion mechanism into the T-POD and activate the expansion mechanism. After this, the zond (an expansion mechanism) will lock in through the bottom of SSETI Express and with this, finalize the docking. If during docking or before it is already determined that docking is not possible (due to for example SSETI Express spinning too fast), SERUM can employ the secondary catching method. This method consists of a net which will capture SSETI Express and allow SERUM to de-orbit with SSETI Express, to remove it from being debris for other (future) spacecraft. If this is also not possible or does not succeed, SERUM itself will initiate the end-of-life phase by itself.

Once docked, the repair of SSETI Express can begin. SERUM is equipped with two mechanisms to do so. The first strategy that is tried, is bypassing the electrical fault by injecting power directly into the system. After this strategy, the shunt resistor inside SSETI Express will be cut. If the bypass was successful, it will be done to demonstrate the technology of in-orbit servicing, otherwise it's a backup solution to fix SSETI Express. This will be done by first piercing through SSETI Express's outer skin and subsequently, the connection will be intercepted using a modified T-tap, a device to intercept a connection instead of cutting it. If either method is successful, SERUM will stay docked to SSETI Express for the rest of its operational lifetime.

The end-of-life phase is the final phase in SERUM's operational lifetime. The first step will be the deployment of the drag sail. This will be done either if none of the methods succeeds in fixing SSETI Express or after fixing is successful and SSETI Express has been working again for 3 months. After this, the spacecraft will

be completely shut down and the drag sail will do its work. Only just before re-entering the atmosphere, the spacecraft will turn on again, contact the ground station, perform calculations, and then, a final burn will be performed to make sure the remains of SERUM and possibly SSETI Express do not land in an inhabitant area.

4.2. Project Design and Development Logic

The Project Design and Development Logic shows the order of activities to be executed after DSE ends. For SERUM, this was already included in the functional flow diagram, and can be seen in Figure 4.1. Up to this point in the DSE, blocks 1, 2 and 3 were executed. The post-DSE activities can be seen from block 4 (manufacturing) onward and entails manufacturing, verification and validation, operations/utilization and finally project closure.

4.3. Functional Flow Diagram

A functional flow diagram is a visual representation of the various functional areas or stakeholders within an organization and how they interact with each other in a logical sequence of tasks or processes. It helps to identify the sequence of steps, inputs and outputs involved in a process and provides a clear understanding of the flow of information or materials within an organization/mission.

Figure 4.1 and Figure 4.2 illustrate the functional flow diagram of the SERUM's mission, which encompasses the entire process from mission analysis to project closure.

The operational phase of the rescue mission receives particular attention, with logical steps defined for various functions related to the status of the SSETI Express satellite. For instance, if the SSETI Express satellite is spinning at a higher-than-anticipated rate and poses a docking hazard, the repair satellite will abort the docking process and de-orbit without attaching to the SSETI Express. In addition, the diagram visually represents certain logical loops, which offer a more profound understanding of subsystem design by enabling consideration of additional functions and their relationships.

4.4. Functional Breakdown

A functional breakdown structure is a hierarchical diagram that outlines the functions required to achieve a specific mission. It breaks down the overall objective into smaller, more manageable and interconnected functions that make up the mission. Each function is then further broken down into sub-functions until the desired level of detail is achieved. The diagram helps to ensure that all necessary functions are identified, and provides a basis for estimating resources, developing schedules, and tracking progress.

The functions of SERUM's mission are presented in Figure 4.3, which outlines the process from mission analysis to project closure. The operational phase of the mission receives the most emphasis as it has a significant impact on the design options of the system.

4.5. Gantt Chart

The tasks outlined in the functional flown diagram are shown in Figure 4.4, where their estimated start and end date are visible. Furthermore, it clearly shows how some processes are performed in parallel, whereas others are directly dependent on previously performed tasks. The spacecraft detailed design is planned to be finished in Q1 2025. Manufacturing, assembly and integration is planned to be done in Q1 2026 and final verification and validation in Q1 2027. Launch is expected to occur in Q2 2027, after which the spacecraft will perform its mission until de-orbiting around 2035. In the last phase, the ground support equipment will be terminated, and the mission will be reviewed in Q3 2035.

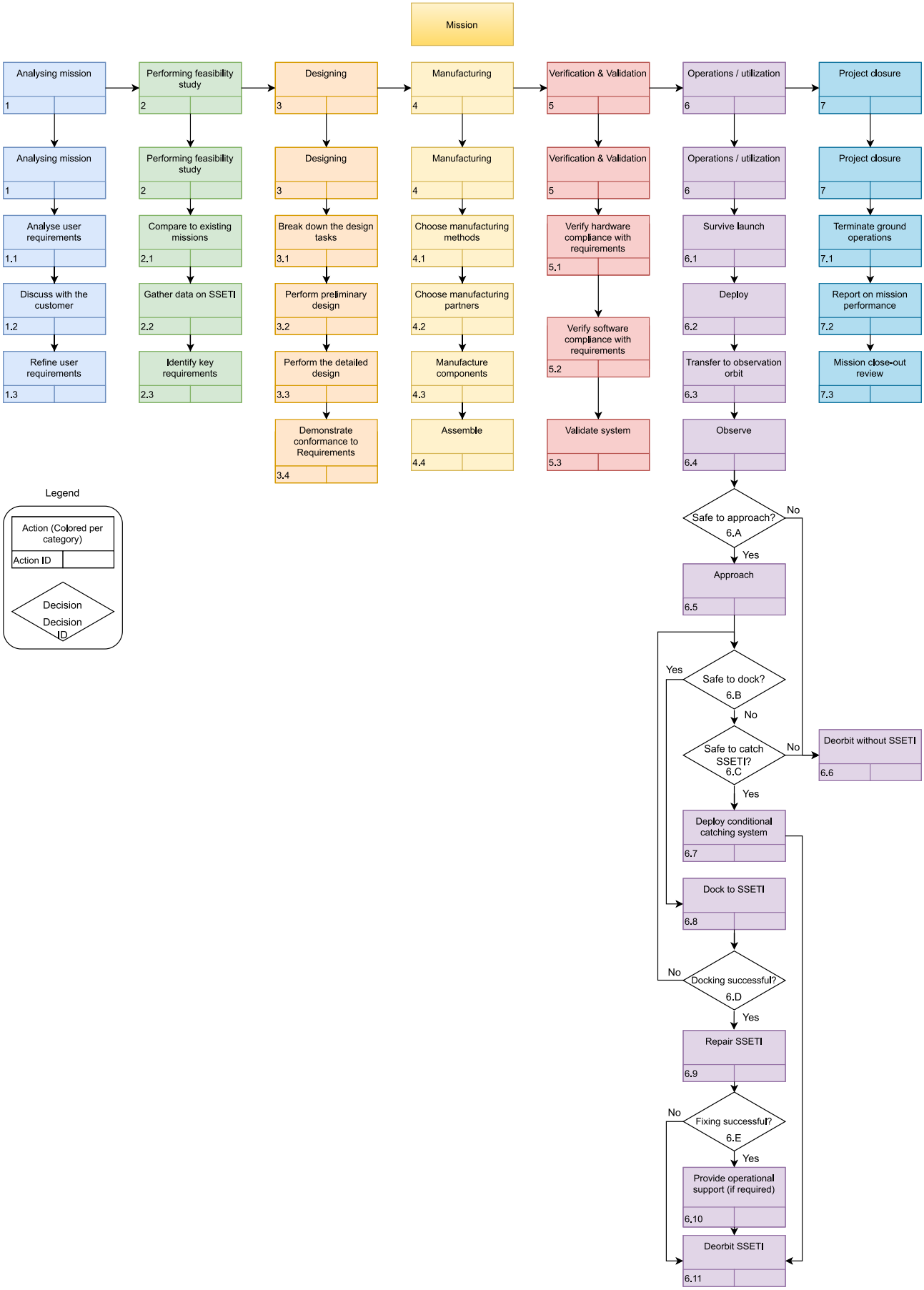

Figure 4.1: Functional Flow Diagram, Part 1

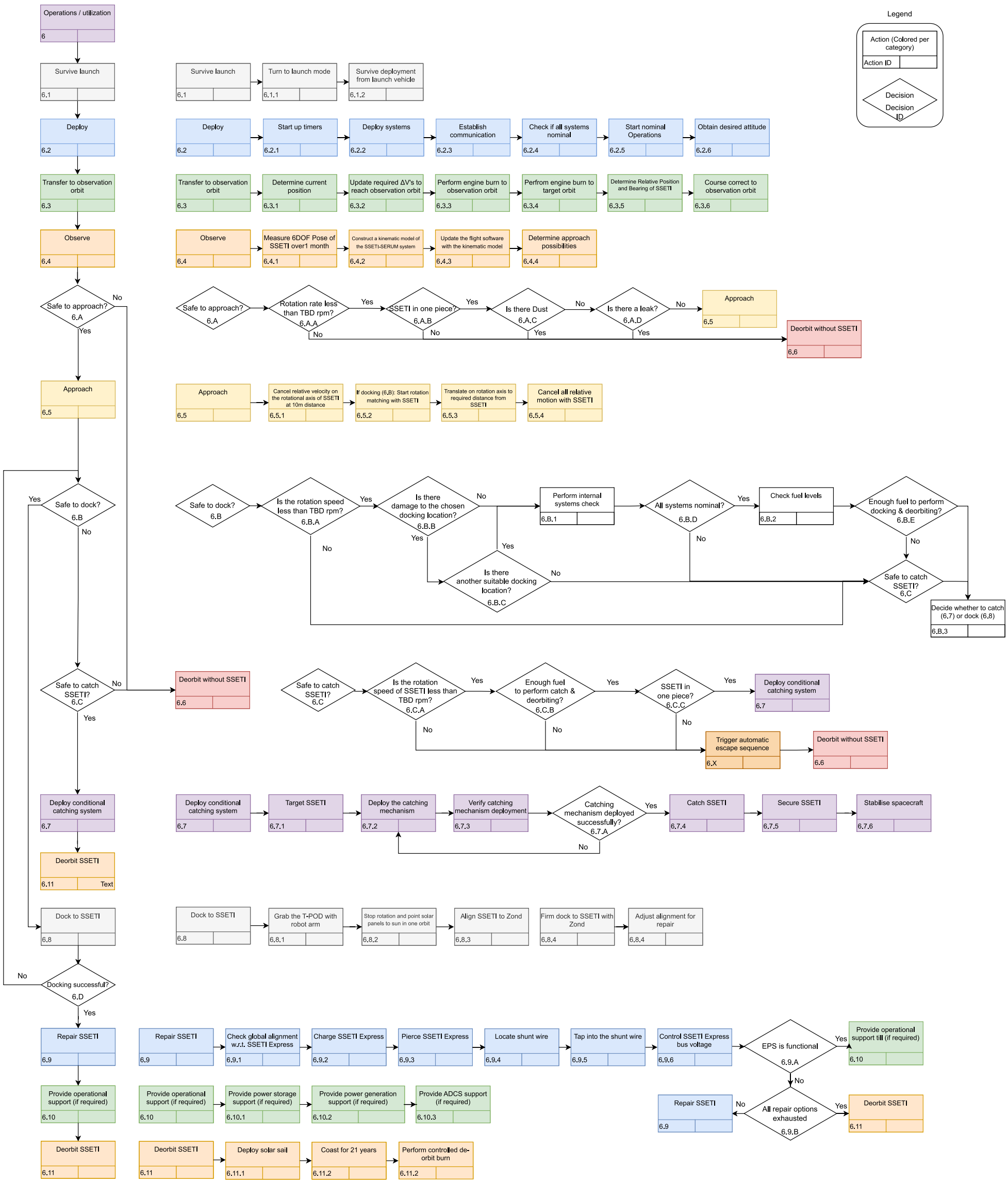

Figure 4.2: Functional Flow Diagram, Part 2

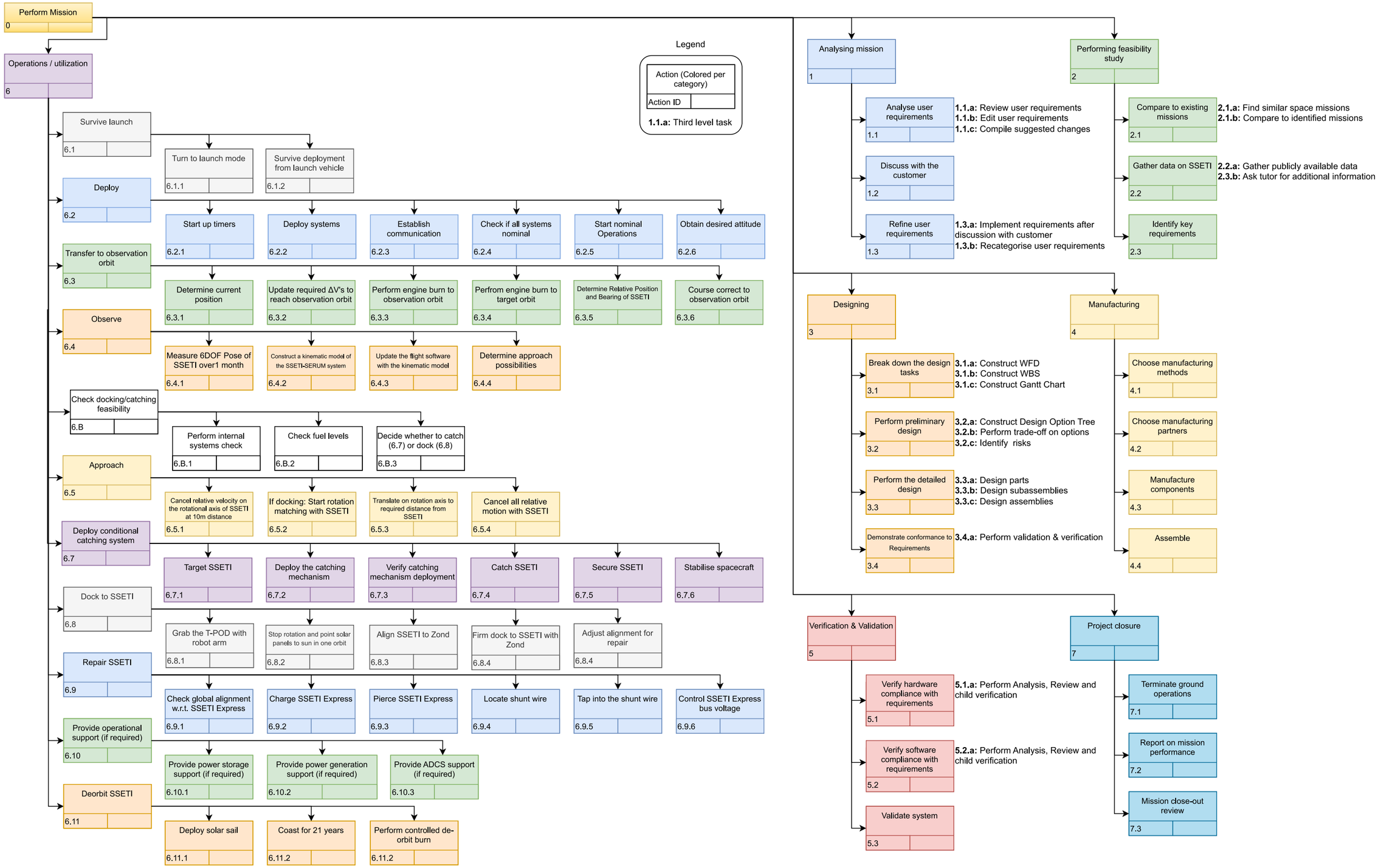

Figure 4.3: Functional Breakdown Structure

Figure 4.4: Project Gantt Chart

ID	Name	2018	2023	2028	2033	2038
1	Designing					
2	Detailed design					
3	Verify compliance with requirements					
4	Manufacturing, assembly & integration					
5	Choose manufacturing methods & partners					
6	Manufacture components					
7	Assemble & integrate spacecraft					
8	Verification & Validation					
9	Verify hardware compliance with requirements					
10	Verify software compliance with requirements					
11	Validate system					
12	Operations & logistics					
13	Integration in launch vehicle & launch					
14	Deployment phase					
15	Transfer to target orbit					
16	Observing target in relative orbit					
17	Approach attemps					
18	Docking & repair					
20	Nominal mission					
21	De-orbiting					
22	Project closure					
23	Terminate ground equipment					
24	Report on mission performance					
25	Mission close-out review					

5 Payload - Docking

This chapter details the design process for the docking subsystem. Its task is to permanently dock to SSETI Express to facilitate a smooth repair scenario. In Section 5.1 the design decisions made in the midterm report are summarized. A first design iteration for the chosen configuration is given in Section 5.2 and Section 5.3, which will be supported by the sensors, detailed in Section 5.4. In Section 5.5, the capture procedure, including the required torques by GNC are given. After these descriptions the budgets for the entire docking subsystem can be found in Section 5.6. Finally this chapter is concluded in Section 5.7, including a visual overview in Figure 5.10 and Figure 5.11 for the docking subsystem's sensors and mechanisms respectively.

5.1. Docking Design Overview

The design of the docking subsystem is, as is the case for most subsystems, driven by the user requirements and some constraints. A literature study of docking and berthing methods resulted in a variety of design options. Only one of the identified design options was able to meet the driving docking system requirements. First and foremost, MIS-010-DOCK-001 is the most driving requirement for the docking subsystem. The feature that would be chosen to dock to, will rotate about some, yet unknown, axis of rotation. Furthermore, for the sustainability of space exploration and in light of the commercialization of space, MIS-002-DOCK-001 drives the entire spacecraft design. For docking this means that a harpoon system will not be used out of fear of potential damage to the solar panels and that additional caution is needed to prevent generating additional space-debris above all else. A design similar to Clearspace-1[1], with a large spider-like grabbing system, is not chosen for similar reasons. In addition to the danger of damaging SSETI Express' solar panels during the collision, possibly resulting in debris, this design option was found to be likely to become too heavy. A net-capture option, as described in Chapter 8 would not create debris for spacecraft without vulnerable appendages. However it will impair the repair and accessing of the internal components of SSETI Express. Thus a net is also not an option because it would not satisfy driving requirements SYS-007-DOCK-001 and SYS-010-DOCK-001.

By inspecting pictures and other documentation on SSETI Express, it was determined that the mechanical interface ring and the T-PODs for the cubesats are the only geometrical features of SSETI Express that could be used to capture SSETI Express without severely damaging its outer panels and thus compromising SYS-011-DOCK-001 (Stefano Speretta, interpersonal communication, May, 2023). The two spacecraft should remain docked for the rest of the lifetime in accordance to MIS-005-DOCK-001 and to mitigate the risk of RI-PAY-7. Thus the docking subsystem should be able to withstand loads generated during the accessing phase, as described in Chapter 6. Additionally the connection should be intact, even in the case of a shut-down such that the spacecraft are ensured to remain connected. The mechanical interface ring will be the best mounting point to establish a stiff connection for these purposes. The mechanical interface ring should however be approached with great caution, because the extruding segment of the mechanical interface ring is very short and the inside hole is close to components belonging to the fuel tank. To work around this problem, it was determined that SSETI Express' relative motion with respect to SERUM should first be controlled before it is attempted to dock with the mechanical interface ring. The concept of the capture and docking procedure can be found in Figure 5.1. The final design option that was ruled out, magnetic and ionic capture methods, are not feasible because the Debye Shielding Effect would render these methods impossible unless the system is a few millimeters removed from SSETI Express. Thus, it is chosen that a finer robotic arm shall first capture SSETI Express, using the T-Pods to control the relative motion between SSETI Express and SERUM.

[1] https://www.esa.int/Space_Safety/ClearSpace-1

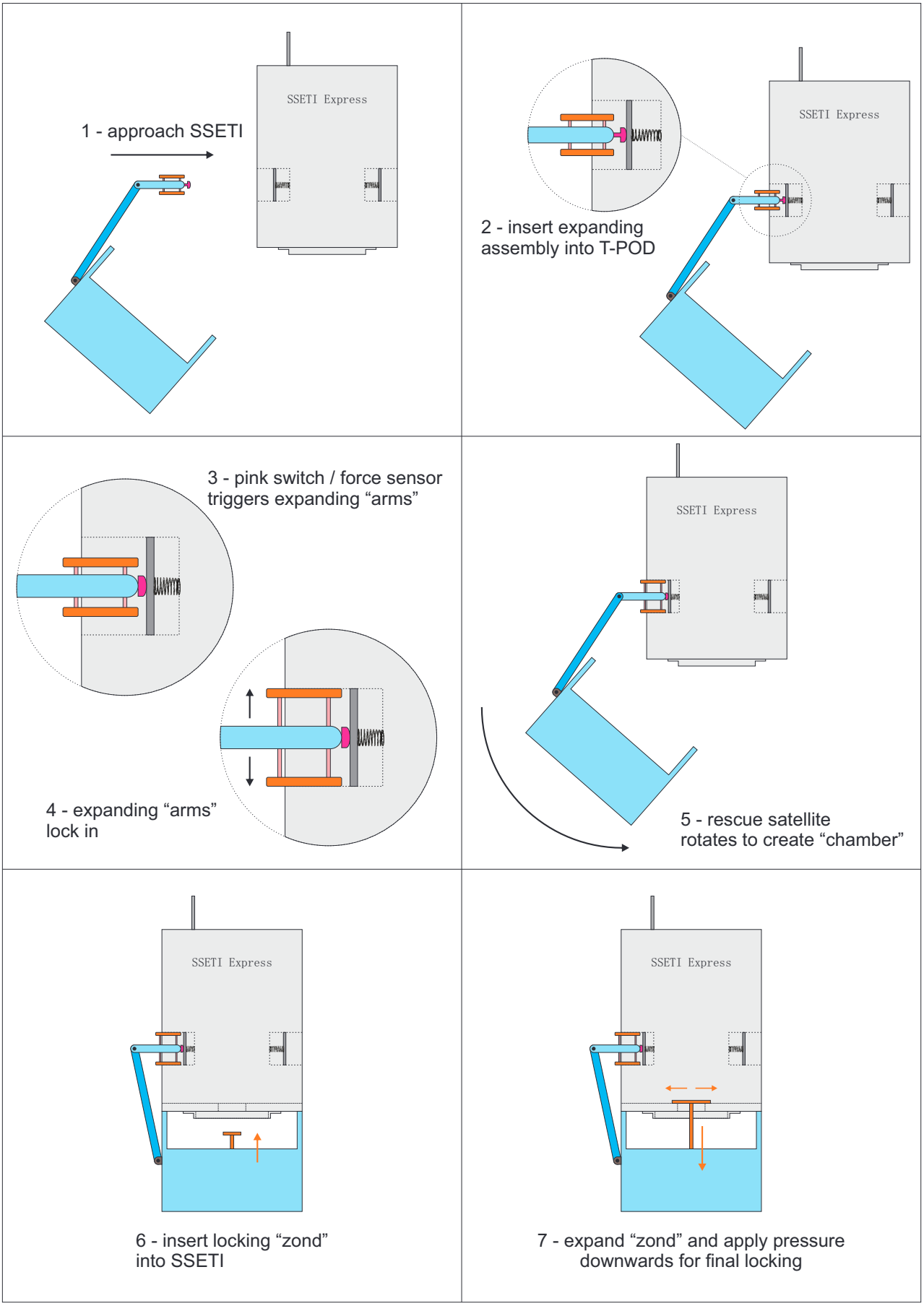

Figure 5.1: Capture & docking procedure

The doors of the T-PODs and the ejection mechanism of the T-PODs are not useful features to attach to because they are both designed to move/pivot and are thus both harder to latch on to and less reliable as a connection. Instead there will be a mechanism that expands into the sides of the T-POD, further detailed in Section 5.2. After a successful capture-procedure, SSETI Express will be re-positioned and docked with the "Zond", the design of which is further proposed in Section 5.3. The Zond has a different expansion mechanism that maintains a fail safe connection even in the event that SERUM becomes inactive, satisfying MIS-005-DOCK-001 in a redundant manner. It will, together with the encapsulement clamp down SSETI Express after docking. The encapsulement is 15 cm extension of the side panels of SERUM that provides opposite forces to the clamping of the Zond and creates a closed environment between SERUM and SSETI Express. This design mitigates the possible results of RI-PAY-1.

In order to dock to SSETI Express, it is required to know where it is. For this a sensor sweet is needed. This sensor sweet can determine the position and bearing of SSETI Express from a distance of 1 km (DOCK-001-OBS-001), determine the 6-DOF of SSETI Express (pose determination) at a range of 10 m to 1.5 m (DOCK-001-OBS-002 and DOCK-001-OBS-003). In addition it can track the T-POD from a distance of 2 m to 0.2 m (DOCK-001-OBS-004). This is achieved by a optical telescope, two sets of three event cameras and a single event camera mounted on the docking arm. The reasoning and sizing of the sensor sweet is described in Section 5.4.

The capture method is possible independent of SSETI Express' axis of rotation, as long as it rotates at a rate equal to or smaller than 1 r/min. SERUM will then align itself and match SSETI Express' rotation on that axis. This procedure is further explained in Section 5.5.

5.2. Expansion Mechanism and Robotic Arm Design

The expansion mechanism and robotic arm are responsible for the capture of SSETI Express. The development of novel components drives a large part of the cost for space-missions. To cut costs it was chosen to select a robotic arm commercially available. For the capture, the distance between the bodies of the two spacecraft will remain at least half a meter apart. With the current estimation of SERUM having the basic dimensions of 56 cm X 56 cm X 56 cm excluding the encapsulement with a depth of 15 cm, it was found that a robotic arm with roughly 1.2 m range should be used. A customised version of the KRAKEN by Tethers Unlimited was chosen[2]. It would have three segments, each with length 0.5 m and medium joints. The mass of this arm would be approximately 11 kg with a cost of approximately 1.78 MEUR (Robert Hoyt, interpersonal communication, June, 2023). This arm is sufficiently long, standing at a total length of 1.5 m, sufficiently strong, with repeated peak torque 36 N m and is easily integrateable because of its compatability with ROS (Robot Operating System). A rough model of the Kraken arm can be found in Figure 5.2.

The expansion mechanism is sized such that it can expand to dimensions slightly larger than the corners of the T-POD, such that strong friction forces can be used. The T-Pod has a cross-section of 10 cm x 10 cm but it is not known exactly how deep the neutral state of the spring is. A video of a test of the T-Pod was on Earth analyzed (Stefano Speretta, interpersonal communication, May, 2023). It could be determined from this video that the back plate would at least be 5 cm deep. Because all corners of the T-Pod are at the same distance from the center of its cross-section, neglecting production margins, it was chosen to have all expanding ridges be driven by the same actuator. A screw is driven by an electrical motor, forming the actuator that controls the expansion. The loads exerted on the expansion mechanism are mainly carried by the outer tube, which contains the screw. The ridges are equipped with small teeth to improve friction on the outside of the T-Pod. The ridges are restricted from going beyond perfectly outward from the center and are aimed toward the actuator such that they brace against any pulling force. The design of the expansion mechanism is provided in Figure 5.3a and Figure 5.3b.

Finally, the next design iteration should include a detailed design on how to dissipate likely potential differences between SERUM and SSETI Express to manage RI-POW-0 and satisfy SYS-003-DOCK-002. This can be done by creating an electrical path between the tip of the expansion mechanism and the rest of SERUM. This path needs to have a resistance large enough such that a safe discharge can occur but small enough such that the dissipation will be completed within a few minutes at most. The Zond will need a switch to electrically isolate it from the rest of SERUM as it would create a closed loop when the bypass or the repair subsystems are in electrical contact with SSETI Express. This provides flexibility on how to prevent charge build-up after the capture procedure.

[2] https://www.tethers.com/wp-content/uploads/2022/10/KRAKEN.pdf

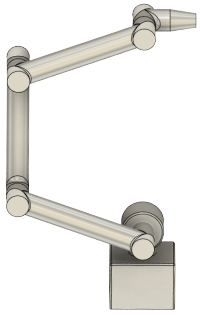

Figure 5.2: Kraken robotic arm with three 0.5 m segments and medium joints [3]

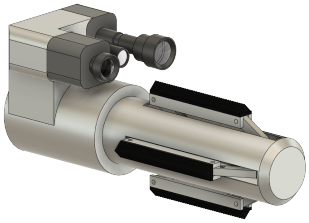

(a) Expansion mechanism retracted

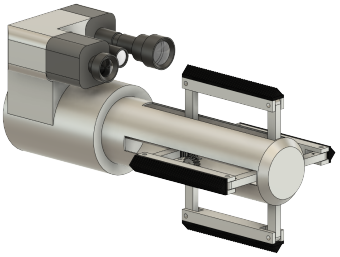

(b) Expansion mechanism deployed

Figure 5.3: Expansion mechanism

5.3. Zond Design

The Zond will serve to clamp down on SSETI Express and provide a rigorous connection between the two spacecraft. The encapsulement will have a nominal depth of 15 cm beyond the side of SERUM. The side panel of SSETI Express has a thickness of 3.2 cm with a 1.5 cm distance between the closest component of the propellant tank. Because of the narrow margin through which some bracing system has to be deployed, it was decided to use a pulley expansion mechanism, which can extend purely in a radial direction. It has the additional benefit of remaining closed unless a torque acts upon the inner screw of the mechanism, thus satisfying SYS-005 even in case the power goes down during the mission. The hole in the honey comb panel in the middle of the mechanical interface ring has a diameter of approximately 11 cm. To allow for margins for the docking, the retracted diameter of the mechanism is 9 cm with the expanded diameter being 14 cm. For flexibility of the docking procedure it was chosen that the Zond shall be able to expand 5 cm beyond the 18.2 cm distance from SERUM for the clamping side. Additionally it shall be able to retract to up to 5 cm smaller than 18.2 cm, such that the sides of the encapsulement can deform to better close the space and that the Zond can be safely inside of the encapsulement. More detail is provided in Chapter 6. This design iteration of the Zond is visualized Figure 5.4a, Figure 5.4b and Figure 5.4c.

(a) Zond retracted

(b) Zond extended

(c) Zond fully deployed

5.4. Docking Sensors

In terms of spacecraft complexity, sending down a video stream and letting ground controllers navigate SERUM and dock to SSETI Express, would be preferred. "Time delays in human communication, calculation, and commands, however, prevent ground controllers from directing the servicer quickly and precisely enough to execute the final capture phase of the rendezvous."[4]. The full docking procedure will thus have to be performed autonomously. For this, NASA developed the Raven module for the ISS in 2015 [5]. This demonstrates the autonomous position determination of other SC within a range of 1 km with full 6-DOF pose determination when the visiting SC's subtended angle of the vehicle is ≥30 % the sensor's FOV" [7]. For SSETI Express this translate into an effective 6-DOF determination range of ±12 m as can be seen in Figure 5.5.

[4] https://nexis.gsfc.nasa.gov/Relative_Navigation_System.html
[5] https://nexis.gsfc.nasa.gov/Raven.html

Thus in order to be able to dock to SSETI Express (SYS-003-DOCK-001), SERUM shall have to be able to determine the relative position and bearing from a distance of 1 km (DOCK-001-OBS-001) and the 6-DOF of SSETI Express (pose determination) at a range of 10 m to 1.5 m (DOCK-001-OBS-002 and DOCK-001-OBS-003). The range of 1km for position determination stems from the approximate accuracy of a TLE in LEO [8]. A Raven like system would be an obvious choice to satisfy these requirements, however, the size and mass of the Raven system makes it incompatible with SERUM. Additionally, the docking procedure itself requires the docking arm to grab onto the T-POD. Thus the docking sensors will have to be able to track the T-POD from a distance of 2 m to 0.2 m (DOCK-001-OBS-004). The position and bearing determination is discussed in Subsection 5.4.1, pose determination in Subsection 5.4.2 and feature tracking in Subsection 5.4.3. The computational power required for these systems is discussed in Section 10.2.

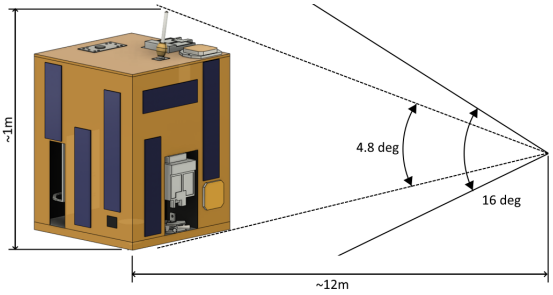

Figure 5.5: The field of view of the Raven Viscam instrument with SSETI Express shown with a subtended angle of 30 % (4.8°) of the sensor's FOV (not to scale)

5.4.1. Position and Bearing Determination

LiDAR systems with a range of 1 km are very heavy. For example the RVS 3000-3D has a mass of 13 kg [9], more than the entire original payload mass budget. Additionally, when compared to small optical systems, small LiDAR systems are not readily available as COTS systems. An optical camera can also perform the position and bearing determination of SSETI Express due to a-priory knowledge of its size [10].

From 1 km away (r) SSETI Express will cover 0.052 54° (α) in the sky. For a ± 30 m positioning accuracy (a), each pixel has a required FOV ($FOV_{pixel,req}$) of 0.026 m as calculated with Equation 5.1 where h is the height of SSETI Express (917 mm). This is equivalent to an AFOV of 0.0148° per Equation 5.2.

The Dragonfly Aerospace Chameleon imager has a AFOV of 2.3° and a resolution of 2000 pixels. [11] Thus the AFOV per pixel is 0.001 15° thus it meets the accuracy requirement of 0.0148° calculated above. SSETI Express will fill up the imager AFOV at a distance of 30 m determining the minimum working range. For ranges closer than 30 m the cameras from the pose positioning can be used for location and bearing determination as described in Subsection 5.4.2.

$$FOV_{pixel,req} = h(1 - \frac{r + a}{r}) \tag{5.1}$$

$$AFOV_{req} = \frac{pix_{sensor}}{pix_{req}} \cdot \alpha \tag{5.2}$$

5.4.2. Pose Determination

To determine the 6-DOF of the visiting vehicle, the Raven system uses a combination of LiDAR and a standard camera to perform feature recognition. As previously discussed, it is preferred not to use LiDAR systems for SERUM. Instead of using LiDAR and standard cameras to determine the perform feature, recognition event based cameras can be used [12]. This system uses three small light weight event cameras to triangulate and track features in 3D. Combining the event based camera sensor method with the navigation algorithms of the Raven system allows for a light weight, low volume and COTS (from a hardware perspective) solution to navigate to and determine the tumbling characteristics of SSETI Express.

Full feature tracking has been demonstrated with a 640×480 pixel resolution such as the DVXplorer Mini [13], which costs 3400 EUR. When taking the 30 % the sensor FOV as the minimum size required for pose determination from the Raven system, this results in a at least 144 pixel image of SSETI Express as seen in Figure 5.6. This is a similar level of detail as is used for the Raven system [7, Figure 10], it is thus expected that this is sufficient detail.

Given the 10 m maximum range (DOCK-001-OBS-002), taken as the working distance (WD), the required lens focal length is calculated. The required FOV is equal to the height of SSETI Express divided by 30 %. The required focal length (f_{min}) is than cal-

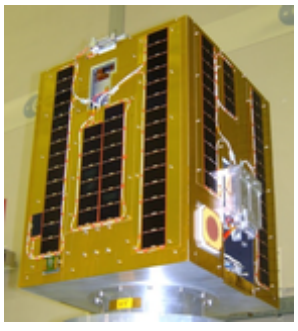

(a) Original image scale to a height of 144 pixels (Stefano Speretta, interpersonal communication, May, 2023)

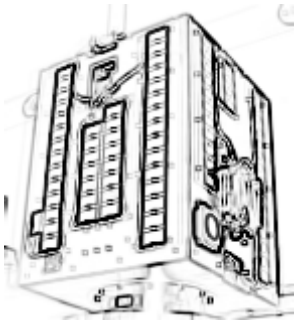

(b) After Prewitt edge detection

Figure 5.6: Simulation of the event based camera output by a edge detection analogy using Prewitt edge detection

culated with Equation 5.3 [6] where H is the height of
the sensor, 5.76 mm. From this equation a focal length of 31 mm is required for this sensor. This is equivalent to a 20.5 mm focal length for a 2/3" image sensor. This leads to the LM12-10MP-25MM-F2.5-1.5-ND1[7], which costs 99 EUR. This system has a minimum working of 4.9 m at which point SSETI Express takes up the full sensor.

$$f = \frac{H \cdot WD}{FOV} \tag{5.3}$$

Similarly, taking the minimum range of 2 m results in a maximum focal length of 12.5 mm. This leads to the choice of the LM12-5MP-08MM-F2.8-1.8-ND1[8]. This results in a maximum WD of 6.6 m. Thus having 2 sets of cameras, one with a 31 mm lens and one with a 12.5 mm lens covers the full range required by DOCK-001-OBS-002 and DOCK-001-OBS-003.

To increase the accuracy of the pose determination system the long range cameras should be as far away from each other as possible. The close range cameras have to be closer together to ensure their FOVs overlap. Additionally, to ensure continues pose determination in the final docking approach maneuver, the cameras will have to face the side of SERUM pointed to SSETI Express. This leads to the camera positioning as shown in Figure 5.10.

To determine the position determination range of the pose cameras Equation 5.3 was used with a f of 31 mm and H of 5.76 mm. To find the FOV required it was taken the SSETI Express express has to take up at least 10 pixels on the sensor. This the FOV required is $640/10 \cdot 0.917$ m$=58.6$ m. This results in a working distance of 315 m.

$$WD = f\frac{FOV}{H} \tag{5.4}$$

5.4.3. Feature Tracking

To track the T-POD from a distance of 2 m to 0.2 m DOCK-001-OBS-004, the advantage of a-priory knowledge of the T-POD dimensions can be used. Forrai et al. [10] developed a method to track an object in 3D using a single event camera if the object's size is known. This method is capable of running on on-board computers such as the NVIDIA Jetson Orin with a frequency of 100 Hz.

This event based object tracking requires that the type of path the object follows is known. Due to the observation phase of the SERUM mission, the expected path of the T-POD with respect to the docking arm is known. Thus, this method can be used directly by SERUM to track the T-POD.

For single arm camera the same even camera, the DVXplorer Mini, is used. To determine the focal length of the lens the same sizing process as described in Subsection 5.4.2 was performed. This results in a focal length of 6.3 mm is required for this lens, equivalent to 5.3 mm focal lenght for a 2/3" lens. This leads to the choice of the LM12-10MP-05MM-F2.5-2.3-ND1[9] 5 mm lens, which costs 99 EUR. This results in a view of the T-POD from 0.2 m as seen in Figure 5.7.

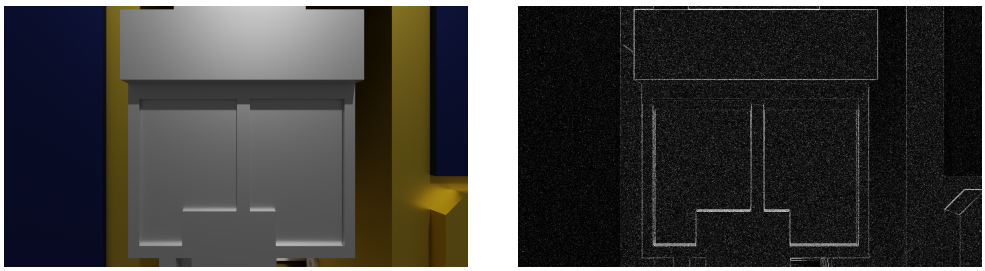

(a) Real color view of the T-POD (b) After Prewitt edge detection

Figure 5.7: Simulation of the event based camera output by a edge detection analogy using Prewitt edge detection

[6] https://www.edmundoptics.eu/knowledge-center
[7] https://www.get-cameras.com/LENS-M12-10MP-25MM-F2.5-2/3-LM12-10MP-25MM-F2.5-1.5-ND1
[8] https://www.get-cameras.com/LENS-M12-5MP-8MM-F2.8-1/1.8INCHLM12-5MP-08MM-F2.8-1.8-ND1
[9] https://www.get-cameras.com/LM12-10MP-5.4MM-F2.5-2.3-ND1-LM12-10MP-05MM-F2.5-2.3-ND1

5.4.4. Sensor Time Line

With the four sensor packages described above, continues tracking of SSETI Express can be performed from a distance of 1 km to a distance of 0.2 m. Figure 5.8 shows how each sensor phase overlap to form contineus coverage. These four phases are: Chameleon Imager, LR Pose Cameras, SR Pose Cameras and Arm Camera. When SERUM is further than 20 m away from SSETI Express only position and bearing determination is performed. When SERUM is closer than that, full 6-DOF determination can be performed.

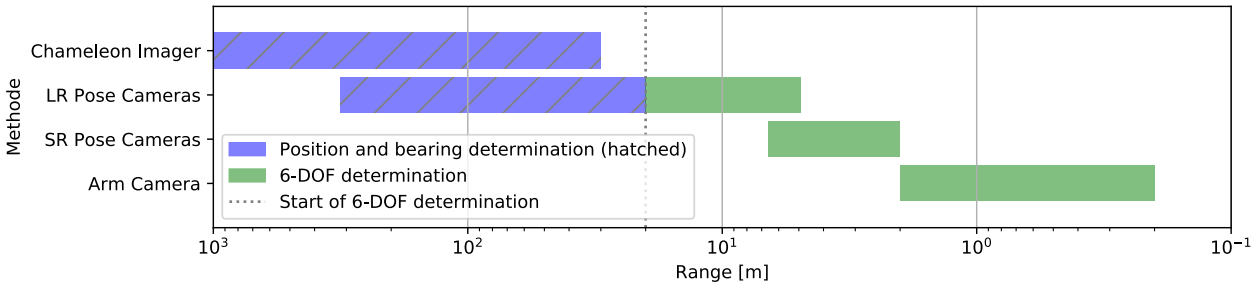

Figure 5.8: Docking sensor range diagram

5.5. Capture Procedure

As mentioned in Chapter 9, it is possible to have 10 minutes of continuous communication during the docking phase. These 10 minutes will unfortunately not all be available to perform a relatively long capture procedure. To avoid a collision between the spacecraft, they will orbit each other at a distance of 10 m when the communication initiates. After 2 minutes, SERUM will still be at a 10 m distance from SSETI Express but will have match SSETI Express' rotation. The y-axis of SERUM will be aligned with SSETI Express' axis of rotation and the angular velocity around this axis will also be matched. By 4 minutes after the onset of communication, the distance between the two spacecraft will be 0.5 m, which is the closest the spacecraft will be before a successful capture-procedure. During this period, the robotic arm will also be positioned such that it will have a 0.5 m distance from the T-POD when the capture attempt starts. Its exact position will thus depend on the kinematics of SSETI Express. The movement of the robotic arm will cause a change in the inertia tensor of SERUM and thus it will need to create torques to maintain this rotation. The fifth and sixth minute of communication is when SERUM is allowed to attempt capture. Within this time the robotic arm will close the gap between itself and the T-Pod, insert the expansion mechanism in the T-Pod and activate the expansion mechanism.

In case the capture is successful, SERUM will then start decelerating SSETI Express' rotation for two reasons. Most importantly, this allows the spacecraft to face the sunlight for a longer time, which allows it to charge the battery using the solar panels. Second, this allows SERUM to maneuver SSETI Express without gyroscopic effects changing the rotation significantly from how an object in rest would react. Once the two spacecraft are rotating at a manageable rate, SERUM will start orienting its solar panels to the sun. This procedure will take place during the eclipse after capture. In case the capture is unsuccessful, SERUM will have two minutes to remove its arm from the proximity of SSETI Express. When the arm is at a save distance, SERUM will perform a burn to once again orbit SSETI Express at a save distance when the communication ends. Before the docking starts, the mechanical interface ring of SSETI Express should be directly facing the Zond at a distance of between 0.3 m and 0.5 m. To ensure correct alignment and to reduce the sizing for the robotic arm and GNC, five more communication windows are scheduled solely to prepare for docking.

Docking itself will be relatively uneventful. Again there will be 10 minutes available for communication. In the first minute of docking, SSETI Express will be brought up to 5 cm from the Zond which will be fully retracted. The alignment will then be controlled at ground-station. If SERUM gets the green light from ground-station, it will expand the Zond such that it fits between the propellant tank and the honeycomb panel. The pulley expansion mechanism will then be expanded to permanently establish a connection with SSETI Express. Finally, the Zond will be retracted again until it is loaded with 500 N of tension. Thus the encapsulement will be loaded in compression for 500 N.

SERUM's rotation during the capture attempt will likely not be around its primary axis of rotation because moving the robotic arm will change it's location and orientation. Thus, the GNC system will have to provide torques to maintain the same rotation as SSETI Express. The torques needed are evaluated with the following formula:

$$M_{cm} = \frac{dB^b_{cm}}{dt} + \Omega^b_{bI} \times B^b_{cm} \tag{5.5}$$

$$M_{cm} = \frac{dI^b}{dt} \cdot \Omega^b_{bI} + I^b \cdot \frac{d\Omega^b_{bI}}{dt} + \Omega^b_{bI} \times I^b \cdot \Omega^b_{bI} \tag{5.6}$$

In the inertia tensor, the geometry of the spacecraft was discretized in the form of lumped masses in 3D (x,y,z), which is a class that was made in Python containing a mass, position-vector and velocity-vector. Assuming that the centroid has already been determined and that x,y,z would be the coordinates of a lumped mass with respect to the centroid, the components of the tensor can be calculated as:

$$I^b_{oo} = \sum_{i=1}^{n} M_i \cdot (p_i^2 + q_i^2), \qquad I^b_{op} = \sum_{i=1}^{n} M_i \cdot o_i \cdot p_i \tag{5.7}$$

In Equation 5.7 o,p and q can be either of x,y or z. Since the robotic arm is moving, the inertia tensor will also have a time derivative. This time derivative will be a tensor containing the time derivative of its components, for which:

$$\frac{dI^b_{oo}}{dt} = \sum_{i=1}^{n} M_i (2p_i \cdot \frac{dp_i}{dt} + 2q_i \cdot \frac{dq_i}{dt}), \qquad \frac{dI^b_{op}}{dt} = \sum_{i=1}^{n} M_i \cdot (\frac{do_i}{dt} \cdot p_i + o_i \cdot \frac{dp_i}{dt}) \tag{5.8}$$

$$\frac{dI^b_{oo}}{dt} = \sum_{i=1}^{n} M_i (2p_i \cdot v_{p,i} + 2q_i \cdot v_{q,i}), \qquad \frac{dI^b_{op}}{dt} = \sum_{i=1}^{n} M_i \cdot (v_{o,i} \cdot p_i + o_i \cdot v_{p,i}) \tag{5.9}$$

In Equation 5.6 all vectors are expressed with respect to an inertial frame. Because the body frame of SERUM would rotate with respect to this inertial frame, every calculation in case of a time-variant simulation would need a coordinate transformation to obtain the required torques with respect to the SERUM body frame. The GNS system must be sized for these torques.

Luckily, the inertial frame can be chosen arbitrarily. To not further complicate the mathematics, the torques are calculated for one specific instance, with the inertial frame being the exact same as the SERUM body frame, except for the fact that it does not move with the body beyond that point. As a result, the moments that are acquired directly translate to the torque that GNC needs to provide around the SERUM body reference frame.

To verify if GNC is sized correctly for the approach, a worst case scenario can be created. This will be when SSETI Express is rotating at $1\,\mathrm{r/min}$, as given by MIS-010-DOCK-001, while the arm is moving outwards, which slows down the spacecraft. In this scenario, GNC should still be able to maintain the rotation. As a result $\frac{d\Omega^b_{bI}}{dt}$ will be equal to the null-vector since it is the angular acceleration of SERUM. Since SERUM will be facing SSETI Express while rotating about its y-axis at $1\,\mathrm{r/min}$, $\Omega^b_{bI} = 0.1047\bar{e_2}$.

For this iteration a conservative simplified approximation for SERUM's mass distribution will be used. The robotic arm will weigh $4\,\mathrm{kg}$ for each section of $0.5\,\mathrm{m}$ and $3\,\mathrm{kg}$ for the subsystems at the. The rest of the spacecraft is a modified version of a cube with a distributed mass of $180\,\mathrm{kg}$ and a side-length of $0.56\,\mathrm{m}$. This calculation is thus for approximately the heaviest that SERUM is allowed to be. A cube with a distributed mass has a radius of gyration of 0.289 times that side-length. To additionally simulate the non-uniformity of SERUM, it is chosen that along each principle axis there is a lumped mass of $36\,\mathrm{kg}$ on one side and $24\,\mathrm{kg}$ on the other side. The robotic arm is assumed to start at the middle of a side-panel and proceed as displayed in Figure 5.9.

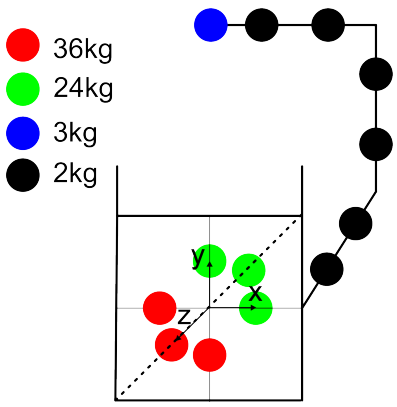

Figure 5.9: Lumped mass configuration capture torque calculations

For the change in inertia, it is chosen that the arm travels towards the center at $0.0167\,\mathrm{m/s}$. In case a maneuver toward the T-Pod of half a meter with constant acceleration in the first half and constant deceleration in the second half and a maneuver time of $60\,\mathrm{s}$ is used, this would be the peak velocity. The discussed data results in the following vectors and matrices used in Equation 5.6:

$$I^b_{approx} = \begin{bmatrix} 12.68775 & -0.58 & 0.0 \\ -0.58 & 3.94 & 0.0 \\ 0.0 & 0.0 & 13.49 \end{bmatrix} \text{kg m}^2 \quad \left| \quad \frac{d}{dt} I^b_{approx} = \begin{bmatrix} 0.0 & 0.1326 & -0.0015 \\ 0.1326 & 0.0049 & 0.0 \\ -0.0015 & 0.0 & 0.0049 \end{bmatrix} \text{kg m}^2 \right.$$

$$\Omega^b_{bI} = \begin{bmatrix} 0 \\ 0.10478 \\ 0 \end{bmatrix} 1/\text{s} \quad \left| \quad \frac{d}{dt} \Omega^b_{bI} = \begin{bmatrix} 0.0 \\ 0.0 \\ 0.0 \end{bmatrix} 1/\text{s}^2 \right. \quad \left| \quad T^b_{approx} = \begin{bmatrix} 0.0139 \\ 0.0005 \\ 0.0064 \end{bmatrix} \text{Nm} \right.$$

With the required torque during the capture calculated, a new torque requirement has been born for the GNC subsystem, which will be investigated in Chapter 12. It would technically be possible for CDH to use Equation 5.6 to control the GNC system. However this would only be a small fraction of the contents of a control system. For example, Equation 5.6 does not contain any decision-making, image-processing or sensor-fusion. To further develop the control system would go far beyond the scope of this report, thus it will not be performed at this stage.

5.6. Docking Subsystem Budgets

This section contains the mass, power and monetary budgets for the docking subsystem. Components that would be developed specifically for this mission use mass estimations based on preliminary CAD models. The mass estimations for the docking subsystem can be found in Table 5.1

Power usage for the subsystems are reported for different use-cases separately if applicable. It is kept in mind that Table 5.2 is used for sizing the EPS system. For that purpose the power usage of the Expansion mechanism and Zond can be ignored because they will only consume power during the few seconds that it takes their small actuators and motors to deploy. As a result, their consumption will be left blank.

Estimating the development cost of the payload is important for the budget of the whole satellite. However, many of the presented components are custom-built and there is no direct source for the specific cost of development. Therefore, when similar components do not exist or no similar components are found, the cost estimations will be made based on the development cost and mass of a space-grade system/mechanism that is similar in underlying physical principles. Canadarm and its development cost suit these criteria. The correlation is then applied to the mass of the piercing mechanism. Canadarm's mass and development associated cost are 328.82 MEUR [10], adjusted for the financial year of 2023, and 410 kg[10]. Applying this estimation method, Table 5.3 presents the total cost of the docking.

Table 5.1: Mass estimation of the docking subsystem

Item	Mass (kg)	(Estimation) Method
Expansion mechanism	0.716	CAD
Zond	2.64	CAD
KRAKEN Robotic arm	11	COTS[11]
DVXplorer Mini (x7)	0.3	COTS[12]
VizCam	0.04	COTS[13]
Lenses	0.06	COTS[14][15][16]
Dragonfly Aerospace Chameleon imager	1.6	COTS[17]
	16.36	

[10] https://www.thecanadianencyclopedia.ca/en/article/canadarm
[10] https://www.tethers.com/wp-content/uploads/2022/10/KRAKEN.pdf
[11] (Robert Hoyt, interpersonal communication, June, 2023)
[12] https://shop.inivation.com/collections/dvxplorer-mini
[13] https://shop.inivation.com/collections/dvxplorer-mini
[14] https://www.get-cameras.com/LENS-M12-5MP-8MM-F2.8-1/1.8INCHLM12-5MP-08MM-F2.8-1.8-ND1
[15] https://www.get-cameras.com/LENS-M12-10MP-25MM-F2.5-2/3-LM12-10MP-25MM-F2.5-1.5-ND1
[16] https://www.get-cameras.com/LM12-10MP-5.4MM-F2.5-2.3-ND1-LM12-10MP-05MM-F2.5-2.3-ND1
[17] (Dragonfly Aerospace (Pty) Ltd., interpersonal communication, June, 2023)

Table 5.2: Power estimation of the docking subsystem

Item	Power (W)	Time	Energy (Wh)	Phase
Expansion Mechanism	-	-	-	Capture and docking procedure
Zond	-	-	-	Docking procedure
Robotic arm	10	10 min	1.67	Capture and docking procedure
DVXplorer Mini (x3)	0[18]	-	-	Observation, capture and docking procedure
DVXplorer Mini (x1)	0[18]	-	-	Capture procedure
Chameleon imager	0[18]	-	-	Approach
VizCam	0[18]	-	-	Capture procedure

Table 5.3: Cost budget contribution of the docking subsystem

Sub-components	**Cost [**kEUR**]**	**Quantity**	**Total cost [**kEUR**]**	**(Estimation) Method**
Expansion mechanism	574	1	574	Cost-Mass relation (Canadarm)
Zond	2640	1	2640	Cost-Mass relation (Canadarm)
KRAKEN Robotics Arm	1780	1	1780	COTS[11]
DVXplorer Mini	3.5	7	24.5	COTS[19]
LM12-5MP-08MM-F2.8-1.8-ND1	0.059	3	0.177	COTS[20]
LM12-10MP-25MM-F2.5-1.5-ND1	0.1	3	0.3	COTS[21]
LM12-10MP-05MM-F2.5-2.3-ND1	0.1	1	0.1	COTS[22]
Dragonfly Aerospace Chameleon imager	190	1	190	COTS[23]
			5209.08	

The mass of the docking subsystem comes mostly from the weight of the Kraken robotic arm. This weight can not be avoided or reduced, unless a superior alternative is identified in a later stage. This alternative should also be an off-the-shelf product or else it is will be considerably more expensive. It also needs to be noted that the current iteration of the Zond has quite a high mass, and as a result cost, because it has been designed with 3.5 mm thick aluminum. This thick design is a safe compensating for the lack of resources for a more detailed analysis in this phase. The high mass will likely result in an overestimation of the cost because a heaver ,relatively simple, mechanism should not necessarily be more expansive. For example, the Zond would likely be more expensive to develop if it was made with CFRP, even though this design would be considerably lighter.

5.7. Conclusion

The docking subsystem is the first part of the payload that SERUM will need during its lifetime. To determine SSETI Express' location, bearing and pose for docking, a sensor sweet is included. The sensor sweet consists of an optical telescope for long ranges, two sets of three event cameras for medium to close ranges, and a single event camera for the final capture phase. This configuration allows continuous coverage from a distance of 1 km all the way to being docked with SSETI Express. The usage of event cameras is a novel approach

[18] Powered by the payload computer

[19] https://shop.inivation.com/collections/dvxplorer-mini

[20] https://www.get-cameras.com/LENS-M12-5MP-8MM-F2.8-1/1.8INCHLM12-5MP-08MM-F2.8-1.8-ND1

[21] https://www.get-cameras.com/LENS-M12-10MP-25MM-F2.5-2/3-LM12-10MP-25MM-F2.5-1.5-ND1

[22] https://www.get-cameras.com/LM12-10MP-5.4MM-F2.5-2.3-ND1-LM12-10MP-05MM-F2.5-2.3-ND1

[23] (Dragonfly Aerospace (Pty) Ltd., interpersonal communication, June, 2023)

that decreases the computational load, power consumption and mass of the docking system significantly when compared to existing systems such as NASA's RAVEN[7]. A model of all the sensors integrated in SERUM can be seen in Figure 5.10. During the 10 minutes of ground-station communication, SERUM will go from an orbit $10\,\mathrm{m}$ removed from SSETI Express to an orbit $0.5\,\mathrm{m}$ removed from SSETI Express, while on its axis of rotation and matching that rotation. Next SERUM will insert the expansion mechanism, which will be custom build and is shown in Figure 5.3a and Figure 5.3b, to establish a first connection. This connection will then be used to safely dock with the Zond, depicted in Figure 5.4a, Figure 5.4b and Figure 5.4c, which creates a rigid connection for the repair. A model of the full integrated docking system can be seen in Figure 5.11. It was calculated in Section 5.5 using the expanded equations of motion, given in Equation 5.6, that the highest torque needed about the principal axes of SERUM during the capture procedure is $0.0139\,\mathrm{N\,m}$, which needs to be within the capabilities of the GNC subsystem. Finally, the total mass of the docking subsystem amounts to $16.36\,\mathrm{kg}$ with a cost, including development, of 5.21 MEUR . Both the mass and cost budgets are likely to decrease with the next design phase, mainly driven by a more efficient Zond design.

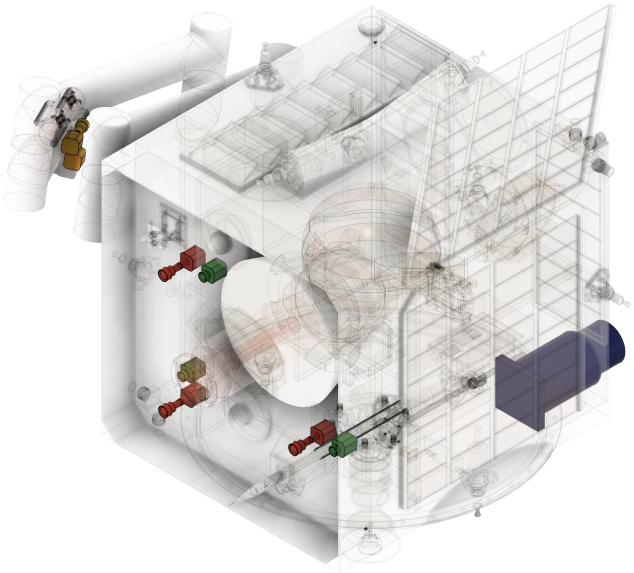

Figure 5.10: Position of posing cameras integrated in SERUM

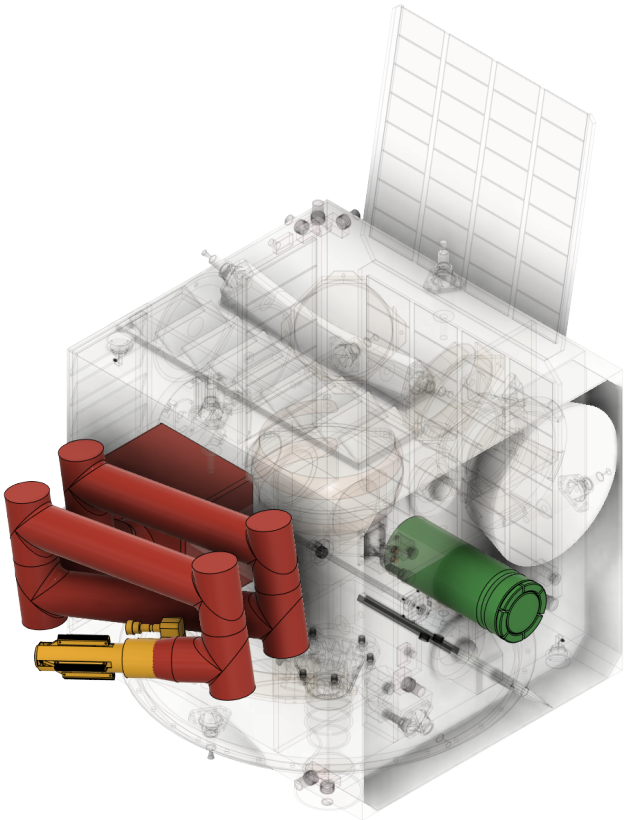

Figure 5.11: The docking subsystem integrated in SERUM

6 Payload - Repair

In order to fulfill SERUM's mission, it is crucial to restore the initial functionality of SSETI Express. According to its mission objectives, SSETI Express' tasks include capturing images of Earth, serving as a transponder for the global amateur radio community, and (the already accomplished task of) deploying three picosatellites.

Essentially, the restoration of SSETI Express' functionality relies on resolving the failure of its EPS. As detailed in Chapter 3, this can be achieved by either enabling direct charging of the battery through the pre-launch connector or replicating the functionality of the faulty MOSFET by intercepting the wires connected to the shunt.

After considering various approaches, a Design-Option-Tree was created to explore potential solutions for these tasks. Subsequently, the feasibility of each option was evaluated, leading to a trade-off analysis among the concepts. A summary of the trade-off process can be found in Section 6.1. In Section 6.2 and Section 6.3, the chosen detailed repair methods are discussed. Additionally, Section 6.4 outlines the sequence of operations involved in the repair process. To ensure the successful revival of SSETI Express, a method for confirming its functionality is presented in Section 6.5. Furthermore, the budgets for the repair subsystem are provided in Section 6.6, and a conclusion is reached in Section 6.7.

6.1. Trade-off Summary

In order to carry out repair operations, access to the EPS system within SSETI Express is required. Considering that the satellite lacks convenient openings for instrument entry, two options were considered: creating a hole in one of the spacecraft walls or completely removing a wall. However, removing an entire panel was deemed impractical due to the presence of delicate solar panels covering it and the wiring running across multiple walls. Cutting and reattaching these wires would introduce significant challenges, making the panel removal approach infeasible. Hence, a trade-off considered options for making a hole in SSETI Express' wall.

While creating a hole through aluminum may initially appear straightforward, it is important to consider one of the mission requirements, which strictly prohibits the generation of debris at any stage. Consequently, the primary trade-off criterion, accounting for 60% of the decision-making process, is the potential for debris generation. The secondary criterion, weighing 40%, is complexity. Given the unique nature of the task, it is desirable to minimize the use of complex systems, as they introduce additional points of potential failure. The four candidates for creating the hole were laser cutting, regular drilling, friction drilling and piercing. Due to one large piece and many small chips generation, laser cutting and regular drilling respectively scored poorly in the trade-off. On the other hand, piercing and friction drilling (indicated in Figure 6.1) seemed viable, as they move the pliable aluminum out of the way, rather than detaching it from the bulk piece.

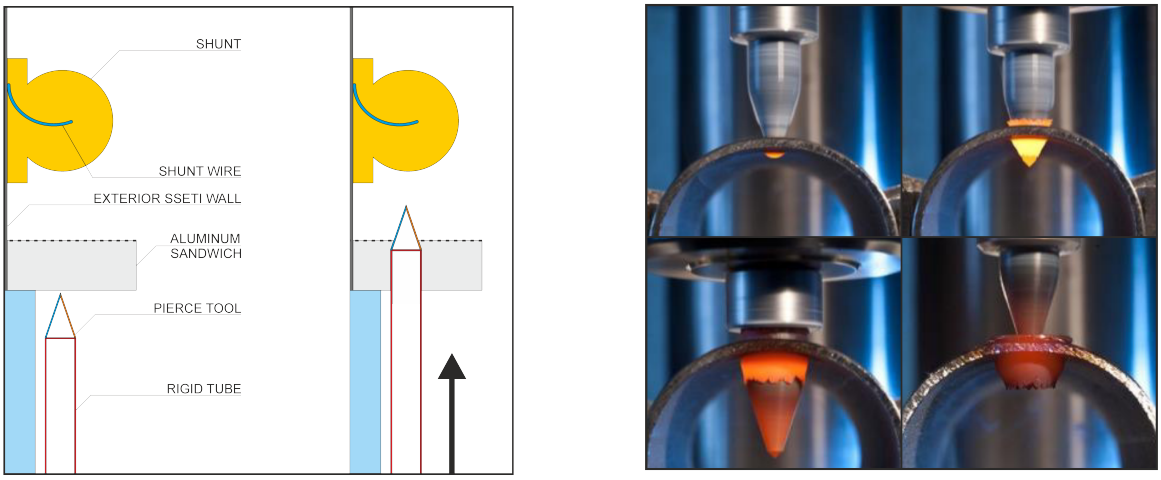

(a) Illustration of the piercing method

(b) Illustration of the friction drilling method [1]

Figure 6.1: Plausible methods for creating a hole in SSETI Express

Ultimately, limited literature existed to support either option in terms of debris generation. Consequently, a

straightforward demonstration was proposed to test the viability of the piercing method. While there was an intention to evaluate the friction drilling method as well, time constraints prevented adequate preparation for this more intricate approach. The details of the piercing test can be found in Chapter 7. In summary, the demonstration successfully showcased the possibility of debris-free piercing, leading to the selection of this method as the winner in the trade-off analysis.

Next, with the hole creation covered, the actual EPS circuit fixing methods were considered. The options were an endoscopic arm intercepting the shunt wire and a bypass connector, charging SSETI Express directly from the outside. Though initially, these options were traded-off on various criteria, it was concluded that they both shall be used. By adopting this approach, the risk of an unsuccessful repair would be minimized, as the availability of a backup option would provide an additional layer of mitigation of several payload related risks.

In summary, the trade-off analysis for the repair payload led to the selection of a battery charging connector as the primary fixing method. This approach involves directly charging the battery of SSETI Express from the exterior and bypassing the malfunctioning portion of the EPS circuit. Additionally, as a backup strategy, a piercing tool and an endoscopic robot arm will be utilized in unison. This backup method involves creating a hole in the spacecraft and intercepting the shunt resistor wire, effectively assuming the control functions previously performed by the failed MOSFET. Section 6.2 and Section 6.3 explore these methods in detail.

6.2. Bypass Strategy

The first strategy that will be tried to repair SSETI Express is to bypass the electrical fault by injecting power into the system as described in Chapter 3. This method works by feeding power directly into the battery of SSETI Express, which will not be dissipated by the faulty shunt circuit due to the presence of several diodes. In this way, the original solar cells are not of use anymore and the satellite will be kept powered by SERUM. This section goes into the details of how this repair procedure will be executed.

The battery charge stud is located on the aft side of SSETI Express, countersunk in the aluminum honeycomb panel, with its main purpose being trickle charging the battery before launch and regular charging during the integration and testing phases.

It provides a direct electrical connection to the positive electrode of the battery, and the negative electrode is grounded to the structure of SSETI Express. In order to make electrical contact, a custom connector is designed, visible in Figure 6.2a, which makes use of 2 pogo pins, that will provide a sturdy, vibration-proof connection. One of the pins connects to the battery stud, whereas the other connects to the (grounder) structure, thereby making it possible to inject power.

To minimize physical interference during docking, the connector remains in a retracted position only until the zond is confirmed to have made a solid connection between SERUM and SSETI Express, and the correct orientation has been achieved. After this, the connector will be extended such that the pogo pins engage with the contacts and an electrical connection is made. For this purpose, a scissor mechanism has been designed, shown in Figure 6.2b, which will convert rotational motion of a servomotor into pure vertical motion of the connector.

To allow for minor misalignments between the two satellites, a compliant stage is used for passive alignment through the use of filleted pins that engage with the cavity in the honeycomb panel. The mechanism uses thin, metal flexures that allow the assembly to translate in the x-y plane and rotate in the z-axis, whilst achieving high stiffness in the other degrees of freedom. The full assembly of the connector, extender, and interstage can be seen in Figure 6.2d.

During the connector extension process, a camera and force sensor will be used for making sure that the alignment between the stud and the connector is sufficient for good contact. If this is initially not the case, the docking arm can be used to reposition SERUM to achieve good alignment. After contact has been made, the voltage between the stud and the ground is measured, and is expected to be non-zero, indicating that contact with the battery has been made.

As SSETI Express battery has been depleted completely for a period of over 17 years, it cannot be predicted in what state it is and if it can be used in any capacity. For that reason, the assumption is made that SSETI Express shall be powered directly by the solar panels and battery of SERUM, resulting in a required $20\,\mathrm{W}$ power draw, which accounts for the nominal power draw ($12\,\mathrm{W}$) and possible losses induced by a malfunctioning battery ($8\,\mathrm{W}$).

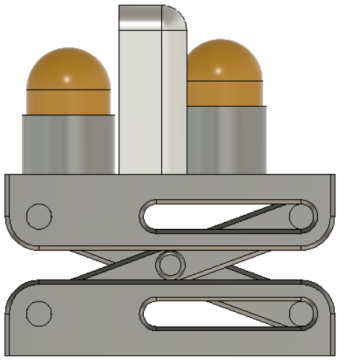

(a) Side view of the stud connector and extender mechanism in stowed mode

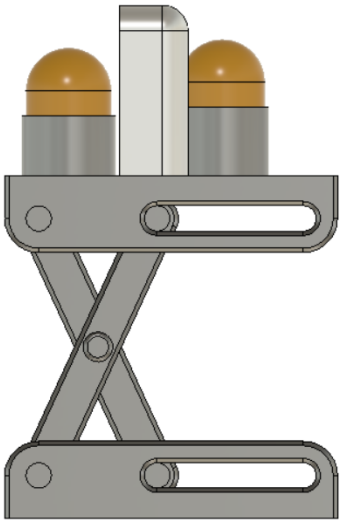

(b) Side view of the stud connector and extender mechanism in deployed mode

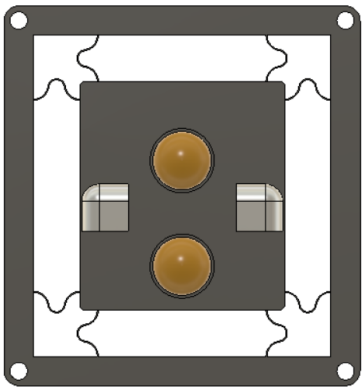

(c) Top view of the full stud connector assembly

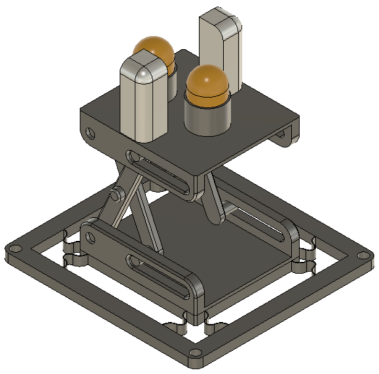

(d) Isometric view of the full stud connector assembly

Figure 6.2: CAD renderings of the mechanism for connecting to the battery stud, the pogo pin contacts are indicated in gold and the alignment pins are indicated in white.

6.3. Shunt Cutting Strategy

In the event that the bypass strategy in Section 6.2 fails, or if it succeeds, purely as a technological demonstrator, the shunt resistor inside SSETI Express will be intercepted. As described in Chapter 3, the shunt resistor is currently dissipating all of the power generated by the onboard solar arrays which lowers the bus voltage to the point that SSETI Express' battery cannot charge and the system cannot operate. The shunt resistor was included onboard SSETI Express as part of the voltage regulation circuit, and simply removing it from the system could potentially cause damage from the bus voltage rising above the nominal $28\,\mathrm{V}$. While this is unlikely since the open circuit voltage of SSETI Express will be $33.8\,\mathrm{V}$ (Subsection 3.3.1) and Table 3.1 shows that the voltage ratings of the components inside SSETI Express are all above $33.8\,\mathrm{V}$, this is deemed an unacceptable risk.

6.3.1. Intercepting Wiretap

Instead of cutting the wire to the shunt resistor, the connection will be intercepted using a modified T-tap. This will divert the connection through SERUM, which can use a MOSFET to switch the shunt resistor in and out of the circuit, as SSETI Express originally did. This way, the shunt functionality is not lost, and the voltage on SSETI Express' bus can be kept in the nominal range. Figure 6.4 shows a commercially available T-tap that inspired the design, Figure 6.5a shows the proposed design to be used on SERUM in an open position, and Figure 6.5b shows a closed position, with the top of the wiretap made transparent. The brass plates on the sides cut through the wire's isolation and into the conductive center. The plastic body of the wiretap forces the wire

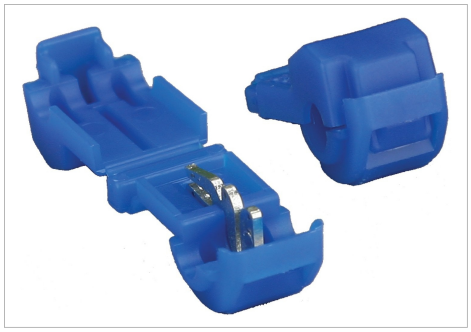

Figure 6.4: A standard T-tap connector[2]

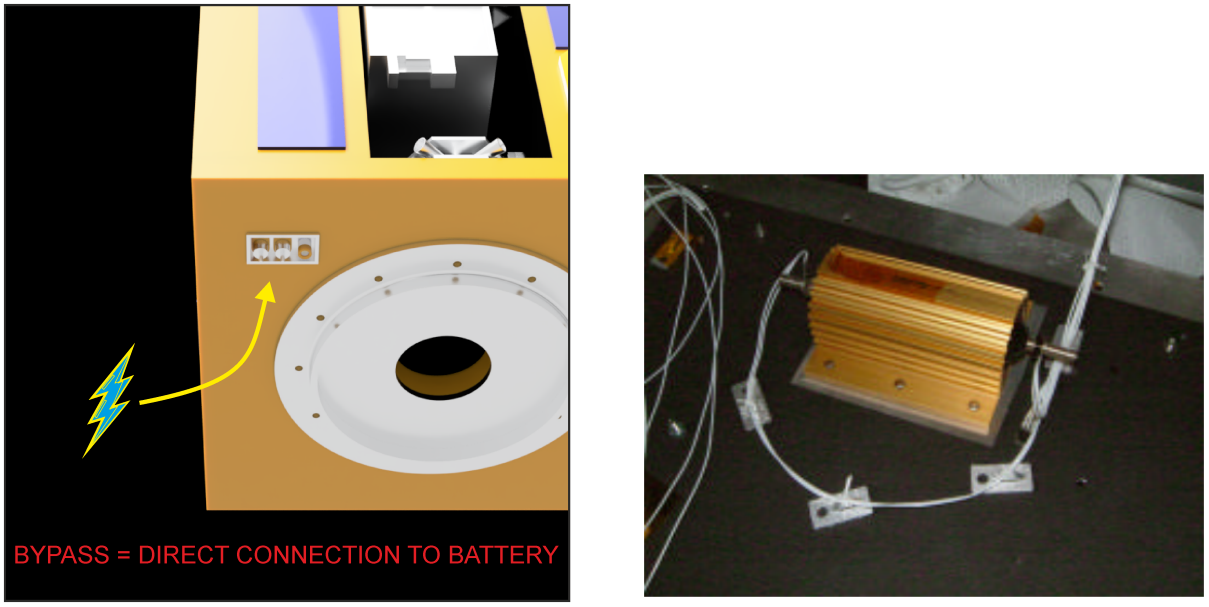

(a) Battery stud connector on CAD model of SSETI Express

(b) Shunt resistor inside SSETI Express

Figure 6.3: Repair options - relevant components

into the groove, and the non-conductive ceramic blade (in white) severs the electrical connection, re-routing it through the blue and green wires coming out of the back of the wiretap.

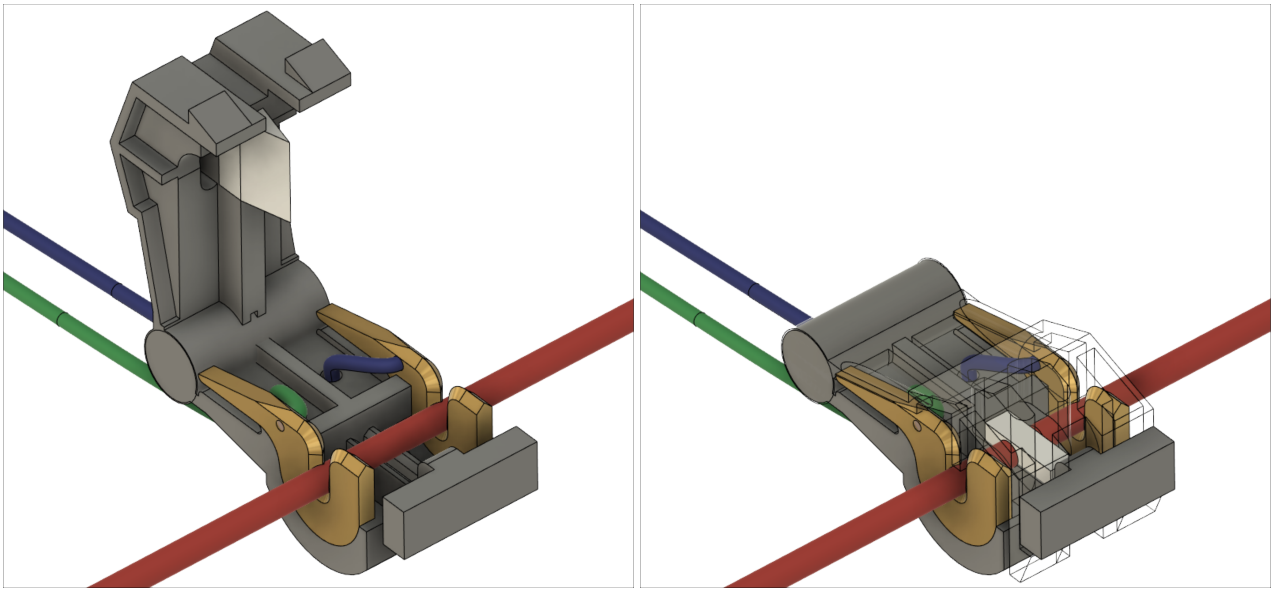

(a) Modified connection intercepting wiretap, open

(b) Modified connection intercepting wiretap, closed

Figure 6.5: CAD model of connection intercepting wiretaps

Unfortunately, such wiretaps are designed to be installed by a human, space for which has not been allocated aboard SERUM. Subsection 6.3.3 will elaborate on how the wiretap will be installed on the shunt resistor's wire.

6.3.2. Piercing Mechanism

In order to install the wiretap on the shunt resistor wire, access to the inside of SSETI Express is required, specifically to the shunt resistor itself, or the EPS box, as these are the two places where the cable is accessible. As the EPS box has many wires running into it, it was deemed easier to tap the right wire close to where it is connected to the shunt resistor. Figure 6.3b shows the shunt resistor inside SSETI Express, with the wires clearly exposed.

In the midterm report two methods of accessing the inside of the spacecraft: thermal drilling and piercing, were traded off. Piercing won the trade-off but it was not certain if it would not generate any debris, so thermal drilling was kept as a backup option. In order to verify that piercing the aluminum honeycomb panel on SSETI Express

would not generate any debris and therefore comply with requirement MIS-002, a test was performed. The details of the test can be found in Chapter 7. The result was positive, with the test honeycomb panel being pierced successfully without generating any debris.

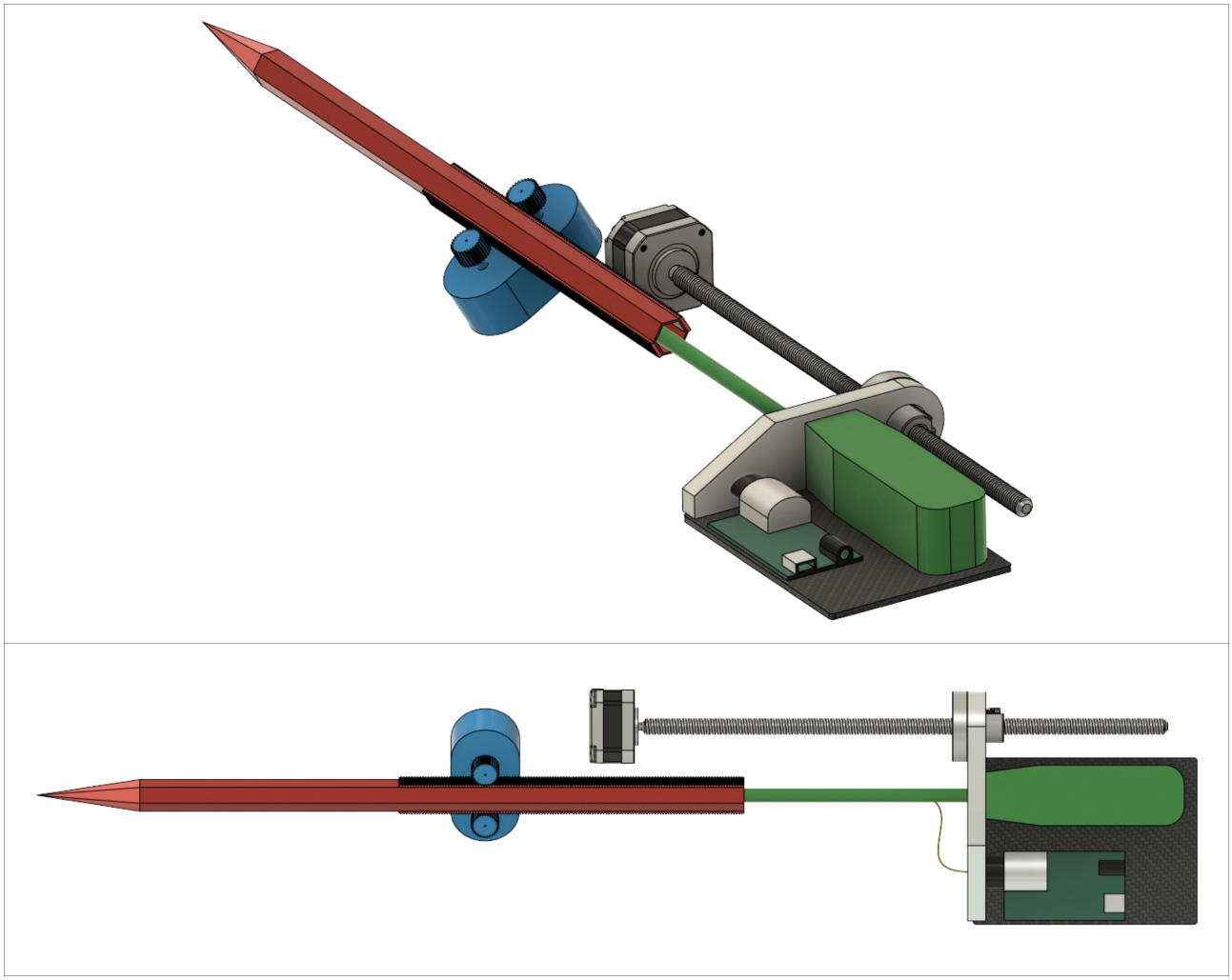

Figure 6.6: CAD model of the piercing mechanism

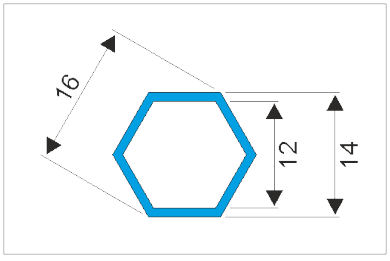

Figure 6.7: Cross section of the piercing tube

The doubts about the piercing solution have been clarified: a slow moving piercing tool can puncture an aluminum honeycomb panel, and it can do so without generating any debris. The test was conducted on a 250 kN press, the dry mass of which was likely not going to fit within the mass budget, so a custom piercing tool had to be designed. Figure 6.6 shows two views of the result. The red component is the piercing tool itself, which consists of a spike, a tube and a gear rack. The shape of the tube is inspired by the piercing tool used to conduct the test, a hexagon with a simple tapered tip. The cross-section of the tube can be seen in Figure 6.7, and will be made out of a material harder than aluminum, as it needs to pierce aluminum panels. The tip of the tube swings open hinged on one of the sides of the hexagon and its cross section is hollow for weight savings, and also to allow an endoscopic arm with endoscopic camera to pass through the center of the tube (Subsection 6.3.3). The motor and gearbox assembly is shown in blue in Figure 6.6 and interfaces with the racks on the sides of the tube to force it forwards through the aluminum sandwich panels on SSETI Express. The tube has a length of 350 mm with a maximum stroke of 150 mm and a tip length of 60 mm.

6.3.3. Endoscope

In order to install the wiretap on the shunt resistor wire inside SSETI Express an endoscopic arm will be used. This solution was chosen because endoscopic arms require only very small access holes and have the entire mechanism attached to the manipulator through a thin tube. As endoscopic arms are very complex mechanisms, it was decided to use one developed by another research team. The paper titled ”Design of a Novel

4-DOF Wrist-Type Surgical Instrument With Enhanced Rigidity and Dexterity" [14] by Man Bok Hong and Yung-Ho Jo was used as an example of the required capabilities. Some modifications were made to the effector to suit SERUM's mission.

The endoscopic arm consists of a box with the control electronics and actuators (4 motors, one per DoF) and a long 8 mm diameter tube connected to the manipulator on the other end. Figure 6.8a shows the complete setup and close ups of the manipulator and actuator box. A custom manipulator will be used aboard SERUM, but the one developed by [14] is shown in Figure 6.8b and it's motion range is visible in Figure 6.8c.

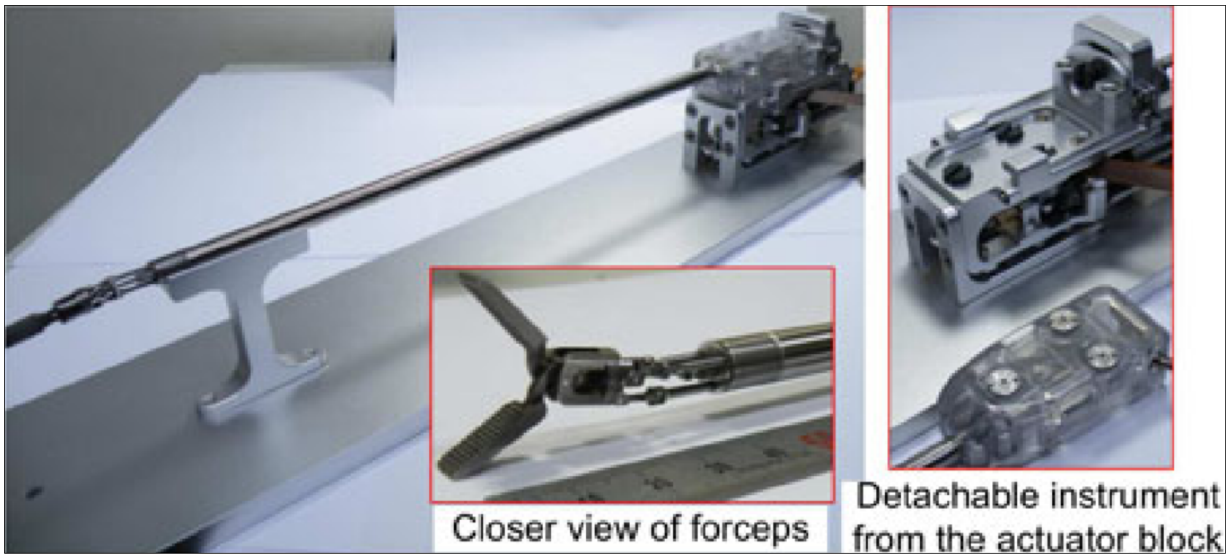

(a) View of the entire endoscopic arm

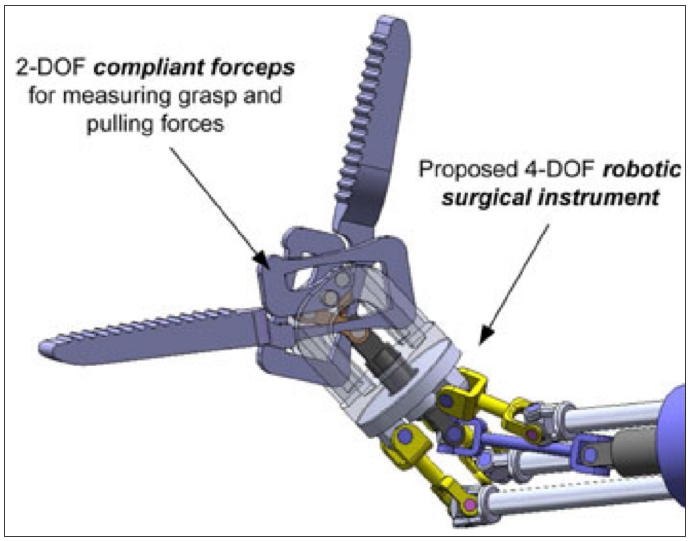

(b) Manipulator of the endoscopic arm

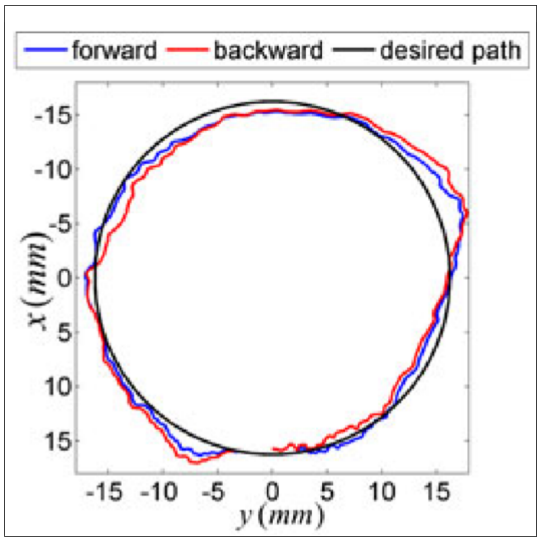

(c) Range of the manipulator, x-y plane

Figure 6.8: Endoscopic arm showcase [14]

6.3.4. 4-DOF Endoscopic Wiretap

For SERUM's mission, everything except the grabbing manipulator will be used. The manipulator will be replaced by the wiretap described in Subsection 6.3.1. The DOF that was previously used to actuate the gripper will be used to open and close the wiretap. Figure 6.9 shows a close up of the wiretap discussed in Subsection 6.3.1 connected to the endoscope covered in Subsection 6.3.3. The complex joint of the endoscope which was shown in Figure 6.8b has been simplified to a ball in all the following figures.

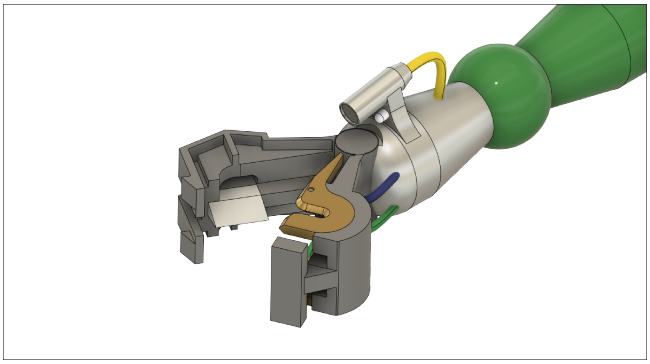

Figure 6.9: Close up of wiretap integrated into endoscopic arm

The green shaft is the tube connecting to the endoscope's actuator box. A small silver camera (ScoutCam) with a yellow wire represents a commercially available endoscopic camera[3] made by a company that produces other space rated cameras. It overlooks the previously presented wiretap. The entire mechanism is small enough to fit inside the piercing tube. Figure 6.10 shows a sequence of figures that illustrate the working principle of the mechanism. First, SSETI Express is pierced with the piercing tool. Once the piercing tool has extended the predetermined distance, the cap will swing open inside the spacecraft, and the endoscopic wiretap assembly will emerge from inside the tube thanks to the independently mobile sled discussed in Subsection 6.3.5. Based on pictures of SSETI Express (Stefano Speretta, interpersonal communication, May, 2023), the opening maneuver of the cap will be possible and will not interfere with any of the components around it. Small lights built into the camera (shown as separate LED's in Figure 6.9) then activate, the wiretap opens and the 3 DOF joint begins to move as the wire of the shunt resistor is located. When the wire has been found, the wiretap is moved into position and closed around the wire, severing the electrical connection and re-routing the connection through SERUM.

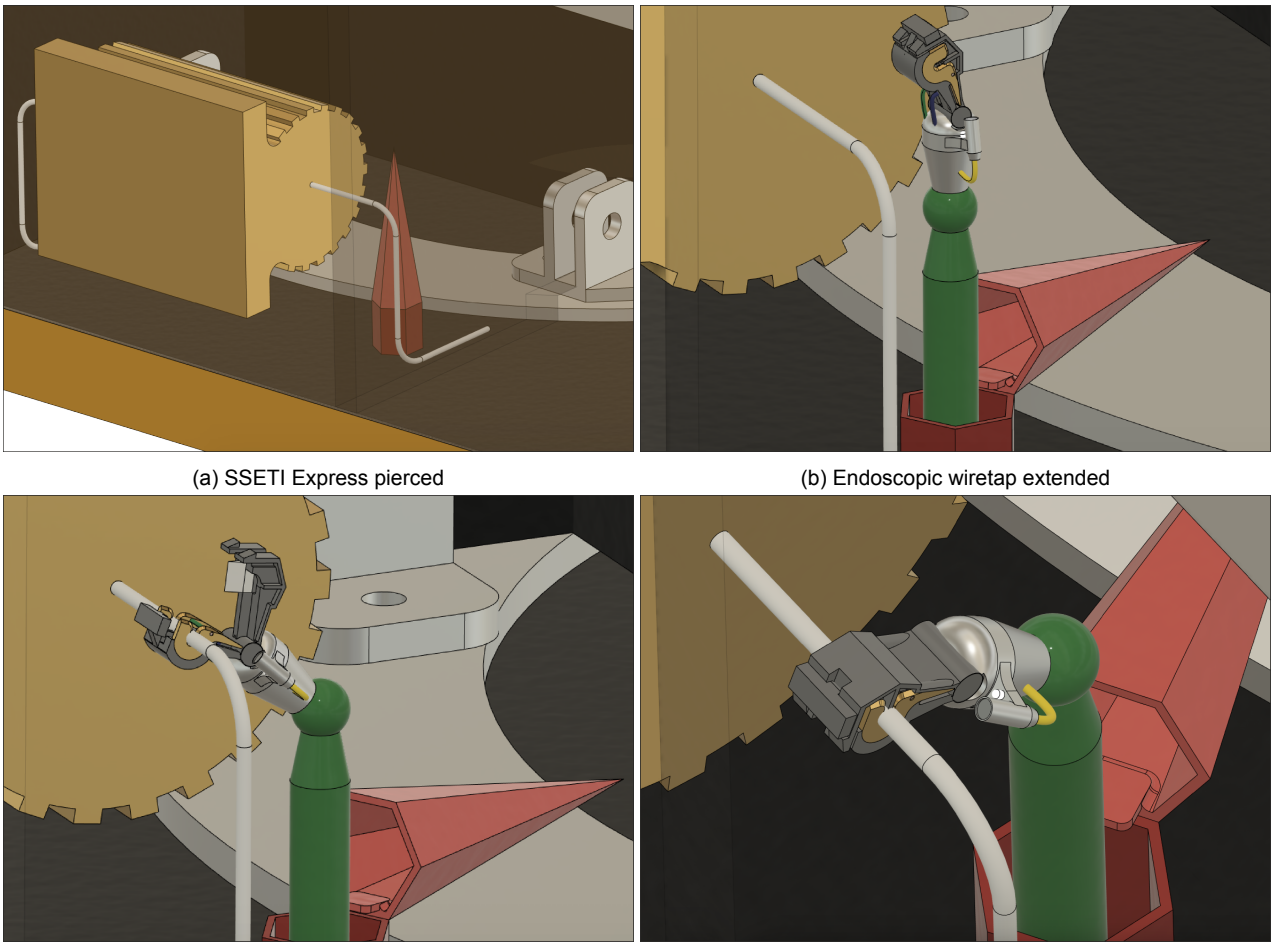

(a) SSETI Express pierced

(b) Endoscopic wiretap extended

(c) Endoscopic wiretap locating wire

(d) Endoscopic wiretap closed on wire

Figure 6.10: The figures show the process of locating the shunt resistor wire with the endoscope and attaching the endoscopic wiretap to it in order to route the connection through SERUM. Some of SSETI Express' panels have been made translucent for better visibility of the operation.

6.3.5. Mounting Sled

The endoscopic arm base and endoscopic camera control board are both mounted to an independently moving base, which is shown in black in Figure 6.6. It is actuated with a ball screw driven by an electric motor for high precision, as the position of the sled directly determines the position of the endoscopic arm tip in that axis (the endoscopic arm cannot extend / retract). The motor is located next to the piercing tube extension motor for convenient wiring.

6.3.6. Voltage Regulator Design

Assuming a linear power regulation system, some aspects need to be taken into account regarding the design of this voltage regulator. As the electrical load of SSETI Express is constantly varying, the duty cycle of the

[3] https://www.odysight.ai/wp-content/uploads/2022/03/ScoutCam-Starter-Kit-brochure-for-web-FINAL.pdf

regulator will have to be adjusted actively depending on the voltage of the bus. To achieve this, an op-amp circuit, similar to the original in SSETI Express' EPS, is proposed, visible in Figure 6.11. The intercepted line that connects to the main bus is compared to a set reference voltage, such that power is dissipated until the main bus stabilizes at $28.8\,\mathrm{V}$.
For this method to function, a common ground connection between the two satellites is required as well, which is achieved through the battery stud connector described in Section 6.2, which connects to the grounded structure of SSETI Express.

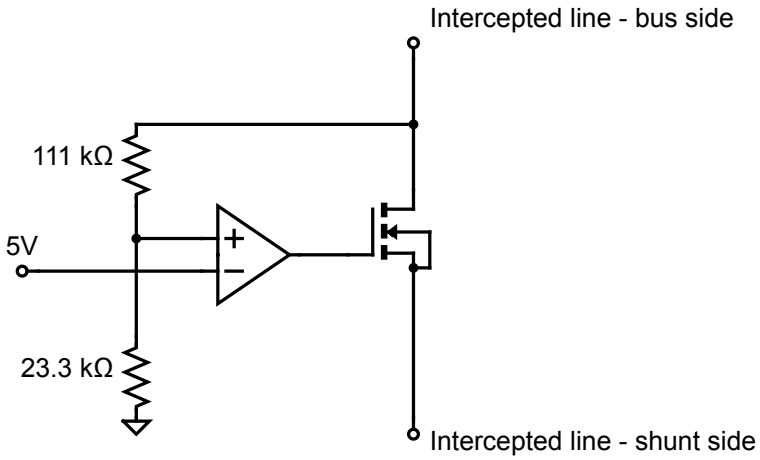

Figure 6.11: External voltage regulator circuit

6.4. Operations

The entire procedure will be performed by a ground-based operator. The piercing process is fairly autonomous, as the tool needs to slowly travel a fixed, predetermined distance. Locating the wire is the operator's primary task, for which they will use a live feed from the ScoutCam. The camera's resolution is 400x400 pixels, with a color image. A simulated view from the camera can be seen in Figure 6.12. The white column is the shunt resistor wire, the gold is a blade for cutting into the wire and the pinkish wedge is the ceramic knife to sever the wire. Most of the interior panels on SSETI Express are painted black for thermal regulation purposes, making navigation difficult. The pre-planned entrance point for the device is however very close to the shunt resistor which is a brass color, so it should be fairly easy to locate simply by swiveling the camera around. A flow chart of the full repair operation, including both repair strategies, can be found in Figure 6.13.

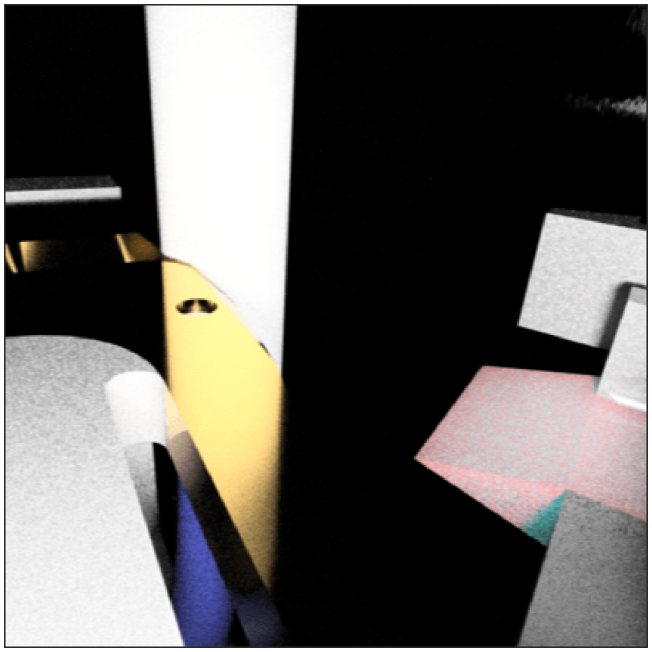

Figure 6.12: Simulated view from the ScoutCam

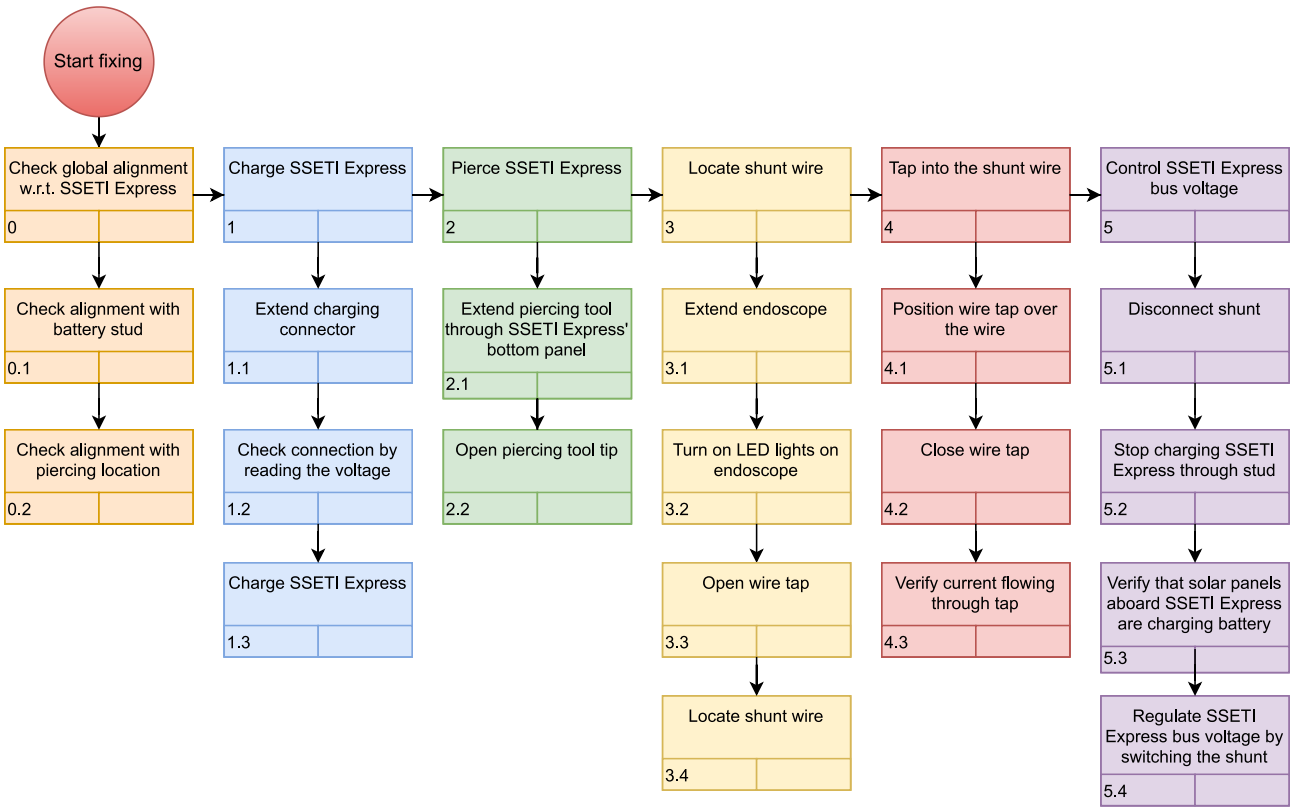

Figure 6.13: Flow chart of repair operations

6.5. Confirmation

Once the proposed fixes have been implemented their efficacy needs to be verified. This will be done with the following means:

- Monitoring voltage on battery stud
- Monitoring current flowing through wiretap
- Monitoring SSETI Express' outgoing communication signals

Monitoring the voltage on the battery stud is very simple, a voltmeter will be included aboard SERUM for this purpose. It should be noted that SSETI Express cannot be charged and monitored at the same time. The expected outcome is that initially the voltage is below $14\,\mathrm{V}$, since the spacecraft is currently unresponsive (Chapter 3). After charging through the stud, the voltage is expected to increase, eventually reaching the nominal battery voltage of $24\,\mathrm{V}$.

Once the wiretap has intercepted the wire leading to the shunt resistor, the current flowing through the shunt can be monitored. The shunt should be discharging all of the current generated by the solar panels on SSETI Express if it is installed correctly. When the shunt is disconnected, no current will flow, as it will be redirected to the rest of the spacecraft bus to, amongst others, charge the battery. Once the bus voltage reaches nominal, the shunt can be used to perform its intended function - regulating SSETI Express' bus voltage. The shunt can be connected and disconnected by SERUM in order to discharge excess power from the solar panels.

SERUM uses different communication bands than SSETI Express (Chapter 9) due to the interference this would cause when SSETI Express is brought back online. In order to check if SSETI Express is functioning as intended, the original ground station will be informed that SSETI Express has been fixed and should be transmitting. It is geographically close to SERUM's ground station as it is located in Alborg, Denmark. This avoids the weight of an additional antenna aboard SERUM.

6.6. Budgets

This section covers the mass, power and cost budgets of the whole repair subsystem, including the bypass, piercing and other components, such as LED and camera.

6.6.1. Mass

The mass budget of the repair subsystem is presented in Table 6.1. As the majority of the components are custom-design, the estimation method to determine their mass is applying the correct materials in CAD, and matching their volumetric dimensions to the reference parts (e.g. endoscope and its control box).

Table 6.1: Mass estimation of the repair subsystem

Item	Mass (kg)	(Estimation) Method
Bypass mechanism	0.3	CAD
Global LED	0.278	Datasheet[4]
Global Camera	0.04	Datasheet[5]
Pierce & Fixing mechanism	1.8	CAD
Tube	-	CAD
1.8 mm Camera	-	CAD
Endoscopic arm	-	CAD
Wiretap connector	-	CAD
Mounting sled	-	CAD
	2.418	Various

6.6.2. Power

The power budgets are presented in Table 6.2. The two notable phases of power consumption are Sleep & bypass and Repair. While the bypassing phase uses the most energy, as it directly supplies SSETI Express with 20 W for 3-months, the most intensive action is piercing.

From the piercing demonstration, covered in Chapter 7, it was concluded, that a total of 50 W h or 179 950 J of energy is needed to make a hole in the aluminum honeycomb sandwich panel. However, this energy value does not account for the losses of the piercing instrument itself. The chosen linear actuator type uses a rack and pinion system that achieves efficiencies of over 90%, whereas the brushless DC motors driving it averages 80% - 90%[6]. The system as a whole will have an efficiency of approximately 76.5%. Integrating the worst case force graph (Figure 7.4a) yields 50 W h of energy required to pierce. Therefore, adjusted for the inefficiencies of the instrument, the total required energy becomes 65 W h or 234 000 J. As energy equals time multiplied by power, one of these variables can be chosen freely for the sizing of the instrument. In the conducted tests (Chapter 7), piercing took 135 s at an average (theoretical, not accounting for mechanism efficiency) power of 1740 W. However this is not possible for a spacecraft the size of SERUM, so it was decided that 130 W of power would not affect the sizing of the EPS, while also giving a reasonable time of 30 min for the piercing tool to travel through the bottom panel of SSETI Express.

Table 6.2: Power estimation of the repair subsystem

Item	Power (W)	Time	Energy (Wh)	Phase
Bypass connector alignment	1.5	10 min	0.3	Initiate bypass
Global LED	4.3	10 min	0.7	Initiate bypass
Global Camera	0.3	10 min	0.1	Initiate bypass
Bypass (powering SSETI Express)	20	3 months	43830	Sleep and bypass
Piercing	130	30 min	65	Repair
Endoscope (attaching wiretap connector)	48	10 min	8	Repair

Note that if the bypass method does not work, the repair phase will start sooner than after three months. If the

[2] https://thermdrill.com/wp-content/download/guidebook.pdf
[3] https://www.amazon.com/Install-Bay-3MBTT-T-Tap-Connector/dp/B001JT72D4
[4] https://www.sierraspace.com/spaceflight-hardware-catalog/
[5] https://www.skyfoxlabs.com/pdf/piCAM_Datasheet_rev_B.pdf
[6] https://www.telcointercon.com/article/bldc-motor

bypass method does work, the repair phase will start after three months and will be performed for the sake of technology demonstration.

6.6.3. Cost

As in Section 5.6 the prices of custom-built components are determined using the ratio between development cost and mass of the Canadarm[10]. It is important to note that the fine nature of the components of the repair subsystem might cause development cost per kilogram to be higher than what was found for Canadarm. This is an uncertainty that will have to be accepted in this stage of design.

Table 6.3: Cost estimation of the repair subsystem

Item	Cost (MEUR)	(Estimation) Method
Global Camera	0.0033	Datasheet[7]
Rest of the Repair payload	1.9072	Cost-Mass relation (Canadarm)
	1.9104	Various

6.7. Conclusion

In order to repair SSETI Express, first the bypass strategy will be executed: using SERUM to power SSETI Express through the pre-launch connector, bypassing the faulty part of the circuit. It will be executed using the designed stud connector (see Figure 6.15a) and for the connection maneuver a camera and force sensor will be used. If this does not work, the shunt cutting strategy will be executed: intercepting the shunt resistor connection and diverting the connection through SERUM, which will be able to switch the shunt resistor in and out of the circuit. For the shunt cutting strategy, a piercing tool will be used (see Figure 6.15c) to pierce through the bottom panel. Once inside, the tool will open up and reveal the endoscope which will use a camera and LED (see Figure 6.15b) to search for the wire to be intercepted. The endoscopic wiretap will then close on the wire and from that moment a MOSFET on SERUM will switch the shunt resistor in and out of the circuit. If the bypass strategy does work, SSETI Express will operate for three months (the operational lifetime it was originally designed for). After that, the shunt cutting strategy will be executed as a technology demonstrator. To check if SSETI Express has been fixed, the voltage on the battery stud, the current flowing through the wiretap and SSETI Express' outgoing communication signals will be monitored. The repair subsystem integrated in SERUM is shown in Figure 6.14.

[7] https://www.skyfoxlabs.com/pdf/piCAM_Datasheet_rev_B.pdf

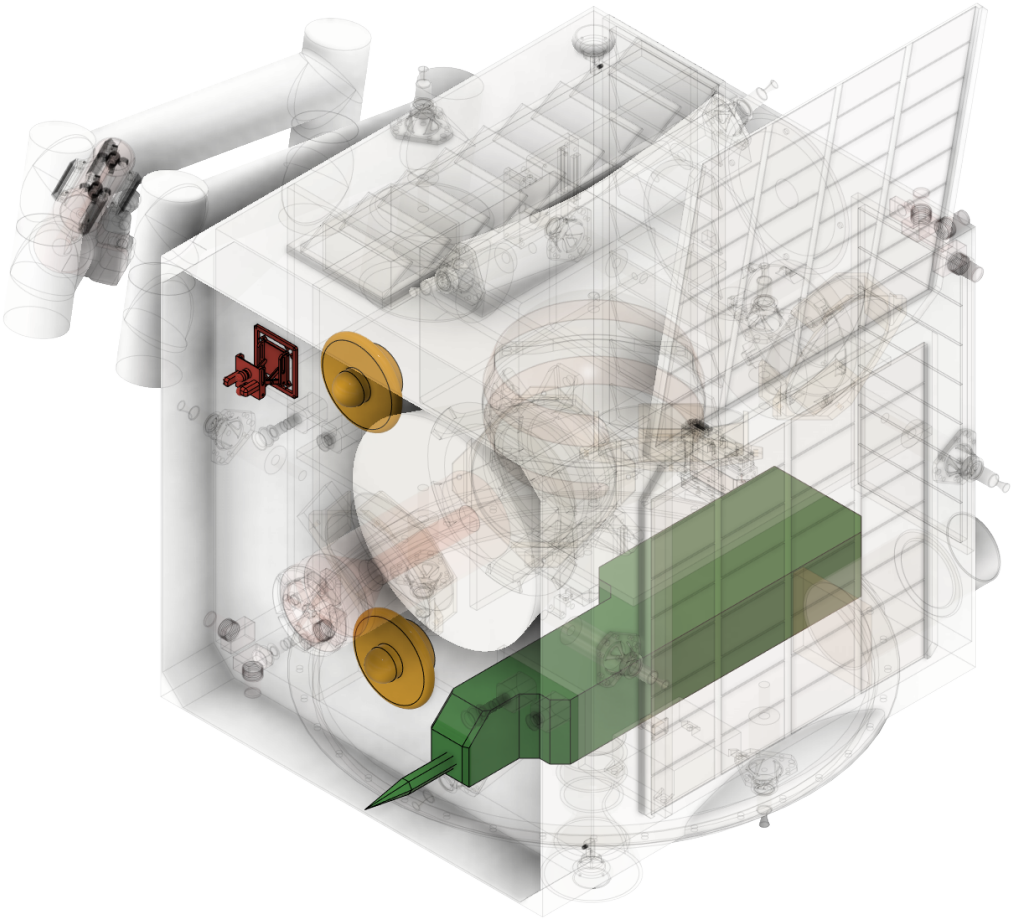

Figure 6.14: The repair subsystem integrated in SERUM

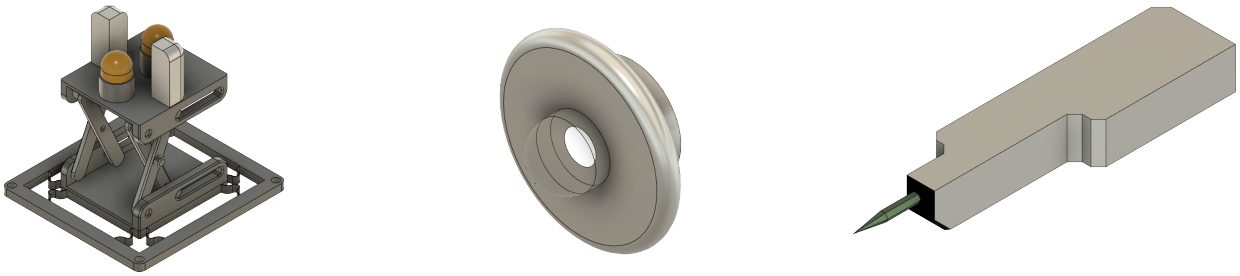

(a) The pre-launch charging connector (b) The global LED (c) The piercing & shunt intercepting tool

Figure 6.15: Components of the repair subsystem

7 Piercing Demonstration

During the trade-off phase of selecting repair instruments, it was determined that piercing and friction drilling methods could be suitable options. It was decided that if feasible, a test would be conducted. However, due to the higher complexity associated with the friction drilling method, the idea of testing it was discarded. On the other hand, piercing appeared to be a viable option. As a result, after engaging with various university staff members and acquiring the necessary materials, a penetration test was carried out.

7.1. Introduction

The piercing test had two main objectives: firstly, to explore the hypothesis that a slow, sharp instrument could penetrate aluminum without generating detached material or debris, considering aluminum's plasticity. As debris generation during any stage of the mission would violate a mission requirement (MIS-002), this is of utmost importance. Secondly, quantifying the required force for piercing through aluminum sheets proved challenging, as existing research primarily focuses on high-speed impacts or blanking/shearing operations, which differ from piercing operations.

The composition of SSETI Express' bottom panel is illustrated in Figure 7.1. While it differs from the manufactured panel described in the subsequent section due to material availability and time constraints, the skin thicknesses are comparable. Furthermore, the honeycomb structure, squeezed to the sides by the piercing tool, offers minimal resistance. Hence, it is considered that the test would be representative of piercing SSETI Express' panel, particularly at the early stage of mission design as outlined in this report.

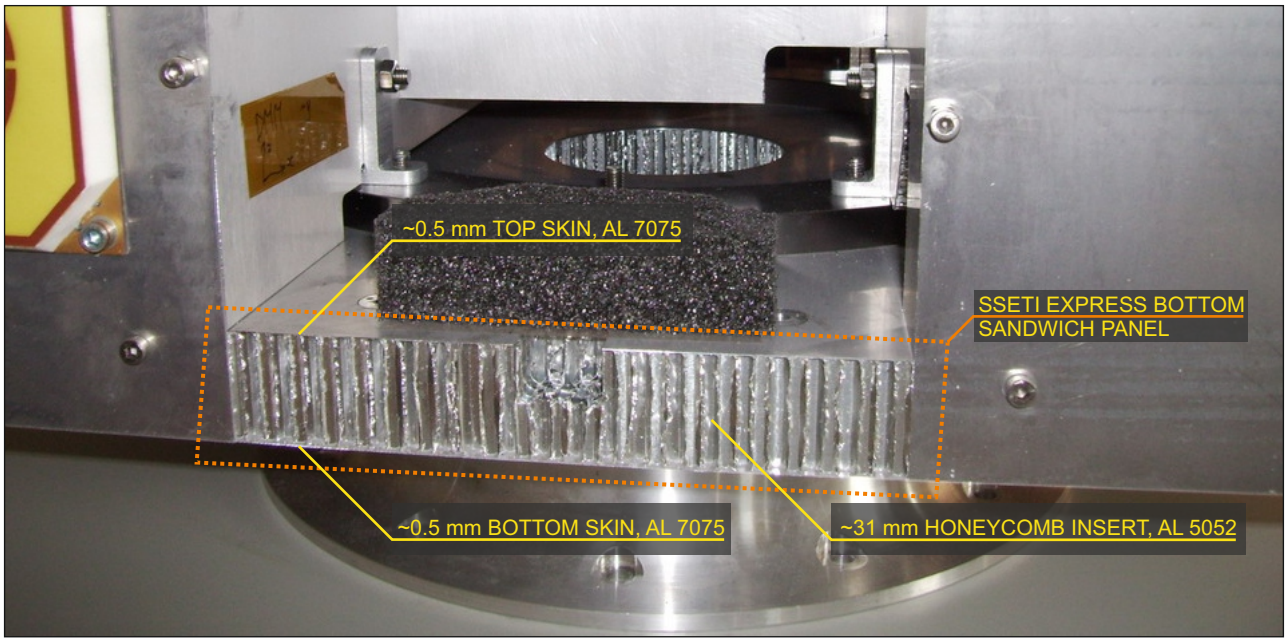

Figure 7.1: SSETI Express' panel to be pierced through (Stefano Speretta, interpersonal communication, May, 2023)

7.2. Manufacturing an Aluminum Honeycomb Panel

Obtaining an entire panel was quickly determined to be unfeasible. Nevertheless, it was possible to acquire the individual materials required for manufacturing one. As a result, this section focuses on detailing the process of creating the panel, presented in Figure 7.2.

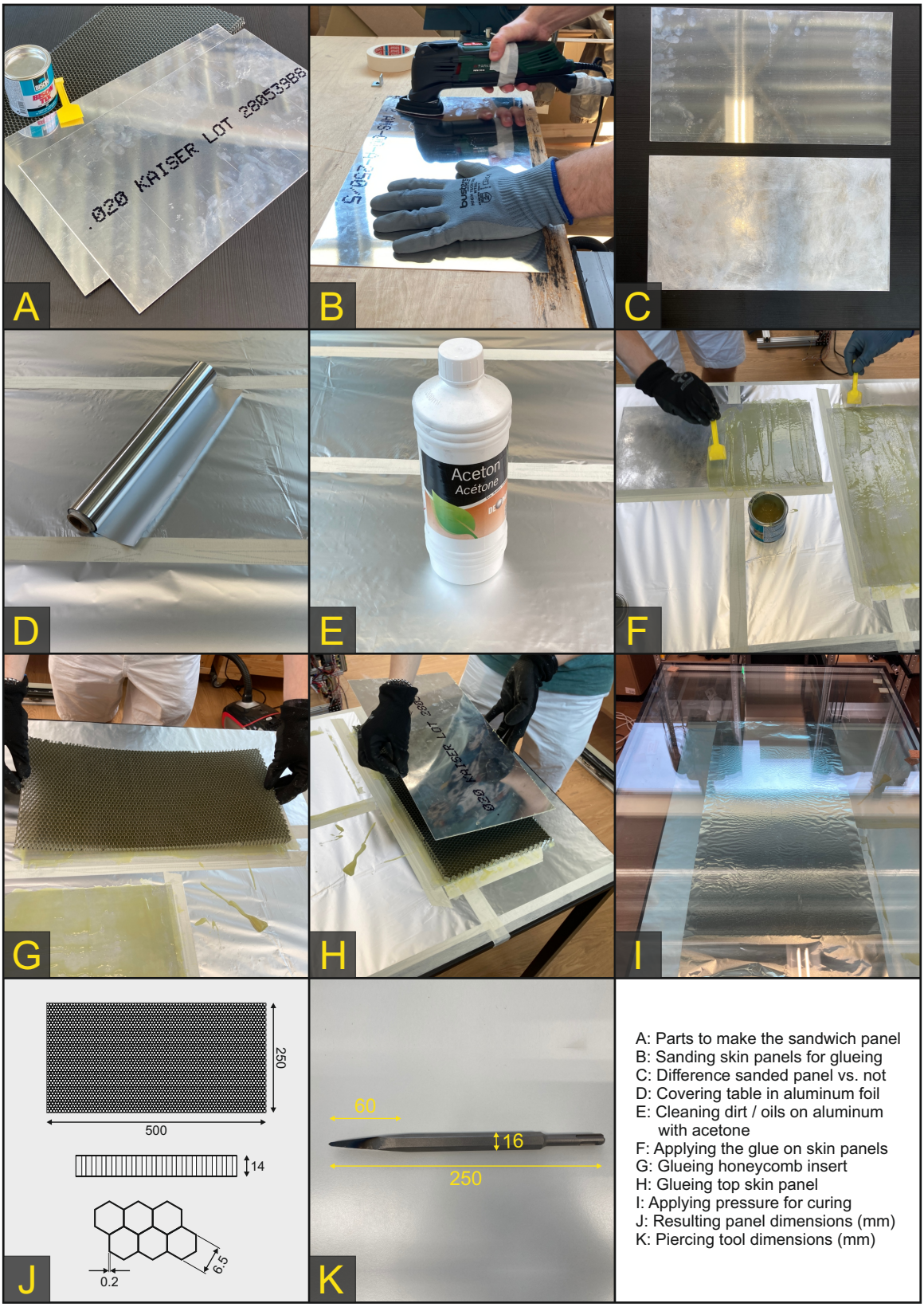

Figure 7.2: Aluminum honeycomb panel manufacturing process

First, in part 'A' the separate parts are visible. The glue used was 'BISON TIX'[1], which in hindsight proved to be a poor choice in terms of shear strength. However, since the bending stiffness was not of a huge importance for the test, the results are usable. The aluminum skins used were 0.5 mm thick aluminum sheets (ams-qq-a-250/5[2]). The specific aluminum alloy type of the 13 mm aluminum honeycomb insert is unknown. In the

[1] https://www.bison.net/en/product.1505375

[2] https://www.smithmetal.com/ams-qqa-250-5-2024.htm

subsequent steps, part 'B' and 'C' demonstrate the sanding process carried out to roughen the surface of the sheets for better adhesion during gluing. Part 'D' shows the table covered with aluminum foil as a protective measure. To ensure optimal bonding strength, all aluminum pieces were cleaned with acetone, as depicted in part 'E'. The application of glue and the assembly of the parts is illustrated in parts 'F', 'G', and 'H'. Approximately 50 kg of glass sheets were placed on top of the panel for overnight curing. Lastly, part 'J' and 'K' display the resulting dimensions of the panel and the piercing tool, respectively.

7.3. Performing the Test

The test was performed in Delft Aerospace Structures and Materials Laboratory under the supervision of a Mechanical Testing Lab technician. Figure 7.3 presents various aspects of the test.

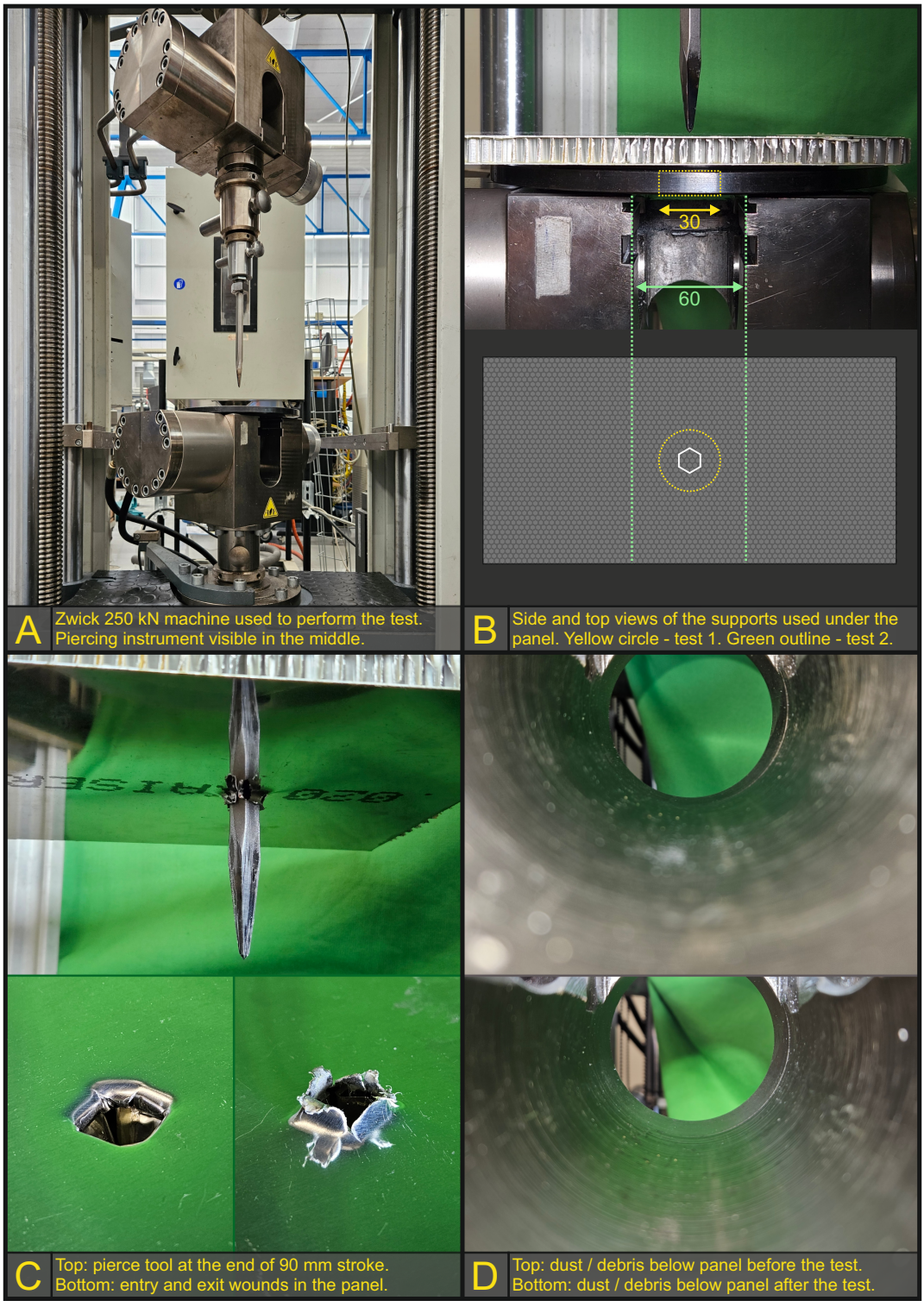

Figure 7.3: Details of the piercing test

Part 'A' highlights the testing machine utilized for the experiment. To acquire data, the sampling rate was set at 10 Hz. The stroke length was chosen intentionally to be 90 mm, representing the total distance the tool would have to travel in case it were to pierce SSETI Express. The time taken to cover that distance was set to 135 s.

Part 'B' outlines the two distinct types of supports employed beneath the panel. In test 1, the entire bottom of the panel was supported, except for a 30 mm diameter hole through which the piercing tool (indicated by a white outline) would pass. In test 2, the support covered a smaller area beneath the panel, leading to increased bending loads, since the supports were positioned farther from the applied force location.

In part 'C', the tool is depicted at the end of its travel, extending beyond its conical section. The entrance and exit holes demonstrate the cutting and bending of the aluminum without any detached pieces or debris.

Finally, in part 'D', the images illustrate the presence of dust or debris under the test rig before and after the experiment. While the focus may not be consistent between the two images, it is still possible to observe the tracking of dust particles and conclude that no significant debris was generated during the experiment.

7.4. Results and Analysis

Before covering the results of the tests, some general observations can be made:

- The test was performed at a different temperature than SSETI Express's exterior structure might be. This information shall be quantified in later stages of the design, but for this phase, it is deemed too in-depth.
- The aluminum alloys used in the test and on SSETI Express are different, but both high strength aerospace grade alloys, with the skin thicknesses roughly matched.

Figure 7.4 presents the results of the two performed tests.

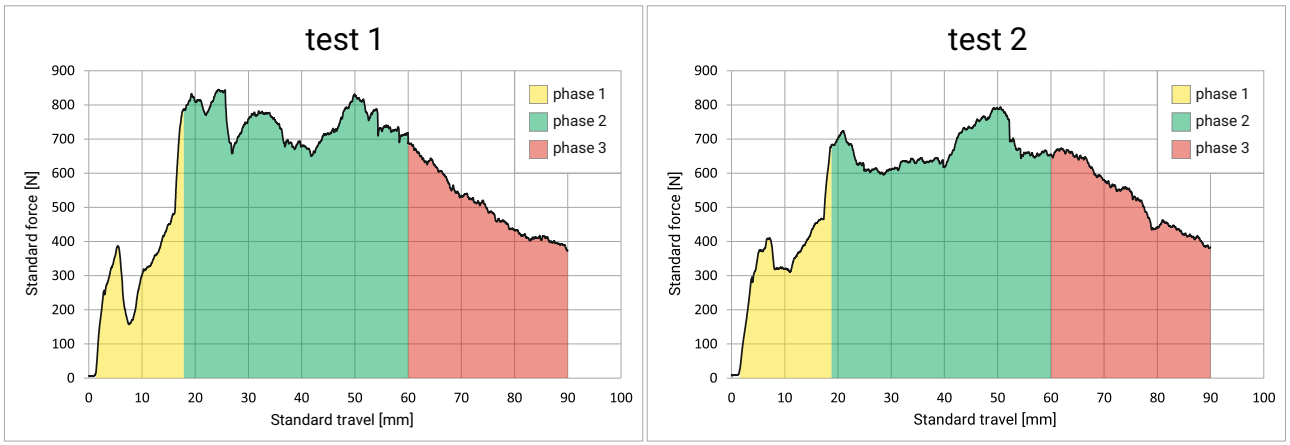

(a) Force versus distance travelled in the first piercing test with greater support

(b) Force versus distance travelled in the second piercing test with lesser support

Figure 7.4: Two tests illustrating the force needed to pierce 90 mm through an aluminum honeycomb sandwich panel presented in Figure 7.2

The analysis of the figures yields the following statements:

- Phase 1 (yellow region) illustrates the rising force phase of the test, where the piercing tool enters the panel through the first skin, travels through the honeycomb insert and pierces through the second skin. The travel of the tool in this phase roughly corresponds to the 14 mm total thickness of the panel.
- Phase 2 (green region) illustrates the relatively constant force phase of the test. This happens during the approx. 60 mm conical section of the tool, where the dominant force is mainly shear from the aluminum around the circumference of the tool being pushed outwards.
- Phase 3 (red region) showcases the declining force after the tool has traveled far enough such that its cross-sectional area does not change through the panel anymore. This is supported by the geometry of the tool presented in picture 'K' in Figure 7.2.
- The area under the graph can be calculated by integration, when units are transformed to SI standard. The resulting value is energy in Joules. For ease of battery sizing in the EPS subsystem (Chapter 13), the energy is converted to Wh (watt-hour).

- The total amount of theoretical energy needed to perform test 1 is $50\,\mathrm{W\,h}$. For test 2 it is $49\,\mathrm{W\,h}$.
- The maximum force in test 1 is $845\,\mathrm{N}$ and $793\,\mathrm{N}$ in test 2.
- The differences in peaks and troughs between the two tests are justified by different supports underneath the panel, see image 'B' in Figure 7.3. Where in test 1 the panel was almost fully supported underneath and experienced little bending, the support in test 2 was much further from the applied force and the panel got visibly bent.
- Aluminum honeycomb sandwich panels are known for their stiffness. However, the glue used in manufacturing the panel in Figure 7.2 was different from the typically used epoxies such as Araldite 420 A/B, due to availability. As a result, the panel had poor bending stiffness. Nevertheless, observing the total energy consumption between the two tests to be practically the same proves that a poor support (of SSETI Express' bottom panel) should not be a problem when piercing through the bottom panel of SSETI Express, especially considering it is well supported by a titanium load spreading ring nearby.

7.5. Conclusion

From the performed tests, it was concluded that piercing the bottom panel of SSETI Express does not generate debris. Additionally, for this stage of mission development, it can be reasonably assumed that the differences in the required piercing force and total energy consumption are minimal between the test panel and the bottom panel of SSETI Express. Of course, for more detailed design phases, a second test should be performed, replicating SSETI Express' bottom panel exactly and matching environmental conditions as well. For now, the values in Table 7.1 will be used as a reference for the design of the repair payload.

Table 7.1: Relevant panel test values

Total energy [J]	**Total energy** [W h]	**Max force** [N]	**Total travel** [mm]	**Debris created?**
179 950	50	845	90	No

8 Payload - End of Life

This chapter will describe the End of Life (EOL) subsystem. This subsystem will make sure that SERUM will de-orbit together with SSETI Express when SSETI Express' operational lifetime is declared to be over. It will also make sure that SERUM de-orbits itself in case of mission failure. Section 8.1 will describe the need for a secondary catching method and explain the chosen method. Section 8.2 will describe the need for a controlled de-orbit and the used method will be designed. Which components to use for the EOL subsystem will be described in Section 8.3 and their architecture will be shown in Section 8.4. Section 8.5 will describe the mass, power and cost budgets.

8.1. Secondary Catching Method

In case docking with SSETI Express is not possible and therefore it cannot be repaired, it is still desired to have it de-orbited within 25 years (MIS-005). To know if it is needed to have a secondary catching method in order to de-orbit SSETI Express quicker than naturally, a simple simulation of its natural de-orbit time was executed in DRAMA-OSCAR. The first step was to calculate the average cross-sectional area of the spacecraft using DRAMA-CROC. The option 'Random tumbling satellite' was used for this, since SSETI Express can be tumbling about an arbitrary axis (SYS-003) so it is not known which side will be in front the most. The next step was to simulate the trajectory of SSETI Express starting at the oldest Two Line Element (TLE) recorded in Space-Track [1], the one from 30-10-2005, which was a few days after launch. The C_d was iterated till the resulted simulated TLE on 02-06-2023 corresponded with the actual known TLE of SSETI Express at that moment[1]. In Figure 8.1 it can be seen that for a drag coefficient of 4.4, the simulated semimajor axis corresponds to the measured one.

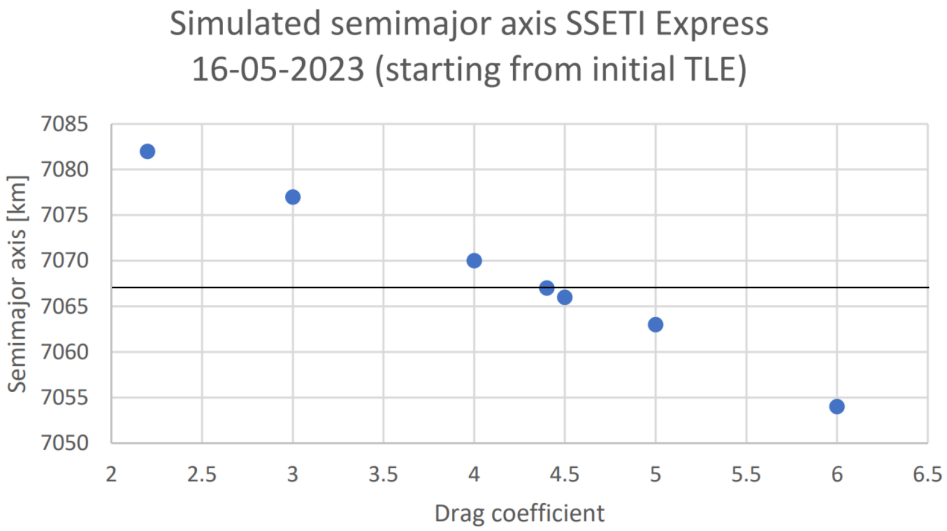

Figure 8.1: Simulated semimajor axis on 16-05-2023 resulting from different drag coefficients of SSETI Express compared to the real semimajor axis on 16-05-2023 according to Space-Track

The found drag coefficient was 4.4. Knowing the average cross-sectional area, the drag coefficient and the old TLE, it was now possible to simulate the natural decay of SSETI Express. For the simulation, 'Solar & Geomagnetic Activity' was chosen with 'Best Case/Worst Case' with a 'Confidence Interval of 95%'. Meaning that for the nominal case, the latest prediction of the solar and geomagnetic activity is used. For the best and worst case, data is used that is 95% higher or lower respectively than the mean cycle values. The resulting natural decay of SSETI Express can be seen in Figure 8.2. The best case values give a very quick de-orbiting time, this is because 95% lower values than the nominal ones is quite a lot and it can be seen that increasing

[1] https://www.space-track.org/#/gp

the solar and geomagnetic activity also has a stronger effect on the decay time than lowering it. However, since a 95% confidence interval is high, it is certain that the upper and lower limits on the de-orbiting time will not be exceeded, resulting in a reliable design.

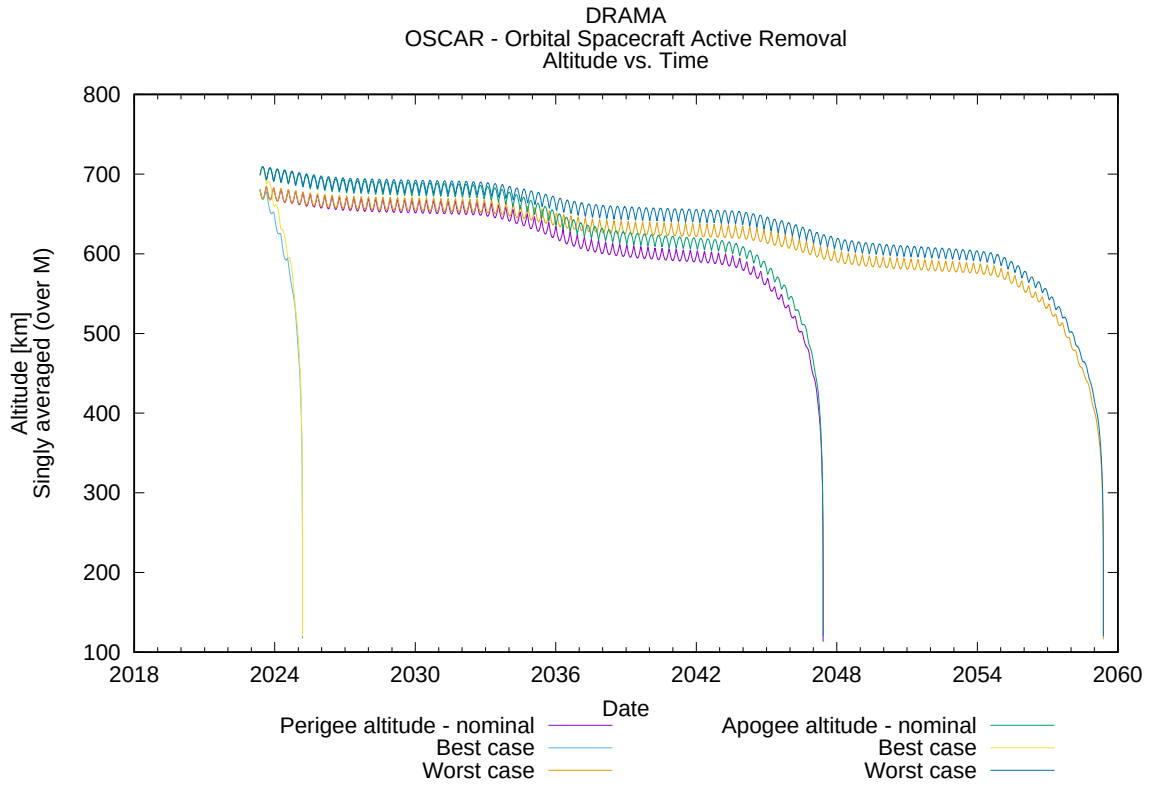

Figure 8.2: DRAMA simulation of SSETI Express' orbit over time

In the quickest scenario, SERUM will arrive in 2029 (as described in Chapter 4) and when it is not possible to dock to SSETI Express the de-orbit window will start immediately, meaning both of the spacecraft should be de-orbited by 2054. Since in the worst case, it can be seen that SSETI Express will not de-orbit within 25 years, a secondary catching method is desired (connecting to SSETI Express without docking to it). This also results in a need for a de-orbit method able to de-orbit the SSETI Express/SERUM combination.

Currently, two methods for catching uncooperative space-debris have been demonstrated in orbit. Those being the use of a harpoon and the use of a net, both of which have been demonstrated successfully with the RemoveDEBRIS program consortium [15]. Since the harpoon technique has a big risk of creating debris (which would not comply to MIS-002), it was decided during the midterm phase that it will not be an option to use it as a secondary catching method. Therefore, the net will be used, which has a low chance of creating debris.

8.2. De-orbiting Subsystem

The de-orbiting subsystem will make sure that SSETI Express and SERUM or, in case of mission failure, only SERUM, will be de-orbited within 25 years.

To know whether a controlled de-orbit is necessary or not, it was first checked if SSETI Express will fully burn-up during re-entry in the atmosphere using DRAMA-SARA. SSETI Express was simulated by creating a 3D model including the dimensions, mass and materials of its main components (such as the side panels, rings, tank, battery, T-pods, etc.). Simulating the final de-orbit stage with this model showed that all components would burn up in the atmosphere except for the titanium rings. This means that a controlled de-orbit will be necessary (independent of whether or not SERUM will fully burn up, which therefore will not be simulated).

In the midterm report, a trade-off was made between the possible de-orbiting subsystems: propulsive de-orbiting, a drag augmentation device and an electrostatic plasma break. This resulted in choosing a drag augmentation device, since it is a lightweight system with a TRL of 8 that can be passive after deployment and could possibly be controllable. Propulsive de-orbiting is almost three times heavier and is an active system, whilst the de-orbiting subsystem should preferably also still function when not all functions of the spacecraft are working anymore since it is an end-of-life system. The electrostatic plasma break was not chosen because it

is not very well controllable, not fully passive and it only has a TRL of 6.

However, later research revealed that controllable drag sails are not yet in a high state of development. Designing a controllable drag sail would be an option, but testing that thoroughly would take up a too big chunk of the budget. Therefore, it is decided to use a combination of a drag sail and propulsive de-orbiting, using the main propulsion system. First, the drag sail will lower the orbit of the spacecraft considerably. At a height of about 140 km (the height from which DRAMA starts handling it as a re-entry maneuver [16]), the propulsion system will do a final burn, assuring the ability to control the location of the impact track. Calculating the amount of fuel needed for a controlled de-orbit from 140 km down to the surface of Earth using DRAMA, results in 2.06 kg propellant needed for the de-orbiting maneuver. It should be noted that this is an upper limit, since drag could also take up a role. The amount of ΔV needed was also calculated by hand, but that number was slightly higher so the one simulated by DRAMA was taken since that is already an upper limit. The orbit can get less precise (and thus needing less ΔV) if an optimization of the re-entry track is done making it enter above less populated areas [17]. The current chosen fuel tank can be extended to support the extra amount of fuel needed for de-orbiting, for the upper limit of propellant needed this would mean that the tank requires 1.7 L more volume and would weigh 77 g more (as described in Section 11.6).

Only using propulsive de-orbiting was decided against, because for that about 10.90 kg of fuel would be needed according to DRAMA-OSCAR (11.3 kg including tank mass) which is about three times as much as the 3.7 kg needed for the propulsive de-orbiting combined with the drag sail mass. Although, in a later stage this option could be worked out to see if enlarging the propellant tank (which probably also means enlarging the dimensions of SERUM) and increasing the mass would outweigh the risks of getting the spacecraft out of sleep mode after 21 years (RI-PAY-25).

8.3. Components Selection

The RemoveDEBRIS consortium proved the use of a net in space [15], which was developed by Airbus Defense and Space. The plan is to buy this design from them, since it is suited for catching a spacecraft with the mass and size of SSETI Express [18]. In the design, there is no component that is not redundant [19], which mitigates the risk of the net not being able to deploy or close (RI-PAY-17 and RI-PAY-19). Figure 8.3 shows an artist impression of net capture technology.

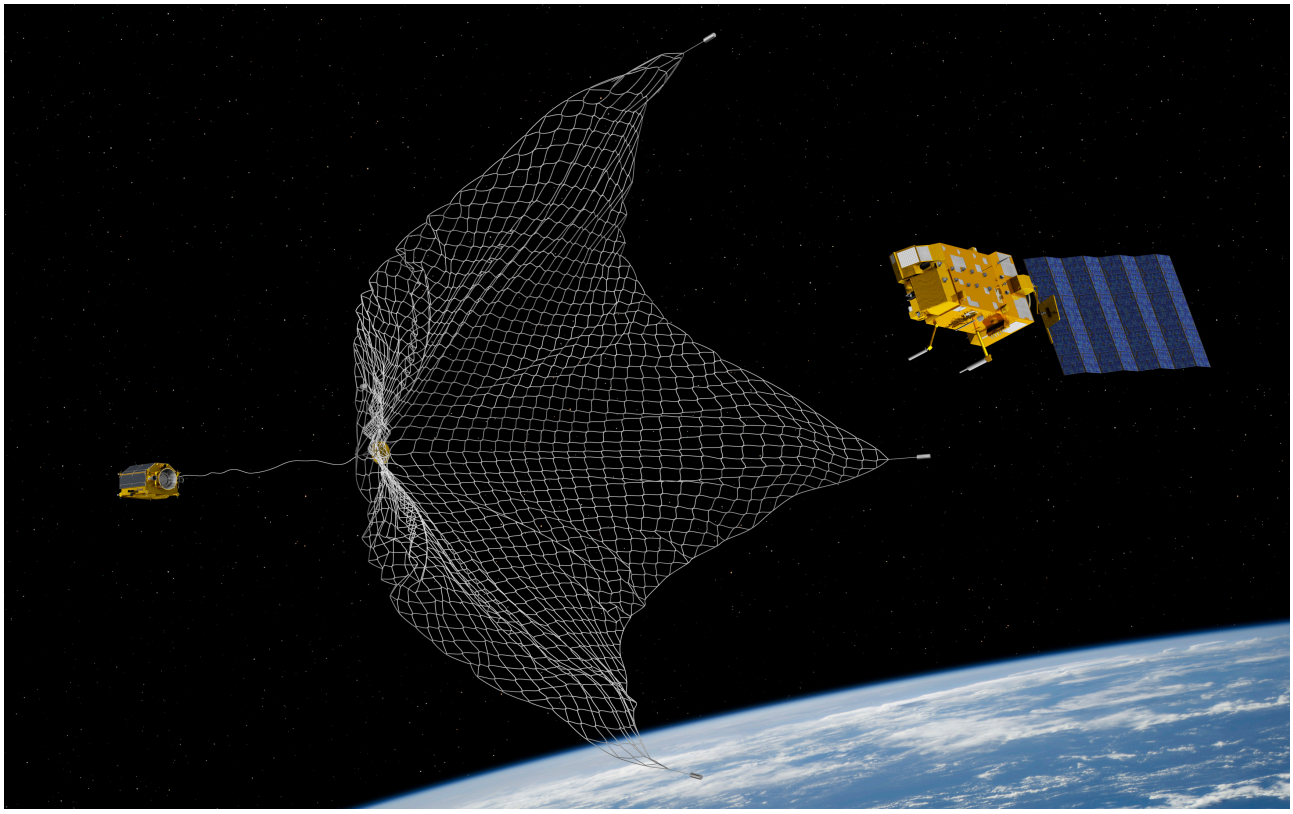

Figure 8.3: Artist impression of a net capture technology[2] (Picture credit: ESA–David Ducros, 2016)

To determine the necessary drag sail size, the worst case de-orbit scenario is used, in which SERUM docks to SSETI Express in 2029 but cannot fix it and thus de-orbites in the same year. In DRAMA-OSCAR, the simulated

TLE of SSETI Express in 2029 is used as the starting position. As an assumption for the drag coefficient of the SERUM/SSETI Express combination, the in Section 8.1 found drag coefficient for SSETI Express is used. The drag coefficient of the drag sail was assumed to be 2.3 [20]. The option 'de-orbit with drag sail' was used and the drag sail area was iterated until the worst case de-orbit time was 25 years. This resulted in a required drag sail area of about $5.5\,\mathrm{m}^2$. An off-the-shelf drag sail from Nakashimada Engineering Works was found with a cross-sectional area of $6\,\mathrm{m}^2$ [3], see Figure 8.4.

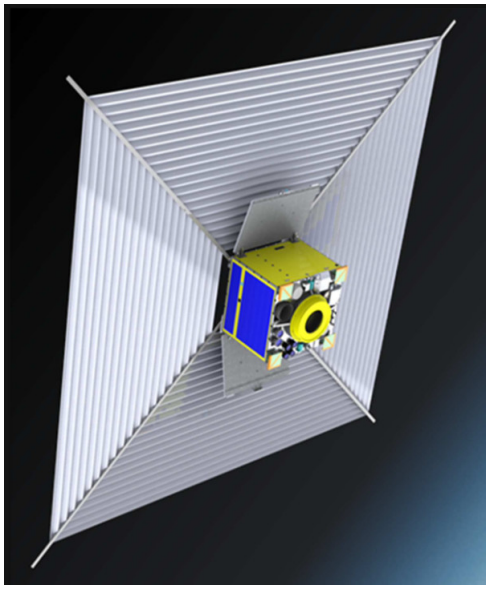

Figure 8.4: The Nakashimada Engineering Works De-Orbit Mechanism (DOM)[4]

Figure 8.5 shows the de-orbit trajectory using the off-the-shelf drag sail, it can be seen that the de-orbit will take 21 years (thus complying to MIS-005). It was required to de-obit within 25 years, which means that there is a 4 year margin which mitigates the risk of the drag sail only partly deploying (RI-PAY-23). Note that the earliest de-orbit time is later than the simulated natural de-orbit time of SSETI Express (see Figure 8.2), which is as expected, since the effect of the drag sail is less than the effect of SERUM docked to SSETI Express being a lot heavier than just SSETI Express on its own.

[3] https://satsearch.co/products/nakashimada-dom-de-orbit-mechanism

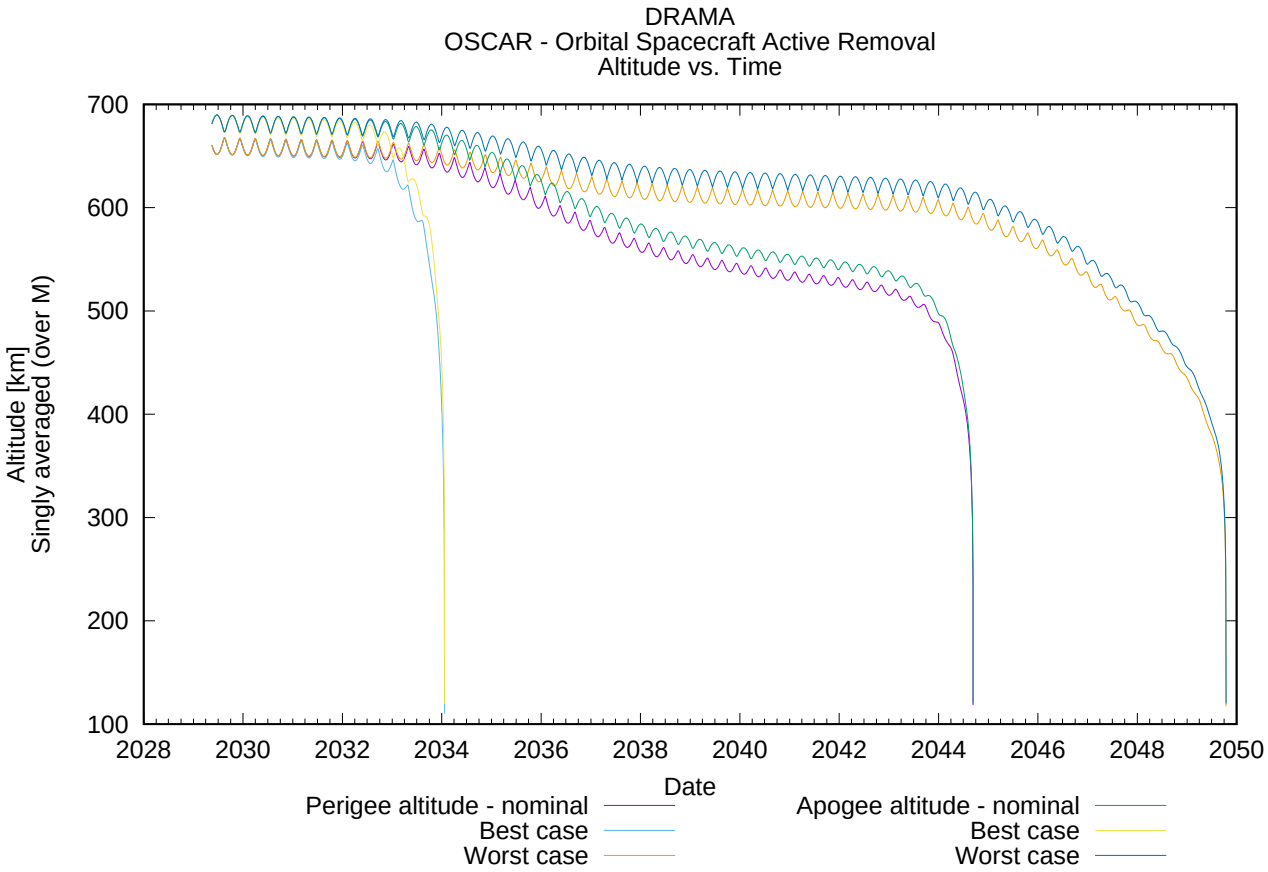

Figure 8.5: DRAMA simulation of the orbit of SERUM docked to SSETI Express using a 6 m^2 drag sail from 2029 onwards

For the final de-orbiting phase, the main propulsion system of SERUM will be used.

8.4. Architecture

The dimensions of the drag sail were found in the data sheet of the chosen drag sail [21] and the dimensions of the net were found in one of the articles written about the RemoveDEBRIS mission [18]. Figure 8.6b shows the stored drag sail and the stored net can be seen in Figure 8.6a. In Figure 8.7 the location of the drag sail, net and main propulsion system in SERUM can be seen.

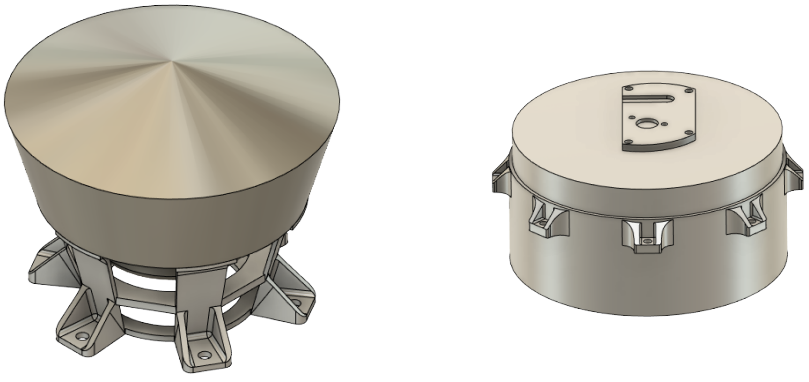

(a) The net in stored position

(b) The drag sail in stored position

Figure 8.6: Components of the EOL subsystem

It can be seen that the net is not placed in the middle of the spacecraft. When the net is deployed, the robotic arm will attach the tether to a hook at the zond (which will be designed in a later phase). This will make sure that the force through the tether acts close to the center line of SERUM. The drag sail is positioned on its own side, which reduces the risk of the drag sail entangling whilst deploying and creating debris (RI-PAY-24).

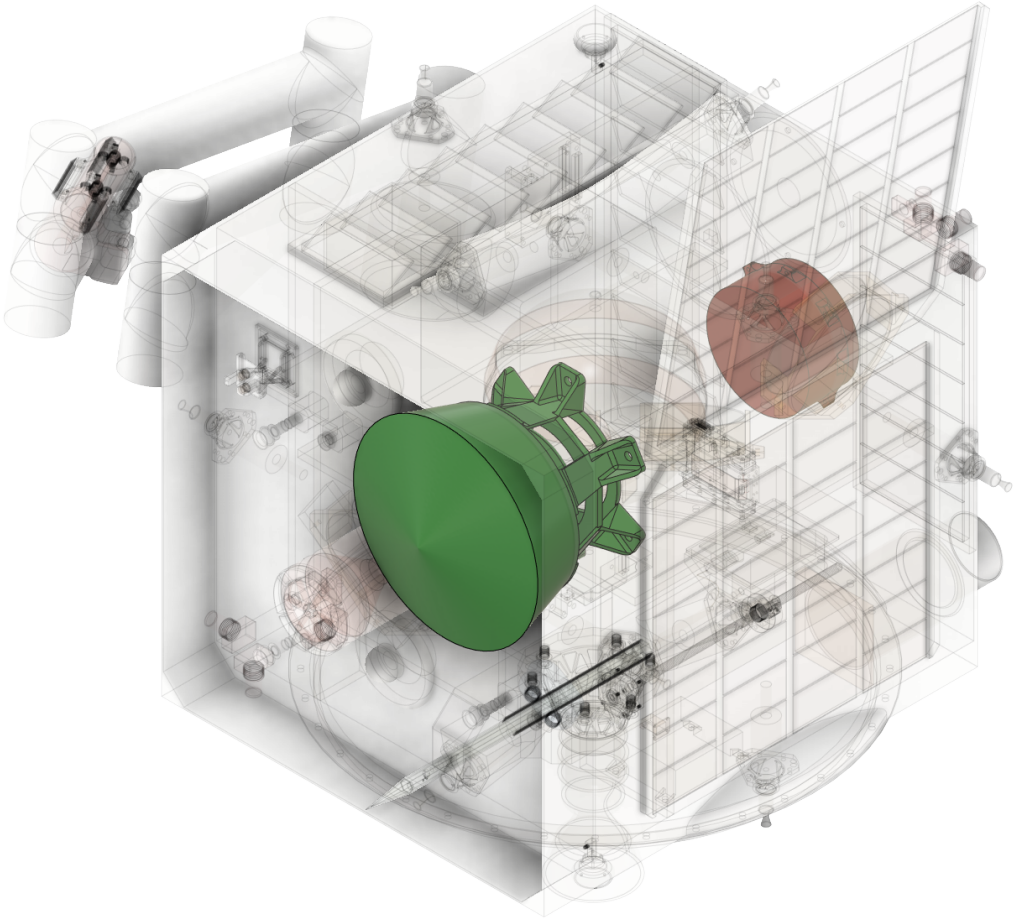

Figure 8.7: The EOL subsystem integrated

8.5. Budgets

This section will describe the mass, power and cost budget of the EOL subsystem.

8.5.1. Mass Budget

Table 8.1 shows the current mass budget of the EOL subsystem. The mass of the targeting system for the net is not included, since the targeting system for docking can be used (as described in Subsection 5.4.1) which is located on the same side of SERUM as is needed for the net. The mass of the maximum required propellant and the tank extension were calculated in Section 8.2, but will be included in the mass budgets of astrodynamics and propulsion.

Table 8.1: Mass budget contribution of the EOL subsystem

Sub-components	**Mass** [kg]
Net	6[22]
Targeting system	0
Drag sail	1.6 [21]
Tank extension	0.092
	7.69

8.5.2. Power Budget

The drag sail only requires 5 W of power for deploying, which will last maximum 120 seconds [21]. The power required for the net is assumed to be the same as for the drag sail, since for both systems the power is used

[3] https://www.esa.int/ESA_Multimedia/Search?SearchText=net&result_type=images

[4] https://satsearch.co/products/nakashimada-dom-de-orbit-mechanism

for deployment. The power of the net is not in the power budget described in Table 13.1 because it happens in another orbit cycle than the drag sail deployment so the power reserved for the drag sail can be interchanged for use for the net. The net also uses power for closing, but that is coming from super-capacitors located in the masses at the end of the net [23] so will not be included in the power budget. After the drag sail is deployed, SERUM will go into sleep mode for 21 years, only its receiver and computer will be on. Once in a while a signal will be send from a ground station to check if SERUM is still alive. At that point, the transmitter will be turned on for sending down telemetry data. When SERUM is approaching the $140\,\text{km}$ altitude, a command will be send to wake it up. After which the propulsion system will be heated for the final burn, which exact moment and direction will be calculated on Earth, using an optimization method to assure a re-entry track with the least chance of causalities.

8.5.3. Cost Budget

The drag sail will cost about $44\,500$ EUR according to contact with SatSearch about the product[5]. The net design will be bought from Airbus Defense and Space. Since it is not known if at the moment of buying it, it will already be in series production by Airbus, it might be more expansive than normal off-the-shelf products. It is assumed that the cost could be four times as high as the cost for the drag sail. Both products are a newly developed product of about the same size and level of difficulty, because series production might not be started yet and because the development process or the needed materials could be more expensive for the net, the estimated price is four times the drag sail price which results in $178\,000$ EUR.

8.6. Conclusion

The EOL subsystem will use a net to be able to catch SSETI Express in case docking is not possible. A drag sail will be used when either SERUM, or SERUM docked to SSETI Express or SERUM connected via a tether to SSETI Express catched by the net needs to be de-orbited. A final burn will be done using the main propulsion system in order to ensure a controlled de-orbit in a non-populated area.

[5] https://satsearch.co/products/nakashimada-dom-de-orbit-mechanism

9 Communications

The communication subsystem is responsible for all communication of SERUM with the groundstation. This is crucial for mission success, as the communication system is the only way to receive information from the groundstation and send the necessary data, images and videostream down.

In Section 9.1 a short overview of the communication system and what is required from it is presented. Then, in Section 9.2 a trade-off (including sensitivity analysis) for the frequency band is performed. After that, a decision on the antenna, modulation and ground station is made. The latter will also include a description of SERUM's overpass time over the chosen ground station and coding scheme chosen. In Section 9.3 a link budget for the chosen frequency bands is shown. After that, in Section 9.4, off-the-shelf components for the communication subsystem are chosen and their integration in SERUM is pictured. In Section 9.5, a mass, power and cost budget for the subsystem are shown. Then, in Section 9.6, a communication flow diagram is presented. Finally, the chapter is concluded in Section 9.7.

9.1. Communication System

From the midterm report, it became clear that to properly design the spacecraft communication system, the spacecraft's lifetime is divided into phases, which necessitate different requirements from the communication system. These are the same phases as defined in Chapter 4.

1. **Pre-deployment**
   No communications necessary.
2. **Deployment from launcher till deployment of spacecraft**
   Being able to do simple communication with Earth.
3. **Travel to SSETI Express**
   Being able to do simple communication with Earth.
4. **Docking to SSETI Express**
   Should be able to communicate continuously during procedure time and send videostream down.
5. **Repair SSETI Express**
   Should be able to have a video connection, but not continuously.
6. **Supporting SSETI Express operations and/or de-orbiting**
   Being able to do simple communication with Earth.

From these requirements it becomes clear that for three phases (phase 2,3 and 6) simple telecommunication is sufficient. To perform this, there will be up- and downlink communication and thus two frequency bands are required, spaced far enough not to interfere with each other. The downlink communication will consist of data collected by the spacecraft, for example telemetry and payload data. When looking at satellites already in LEO, it shows that ± 30 kbps is needed for sending data down [24]. The uplink will require a smaller data rate, as data will have to be send down (which can include images) and only commands will be send up. Again from [24] it can be seen that approximately ± 10 kbps is necessary for sending commands up. However, during phase 4 (docking) and phase 5 (the repair) a videostream has to be transmitted down. As more information must be transferred to the ground station (namely video), wideband communication channels, with greater data capacities, become more attractive. This only requires downlink and thus one frequency band. The video format of DVB-S2 (Digital Video Broadcast by satellite standard version 2), is widely used for video broadcasting [25]. For standard video resolution, a data rate of ± 5 Mbps is required [26]. To accomodate these data rates, S-, UHF-, and X-band are traded off for the 'simple' telecommunication of phases 2,3 and 6, whereas for the video connection (phases 4 and 5) higher frequency bands Ku- and Ka-band are traded off.

9.2. Trade-off

In this section, a trade-off for the frequency band will be performed. This will be done twice, once for phases 2,3,6 and once for phases 4 and 5. After that, a selection on the antenna, modulation scheme and ground station will be made. Next to that, the overpass time over the chosen ground station and the encoding scheme will be discussed.

9.2.1. Frequency Band

Before performing the trade-off, the trade-off criteria and their weights were determined. These criteria and weights will be used for both trade-offs.

- **Bandwidth, 0.3:** A higher bandwidth results in a higher data transfer rate and thus a higher performance[1]. This is important for both the 'normal' telemetry as the spacecraft will have limited time in contact above the ground station and thus a higher data rate makes it possible to transmit and receive more data but also for the video stream, as this requires a relatively high data rate in order to ensure proper functioning. Therefore, bandwidth is given a high weight.
- **Power, 0.3:** The mission has a power budget, which has to be adhered to in order to ensure proper functioning. It is not desired to raise the power requirement for the mission a lot because of one subsystem and thus the power is of high importance, with a high weight.
- **Mass, 0.2:** For the entire mission it is desired to keep the mass low and within the budget defined for the communication subsystem. However, there is some room for margin as the launch vehicle allows higher mass than was found in the first mass budget, therefore the weight is lower.
- **Cost, 0.2:** For the entire mission it is desired to keep the cost low and within the budget defined for the communication subsystem. But compared to mass, power and bandwidth it is deemed less important to ensure proper functioning of the spacecraft. Also for the video stream, as this is only during a short time of the spacecraft operational lifetime. Its weight is therefore lower.

Table 9.1: Trade-off table phase 2,3,6

Criteria / Options	*Bandwidth*	*Power*	*Mass*	*Cost*	*Total score*
Weights	0.3	0.3	0.2	0.2	
UHF-band (300-1000 MHz	Y: Low.	L: Medium power.	Y: Highest mass.	G: Low cost.	3.7
S-band (2-4 GHz)	L: Medium.	G: Low power.	L: Medium mass.	L: Medium cost.	4.3
X-band (8-12 GHz)[2]	G: High.	L: Medium power.	G: Lightest mass.	G: Low cost.	4.7

Phases 2,3,6 For the bandwidth, a higher frequency results in a higher bandwidth. This can be seen in the scoring for bandwidth.

It holds that the higher the frequency of the band, the more prone to interference the signal is. However, since the UHF-band has a smaller frequency spectrum there is a lack of available frequencies on the spectrum, causing interference[3]. Also, X-band provides extremely good rain resilience and as X band satellites typically have at least 4° separation between the satellites, the chances of adjacent satellite interference is also less[2]. For almost all bands (in both Table 9.1 and Table 9.2), it holds that a higher frequency equals a shorter wavelength (as $v = f\lambda$), and these shorter wavelengths can be effectively captured by smaller antennas, making higher frequency bands lighter. At the same time, a higher frequency means more signal attenuation (requiring more power to maintain strength over longer distances) and the smaller antenna means that less power is coming from the signal, which also has to be compensated by increasing transmitted power. This can be seen in the trade-offs, where higher frequency also requires more power. As mentioned before, X-band has exceptional little interference, making the power requirement lower than expected for the higher frequency. For UHF, this power requirement is thus higher than expected, as a result of the higher change of interference.

For the cost, different aspects have to be taken into account. For the equipment, it can be said that a higher frequency range requires more specialized components and technologies and thus increases the cost. For infrastructure, the same as for equipment holds, where the higher frequency requires more precise antennas and in general more specialized equipment, making it again more expensive. It can thus be concluded that the higher the frequency band, the higher the cost. However, for X-band, it has proven cost effective for numerous aspects such as price per MHz, price per Mbps and limited capital cost for related equipment, making X-band score better than expected for its high frequency, on the cost criterion [2].

From Table 9.1, it can be seen that both S- and X-band score high. Since two bands have to be selected for phases 2,3,6 (one for uplink and one for downlink), it is therefore decided to select both S-band and X-band. S-band is selected for uplink and X-band for downlink, as X-band has a higher bandwidth and thus a higher

[1] http://www.aidforum.org/topics/technology-data/ka-vs-ku-band-which-is-the-best-for-satellite-broadband/

[2] http://www.milsatmagazine.com/story.php?number=1530000863

[3] https://blog.iseekplant.com.au/blog/problems-with-uhf-radios#:~:text=UHF%20Radio%20Interference,-If%20you%27ve&text=It%20can%20be%20caused%20by,data%20often%20missing%20its%20target

data rate, which is beneficial as more data is probable to be send down than up. The sensitivity analysis for phases 2,3 and 6 can be seen in Figure 9.1.

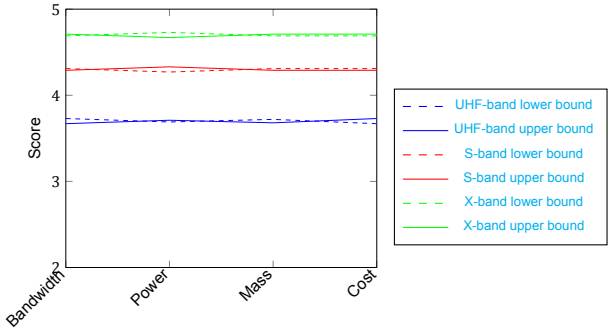

Figure 9.1: Sensitivity analysis for phases 2,3 and 6

Table 9.2: Trade-off table phase 4 and 5

Criteria / Options	*Bandwidth*	*Power*	*Mass*	*Cost* [1]	*Total score*
Weights	0.3	0.3	0.3	0.2	-
Ku-band (12-18 GHz)	Y: Once Ku bandwidth.	G: Lower.	L: Higher.	Y: 800-1400 $/Mbps/-month.	3.8
Ka-band (26.5-40 GHz)	G: Twice Ku bandwidth.	L: Higher.	G: Lower.	G: 250-400 $/Mbps/-month.	4.7

Phases 4 and 5 For the bandwidth, the higher a frequency of a band, the higher the bandwidth. For Ka-band, the bandwidth is double that of the Ku-band [4]. This thus increases the performance, as explained before.

On the other side, the higher the frequency, the more a signal is to interference, making the Ka-band more prone to atmospheric phenomena. This thus results in Ka-band requiring more power to compensate for this loss [5].

The higher frequency of Ka-band results in a shorter wavelength, which requires smaller systems, components and antennas compared to Ku-band [4]. This thus allows smaller, lightweight and often more cost-effective terminals to be operated making a Ka-band system lighter than a Ku-band system [5].

From the trade-off in Table 9.2 it can be concluded that Ka-band is the best option for phases 4 and 5. This is confirmed by a sensitivity analysis, as can be seen in Figure 9.2.

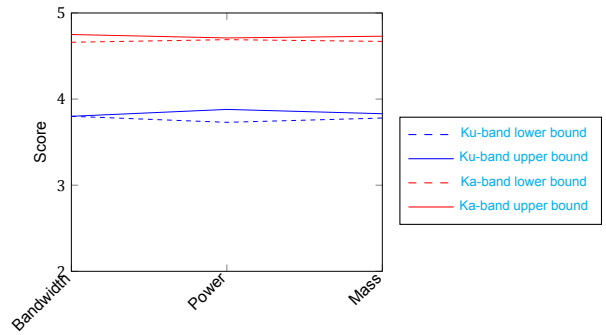

Figure 9.2: Sensitivity analysis for phases 4 and 5

[4] https://resources.pcb.cadence.com/blog/2023-comparing-the-ka-band-vs-the-ku-band
[5] https://www.getsat.com/knowledge-base/ku-band-vs-ka-band/

9.2.2. Antenna

Different types of antennas, with different radiation patterns exist. The most simple one, the isotropic antenna, radiates in all directions equally, also called omnidirectional. Directional antennas concentrate their radiation in patterns (lobes or beams). Ideally, all energy is concentrated into one main beam, but in reality there are often many small side lobes that radiate in unwanted directions. An antenna gain is created if a directional antenna focusses its energy into a smaller solid angle, which means that more of the radiated energy reaches the satellite or ground station [27].

For the different phases and thus different bands differentiated before, different antennas are required. For the X-band, which will send the spacecraft telemetry down, it is important that after deployment, the spacecraft always beeps (with for example an omnidirectional low gain antenna). Since rideshare is used, all launched satellites are relatively close and it is therefore difficult to distinguish SERUM. When switching on the omnidirectonal antenna, once far enough away from the launcher, the ground station will at some point pick up on SERUM, connect and secure link and that way know where SERUM is. Also for the Ka-band, an omnidirectional antenna is required as when docking and repairing, SERUM is either matching its rotating to SSETI Express or is already docked to SSETI Express, which might be spinning in an unknown way and thus no pointing to the ground station can be guaranteed. To ensure that the videostream can always be send down, two Ka-band antennas are included in the design on opposite sides of SERUM, as this guarantees reception of the signal, even the case of extreme rotation. For the receiving S-band antenna, also an omnidirectional antenna is required, as SERUM needs to be able to receive commands at any moment from the groundstation. Both when being launched and when matching SSETI Express' rotation, it is unsure how SERUM will rotate and thus an omnidirectional antenna is required.

9.2.3. Modulation

Modulation is the technique in which the baseband signal is put onto a radio frequency carrier that can be transmitted. This can be done by varying either the carrier's amplitude, frequency or phase in accordance with the signal. Modulation can be done in two ways. The first is analog, in which the carrier wave properties are varied in accordance with change in information signals amplitude, this is easily implementable but prone to variations and noise. The other option is digital, in which a digital string of data is represented by a digital waveform. This can again be done in two ways. The first is with a constant envelope (FSK, PSK), this is preferred for satellite communication as it reduces side-lobe generation. The second is with a non-constant envelope (ASK, QAM). The general advantage of digital modulation over analog is that digital modulation allows compression and error correction coding, which will be discussed later [28].

When comparing the different digital modulation options, PSK is preferred of all digital techniques as it has the best spectral efficiency [28] and lowest probability of error [29]. Within PSK, different modulation schemes excist. Quadrature PSK (QPSK) is the one that is found most in satellites. Compared to binary PSK (BPSK) it has a better bandwidth efficiency, which is the amount of bandwidth required to accommodate a given amount of data. QPSK is equivalent to two BPSK schemes combined, resulting in doubling of the possible data rate but also a higher probability of error. Furthermore, QPSK chipsets are widely available, making it a more cost effective method as well. Lastly, QPSK is in LEO the most tolerant scheme for Doppler shift [29]. Furthermore, there are also two special higher order modulation formats (16 and 32 asymmetric PSK), these are a combination of ASK and PSK at higher bit rates. A different alternative is quadrature amplitude modulation (QAM) which has a rectangular constellation diagram [27]. The downside of QAM is the very high C/N ratio, making it not useful for satellite communication [28]. For SERUM it is therefore decided that QPSK is used.

9.2.4. Ground Station

For the phases 4 and 5, Ka-band needs to deliver the video stream to the ground station. Typical LEO missions have one or two ground stations, delivering 5-15 minutes of connectivity [6]. A similar to SERUM repair mission, is the ELSA-d mission. Also orbiting in LEO, ELSA-d performed rendezvous and magnetic docking technologies. To do so, it requires long, almost entire globe coverage to acquire 20-30 minutes of constant contact. This is achieved with 16 grounds stations in 12 countries. With this number of groundstations it is possible to go from one antenna to another without any loss of data [7] [8]. However, for SERUM it was decided that this is a bit redundant and that the mission could also be performed with either one or two groundstations, as stated above.

Different ground station cooperations have been looked into, such as SSC (Swedish Space Cooperation), Groundcom.space and KSAT (Kongsberg Satellite Service). It was decided to use (a) KSAT groundstation(s),

[6] https://astroscale.com/elsa-d-leading-the-way-with-innovative-ground-station-solutions/

[7] https://spacenews.com/astroscale-breaking-new-ground-for-on-orbit-servicing-demonstration/

[8] https://www.eoportal.org/satellite-missions/elsa-d#key-commercial-and-mission-factors

as these cover the poles and SERUM with SSETI Express will pass over these poles multiple times during the day. These passes will then give approximately 10-15 minutes of time to first practice the docking maneuvre, with camera feed being send down and once the maneuvre is finetuned, perform it for real. This is first done with one groundstation, however if during the trying of the maneuvre, it turns out more connected time is necessary, a second ground station of KSAT (at for example the other pole) can be added.

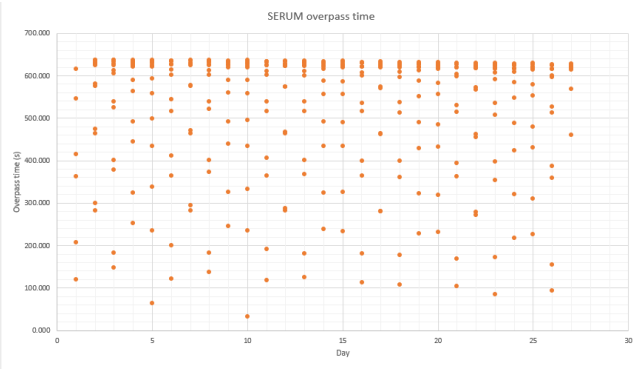

(a) SERUM overpass time over Svalbard

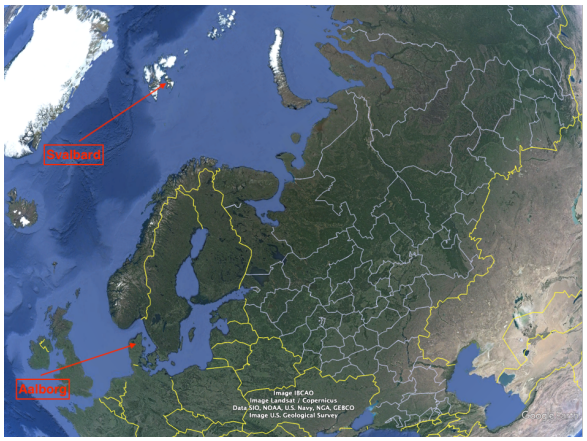

(b) Location of SERUM and SSETI Express ground station

Figure 9.3: Groundstation overpass time and location

Overpass time From the groundstations available at KSAT, it was decided on antennas in Svalbard, in Norway. This ground station, located at a latitude of $78.2\,°C$ and longitude of $15.4\,°C$, has five operating satellite, operating in S-, X- and Ka-band [30]. With the use of GMAT an estimation of the amount and duration over overpasses was made. Over the simulation of 27 days, SERUM passed over the groundstation 341 times, which gives an average of 12.6 times per day. In Figure 9.3a, the overpass time of the passes of the 27 simulated days can be seen. To first practice and after some time perform the docking maneuvre, a plan for a 10 minute procedure was set up. An overpass time of at least 10 minutes (600 seconds) is therefore defined as a 'good pass. It can be seen that almost every day has at least one good pass, with longest pass times of 637.415 seconds (day 2) and the shortest 33.169 seconds (day 10). However not all passes are that short and shorter passes of for example 6 or 7 minutes can be used to exchange data.

SSETI Express makes use of two groundstations, a main station in Aalborg Denmark and another one at the same location as SERUM in Svalbard [9]. This is another advantage of the selected groundstation, as the Aalborg station is in the same time zone, making contact between operators easy. This is even more convenient for the station located also in Svalbard, where the controllers of both SERUM and SSETI Express will be located very close together, allowing easy data exchange and consulting. The locations of both SERUM and SSETI Express can be seen in Figure 9.3b.

Coding Coding can be used for several purposes, such as encryption, compression or adding redundancy to the signal. There exist two types of coding schemes, BEC (bi-directional error correction) and FEC (forward error correction). BEC entails that once an error is detected, the signal is send again. In FEC however, when an error is detected, it is corrected by the receiver and thus the signal does not have to be send again. This also allows the link to operate at a lower BER than usual, which translates into an additive gain in the link budget. The downside however of this additive gain is that a lower number of useful bits is actually sent over the channel [31]. Examples of the different encoding schemes are convolutional codes, turbo-codes and LDPC (low density parity check). From these, LDPC is the newest but also best performing one, giving an extremely high rate and adding 10 dB of coding gain, depending on the rates [32]. When looking at KSAT and the encoding and decoding offered by its antennas, it is found that LDPC is also covered [10]. This confirms the choice of encoding scheme.

9.3. Sizing

In order to ensure proper functioning of the communication subsystem, the obtained signal-to-noise ratio must be higher than the required signal-to-noise ratio by a margin of at least 3 dB. This required signal-to-noise ratio, can be read in Figure 9.4 [33], and [32]. The modulation, as stated above, depends on the chosen parts. The

[9] https://www.eoportal.org/satellite-missions/sseti#orbit

[10] https://www.ntnu.no/wiki/display/NSSL/Specifications+of+Available+Ground+Stations

Bit Error Rate (BER) is the number of bits in error divided by the total number of bits sent. This is usually assumed to be an average over some period of time, namely one error for every million bits sent, leading to a 'normal' BER of 10^{-6} [27].

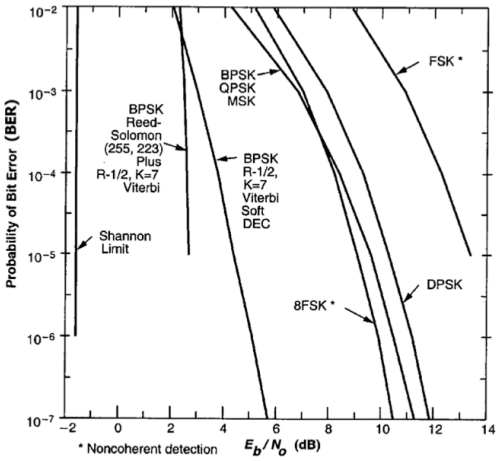

Figure 9.4: Transmission path loss as a function of frequency [33]

The obtained signal-to-noise ratio has to be calculated. Therefore, the following aspects are taken into account:

- Transmitter Power: The power transmitted by the transmitter. Sometimes, only an EIRP (Effective Isotropic Radiated Power) is given, this is the transmitted power, multiplied with the transmitter loss factor and transmitting antenna gain.
- Loss factor transmitter and receiver: Both in the receiver and transmitter there is a loss in power due to the handling of the signal sending process. Since this value is not known for the components, a general value of -0.97 dB for both transmitter and receiver is used [33].
- Transmitting antenna gain: The gain of the transmitting antenna, as discussed in Subsection 9.2.2.
- Transmission path loss: Loss of signal due to atmospheric effects and scattering due to objects in the transmission path. This value is dependent on the rain attenuation and frequency chosen. It also depends on the elevation angle, for which in the link budget the 'worst' case, being the biggest loss is chosen. The attenuation is then calculated according to [34] and [35].
- Free space loss: Loss of signal due to the square law, causing the signal to be spread over an area. This can be calculated with:

$$L_s = \left(\frac{\lambda}{4\pi S}\right)^2 \tag{9.1}$$

$$S = \sqrt{(R_E + h)^2 - R_E^2} \tag{9.2}$$

- Antenna pointing Loss: Loss of signal because the distribution of the signal over an area according to the square law is not uniform. This can be calculated with:

$$L_{pr} = L_{pr_t} + L_{pr_r} = -12\left(\left(\frac{e_{tt}}{\alpha_{1/2t}}\right)^2 + \left(\frac{e_{tr}}{\alpha_{1/2r}}\right)^2\right) \tag{9.3}$$

$$\alpha_{1/2} = \frac{21}{fD} \tag{9.4}$$

  In these equations, e_{tt} is dependend on GNC system pointing accuracy (0.06 for SERUM GNC) and e_{tr} is usually taken as 1/10 of $\alpha_{1/2_r}$ [3].
- Receiving antenna gain: The gain of the receiving antenna.
- Data rate: The required data rate to be send.
- System noise temperature: This is a way to express noise of a system in terms of an equivalent temperature [11]. It can be calculated, but often a certain G/T is given for an antenna. If it not given for an antenna, a system noise can be estimated based on up or downlink and the frequency [36].

[11] https://www.everythingrf.com/community/what-is-noise-temperature

The obtained signal to noise ratio can then be calculated with [33]:

$$\frac{E_b}{N_0} = \frac{P \cdot L_l \cdot G_t \cdot L_a \cdot G_r \cdot L_s \cdot L_{pr} \cdot L_r}{R \cdot k \cdot T_s}$$
$$= P + L_l + G_t + L_a + G_r + L_s + L_{pr} + L_r + 228.6 - 10log_{10}R - 10log_{10}T_s[dB]$$

If certain values are not provided in dB, they can be converted to dB with:

$$X[dB] = 10log_{10}\left(\frac{X}{X_{ref}}\right) \tag{9.5}$$

This is done for all three frequency bands, creating the link budget as can be seen in Table 9.3.

Table 9.3: Link budgets

	Downlink Ka-band	**Downlink X-band**	**Uplink S -band**
Frequency [GHz]	26.5	8	2.1
Ground station antenna	SG12 [30]	SG3 [30]	SG1 [30]
Transmitter Power P [dBW]	8.248[37]	-0.315 [38]	15.8(EIRP)[30]
Loss factor transmitter L_l [dB]	-0.97	-0.97	-
Gain transmitter G_t [dBi]	3 [39]	3 [40]	-
Transmission path loss L_a [dB]	-33	-28.2	-0.5
Gain receiver antenna G_r [dBi]	-	-	7.5
Free space loss L_s [dB]	-176.642	-166.239	-159.622
Antenna pointing loss L_{pr} [dB]	-0.120	-0.120	-0.120
Loss factor receiver L_r [dB]	-0.97	-0.97	-0.97
G/T ground station antenna [dB/K]	47 [30]	37.8 [30]	-
Required data rate R [dB$(bits/s)^{-1}$]	-64.77	-44.771	-40
Boltzmann Constant k [$(J/K)^{-1}$]	228.6	228.6	228.6
System noise temperature T_s [K]	-	-	-27.882 [33]
E_b/N_0 obtained	11.016	13.814	13.807
E_b/N_0 required	8	10.8	10.8
Margin	**3.016**	**3.014**	**3.007**

A few things should be noted. First of all that the link budget is calculated for SERUM's orbit, once docked to SSETI Express, which is a 700 km orbit. The ground station antenna chosen, depends on the frequency band. For both X-band and Ka-band the transmitter power and EIRP (for S-band) is lower than the maximum, to bring the margin closer to 3. The frequency selected, is a frequency in the operating range of both the antenna and transmitter/receiver. This frequency is then used to perform the link budget calculations. In reality however, no frequency is selected yet, as this will be dependent on the ITU and is out of the scope of this design phase. When choosing a frequency in a future design phase, SERUM will adhere to the rules laid down by the International Telecommunications Union. As can be seen, all the bands have a closing link budgets for the current data rate.

9.4. Components Selection

As stated above, three different frequency band systems are in used SERUM. In Subsection 9.2.2 the different types of antennas for the different bands were discussed. When deployed from the launcher, it is assumed SERUM will have a relatively small rotation and thus that it will be possible to connect with the ground station with one omnidirectional X-band antenna. For S-band uplink, an omnidirectional antenna is required to ensure that SERUM can at any time connect with the groundstation. For Ka-band, SERUM has to match SSETI Express's rotation and at the same time send down a continuous video stream. To ensure this and because it is not known how and how fast SSETI Express rotates, the decision for two Ka-band omnidirectional antennas was made on opposite sides of the spacecraft. This way, the transmitter can switch between antennas and keep the video stream going. This leads to the following configuration of the communication subsystem:

- Ka-band
  - 1x Tethers unlimited Swift-KTX
  - 2x Ka-Band Omnidirectional Antenna, SAO-2734030345-KF-R1
- X-band
  - 1x Endurosat X-band transmitter
  - 1x MI-Wave 267 X-band omnidirectional antenna
- S-band
  - 1x Endurosat S-band receiver
  - 1x WiRan S-band antenna

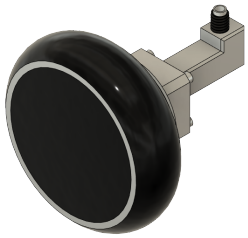

(a) Ka-band antenna

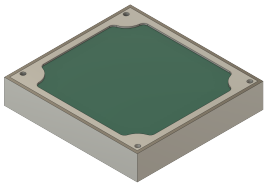

(b) S-band antenna

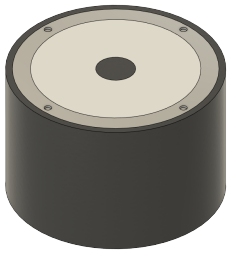

(c) X-band antenna

Figure 9.5: Communication subsystem antennas for different bands

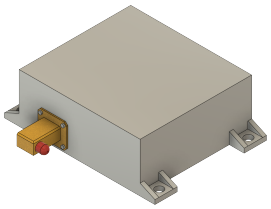

(a) Ka-band transmitter

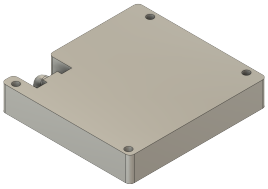

(b) S-band receiver

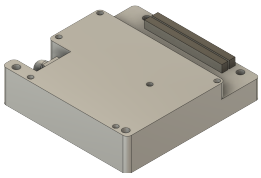

(c) X-band transmitter

Figure 9.6: Communication subsystem transmitters and receiver for different bands

9.5. Other Budgets

The design of the communication subsystem contributes to the mass, power and cost budget. In this section, the communication subsystems budgets are presented.

9.5.1. Mass Budget

In the mass budget, the mass contributions of the selected components can be seen, as well as their summed up total mass. The mass budget for the communication subsystem can be seen in Table 9.4.

Table 9.4: Mass budget contribution of the communication subsystem

Sub-components	**Mass** [kg]	**Quantity**	**Total Mass** [kg]
Ka-band transmitter	0.3	1	0.3
Ka-band antenna	0.085	2	0.170
X-band transmitter	0.275	1	0.275
X-band antenna	0.1	1	0.1
S-band receiver	0.22	1	0.22
S-band antenna	0.102	1	0.102
			1.167

9.5.2. Power Budget

For the power budget two maximum powers are considered. For phases 2,3 and 6, only communication through S- and X-band is performed, requiring a maximum of 30 W. The only exception is in phase 6, between expand-

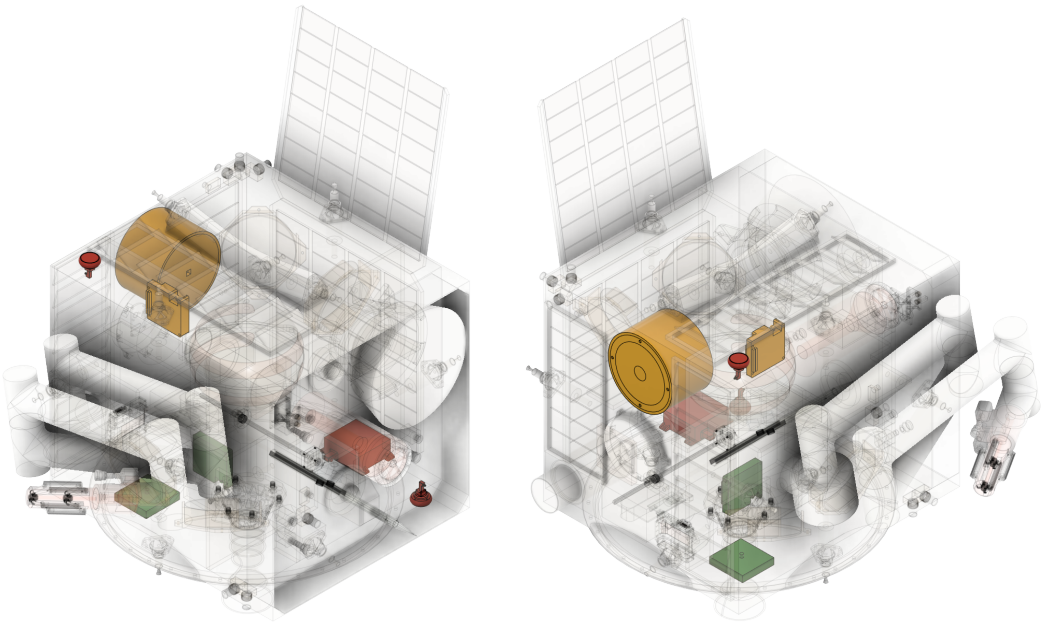

Figure 9.7: Communication subsystem integrated into SERUM with Ka-band in red, S-band in green and X-band in yellow

ing the drag sail and performing the final burn, the communication subsystem will only consume 7 W as it will only have its receiving system (S-band) on, to receive information from the ground station about when to turn back on or in case of emergency earlier. For phases 4 and 5, also Ka-band will have to be send down. In the most extreme case where also at the same time communication will be performed over all bands, a maximum power of 102 W is required. Exceptions are in phase 4 the observing and preheating of the GNC and in phase 5 the punching and sleep and bypass, during all of these only X- and S-band are used and thus a total of 30 W is required. During phase 0 (predeployment) no communication is required, so no power is consumed.

When transmitting on the Ka-band, the system will switch between both antennas, making that the power of one is 50 W, but since they will not be transmitting at the same time, this power consumption will not be doubled. The power budget for the communication subsystem can be seen in Table 9.5.

Table 9.5: Power budget contribution of the communication subsystem

Sub-components	**Maximum Power phases 4,5 [W]**	**Maximum power phases 2,3,6 [W]**
Ka-band transmitter	22	-
Ka-band antenna	50	-
X-band transmitter	18	18
X-band antenna	5	5
S-band receiver	2	2
S-band antenna	5	5
	102	**30**

9.5.3. Cost Budget

The cost of the transmitters/reciver are the known cost of the actual part. For the antennas however the cost of the chosen part is not known and thus an estimate of the cost based on similar antennas is made.

Next to the estimation for the components, the use of the frequency band will also have to be paid. For the exact price, this is difficult to estimate and find. However, a price was found for Ka band, as can be seen in Table 9.2. As no price is known for S- and X-band, the price of the total communication bps for 25 years is calculated with the 250 USD, coming from the Ka-band. This is an estimate as Ka-band will only be used for a certain period of time and this price will not be the same for X- and S-band. In total (with the 5 Mbps, 10

kbps and 30 kpbs summed), 5.04 Mbps will be used for 25 years (in the most extreme case), giving a total of 378 000 USD. The cost budget for the communication subsystem can be seen in Table 9.6.

Table 9.6: Cost budget contribution of the communication subsystem

Sub-components	**Cost [kEUR]**	**Quantity**	**Total cost [kEUR]**
Ka-band transmitter	133.5	1	133.5
Ka-band antenna	10	2	20
X-band transmitter	27.4	1	27.4
X-band antenna	3.56	1	3.56
S-band receiver	11	1	11
S-band antenna	4.45	1	4.45
Spectrum use	-	-	336.420
			536.33

9.6. Communication Flow Diagram

The aim of the communication flow diagram is to show the steps taken by the communication subsystem. To show this, the same phases as defined earlier are used. In phase 1 no communication is necessary, as SERUM is still in the launcher and is not allowed to communicate. In phase 2, the spacecraft will deploy, start up its communications station and try to find the groundstation. Once the groundstation and SERUM have connected, the uplink connection is also established and the link between both is secured. This can take multiple orbits, as SERUM will only be in contact with the ground station for a maximum of 10 minutes every orbit. Once this link is secured, SERUM can check all its systems. In phase 3, SERUM will use the S- and X-band to prepare and acquire information about the transfer. Also during the transfer, when passing over the groundstation, these bands can be used to exchange data and telemetry. Finally in phase 4, Ka-band is used. With S-band the spacecraft can be informed of 'good' (10 minute) passes coming and once this is the case, the Ka-band can be turned used to broadcast a videostream down and practice or eventually perform the docking maneuver. If the pass is to short for this, the pass can be used to exchange again information over the S- and X-band. In phase 5, SERUM and SSETI Express are docked and the overpass can again use Ka-band to stream a video whilst repairing. Also, in phases 4 and 5, if necessary Ka-, S- and X-band can all be used simultaneously. After a succesful repair, S- and X-band will support the up and downlink telemetry for the rest of the operational lifetime. At the end of this lifetime or if the repair fails, S- and X-band will again be used to expand the dragsail. After that, the communication system will be shut down until the final burn. At that point, S- and X-band are again used to determine the correct moment and burntime to prevent the remains coming down in an inhabitant area. This flow is illustrated in Figure 9.8.

9.7. Conclusion

This section described the design of the communication subsystem. It started with dividing the mission in six phases. For phases 2,3 and 6, S- and X-band will be used (uplink and downlink, respectively) and for phases 4 and 5 Ka-band will be used. During phase 0 no communication is required. The KSAT Svalbard ground station is chosen, with antennas SG12 (Ka), SG1 (S) and SG3 (X). This groundstation will be in contact with SERUM on average 12.6 times per day, including multiple 'good' (10 minutes or more) passes. A link budget was made, that is closing for all three frequency bands. Components were selected and with these a mass, power and cost budget was made. The final design leads to a mass of 1.167 kg, 102 W or 30 W of power, depending on the phase and a cost of 536.33 kEUR. Finally, a functional flow diagram showing the communication steps taken throughout the lifetime phases of SERUM was presented.

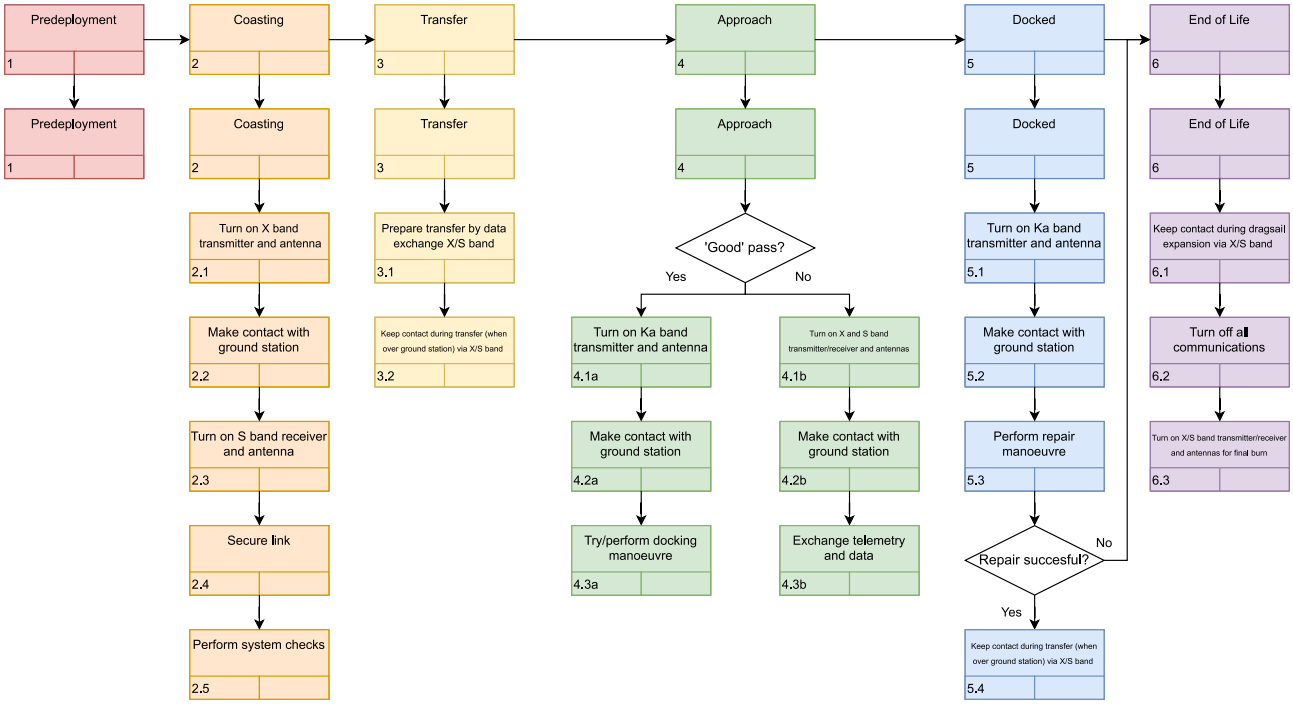

Figure 9.8: Communication Flow Diagram

10 Command & Data Handling

The Command and Data Handling (CDH) subsystem is responsible for processing all incoming and outgoing data. All information coming from the other subsystems is passed by the CDH subsystem, which makes other subsystems act accordingly. Additionally, the CDH computer is responsible for correcting for the Doppler shift for the communication subsystem.

10.1. Architecture

In the midterm report, a trade-off was performed to determine the CDH architecture. Due to latency and communication coverage limitations, it was decided to perform all computer processing required for the mission on board. As the computational workload of the payload is very high with respect to all other subsystems, it was decided to have a dedicated payload computer as well.

10.2. Payload Computer

The payload computer is tasked with performing all computationally intense processing for the payload subsystem. This consists of docking to, repairing and catching SSETI Express. Of these tasks, docking requires the most computational power. Docking to SSETI Express is broken down into three sensor phases as described in Section 5.4: the Chameleon Imager, Pose Cameras and the Arm Camera.

In the Arm Camera phase, feature tracking is performed based on the method developed by Forrai et al. [10]. This method was demonstrated to work on a NVIDIA Jetson Orin with a frequency of 100 Hz. A space rated version of this computer is under development by Spiral Blue and is called the Space Edge Two (SE-2) [41]. As this hardware is proven to work for this purpose, it is taken as the initial choice for the payload computer.

The Pose Camera phase is based on the Raven system [7] and features tracking methods developed by Messikommer et al. [12]. The Raven system uses a Space Cube 2 which employs FPGAs (Field Programmable Gate Array) to increase the computing performance 10 or 100 times [1]. Specifically, it used 2 Xilinx Virtex 5 FPGAs. These can be added to the SE-2 computer through a PCIe (Peripheral Component Interconnect Express) link with a FPGA module such as the DSP-PCIe/104 board [2].

Messikommer et al. used an NVIDIA Quadro RTX 8000 GPU (graphics processing unit) to perform feature tracking with a frequency of approximately 50 Hz [12]. The NVIDIA Quadro RTX 8000 has a processing power of 130 TFLOPS (Terra Floating Point Operations Per Second) with 4608 CUDA cores [42]. The SE-2 has a processing power of 50 TFLOPS with 2048 CUDA cores [41]. It can thus be expected that the performance of the SE-2 is roughly 2.5 times lower. This would mean a tracking frequency of approximately 20 Hz. As the relative velocity between SSETI Express and SERUM is low (Chapter 5), this frequency is considered good enough.

Finally, since the Chameleon Imager phase is not strongly time dependent, a frequency of 1 Hz is sufficient. The SE-2 is assumed to be powerful enough for this phase as well. Thus, the payload computer will consist of a SE-2 computer with an additional FPGA expansion module. It is also capable of performing an automated escape system (SYS-005).

10.3. CDH Interface Diagram

The CDH interface diagram is shown in Figure 10.1. This diagram shows how the CDH is connected with all other subsystems and their components. Each link represents a wired connection. Where available, the used protocol and maximum required data speed is indicated as a label.

10.4. Sizing of Data Storage

One of the primary tasks of the CDH subsystem is the storage of data. From the diagram shown in Figure 10.1 combined with knowledge of which systems are active when, simulations to determine the required storage size were performed. These simulations consist of four phases where only the low speed 30 kbps downlink is used: observation, coast, burn and piercing (see Section 4.3). In addition to these four phases, the docking

[1] https://spacecube.nasa.gov/

[2] https://www.xilinx.com/products/boards-and-kits/1-1pimjb.html

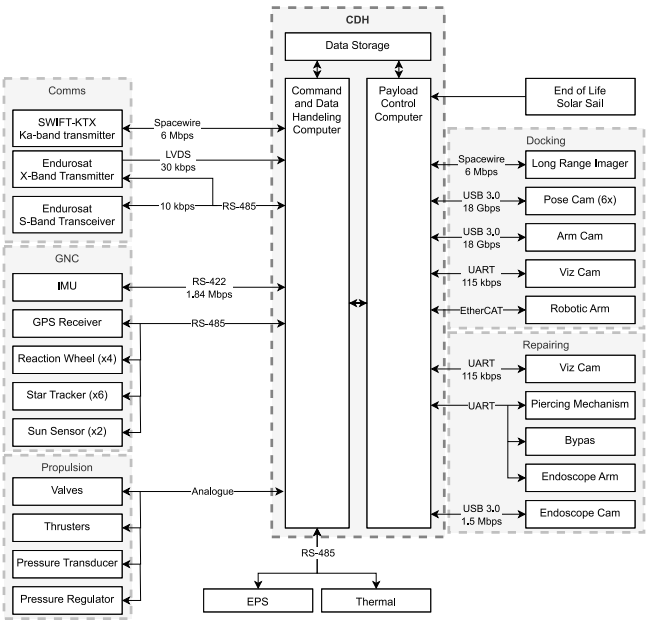

Figure 10.1: CDH interface diagram

phase uses the high speed 5 Mbps downlink. As during this phase the payload computer, with 1 TB internal storage [41], will be active, this phase is simulated separately.

Figure 10.2a shows the simulated stored data in MB for a period of three orbits. The simulation has the communication downlink window at the end of the orbital period. It is clear that the burn phase, when SERUM transfers from its initial orbit to SSETI Express' orbit, is driving the data storage requirement. Thus, the required data storage capacity in the general CDH subsystem is 17.5 MB. It can also be concluded that the piercing and burn phases require multiple orbits to off-load the data that is collected during their respective events. As these events do not repeat, this is no issue. The observation and coast phases are able to off-load all the collected data every orbit and thus make up a stable system.

In Figure 10.2b, it is clear that the docking phase requires almost 300 MB of storage. This is far more than the 17.5 MB of the CDH storage capacity. However, since the payload computer has a build-in storage capacity of 1 TB [41], all docking related data can be stored there. There is thus no need to increase the CDH storage capacity beyond 17.5 MB.

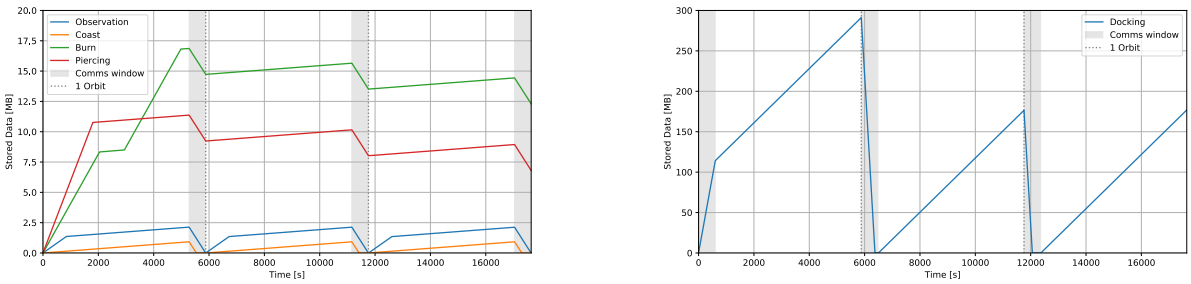

(a) In the low communication rate phases

(b) In the high communication rate phases

Figure 10.2: Storage requirement over three orbits

10.5. Sizing the CDH Computer

Whilst no particular CDH computer will be chosen in this report, a statistical analysis is performed to determine the expected power draw, size and mass. Five on board computers developed for micro-satellites are compared, the average of these five systems is taken to make budgets for the CDH subsystem. Since all five computers fit in a one unit enclosure in the width and length (100 mm by 100 mm), this dimension is taken as the size of the CDH computer. From the statistical analysis it is clear that the full 17.5 MB can be stored within the CDH computer. There is thus no need for a separate storage module.

For the long term EOL phase of the mission, the total radiation dose exceeds the operational limits of COTS

components[3] (21 y with 10 krad/y[4] is a total dose of 210 krad). Thus, in addition to the aluminum shielding discussed in Section 10.6, it is required that the CDH computer consists of radiation hardened components to comply with SYS-004-CDH-001[5].

Table 10.1: CDH computers comparison

Computer	**Power** [W]	**Mass** [g]	**Cost [**kEUR**]**[6]	**Internal Storage** [MB]
Kryten-M3[7]	0.4	62	15	4000
NANOhpc-obc[8]	1.3	60	15	8000
TRISKEL[9]	0.28	100	15	1000
COSOBC[10]	0.5	100	5	4000 (x2)
Eddie[11]	0.1	25	5	16
Average	0.5	70	11	3400

10.6. Shielding

To mitigate the risk of failure of the short term (≤ 8 y) CDH subsystem (RI-PAY-8), the CDH was designed to sustain low-energy particles. A commonly used way of achieving this is by shielding the components within a metal box [43]. A thickness of 3 mm aluminum is required to shield semi-hard components [43]. The components of the CDH all fit within a box with length and width of 100 mm, and using a density of 2.81×10^{-6} kg/mm^3 for level 1 aluminum[44], the mass of such a metal box is calculated as follows:

$$m = 2t\rho((h+w)l + hw) = 2 \cdot 3 \cdot 2.81 \cdot 10^{-6} \cdot ((63+100) \cdot 100 + 63 \cdot 100) = 374g$$

10.7. Budgets

With the entire command and data handling subsystem designed, its mass, power and cost were estimated.

10.7.1. Mass Budget

The current mass budget for the CDH subsystem is shown in Table 10.2.

Table 10.2: Mass budget contribution of CDH subsystem

Sub-components	**Quantity**	**Mass** [kg]
Payload computer (SE-2)	1	0.25
FPGA module[12]	1	0.10
CDH computer	1	0.28
Shielding	1	0.374
		1.004

10.7.2. Power Budget

The current power budget for the CDH subsystem is shown in Table 10.3. During nominal operations, CDH computer will be active, drawing 0.5 W of power. As this power consumption is a rough first estimate is a large 2.5 W margin was added. However, during approach, grab&dock, bypass and repair, also the FPGA module and payload computer will be active. The FPGA module is powered by the payload computer. To account for

[3] https://satsearch.co/products/spacemanic-eddie-the-on-board-computer
[4] https://llis.nasa.gov/lesson/824
[5] https://blog.satsearch.co/2021-01-21-spotlight-how-to-choose-a-satellite-on-board-computer-obc
[6] Provided by satsearch.com as indicative pricing for a theoretical exercise
[7] https://satsearch.co/products/aac-clyde-kryten-m3
[8] https://satsearch.co/products/skylabs-nano-ohpc-obc
[9] https://satsearch.co/products/alenspace-triskel
[10] https://satsearch.co/products/cosats-cosobc-on-board-computer
[11] https://satsearch.co/products/spacemanic-eddie-the-on-board-computer
[12] https://www.rtd.com/PC104/DM/digital%20IO/FPGA6800.htm

the worst case scenario, 13 W of power is budgeted for these phases. Lastly, during observation, only 2 W of power is added compared to the nominal operation, as in this phase, the payload computer is only active $\frac{1}{7}$ of a orbit.

Table 10.3: Power budget contribution of CDH subsystem

Sub-components	**Quantity**	**Power** [W]
Payload computer (SE-2)	1	10
FPGA module[12]	1	0[13]
CDH computer	1	3
		12

10.7.3. Cost Budget

The current cost budget for the CDH subsystem is shown in Table 10.4.

Table 10.4: Cost budget contribution of the CDH subsystem

Sub-components	**Cost [**kEUR**]**	**Quantity**	**Total cost [**kEUR**]**
Payload computer (SE-2)	31.15	1	31.15
FPGA module[12]	1	1	1
CDH computer	11	1	11
Shielding	1	1	1
			44.15

10.8. Conclusion

In conclusion, the CDH will consists of two computers, namely the CDH computer and the payload computer, which adds extra computational power for the requiring phases of the mission. A FPGA module is present for computational acceleration for docking pose determination and lastly, the entire system will be enclosed by an aluminum box, which shields it from low energy radiation. In order to design for the radiation in the 21 years of de-orbit, all components will be hardened. The subsystem was integrated into SERUM as seen in Figure 10.3.

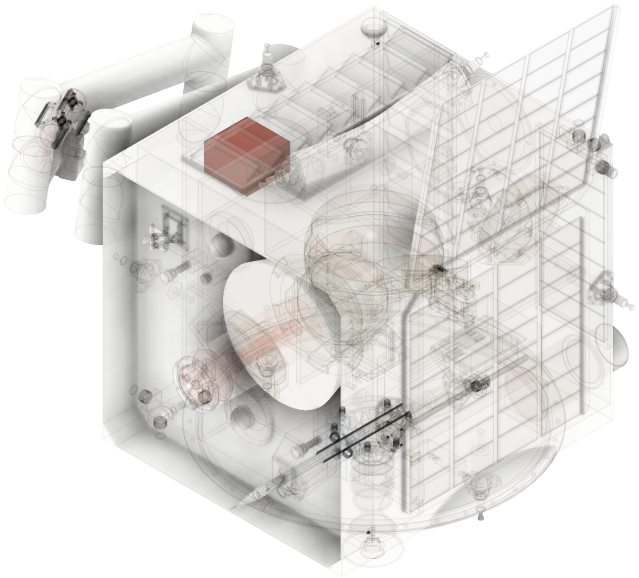

Figure 10.3: The integrated CDH subsystem - only the red computer box

[13] included in the payload computer power consumption

11 Propulsion

This chapter elaborates on the design of the propulsion subsystem. Firstly, Section 11.1 recaps the preliminary design that was presented in the midterm report. Then, Section 11.2 summarizes a literature study on green mono-propellants, which leads to the new insights explained in Section 11.3. With all of this knowledge, a trade-off is presented in Section 11.4. Section 11.5 then outlines the ignition procedure of the chosen thruster. This is followed by the design of the propellant tank in Section 11.6. Lastly, all components will be listed and the architecture of the subsystem will be visualized in Section 11.7. The conclusion on this subsystem can be read in Section 11.8.

11.1. Propulsion System

As was concluded from the midterm report, a mono-propellant is the most suitable type of propulsion considering dry mass, thrust/power, cost and specific impulse. This type of propulsion relies on the exothermic decomposition of a fuel due to ignition or interaction with a catalyst [45]. It outperformed cold-gas with its lower dry-mass and higher specific impulse, electric propulsion with its higher thrust/power and lower cost and bi-propellants with its lower dry-mass and higher thrust/power.

11.2. Green Mono-propellants

As stated by MIS-008-PROP-001, the propulsion subsystem cannot use toxic propellants. The Global Harmonized System of classification and labeling of chemicals (GHS) has defined a scale to score chemicals on their toxicity; the Acute Toxicity Classification (ATC). The scale ranges from 1 to 5, with 5 indicating the least toxic chemicals. According to [46], propellants with an ATC level 3 or higher can be considered green. As the European Chemicals Agency (ECHA) has put the most widely used monopropellant, hydrazine, on the list of Substances of Very High Concern (SVHC) [47], research into green monopropellants is picking up pace.
They can be subdivided into the following categories [45]:

- Energetic Ionic Liquids (EILs)
- Liquid NOx Monopropellants
- Hydrogen Peroxide Aqueous Solutions (HPAS)

Each of these categories will be elaborated on in more detail below. Many characteristics of specific green propellants are depicted in Section 11.2.

11.2.1. Energetic Ionic Liquids

Energetic ionic liquids, or EILs in short, are mixtures of oxidizer salts, dissolved in ionic liquids, premixed with a fuel [45]. Generally speaking, this type of green propellant is used for orbital maneuvers (as it can provide high thrust) and has a high volumetric specific impulse. Several propellants of this type have already been tested, among others ADN- (Ammonium Dinitramide)- and HAN (Hydroxylammonium Nitrate)-based fuels.

One of the most widely tested and readily available green mono-propellant is AF-M315E, or ASCENT. It is a HAN-based propellant that is used in commercially available thrusters for space applications such as the BGT-X5 Green Monopropellant Thruster from BUSEK [1]. ASCENT has relatively high adiabatic flame temperature of $2166\,\mathrm{K}$, which makes it difficult to develop cheap thrusters for its acceleration. It however, has a specific impulse superior to that of hydrazine by 13% [45]. It should be noted that the thrusters using this chemical that were tested in space had a maximum thrust of $1\,\mathrm{N}$ [48], making it feasible for attitude control rather than for orbital maneuvers.

Another EIL that has been tested in space is SHP163, which fuelled the Green Propellant Reaction Control System (GPRCS) on board of the RAPIS-1 spacecraft in 2019 [49]. It again is a HAN-based liquid which has an even higher volumetric specific impulse ($396\,\mathrm{gscm}^{-3}$) on the cost of higher combustion temperatures (up to 2400K) [50]. This propellant is not yet tested in a main propulsion system.

HNPxxx propellants were already tested in vacuum, but have not yet been demonstrated in space. IHI Aerospace

[1] https://www.busek.com/monopropellant-thrusters

Table 11.1: Characteristics of some green propellants [45]

Propellant	Theoretical specific impulse (s) (Vacuum)	Density (g/cm^3)	Volumetric specific impulse ($g\,s/cm^3$)	Chamber Temp. (K)
AF-M315E	266	1.470	391	2166
SHP163	276	1.400	396	2401
HNP221	241	1.220	294	1394
HNP225	213	1.160	245	990
GEM	283	1.510	427	?
LMP-103S	252	1.240	312.48	1903.15
FLP-103	254	1.310	332.74	2033.15
FLP-106	255	1.357	344.6	2087.15
FLP-107	258	1.351	348.5	2142.15
N2O	206	0.745	153.5	1913.15
Nitromethane	289	1.137	328.6	2449
NOFBXTM	350	0.700	245	3200
HyNOx (NOx/ethene)	303	0.879	266.3	3264
NOx/ethanol	331	0.892	295.3	3093
HTP 98%	186	1.430	266	1222
H2O2 90%	172.13	1.390	239.3	1019.3
H2O2 85%	150.5	1.370	206.2	892.65

is however in the process of developing a propulsion system utilizing HPN225 [2, 3]. This propellant has the advantage of a relatively low flame temperature (around 1000K [51]) and a high volumetric specific impulse at the same time.

GEM (Green Electric Mono-propellant), another HAN-based mono-propellant developed by DSSP (Digital Solid State Propulsion)[4], on the other hand, has not yet been tested in vacuum. This liquid could serve as a replacement of the aforementioned AF-M315E, with the advantage of the possibility of electrical ignition and usage of the fuel in multi-mode, meaning that a tank of propellant on board can be used in different propulsion configurations such as cold gas and liquid bi-propellant.

Another widely researched family of green propellants is the ADN-based family, consisting of FLP-103, -101, -106, -107 and LMP-103S, often called High Performance Green Propulsion (HPGP). Of these, LMP-103S is the most mature and is already used in commercially available systems [5]. Even though the volumetric specific impulses of these propellants are lower than that of AF-M315E, the flame temperature is lower and the propellant has more flexibility in terms of ignition methods: they can be ignited electrically, thermally and by use of a catalyst [52].

11.2.2. Liquid NOx Based Monopropellants

Several types of nitrogen-oxygen based mono-propellants have been considered for spacecraft propulsion. Of these, only HyNOx (Hydrocarbons mixed with nitrous oxide) has reached TRL 8, as it (the thruster using it) is expected to be commercially available at the end of 2023 [6]. A Liquid NOx monopropellant is a premixed fuel-oxidizer and reaches very high combustion temperatures (up to $3264\,K$ [45]). Even though it has a higher specific impulse than the other categories of green mono-propellants, its volumetric specific impulse lags that of EIL's and it has the highest flame temperature of all propellant categories considered. NOFB (Nitrogen-Oxigen Fuel Blends), and EUFB (Nitrous Oxide Ethanol) are two other liquids that are under investigation.

[2] https://www.ihi.co.jp/var/ezwebin_site/storage/original/application/e4dc26323756c0d23e7851f7eadbd688.pdf
[3] https://www.ihi.co.jp/ia/en/products/space/pinot/pinot-g/en/index.html
[4] https://dssptech.com/oil-gas/applications
[5] https://www.ecaps.space/hpgp-performance.php
[6] https://www.greendelta.space/

The latter shows better ignitability that the aforementioned propellants and is of high interest, as it allows for self-pressurization, significantly simplifying the propulsion subsystem. [7]

11.2.3. Hydrogen Peroxide Aqueous Solutions

Hydrogen Peroxide Aqueous Solutions are the last category of green mono-propellants. Even though this category performs worse than the aforementioned and even hydrazine, its low adiabatic flame temperature and special characteristics make it an interesting one. HTP (High-Test Peroxide) is especially interesting because it can be used in a multi-mode configuration. Additionally, this category has commercially available systems making use of hydrogen peroxide [8].

11.3. New Insights

Having researched green mono-propellants in more detail, some new insights were gained. First of all, the **availability** of the propellant should be considered. ADN-based mono-propellants for example (more specifically, LMP-103S), are subject of patents, which makes them more scarce and expensive [53]. The chemical is only produced in Sweden by EURENCO Bofors and ECAPS in collaboration on a licence of FOI (Swedish Defence Research Agency) [54][9].

Next to availability, also the **stability** of propellants is of importance. This not only concerns stability in space, but also on the ground, especially when transporting, storing and loading the propellant. Hydrogen peroxide for instance, is explosive when contaminated with impurities or exposed to incompatible materials [55]. Special attention has to be paid when working with these chemicals, increasing complexity and cost of the mission.

Lastly, the **controllability** of the thrust should be taken into account. Especially when docking, providing thrust as fast as possible is advantageous. Some green propellants such as AF-M315E require long preheat times (up to 1 hour) [56]. This specific liquid however, also has cold start capabilities with a lower thrust compared to the preheated performances [57].

Next to these criteria, the team decided to use the fuel for the main propulsion for the GNC actuators (RCS, Chapter 12) as well. This not only saves space, but also reduces complexity and weight significantly. This was concluded as all commercially available thrusters that the team came across were available in a 1 N variant as well.

11.4. Propellant Trade-off

The team aims at using thrusters that have been tested in an operational environment, as research and development of a propulsion system using a novel propellant would stretch the schedule and cost of this project. Therefore, many of the aforementioned options were eliminated, only leaving the green mono-propellants in the list below for the trade-off. All of the comparisons will be made on 22 N thrusters as this is the next smallest standard thrust class for satellites after one newton thrusters. One newton attitude control thrusters will be used for GNC sizing.

- **AF-M315E/ACSENT**
  For this propellant, the GR-22 thruster from Aerojet Rocketdyne was taken as a reference. This thruster can provide 22 N of thrust and is sized for the main propulsion system. Its little brother, the GR-1, is sized for attitude control [57] and was tested in space [48]. This is the only AF-M315E thruster that has flown in space.
- **LMP-103S**
  For this ADN-based propellant, Bradford ECAPS's 22 N HPGP thruster will be used. Even though it has a TRL level of only 7 [10], this thruster was chosen in order to make a fair comparison among thruster with similar thrust performance . A 1 N HPGP thruster is available at TRL 9 and is thus commercially [11]. This is the only ADN thruster with a sufficient TRL for this mission (at least a TRL of 6).
- **HyNOx**
  The only HyNOx thruster (almost) on the market is the HyNOx-22 thruster from GREENDELTA, which

[7] https://artes.esa.int/sites/default/files/D6%20-%20TNO%202018%20-%20R10640%20-%20Final%20Report%20EUFB-ESA-FP.PDF

[8] https://www.satcatalog.com/component/cz-11-600/

[9] https://www.ecaps.space/about-ecaps-general-facilities.php

[10] https://satsearch.co/products/ecaps-22n-hpgp-thruster

[11] https://satcatalog.s3.amazonaws.com/components/860/SatCatalog_-_Bradford_Space_-_1N_HPGP_-_Datasheet.pdf?lastmod=20210710010734

produces 22 N of thrust. It will be released at the end of 2023 but can already be pre-ordered now [12]. GREENDELTA will extend the HyNOx family in the beginning of 2024 with the HyNOx-1 and HyNOx-200.

- **HTP/H2O2**
  For the HTP thruster, the space proven[13] 22 N dual-mode Ocelot thruster from Benchmark Space Systems is taken[14]. The thruster also has one and two newton counterparts, and the whole thruster family has heritage.

The following trade-off criteria were decided upon:

- **Volumetric specific impulse, 0.3**
  Volumetric specific impulse is the theoretical specific impulse in vacuum of a fuel multiplied by the density of the fuel. It can be seen in the third column of Table 11.1. Specific impulse is of high relevance as it is a measure of the efficiency of the fuel, while the density is important as it directly influences the size of the tank required aboard SERUM. Using volumetric specific impulse as a measure combines the specific impulse and the density into one convenient criterion, which is given a weight of 0.3.

- **Stability, 0.3**
  The stability of the fuel plays an important role in overall mission cost, system complexity, and safety. The fuel must be handled on the ground when being loaded into the spacecraft and survive the mission duration in SERUM's fuel tanks. Since safety is extremely important, especially for the engineers and technicians working with the spacecraft, it is given the joint highest weight.

- **Controllability, 0.2**
  This trade-off serves as a selection procedure for both the main propulsion system fuel and the GNC system fuel. For GNC, fast ignition and small minimum impulse bits are important for agile maneuvering, such as will be required during the docking procedure. Since this criterion is of relevance for the GNC system, data for the smaller 1 N thrusters was used in the trade-off. This criterion will take into account the minimum impulse bit, the ignition delay, preheat times and cold start capabilities. Since this criterion is only important for GNC, it is given a slightly lower weight of 0.2. A quantification of the minimum impulse bit can be found in Chapter 12.

- **Availability, 0.2**
  As mentioned previously, not all propellants are widely available. Scarcity of a propellant drives its price up and makes the project more logistically complex. As especially the cost of this mission is a constraining factor, it is important to take availability of the chemicals into account in the trade-off. This criterion has been assigned a weight of 0.2 as it only affects the logistical side of the project rather that the performance of the spacecraft itself.

From the trade-off shown in Table 11.2, it can be concluded that LMP-103S and AF-M315E are both suitable green propellants for this mission. As there is currently more development seen with LMP-103S as compared to AF-M315E, the HPGP thrusters will be chosen, which are depicted in Figure 11.4c and Figure 11.4b. The 22 N version will be implemented in the main propulsion subsystem whereas the 1 N variant will be used by GNC, as this has the great advantage of using the same propellant for both subsystems, not only saving mass and volume, but also cost and complexity. LMP-103S has a relatively good volumetric specific impulse, for reference, hydrazine has a specific impulse of only 239 g s/cm^3 [45].

The propellant is also stable: it is chemically stable, it can be stored for over 8.5 years, it is not sensitive to

[12] https://www.greendelta.space/products/

[13] https://www.benchmarkspacesystems.com/news/post/-press-release-benchmark-space-systems-fires-up-metal-plasma-and-bi-prop-thruster-production

[14] https://3901849.fs1.hubspotusercontent-na1.net/hubfs/3901849/Data%20Sheets/BSS%20Datasheet%20-%20Thrusters%20FEB%202023.pdf

[15] https://dssptech.com/propellant-products

[16] https://ntrs.nasa.gov/api/citations/20140012587/downloads/20140012587.pdf

[17] https://www.bradford-space.com/flight-components

[18] https://www.ecaps.space/assets/pdf/Bradford_ECAPS_Folder_2017.pdf

[19] Multiple documents provide conflicting information on the minimum impulse bit, ranging from 1 mN s up to the listed 70 mN s which is provided in the thruster datasheet

[20] https://satcatalog.s3.amazonaws.com/components/860/SatCatalog_-_Bradford_Space_-_1N_HPGP_-_Datasheet.pdf?lastmod=20210710010734

[21] https://www.greendelta.space/products/

[22] https://3901849.fs1.hubspotusercontent-na1.net/hubfs/3901849/Data%20Sheets/BSS%20Datasheet%20-%20Thrusters%20FEB%202023.pdf

[23] https://3901849.fs1.hubspotusercontent-na1.net/hubfs/3901849/Data%20Sheets/BSS%20Datasheet%20-%20Halcyon%20FEB%202023.pdf

Table 11.2: Trade-off table for the propellant

Criteria / Options	*Volumetric specific impulse [45]*	*Availability*	*Stability*	*Controllability*	*Total score*
Weights	0.3	0.2	0.3	0.2	-
AF-M315E/ASCENT	G: 391	Y: Can be bought with ATF by DSSP permit[15]	Y: 'Critical' safety rating, but safer than hydrazine, long term storeable [57]	G: 8 mN s [16], cold start capable [57]	4.0
LMP-103S	L:312	L: Can be bought by Bradford Space & EURENCO [17]	G: Over 20 years stability. Permitted on commercial aircraft for shipping.[18]	Y: 70 mN s [19] [20], not cold-start capable [58]	4.1
HyNOx	Y: 266.3	O: Firestar Engineering makes NOFBX, but it does not seem purchasable [59].	Y: Long term storable, has caused accidents in the past [60]	L: 50 mN s [21], cold start capable [60]	3.0
HTP/H2O2	Y: 266	G: Easily available	Y: Safe if handled correctly [61], long term storeable in high concentrations [62]	L: 35 mN s [22], cold start capable [23]	3.6

electrostatic discharge and it is not reactive, carcinogenic, corrosive, flammable (vapors) or sensitive to space radiation.[18]. The propellant should however be handled with care: it is explosive when in contact with fire and inhalation as well as ingestion and any contact with the human body should be prevented (it is not immediately deadly). Also impact , friction, heating and direct light should be avoided [24]. The minimum impulse bit suggests that it has worse controllability than hydrazine (10 mN s [25]), but this is not a problem for our mission (as will be quantified in Chapter 12). It should also be noted that the selected thrusters do not have a cold-start capability [58]. This is, however, also not an issue for the mission, neither for the main propulsion system nor for the RCS thrusters. The main propulsion system only needs to be fired a few times during the mission, and the points at which it needs to be used will be known well in advance. Conversly, the RCS thrusters will need to be fired hundreds of times during the mission, but in clusters: after deployment for stabilization, before the main burns and during the approach and docking procedures. The thrusters will need to be preheated for each of these clusters, and potentially kept hot during the approach and docking phases (see Table 11.4 for more information on the power requirements).

The availability of LMP-103S is considered sufficient, as it can be bought commercially, even though it is manufactured at one location only: Karlskoga, Sweden (the propellant as well as the thruster and catalyst are even patented by ECAPS). There, Bradford space and EURENCO Bofors collaborate to manufacture LMP-103S. Bradford Space is part of Bradford Engineering, a company found in 1984 and currently housed in New York City, the Netherlands, Sweden, Luxembourg, and Seattle [26]. EURENCO is solely located in Europe: in France, Belgium and Sweden to be specific [27]. These backgrounds gave the team confidence in the availability of the propellant and doing business with this parties.

The sensitivity analysis on the trade-off (Table 11.2) is presented in Figure 11.1. As can be seen, LMP-103S

[24] https://static1.squarespace.com/static/603ed12be884730013401d7a/t/605916aae0a9e2324c7bc739/1616451243559/LMP-103S+MSDS.pdf

[25] https://www.space-propulsion.com/brochures/hydrazine-thrusters/hydrazine-thrusters.pdf

[26] https://www.bradford-space.com/about

[27] https://eurenco.com/en/who-we-are/

wins when changing the weights of the criteria by 10%.

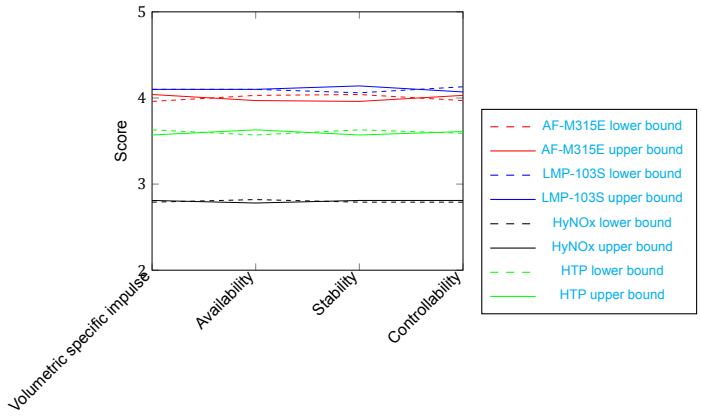

Figure 11.1: Sensitivity analysis for the propulsion subsystem.

11.5. Ignition

LMP-103S can be ignited thermally, electrically and by use of a catalyst [45]. The HPGP thrusters use a catalyst to initiate decomposition of LMP-103S and create thrust. The catalyst, hexa-aluminate, is heated up to 350 °C which takes about 30 minutes [63] (for the 1 N thruster). The heater consumes a power of 8 W to 10 W [20] of power, which equates to 14.4 kJ to 18 kJ of energy per RCS thruster. For longer maneuvering periods (which the RCS thrusters will encounter), the thrusters would need to be kept hot, using the lower boundary of the heater power - 8 W per thruster, 96 W total.

The 22 N HPGP thruster has a heating power of 25 W to 50 W. No information is available on the preheat time of the more powerful thruster, so the working assumption is that the heater has been scaled for the thruster such that the pre-heating time is the same. This would mean 45 kJ to 90 kJ of energy required for preheating.

11.6. Propellant Tank

The thrusters require the propellant to be pressurized: 0.55 MPa to 2.4 MPa for the 22 N thruster [28] and 0.45 MPa to 2.2 MPa for the 1 N thruster [29]. This pressure is achieved by the propellant tank. As the propellant is released, the pressure will drop. In order to assure a sufficient pressure in the tank, a pressurizing gas, or pressurant, is used. This can be either a inert gas (exogenous) or a small amount of cryogenic propellant (autogenous) [30].

Similar to the PRISMA mission (which demonstrated HPGP or LMP-103S on the 1 N thruster), SERUM will use the PEPT-230 propellant tank (seen in Figure 11.4a)[31,32]. This propellant tank is commercially available and is qualified for holding ADN-based 'green' mono-propellants. It can hold up to 4.5 L of propellant (without utilizing the option of a cylindrical mid-section extension), which translates to 5.58 kg of LMP-103S. The PEPT-230 propellant tank can be extended on the cost of extra mass, so that it can hold more propellant. 1 kg of propellant requires 0.81 L of volume [33], which adds 37.28 g of mass to the tank [31,34][64]. It might be necessary to add tank volume for the mission or extra propellant can be loaded to account for more docking attempts (which will be a customer decision). This will be elaborated more on in Chapter 17.

The operating pressure of the tank is 24 bar to 5.5 bar, meaning that the propellant pressure will be reduced to at least 2.4 bar by a PFCV (proportional flow control valve) before entering the thruster. The tank uses gaseous nitrogen or gaseous helium as pressurant, which is separated from the propellant by means of a diaphragm. For this mission, gaseous nitrogen will be used, as it does not react with the ADN-based fuel and is generally cheaper [35].

[28] https://www.satnow.com/products/thrusters/ecaps/36-1262-22n-hpgp

[29] https://www.satnow.com/products/thrusters/ecaps/36-1262-1n-hpgp

[30] https://headedforspace.com/why-and-how-rocket-fuel-tanks-are-pressurized/

[31] https://www.rafael.co.il/wp-content/uploads/2019/03/RAFAEL_SPACE_PROPULSION_2019-CATALOGUE.pdf

[32] https://www.eoportal.org/satellite-missions/prisma-prototype#prisma-propulsion-systems

[33] https://static1.squarespace.com/static/603ed12be884730013401d7a/t/605916aae0a9e2324c7bc739/1616451243559/LMP-103S+MSDS.pdf

[34] https://kyocera-sgstool.co.uk/titanium-resources/titanium-information-everything-you-need-to-know/ti-6al-4v-grade-5-titanium-alloy-data-sheet/

[35] https://static1.squarespace.com/static/603ed12be884730013401d7a/t/605916aae0a9e2324c7bc739/1616451

11.7. Components and Architecture

This section will list the components of the propulsion subsystem, their mass and power requirements and lastly, their configuration.

11.7.1. Component Masses

The propulsion subsystem will use one 22 N HPGP thruster as mentioned above. In case of failure, the attitude control thrusters (the 1 N HPGP thruster) will act as redundancy (mitigating RI-PROP-8). Two of them will be pointing in the same direction as the main thruster (Chapter 12). They will have a combined thrust of 2 N and are able to provide a total impulse of 96 000 N s, which is sufficient to perform the orbital maneuvers (Chapter 12).

Table 11.3 shows the components selected for the subsystem, and their associated masses. The values in italics are estimates based on similar parts, but commercial components that would fit SERUM's mission have not been chosen.

In order to estimate the weight of the plumbing required to connect all of the attitude control thrusters and main engine to the fuel tank, all of the components were positioned approximately in the CAD model of SERUM. Next, the output of the tank was connected with a straight line to each of the thrusters and the lengths were summed. The resultant length was multiplied by 150% to include a margin that accounts for routing the pipes around the components. This leads to an estimated tubing length of 710 cm. 10 mm internal diameter 304 stainless steel is chosen for the tubing [36,37], as it is compatible with many of the chosen components and commonly used in the aerospace industry [38]. The tubing has a mass of 2.765 g/cm, meaning that the estimated mass of the plumbing is 1963 g.

The mass estimation returns a total dry mass of 10.09 kg for this subsystem.

Table 11.3: List of components for the propulsion subsystem and their mass

Component name	**Function**	**Mass** [kg]	**Quantity**	**Total Mass** [kg]
1 N HPGP thruster	Attitude control thruster	0.38	12	4.56
22 N HPGP thruster	Main propulsion thruster	1.1	1	1.1
PEPT-230 propellant tank	Main propellant tank	1.3	1	1.3
Pressurant service valve	Filling pressurant tank	*0.05*	1	*0.05*
Propellant service valve	Filling propellant tank	*0.05*	1	*0.05*
Proportional Flow Control Valve (PFCV)	Control feed pressure	*0.12*	1	*0.115*
Pressure transducer	Senses pressure of propellant	*0.25*	1	*0.25*
Filter	Filters fuel	*0.30*	1	*0.30*
Shape Memory Alloy Valve (SMAV)	Stops fuel flow to thrusters before ejection from LV	*0.40*	1	*0.40*
Plumbing	Routing fuel from tank to thrusters	*1.96*	-	*1.96*
				10.09

11.7.2. Power Budget

The power required by the components of the propulsion system is stated in Table 11.4. For the pressure transducer, which is a component not specifically chosen for this mission, a space rated commercially available option is chosen: the PX5500-I. The other components have power estimates based on available space rated components, but have not been specifically chosen for the mission due to the project time constrains.

Two important assumptions were made with respect to the propulsion system's power budget. Firstly, the

243559/LMP-103S+MSDS.pdf

[36] https://ndiastorage.blob.core.usgovcloudapi.net/ndia/2009/insensitive/8Asjoberg.pdf

[37] https://indico.esa.int/event/234/contributions/3743/attachments/3078/3783/2018CSID_CSmith_CompatibilityOfWeldedPropellantSystems.pdf

[38] https://www.fedsteel.com/insights/steel-pipe-tubing-applications-in-aerospace/

thruster heat-up power is assumed to be the same as the power while it is running. This is a reasonable assumption since the thrusters still need to be heated while they are running [58], only with slightly less power as they are already hot. The power required to keep the thruster valve open slightly increases the power required, so the assumption is that these two effects balance out. The second assumption is that the peak power required momentarily to actuate the valves will be taken care of by the EPS, and the power requirements listed in Table 11.4 are to keep the valves open.

Table 11.4: The power required by each of the components

Component name	Power required	Energy required	Additional information
1 N HPGP thruster	8 W to 10 W [48]	14.4 kJ to 18 kJ	Must be preheated with given power for 30 min before firing
	0.53 W	-	Thruster valves will consume holding power while the thrusters are burning
22 N HPGP thruster	25 W to 31.25 W [48]	45 kJ to 56.25 kJ	Must be preheated with given power for 30 min before firing
	1.56 W	-	Thruster valves will consume holding power while the thrusters are burning
PX5500-I [39]	0.56 W	-	Will be on during the entire mission
SMAV	30 W	0.9 kJ	Single action, only needs to be opened once
PFCV	1.46 W	-	Will be somewhat open during the entire mission, depending on the amount of propellant left

To evaluate the maximum power consumption, one has to note that these systems will never work simultaneously. The maximum power consumption identified is 128.38 W, when 12 GNC thrusters are pre-heated or used (Chapter 12) and the PFCV is fully opened. The nominal power consumption is 0.56 W. When heating or using the main thruster, the consumption rises to 34.83 W. For the final burn, only two 1 N thrusters need to be heated, which then required 28.03 W.

11.7.3. Cost Estimate

The cost of the propulsion subsystem was estimated to be 798 616 EUR (877 600 USD). This estimation was based on an average thruster cost determined from a deal between Bradford space and Broad Reach Engineering of Golden, Colo.[40] and a market analysis [65]. The cost breakdown is listed in Table 11.5. Note that plumbing was not included in this table as this will have no significant contribution to the total cost.

11.7.4. Architecture

The architecture of the propulsion subsystem will be very similar to the one of PRISMA [32], with the main difference being the thrusters connected to the tank. The architecture is schematically visualized in Figure 11.2. Via the service valve, the propellant as well as the pressurant is loaded into the tank. The pressure of the propellant leaving the tank is regulated by the proportional flow control valve (orifice) and measured by the pressure transducer (to check for leaks before opening the latch valve) before it reaches the filter. The propellant then reaches the SMAV (latch valve). Even though each of the thrusters have their own latch valve build in, this overarching valve was added as a safety measure, especially for the launch phase. A special valve was chosen for this application, as reliability is absolutely crucial: failure of this valve blocks all propulsion of SERUM. The valve chosen is very reliable because it makes use of a shape memory alloy which deforms, opening the valve. The valve is redundant by itself and can only be used once [41].

[39] https://www.omega.nl/pptst/PX5500-I.html#description

[40] https://spacenews.com/swedish-space-corp-touts-success-prisma-formation-flying-mission/

[41] https://www.rafael.co.il/wp-content/uploads/2019/03/RAFAEL_SPACE_PROPULSION_2019-CATALOGUE.pdf

Table 11.5: Cost estimation for the propulsion subsystem

Component	Cost [EUR]	Quantity	Total cost [EUR]
Thruster	51,187.50	13	66 5437.50
Propellant tank	24,570.00	1	24 570.00
Fill/drain valve	23,660.00	2	47 320.00
Pressure transducer	318.50	1	318.50
Filter	23,660.00	1	23 660.00
Pressure regulation	27,300.00	1	27 300.00
Isolation valve	10,010.00	1	10 010.00
			798 616

The components are integrated in the architecture which can be seen in Figure 11.2.

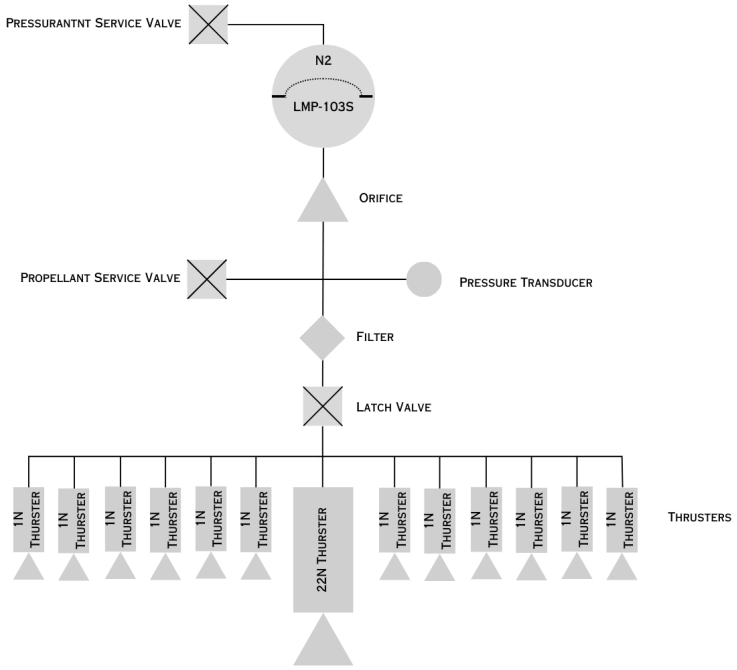

Figure 11.2: The propulsion system's architecture

A CAD model of the propulsion subsystem was made and can be seen in Figure 11.4. Figure 11.3 depicts the propulsion subsystem within the design on SERUM.

11.8. Conclusion

The propulsion subsystem of SERUM uses LMP-103S as propellant. This chemical is labeled as a green-propellant and will be used in mono-propellant configuration. It is supplied by European countries and is stable. One GR-22 thruster from Bradford will make up the main propulsion (see Figure 11.4c), and will be accompanied by 12 GR-1 thrusters for attitude control (as depicted i Figure 11.4b), final burn and redundancy. The propellant tank, visualized in Figure 11.4a, can hold up to $5.58\,\text{kg}$ of propellant, but can be extended with cylindrical sections if the mission calls for more (the cylindrical sections do not contribute to the weight significantly). The entire system weighs slightly more than $10\,\text{kg}$ and costs $798\,616$ EUR. It can be seen, integrated in SERUM, in Figure 11.3.

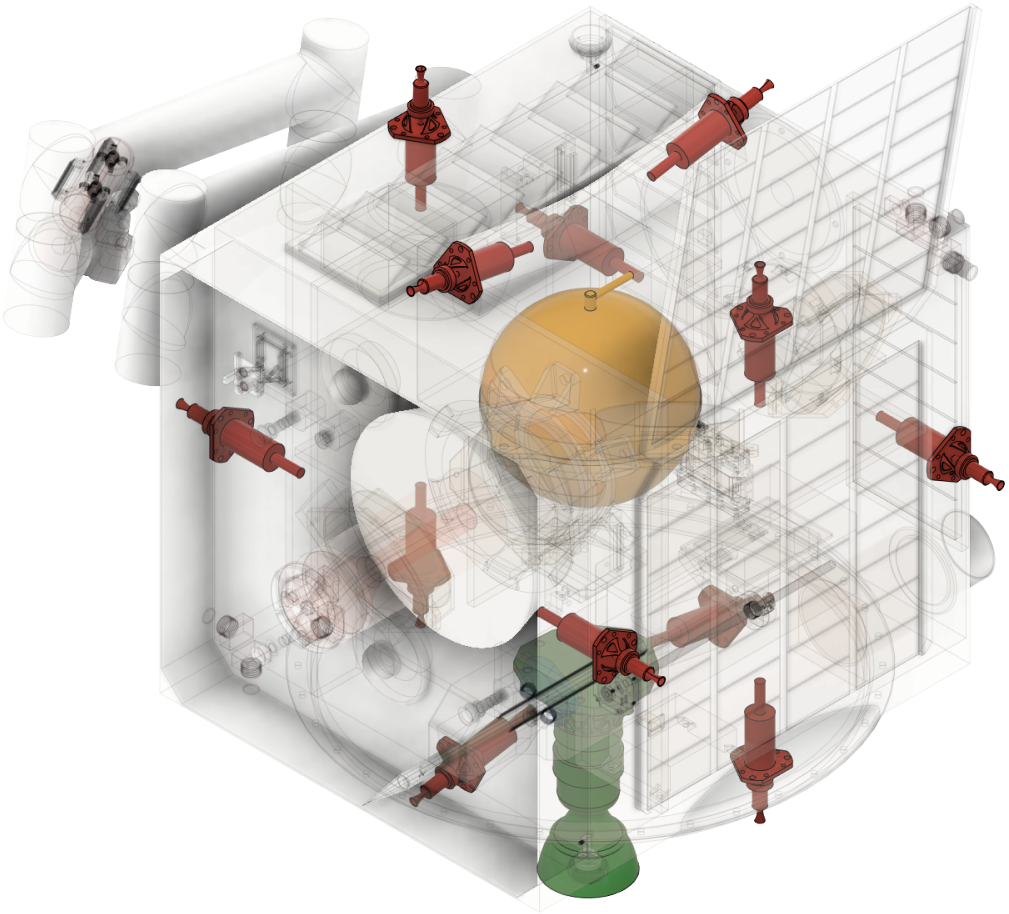

Figure 11.3: The propulsion subsystem integrated in SERUM

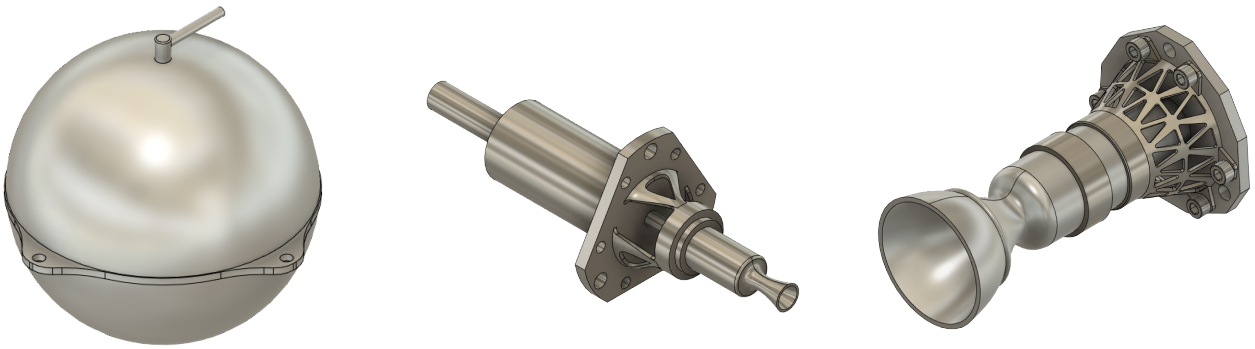

(a) The fuel tank (b) The 1 N thruster (c) The main thruster

Figure 11.4: Propulsion subsystem components

12 Guidance, Navigation and Control

The Guidance, Navigation and Control subsystem (GNC) has the duty of navigating the spacecraft through space, determining where the spacecraft is desired to be, and controlling the spacecraft accordingly.
Section 12.1 states a short summary of the tasks to be performed by the GNC subsystem, Section 12.2 gives a description of the trade-offs performed in the mid-term report and which component configuration is selected according to this. In Section 12.3, the size and required control authority of the system is determined, which is used to select a combination of commercial components in Section 12.4. The position and orientation of these components is chosen in Section 12.5, and finally the mass, power and costs of the subsystems are budgeted in Section 12.6.

12.1. Subsystem Tasks

In this mission, the GNC subsystem will have the following tasks:

- Determine the position and attitude of the spacecraft
- Provide 6 degrees of freedom of control during the approach and docking phase
- Provide attitude control during the full mission
- Detumble the spacecraft after deployment
- Provide feedback for the propulsive maneuvers
- Perform the final de-orbit burn

It should be noted that orbit insertion will be performed by the main thruster of the propulsion subsystem.

12.2. Performed Trade-offs

For the trade-offs, the subsystem has been divided into four main sections, those being: position determination, position control, attitude determination and attitude control.
For position determination, a combination of an inertial measurement unit (IMU) and a GNSS receiver has been selected. For position control, RCS is chosen which will provide 3 DOF in the translation axes.
To select the attitude determination sensors, a trade-off has been made, with the driving criteria Mass, Resolution, Output Rate, Drift and Commercial availability. From this it was decided to use star trackers for highly accurate orientation determination, an gyroscopic sensor for angular rate determination, and a sun sensor for the detumbling phase after deployment. In terms of attitude control, a trade-off has been performed with the criteria being: Mass, Saturability, Commercial availability, Control authority and Consumables required. This resulted in reaction wheels for the main, accurate attitude control, and RCS thrusters for reaction wheel desaturation and high torque maneuvers.
Thus the chosen configuration for the GNC subsystem is as follows:

- GNSS Receiver
- Star Tracker
- Sun Sensor
- IMU
- Reaction wheel
- RCS thruster

12.3. Subsystem Sizing

With the main configuration of actuators and sensors chosen, an estimation has to be made on the control authority that is to be required from the system. Multiple phases in the mission are identified to require GNC control and are the following:

- Detumble after deployment
- Approach SSETI Express

- Match SSETI Express' rotation
- Actuate docking arm and dock
- Detumble SSETI Express

For each of these phases, it is determined what the minimum required GNC forces and torques are, which are required for correct functioning.
As the time window for the approach and docking maneuvers is an order of magnitude smaller than the orbital period, orbital effects are deemed negligible and are therefore ignored in this design phase of the GNC subsystem.

12.3.1. Detumble After Deployment

After SERUM is deployed from the launch vehicle adapter, it is expected to tumble at a rate of at most $2\,\mathrm{deg/s}$ around the roll axis of the launcher, and at most $1\,\mathrm{deg/s}$ around the other two axes [1]. Equation 12.1 states the estimation of SERUM's inertia tensor, based on a cubic shape, homegenous mass distribution and a mass of 91.09 kg. Using the largest expected angular rate, Equation 12.2 gives the maximum angular momentum to be overcome to detumble the satellite, at $0.0166\,\mathrm{kgm^2/s}$.

$$I_{SERUM} = \begin{bmatrix} 4.76 & 0 & 0 \\ 0 & 4.76 & 0 \\ 0 & 0 & 4.76 \end{bmatrix} \mathrm{kg} * \mathrm{m}^2 \tag{12.1}$$

$$L_{max} = I_{max} \cdot \omega = 4.76 \cdot \frac{2 \cdot \pi}{180} = 0.0166\,\mathrm{kgm^2/s} \tag{12.2}$$

12.3.2. Approach

Docking is a time-sensitive maneuver and thus sets a limit on the minimum thruster performance for it to be executed successfully. 120 s have been allocated for this maneuver, in which the spacecraft has to translate itself 10 m from approximately standstill. The absolute minimum thrust required for this operation is calculated using Equation 12.3, resulting in a minimum required thrust of 0.127 N, however, in order to be able to avoid SSETI Express in case unforeseen issues arise, a significant safety margin is desired on this value.

$$F_{min} = m\frac{\Delta x}{0.5t^2} = 91.09\frac{10}{0.5120^2} = 0.127\,\mathrm{N} \tag{12.3}$$

12.3.3. Rotation Matching

For the docking procedure, it is required for SERUM to match the angular rate of SSETI Express, which is approximately $6\,\mathrm{deg/s}$. In this phase, it is preferred to make use of only the reaction wheels due to operation in the vicinity of SSETI Express. Using Equation 12.4, the required angular impulse on the principle axes for this maneuver is at most $0.498\,\mathrm{kgm^2/s}$.

$$L_{max} = I_{max} \cdot \omega = 4.76 \cdot \frac{6 \cdot \pi}{180} = 0.498\,\mathrm{kgm^2/s} \tag{12.4}$$

As this maneuver is time-sensitive, a minimum torque is required to achieve this rotation within the allocated time-frame. A timeslot of 60 s is designated for this, resulting in a minimum required torque of $0.008\,30$ N m.

12.3.4. Docking

For directing the docking arm in a controlled manner during the docking maneuver, it has been determined using Equation 5.6 that at most the torque vector shown in Equation 12.5 needs to be provided by the GNC system.

$$T_{docking} = \begin{bmatrix} \pm 0.0139 \\ \pm 0.0005 \\ \pm 0.0064 \end{bmatrix} \mathrm{N\,m} \tag{12.5}$$

[1] https://storage.googleapis.com/rideshare-static/Rideshare_Payload_Users_Guide.pdf

12.3.5. Detumble SSETI Express

After docking with SSETI Express, the combined body will be detumbled. Since the angular momentum is conserved during the docking process, the angular impulse required for detumbling is equal to the sum of the angular momentum of SSETI Express and SERUM when spinning at a rate of $6\,\mathrm{deg/s}$. Since the ADCS has not been utilized, the inertia tensor of the wet mass configuration is believed to be the closest match to the current inertia tensor, resulting in a maximum moment of inertia of $2.54\,\mathrm{kgm^2}$ around the principal axes [66]. From this, an angular momentum of at most $0.266\,\mathrm{kgm^2/s}$ is anticipated around the principal axes. Combining this with SERUM, results in a angular momentum of at most $0.755\,\mathrm{kgm^2/s}$ for the combined body, which has to be overcome by the moment wheels. This is however counteracting the angular momentum stored from the rotation matching maneuver, such that the after this detumbling, only the angular momentum of SSETI Express is stored in the reaction wheels.

$$I_{SSETI_{wet}} = \begin{bmatrix} 2.54 & -0.083 & -0.025 \\ -0.083 & 2.62 & -0.035 \\ -0.025 & -0.035 & 1.85 \end{bmatrix} \mathrm{kg} * \mathrm{m}^2 \tag{12.6}$$

12.4. Components Selection

From Section 12.3, the minimum required performance of the GNC actuators is derived and is stated in Table 12.1 and Table 12.2. Commercial components are selected that comply with this required performance in the following section.

Table 12.1: Minimum required performance of the moment wheels

Property	Minimum performance
Momentum storage	$0.498\,\mathrm{kgm^2/s}$
Torque	$0.0139\,\mathrm{N\,m}$

Table 12.2: Minimum required performance of the RCS thrusters

Property	Minimum performance
Thrust	$\gg 0.127\,\mathrm{N}$

Thruster As stated in Table 12.2, the thruster are required to provide a force in excess of 0.127. Furthermore, to simplify the overall system complexity the thrusters are desired to share the propellant architecture chosen for propulsion, which uses LMP-103S.
To take advantage of the shared architecture, Bradford ECAPS's 1N HPGP Thruster [2], is selected, which is part of the same product line as the main thruster selected in Section 11.7.

Reaction Wheels The reaction wheels are required to provide a momentum storage of $0.498\,\mathrm{kgm^2/s}$ and a torque of at least $0.008\,30\,\mathrm{N\,m}$. Furthermore a generous safety margin is desired to account for unforseen situations and to reduce the amount of desaturation needed.
Rocket Lab's 1Nms RW-1.0 Reaction Wheel [3] satisfies these requirements and is therefore selected for rotational control on all three axes.

Star Tracker The star sensors are responsible for the highly accurate attitude determination of SERUM, which should be irrespective of the orientation of the spacecraft. To achieve accurate tracking, light leakage from earth should be avoided, resulting in the necessity of having star sensors on all 6 planes of the satellite.
As this amount of sensors can result in significant amount of mass, emphasis in the component selection is laid on the mass and cost of the sensors. This leads to the selection of CubeSpace's GEN2: CubeStar - Miniature Star Tracker [4], a relatively low cost, low mass star tracker.

Sun Sensor To provide tracking directly after deployment, the sun sensor shall need to function in the slew rates experienced after deployment which are stated to be at most $2\,\mathrm{deg/s}$ around the roll axis of the launcher, and at most $1\,\mathrm{deg/s}$ around the other two axes.[5]. CubeSpace's GEN2: CubeSense Sun [6], is selected for this purpose, since it is a low cost component and is of the same product-line as the star sensors, thus easing integration. Furthermore, it has large field of view ($166°$), meaning that two sensors are expected to be enough for almost-continuous tracking.

[2] https://www.ecaps.space/products-1n.php
[3] https://www.rocketlabusa.com/assets/Uploads/RL-RW-1.0-Data-Sheet.pdf
[4] https://www.cubespace.co.za/products/gen-2/sensors/cubestar/
[5] https://storage.googleapis.com/rideshare-static/Rideshare_Payload_Users_Guide.pdf
[6] https://www.cubespace.co.za/products/gen-2/sensors/cubesense-sun/

IMU The inertial measurement unit (IMU) integrates both a MEMS gyroscope and a MEMS accelerometer into a single package. Sensonor's STIM380H [7] is selected for this purpose, since it has a low bias/error rate and has a low mass.

GNSS Receiver For the GNSS receiver, Spacemanic's Celeste GNSS [8] has been selected. It is an low weight GNSS receiver, and is designed for use in CubeSats.

12.5. Component Positioning

The positioning of the components is an aspect that can influence their effectiveness, and is discussed in the following section.

RCS Thrusters The RCS thruster have the task of providing 6 DOF control, meaning they must be able to provide both a pure force and a pure moment. This sets requirements on the positioning of the thrusters, as they must have a moment arm in order to generate moments. Furthermore, the center of the panels is occupied for the payload, propulsion and docking subsystems, thus requiring the RCS thrusters to be mounted near the edges of the panels. In addition, interference of the thruster's exhaust plume with SSETI Express shall be avoided, by angling the thrusters at $10°$. To comply with SYS-007-GNC-001, the longitudinal set of thruster is positioned outside the outer shell, parallel with the side panels, such that they are still functional after having docked with SSETI Express.

Star Sensors To allow continuous tracking, independent of the orientation of SERUM, a configuration of 6 star trackers is selected, where the trackers are mounted on the outer panels of the spacecraft. This configuration has redundancy and ensures tracking while docked to SSETI Express, whilst the mass and cost of the additional sensors is negligibly small when compared to the entire subsystem.

Sun Sensors Two sun sensors are selected for almost continuous tracking when the star trackers are unavailable. They are mounted on the side panels, such that they are not obscured by the solar panels or SSETI Express after docking.

Others The IMU and GNSS receiver are mounted near the CDH, with the GNSS antenna being mounted on the outer panel for optimal reception. The reaction wheels are mounted internally on the outer shell of SERUM, mounted in the corners in a pyramid configuration, such that 3-axis control is still available in case of a single failure as a mitigation strategy for RI-GNC-2. Due to positioning requirements of other subsystem components, the reaction wheels are grouped in sets of 2, and positioned near the corners of the structure.

12.6. Subsystem Budgetting

With the components selected, the subsystem budgets can be defined, which are: the mass budget, the power budget and the financial budget.

12.6.1. Mass & Power Budget

From the selected components, the mass can be seen in Table 12.3, and the power budget is stated in Table 12.4. It can be concluded that the total mass is expected to be 5.91 kg.

As the power draw of the components is variable and depends on multiple aspects, it will be split into the average, steady-state draw, and the expected peak draw. For the steady-state estimate, one active star tracker and one active sun sensor is assumed, and one saturated reaction wheel. This results in a average power draw of 7.47 W. For the peak draw, maximum power draw of the sensors is assumed, and full power actuation of one reaction wheel, resulting in a power draw of 46 W.

12.6.2. Financial Budget

To estimate the cost of the GNC subsystem, a financial budget is created and can be seen in Table 12.5. As the price of the IMU and the GNSS receiver was not provided by the manufacturer, a cost is estimated of 5000 € for both components. This makes the total subsystem cost to be estimated at 435 kEUR , which constitutes 2.2% of the total mission budget.

[7] https://www.sensonor.com/products/inertial-measurement-units/stim380h/

[8] https://satsearch.co/products/spacemanic-celeste-the-gnss-receiver

Table 12.3: List of components for the GNC subsystem and their mass, note that the power required for the thrusters is included in the propulsion susbsystem

Component name	**Function**	**Mass** [kg]	**Quantity**	**Total Mass** [kg]
1 N m Reaction wheel	Attitude control	1.38	4	5.52
Cubestar Star Tracker	Accurate attitude determination	0.047	6	0.282
Cubesense Sun Sensor	Coarse attitude determination	0.015	2	0.030
STIM380H IMU	Angular rate & acceleration sensing	0.057	1	0.057
Celeste GNSS Receiver	Absolute position tracking	0.025	1	0.025
				5.91

Table 12.4: The power required by each of the GNC components, note that the mass of the thrusters is included in the propulsion susbsystem

Component name	**Power required**	**Additional information**
1 N m reaction wheel	0 W to 5.3 W (Steady State), 43 W (Max)	Regenerative breaking possible
Cubesense sun sensor	0.100 W to 0.174 W	Active during large slew rates
Cubestar star tracker	0.165 W to 0.271 W	Constantly active
STIM380H IMU	1.8 W to 2.5 W	Constantly active
Celeste GNSS Reciever	0.100 W	Constantly active

12.7. System control characteristics

With the specific actuators selected, the control characteristics of the spacecraft can be determined, and defines the degree of maneuverability the satellite has. As this mission is largely dependent on precise position and attitude control, it is an important aspect of the design and is described in this chapter, split up between position control and attitude control.

12.7.1. Position Control

Position control is provided by 3 sets of 4 RCS thrusters, which together provide 3 degrees of freedom. The thrusters can generate up to 1 N of force with a minimum impulse of 70 mN s. The thrusters which are oriented along the horizontal plane (assuming the aft of the spacecraft is the launch vehicle adapter ring), are parallel to their respective degree of freedom, such that they achieve maximum efficiency. Thus the thruster force in these two degrees of freedom is simply the addition of of the individual thruster force, resulting in 2 N of force in those two cardinal axes. The thrusters in the vertical axis are angled at 10°, such that they reduce interference of their exhaust with SSETI Express, at the cost of efficiency. This results in a maximum force of 1.97 N. With the spacecraft mass estimate of 91 kg, the position control authority can be seen in Table 12.6. With a longitudinal acceleration of $0.015\,\mathrm{m/s^2}$, the spacecraft can deccelerate from its approach velocity in 5.5 s, thereby verifying SYS-005-GNC-001, which requires the SERUM to abort and revert the approach within 10 s

12.7.2. Attitude Control

Attitude control is mainly provided by the cluster of 4 1 N m s reaction wheels, which are positioned in a redundant pyramid configuration. They have a maximum individual torque of 0.1 N m, and their positioning gives

Table 12.5: Cost estimation for the components of the GNC subsystem, note that the cost of the thrusters are included in the propulsion subsystem (Prices adjusted to Euro FY2023)

Component name	**Cost** [€]	**Quantity**	**Total Cost** [€]
1 N m Reaction wheel	74,102	4	296,408
Cubestar Star Tracker	16,362	6	98,172
Cubesense Sun Sensor	3,330	2	6,660
STIM380H IMU	5,000	1	5,000
Celeste GNSS Receiver	5,000	1	5,000
			411,240

Table 12.6: Position control characteristics of SERUM, showing maximum acceleration and minimum velocity increments

Axis	**Acceleration** [m/s^2]	**Velocity Increment** [mm/s]
x	0.022	1.5
y	0.022	1.5
z	0.022	1.5

them the following effectiveness:

$$T = \begin{bmatrix} \frac{1}{\sqrt{3}} & -\frac{1}{\sqrt{3}} & -\frac{1}{\sqrt{3}} & \frac{1}{\sqrt{3}} \\ -\frac{1}{\sqrt{3}} & \frac{1}{\sqrt{3}} & -\frac{1}{\sqrt{3}} & \frac{1}{\sqrt{3}} \\ \frac{1}{\sqrt{3}} & \frac{1}{\sqrt{3}} & \frac{1}{\sqrt{3}} & \frac{1}{\sqrt{3}} \end{bmatrix} \cdot \begin{bmatrix} M_1 \\ M_2 \\ M_3 \\ M_4 \end{bmatrix} \tag{12.7}$$

Which results in a maximum single axis torque of 0.23 N m, and 0.13 N m in case all three axes are actuated simultaneously. With the spacecraft inertia estimate as given in Equation 12.8, the attitude control authority can be seen in Table 12.7

$$I_{SERUM} = \begin{bmatrix} 4.76 & 0 & 0 \\ 0 & 4.76 & 0 \\ 0 & 0 & 4.76 \end{bmatrix} \text{kg} * \text{m}^2 \tag{12.8}$$

Table 12.7: Attitude control characteristics of SERUM, showing maximum angular acceleration and maximum achievable rates through the reaction wheels

Axis	**Angular acceleration** [°/s^2]	**Achievable rate** [°/s]
x	1.56	15.6
y	1.56	15.6
z	1.56	15.6
Single axis only	2.77	27.7

12.8. Conclusion

This chapter documents the design and component selection of the guidance, navigation and control subsystem of the SERUM spacecraft. The initial configuration that resulted from the trade-offs performed in the baseline report was worked out further and individual phases in the docking and approach maneuvers were identified, from which commercially available components were selected. Those being: the 1 N HPGP Thruster, Rocket-labs RW-1.0 reaction wheel, The CubeSpace star tracker and sun sensor, the STIM380H IMU and the Celeste GNSS Receiver. These components add up to a total subsystem mass of 5.91 kg, which falls within the 20% margin of the initial mass budget. The power usage is estimated at 7.47 W nominally, but peak power is highly dependent on the use of the reaction wheels and is expected to be no more than 46 W. The cost estimate of the components is $411\,240$ EUR or 2.2% percent of the total mission cost, this is 14% of the budgetted cost,

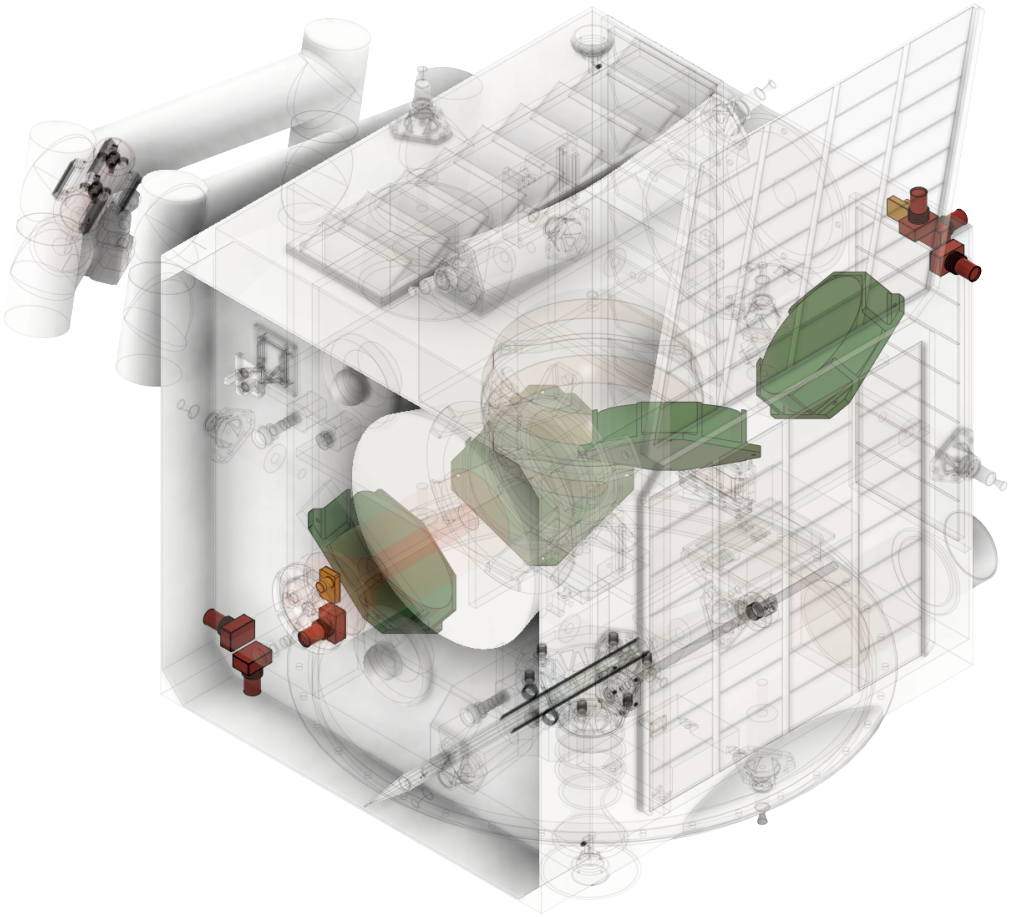

Figure 12.1: Positioning of the GNC sensors and reaction wheels, star trackers shown in red, sun sensors in yellow and reaction wheels in green

thus allowing a generous margin for integration costs. The positioning of the sensors and reaction wheels can be seen in the context of the satellite in Figure 12.1. It show how the moment wheels are in their pyramid orientation, located within the satellite shell. The optical sensors are located on the outer panels facing outward to ensure they function correctly. Not indicated in colour are the RCS thrusters, which can be seen more clearly in Figure 11.3.

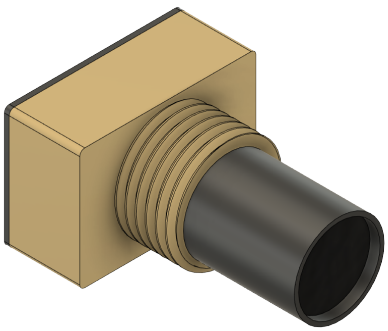

(a) The CubeStar star tracker

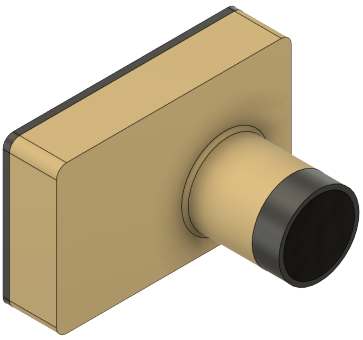

(b) The CubeSense sun sensor

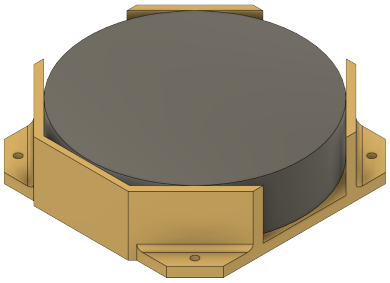

(c) Rocketlab's 1Nms reaction wheel

13 Electrical Power System

The Electrical Power System supplies power to the bus and payload. It has several components which need to be chosen and sized. The conclusions regarding the power generation drawn in the midterm report are recapped in Section 13.1. Then, the method of storing power is discussed in Section 13.2. In order to size the EPS, the eclipses are analyzed in Section 13.3. The power budget of SERUM can then be seen in Section 13.4. This budget is followed by the sizing procedure in Section 13.5. With a final configuration, the depth of discharge is evaluated, as can be read in Section 13.6. The budgets of the ESP specifically are listed in Section 13.7. A conclusion on the EPS configuration can be read in Section 13.8.

13.1. Deployable Solar Panels

From the midterm report, it was concluded that deployable solar panels are the best option for generating power during the mission. They won not only by their good longevity and TRL, but also, in contrast to solar dynamic systems and fuel cells, because of their relative simplicity. In addition, deployable solar panels are scalable. Their power output/mass is not as good as that of solar dynamic systems of fuel cells. However, these options scored unacceptable on complexity and longevity respectively.

13.2. Battery

As SERUM will experience eclipses during which power is required for certain subsystems, the power generated by the deployable solar cells needs to be stored. Additionally, some phases of the mission do not allow SERUM to point its solar panels to the sun. Batteries are the most widely used way of storing power. The far majority of rechargeable batteries put in spacecraft nowadays are lithium-ion batteries. This type of battery has a significantly higher energy density than for example nickel-based batteries [67]. However, when such a battery suddenly releases a significant amount of energy, heat is generated. If this heat is not dissipated correctly, a thermal runaway can occur. This exothermic reaction propels itself and can even cause explosion of the battery. Also, a lithium-ion battery has a strict lower operational temperature bound, which will flow into the requirements on the thermal subsystem (Chapter 14). Still, this battery type is the preferred type for space applications and will therefore be used in SERUM [67].

As was identified in Chapter 4, the final burn will take place more than 20 years after launch and the battery will then be degraded beyond its acceptable performance. Therefore, a super-capacitor will replace its task. A super-capacitor is known for having exceptional cyclability while delivering very low power and will therefore be used for the hibernation when de-orbiting and the final burn [68].

13.3. Eclipses

SERUM experiences an average of 14.4, 2194 s, eclipses per 24 h cycle (445 per month) in the launch vehicle ejection orbit, and 14.4, 2074 s, eclipses per 24 h cycle (445 per month) in SSETI Express' orbit. The time to transfer to SSETI Express' orbit and finish repair is 8 years (MIS-010). This means that the spacecraft could spend the 8 years in the ejection orbit, in SSETI Express' orbit or in a transfer orbit between the two. The transfer orbit is assumed to be an intermediate stage and therefore, it will not be taken into account in calculating the amount of eclipses. The worst case number of eclipses is 42 700 of approximately 2194 s each (result from GMAT simulation).

The piercing, however, does not need to occur as fast as in the demonstration. In order to minimize the power usage of this system, the team chose to assign 130 W to this task, which results in approximately 30 min of piercing time. To further reduce the required power, SSETI Express will not receive any bypass power during this time.

13.4. Power Budget

The final power budget is listed in Table 13.1. As can be seen in the table, different power consumption phases were identified and grouped into six main categories: Pre-deployment, Coasting, Transfer, Approach, Docked and EOL (as mentioned before in Chapter 4). The power requirements for the subsystems differ significantly among these phases and therefore, each of the phases was considered independently (for the explanation of the power required by the subsystems, consult the respective chapters). The times in **bold** will consist of multiple periods and thus eclipses.

Table 13.1: The power budget

Category	Phase	Time	CDH [W]	GNC [W]	PAY [W]	COMM [W]	PROP [W]
Pre-deploy	Pre-deploy	1 min	3.00	25.77	0.00	0.00	0.56
Coast	Coast	**2 weeks**	3.00	4.57	0.00	30.00	0.56
Transfer	Burn 1	35 min	3.00	4.57	0.00	30.00	34.83
	Transfer	**2 weeks**	3.00	4.57	0.00	30.00	0.56
	Burn 2	34 min	3.00	4.57	0.00	30.00	34.83
Approach	Observation	**1 month**	5.00	0.00	0.00	30.00	0.56
	Pre-heat thrusters	30 min	3.00	4.57	0.00	30.00	128.38
	Approach	4 min	13.00	4.57	0.00	102.00	128.38
	Grab & dock	**6 periods**	13.00	4.57	10.00	102.00	0.56
Docked	Initiate bypass	10 min	13.00	4.57	1.50	102.00	0.56
	Piercing	30 min	13.00	4.57	130.00	30.00	0.56
	Repair	10 min	13.00	4.57	48.00	102.00	0.56
	Sleep and power injection	**3 months**	3.00	4.57	20.00	30.00	0.56
EOL	Deploy drag sail	120 s	3.00	4.57	5.00	30.00	0.56
	Sleep	**21 years**	0.00	0.00	0.00	0.00	0.00
	Final burn	30 min	3.00	4.57	0.00	30.00	23.08

Figure 13.1 visualizes the power usage over time. The horizontal axis was cut for the bold phases for readability.

In the pre-deployment phase, the reaction wheels will stabilize the spacecraft while the solar panels will be deployed (the unknown power necessary is not in the power budget but will be supplied by the battery) and pointed towards the sun. This will be thus powered by the battery. During the coasting phase that follows, the solar panels are pointed to the sun while SERUM experiences sunlight and eclipses and the bus is switched on.

Then, the transfer will take place, during which the thrusters need to be pre-heated (which takes $30\,\mathrm{min}$) and kept hot for the burns (Chapter 11). In this category of phases, the solar panels generate power as the reaction wheels will slowly rotate SERUM such that it points towards the sun (they consume almost no power as they break regeneratively). SERUM will wait with the initiation of the burn until it is in sunlight and the battery is charged. Only during the actual burns, when the thrusters need to be aligned with the velocity vector, the solar panels are assumed to not generate power. As these take about $5\,\mathrm{min}$, the battery needs to be designed for providing this power for the eclipse time + 5 min.

Again, SERUM will wait with the initiation of the next phase until it is in sunlight and the battery is fully charged. During approach, SSETI Express will first be observed. This phase takes one month, but the observation itself takes only $\frac{1}{7}$ of an orbit. Therefore, the battery should be able to power the systems for a maximum of eclipse time + $\frac{1}{7}$ of an orbit. The same holds for approach, which is less critical with only 5 min. Pre-heating of the thrusters will be done in sunlight again. Grab and dock on the other hand, will be done in multiple periods. However, this action can only be performed when in contact with ground, which is for a duration of $10\,\mathrm{min}$ per orbit. On top of that, grabbing will be completed within the first orbit, after which SERUM can immediately point its solar panels towards the sun again. Therefore, the battery only has to power SERUM for a duration of an eclipse + $10\,\mathrm{min}$.

As SSETI Express is now docked, SERUM can charge its battery before performing a sequence of servicing operations. During repair, there is the possibility that piercing SSETI Express takes longer than expected (as the piercing demonstration might not be completely representative for space conditions). For this, SERUM could dive into its battery margin (as will be explained later), or do it in multiple stages. $20\,\mathrm{W}$ will be supplied to SSETI Express' (which is included in the payload power), as this is its peak power. As this amount of power will not be drawn by SSETI Express nominally, RI-POW-1 is mitigated.

The 21 years of de-orbit are not taken into account in the sizing of the EPS. For this stage of the design, it is namely assumed that the power generated by the solar panels during this phase (which cannot be oriented to the sun due to the drag sail, but will generate some power) equates the power consumed by the system in hibernation or sleep ($10\,\mathrm{W}$ will be used by communication), for which the super-capacitor will be used. For

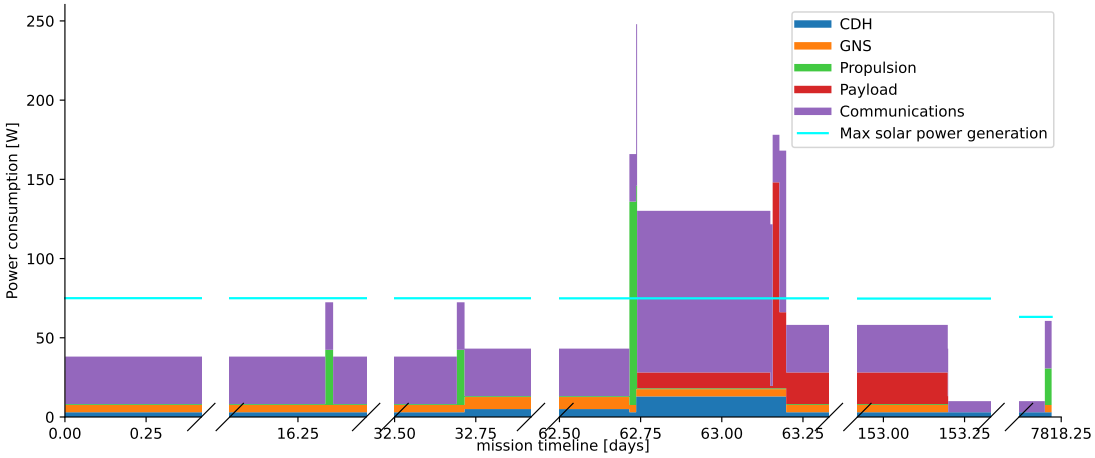

Figure 13.1: The power consumption of SERUM in time

the final burn, SERUM will boot up, fully charge its super-capacitor (which will also be the primary storage for power during hibernation) in sunlight, as well as heat up two 1N engines and perform communications (all from the solar panels). The super-capacitor will then power the final burn, when sunlight is not assured [69]. The energy needed for this maneuver was approximated for a burn time of $200\,\mathrm{s}$:

$$E = Pt = (3 + 4.57 + 23.08) \cdot \frac{200}{3600} = 1.7Wh$$

13.5. EPS Sizing

For sizing the EPS, some assumptions were made:

- $1/3$ of the orbit is an eclipse
- For the phases in which the solar panels can not be pointed, no solar power is generated
- For the phases in **bold**, the solar panels generate full power during $2/3$ of the orbit
- SSETI Express' solar panels do not generate any power
- The solar panels are disconnected when there is excess power and the battery and super-capacitor are fully charged
- The battery's task is taken over by a super-capacitor after drag sail deployment
- The battery can be charged in 1 orbit

First, the battery was sized. In order to do this, the timing of the phases and the eclipses was analyzed. It was identified that the phases that are either (partially) in eclipse by duration or cannot be timed to be in sunlight due to communication requirement are the constraining factors on energy storage:

- *Coasting* lasts multiple periods. This phase requires $9.78\,\mathrm{W\,h}$ of energy in eclipse in case communication is in eclipse as well.
- *Transfer* is similar to coasting and thus also requires $9.78\,\mathrm{W\,h}$ of energy.
- *Observation* also lasts multiple periods. However, the worst case for this phase is having an eclipse and an observation period of $\frac{1}{7}$ of an orbit immediately one after another, as well as communication during this time. The battery then needs to supply $12.86\,\mathrm{W\,h}$.
- During *approach*, no solar power will be generated. The same thing holds for the first *grabbing* cycle, which follows immediately after approach. In the worst case scenario, this sequence of actions in followed by an eclipse (in which the power required equals the coasting power). $42.89\,\mathrm{W\,h}$ will be needed.
- Lastly, *sleep & bypass* will again take several orbits. With communication happening in eclipse, this phase requires $21.52\,\mathrm{W\,h}$ of energy from the battery.

From this analysis, one can see that the grab & dock phase sizes the battery, with a required $42.89\,\mathrm{W\,h}$ of energy. A margin will be added to this, and therefore, a $45\,\mathrm{W\,h}$ battery will be used. This margin has the purpose of mitigating RI-6 (Chapter 19).

Now, as every ecliptic phase can be powered by the battery, the solar powered phases size the solar panel. For this, it was identified that piercing is the critical phase: it required not only the highest power (148.13 W without communication, which uses 5 W h), but also the most energy of all sun-lit phases. As the energy this action requires (79.07 W h) exceeds the battery energy, additional power of the solar panel will be necessary. The required power was calculated as follows:

$$E_{pierce} = 148.13 \cdot 0.5 + 5 = 79.065$$

Now, the power that the solar panel has to provide is (assuming the battery will be maximally used):

$$P_{panel} = \frac{E_{panel}}{t} = \frac{79.065 - 42.89}{0.5} = 72.35W$$

This power is determined for a critical power consumption stage, 63 days into the mission (piercing through the panel). Considering a solar degradation of -0.8% per year [1], the beginning of life power generation of the solar panel should be 75 W. No margin was added as the solar panels are oversized for the majority of the mission (as seen in Figure 13.1) and the battery does have one. Using an average solar power density of 250 W/m^2 [2], this results in an area of 0.3 m^2. It was then checked that this panel area can charge the battery in one orbit (while coasting):

$$E_{panel} = 1.054 \cdot (75 - 8.13) = 70.48$$

This is indeed more that enough to fully charge the battery.

13.6. Depth of Discharge

For calculating the depth of discharge (DoD), it was assumed that the Ka-band will not communicate during eclipse. This is a reasonable assumption as the band will only be used during in European business hours, during which there is thus sunlight on the ground station and in the orbit as well.

Sleep & bypass is the phase with the highest cyclical DoD. The DoD for sleep & bypass was calculated as follow:

$$DoD = 1 - \frac{E_{bat} - E_{eclipse} - E_{com}}{42.89} = 1 - \frac{42.89 - 16.52 - 5}{42.89} = 33.5\%$$

The battery energy is the energy calculated before. The eclipse energy is the energy consumed in eclipse during sleep & bypass (which is $\frac{1}{3}$ of the energy consumed in one orbit). The communications energy is the energy consumed by the low power bands during 10 min.

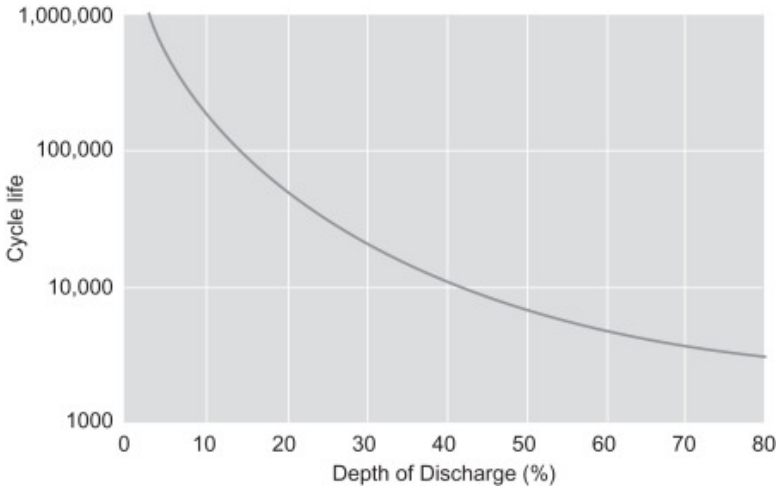

Figure 13.2: A graph plotting the number of cycles against the DoD [68]

As can be seen in Figure 13.2, more than 8000 cycles can be done with this DoD without loss of performance. As this phase will only take approximately 1350 cycles, this will not be a problem.

[1] https://ntrs.nasa.gov/api/citations/19950009355/downloads/19950009355.pdf

[2] https://satsearch.co/products/search/solar%20panel?page=1

The second case is the one with the most cycles, namely $43\,800$ cycles in the 8 years of mission as described in the requirements.

$$DoD = 1 - \frac{E_{bat} - E_{eclipse} - E_{com}}{42.89} = 1 - \frac{42.89 - 4.78 - 5}{42.89} = 22.8\%$$

The eclipse energy is calculated by taking $\frac{1}{3}$ of the coasting energy for one orbit. With this DoD, more that $50\,000$ cycles can be done. Thus, DoD will not be a problem for this mission.

13.7. Budgets

Having designed the EPS, budgeting the systems is required for an understanding of the system mass (Subsection 13.7.1) and cost (Subsection 13.7.2).

13.7.1. Mass Budget

Two solar panels can be fitted on the free side panels of SERUM during launch. These have a combined power of 75 W and an area of 250 W/m^2. The mass was then estimated based on existing panels [3]. The mass of the solar panels including the mechanism to attach them to SERUM will be:

$$m_{panels} = 0.3 \cdot 3.8 + 2 \cdot 0.4 = 1.94kg$$

For the other two components, commercial options were taken as a reference. A 20% safety margin was added to account for small additional components and wires.

Table 13.2: The mass budget of the EPS

Component	**Mass[kg]**
Solar panels	1.94
Battery	0.375[4]
Capacitor	0.472[5]
Margin	20%
	3.34

13.7.2. Cost Budget

With the EPS characteristics determined, it is possible to estimate the cost required for the acquisition of such a system. For estimating the cost of the super-capacitor, the cost per kW h was sourced [6] and then adapted to the necessary capacity leading to a cost of 658.39 EUR. For the solar array, the area sizing was used as the benchmark for the cost. The cost was found [7] and determined for the panel area of 0.3 m^2. The cost was then calculated to be $154\,245$ EUR. The battery was found to cost $20\,020$ EUR [8].

Table 13.3: The mass budget of the EPS

Component	**Cost [**EUR**]**
Solar panels	154 245
Super-Capacitor	658.39
Battery	20 020
	174923.39

[3] https://satcatalog.s3.amazonaws.com/components/1209/SatCatalog_-_SparkWing_-_SmallSat_Solar_Array_-_Datasheet.pdf?lastmod=20210809221934

[4] https://satsearch.co/products/ibeos-14v-modular-smallsat-battery

[5] https://batteryuniversity.com/article/bu-209-how-does-a-supercapacitor-work

[6] https://batteryuniversity.com/article/bu-209-how-does-a-supercapacitor-work

[7] https://www.pumpkinspace.com/store/p154/CubeSat_Kit%E2%84%A2_Fixed_Solar_Panels.html

[8] Obtained from contact with ibeos

13.8. Conclusion

In conclusion, SERUM will be equipped with a 45 W h lithium-ion battery (depicted in Figure 13.4a) to power the approach and first obrit of grab & dock, solar panels which can provide 75 W of power (seen in Figure 13.4b) to power piercing and a super-capacitor which can store at least 1.7 W h for the final burn. There is a margin on the battery, but not on the solar panels, as these are oversized for the majority of the mission (see Figure 13.1). The margin on the battery aims to mitigate RI-6 and make later design iterations easier, the same holds for the fact that the solar panels are generally speaking oversized. The system will weigh approximately 3.4 kg and cost about 174 923.39 EUR. Figure 13.3 depicts the EPS, integrated in SERUM.

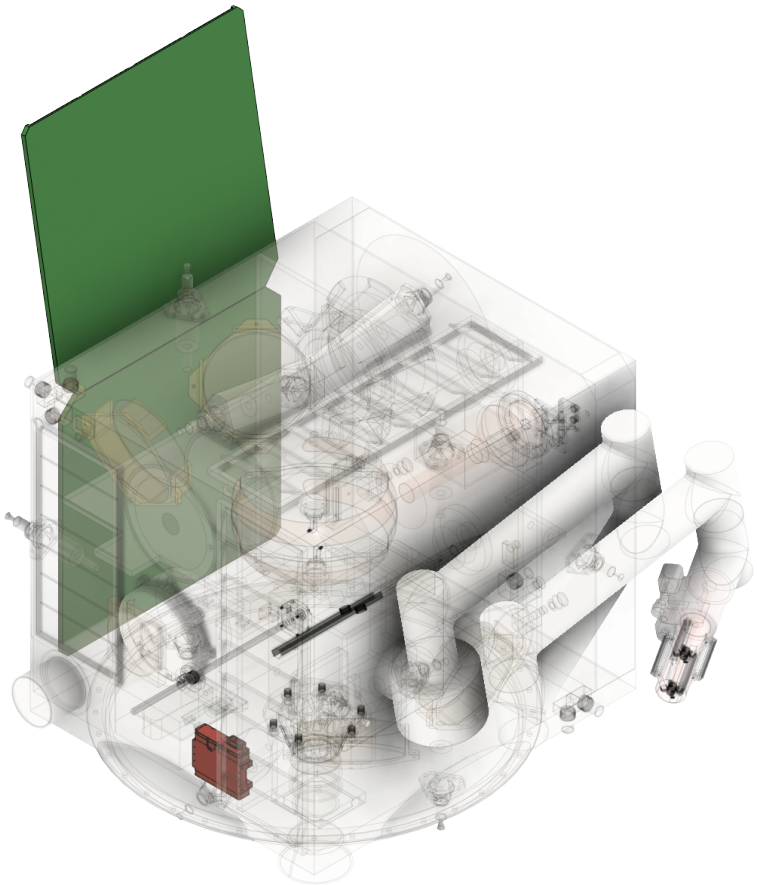

Figure 13.3: The EPS integrated in SERUM

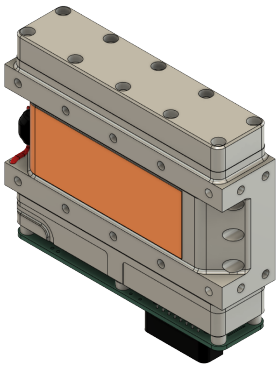

(a) The battery

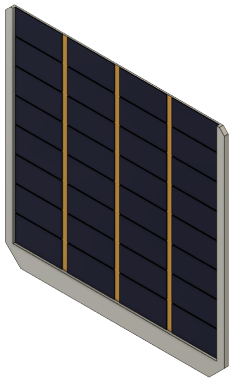

(b) One of the solar panels

Figure 13.4: Components of the EPS subsystem

14 Thermal Control System

The thermal control system is tasked with keeping all spacecraft components within their operational temperature ranges. After the selection of the payload, GNC, CDH, propulsion, communications and EPS components, the most limiting components (both in maximum and minimum operational temperature) are identified and taken as design limits. In SERUM's case, this is the chosen PEPT-230 propellant tank, which has an operational temperature between $10\,°C$ to $49.85\,°C$. In this chapter, the effect of the orbital environment on SERUM's thermal behavior is first investigated in Section 14.1. Then, the subsystem itself will be sized depending on the use of passive or active thermal control in Section 14.2. Finally, the components and budgets are listed in Section 14.3

14.1. Thermal Environment

There are three fundamental ways of transferring heat: radiation, conduction and convection. The lack of an atmosphere makes the latter two impossible in space. This leaves us with radiation being the only method for the spacecraft to dissipate or absorb heat from its environment. Figure 14.1 shows the sources of heat absorption and emission in space.

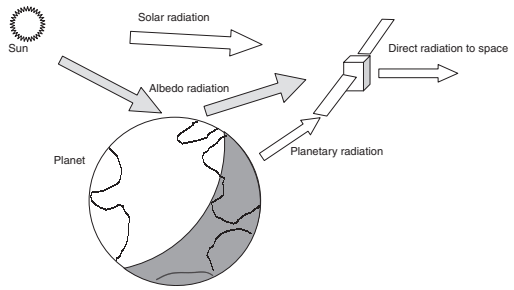

Figure 14.1: Typical spacecraft thermal environment [70]

As can be seen from Figure 14.1, the spacecraft receives direct incident solar radiation (Q_{inc}), albedo radiation or solar radiation reflected from the Earth (Q_{alb}), and Infrared radiation from the hot Earth (Q_{IR}). The spacecraft itself generates internal heat (Q_{int}) and radiates heat depending on its own temperature (Q_{rad}). Together, these heat sources generate the net heat of the spacecraft (Q_{net}) as follows (in [W]) [70]:

$$Q_{net} = \alpha Q_{inc} + \alpha Q_{alb} + \alpha_{IR} Q_{IR} + Q_{int} - \epsilon Q_{rad} \tag{14.1}$$

Where α is the solar absorptivity and ϵ is the emissivity of the surface finish. For α_{IR}, Kirchoff's law states that the planetary infrared radiation absorptivity equals the spacecraft emissivity:

$$\alpha_{IR} = \epsilon \tag{14.2}$$

A positive Q_{net} will heat up the spacecraft while it will cool down when negative. It is desired that Q_{net} either equals 0 at its equilibrium temperature or it fluctuates between illuminated and eclipsed mode in the right way to keep the steady-state temperature range within bounds. It was chosen to do a first level simulation of these fluctuations for a few orbit cycles. But first, all relative parameters need to be identified.

The sun radiates about $3.856 \times 10^{26}\,W$ of power into space. Applying the inverse square law, this results in a solar intensity (J_s) of about $1371\,W/m^2$ [70]. The solar intensity can normally be assumed to be constant, but in this analysis, the extreme cases will be considered: the hot case (Earth perihelion) being $1420\,W/m^2$ and cold case (Earth aphelion) being $1360\,W/m^2$ [71]. The solar incident heat absorbed is defined as:

$$Q_{inc} = J_s A \tag{14.3}$$

Where A is the area of the spacecraft absorbing the sunlight.

Part of the incoming solar radiation is reflected by the Earth and is absorbed by the spacecraft. This is called the albedo radiation. The albedo heat absorption is defined by:

$$Q_{alb} = a F_{alb} J_s A \tag{14.4}$$

With a being the albedo factor (the percentage of solar radiation reflected). In this case, albedo factors of 0.30 (hot) and 0.23 (cold) are used [71]. F_{alb} is the visibility factor which is dependent on the orbital altitude and the angle between the solar vector and its projection on the spacecraft's orbital plane [70]. For this phase of the design, it is assumed to be constant and close to the visibility factor used in the infrared calculations in Equation 14.6.

The heat absorption of the Earth's infrared radiation is calculated as follows:

$$Q_{IR} = F J_{IR} A \tag{14.5}$$

The planetary radiation intensity (J_{IR}) equals $244\,\mathrm{W/m^2}$ (hot case) and $218\,\mathrm{W/m^2}$ (cold case) [71]. And the visibility factor F equals the Earth radius R_E divided by the (circular) orbit radius $R_E + h$ (with h being the spacecraft altitude) in Equation 14.6.

$$F = \left(\frac{R_E}{R_E + h}\right)^2 \approx F_{alb} \tag{14.6}$$

14.2. Sizing

In this section, the thermal control subsystem will be sized. First, the possibility of passive control by choosing the right coatings is explored. Then, passive or active components need to be chosen, if necessary. Passive thermal control is always preferred over active control, as it is more reliable and it doesn't require power. The choice of a surface finish with different absorptivity (α) and emissivity (ϵ) might cause the spacecraft to stay within thermal limits.

Before starting with the thermal cycles simulation, some assumptions are established:

- The spacecraft is assumed to be a uniform cube with length l = $0.56\,\mathrm{m}$, absorbing heat on one surface area only, and emitting heat from it's five exposed surface areas while docked [71].
- The deployable solar arrays are not included in this analysis they are relatively small (see Chapter 13) and usually absorb and radiate much more heat than the spacecraft itself [72]. Including them will make the analysis too detailed for this stage of the design.
- The spacecraft has a uniform heat distribution: it conducts internal heat evenly and instantly. The spacecraft has an assumed specific heat capacity (C_p) of $900\,\mathrm{J/(kg\,K)}$, which is the specific heat of aluminum and an average estimation of high and low ends of satellite component specific heat capacities [73].
- The spacecraft itself is assumed to have a mass of $80\,\mathrm{kg}$ in docked configuration.
- The spacecraft is thermally isolated from SSETI Express while docked. This assumption is made because little information on emitted heat from SSETI Express is known.
- The thruster heat radiation and conduction during burn is not considered. They are positioned on thin support structures which are assumed to not conduct a significant amount of heat.
- Large peak powers for short amounts of time are disregarded as it is assumed that this heat will not reach the centrally placed propellant tank in the short period the heat is generated. If the thermal cycle only tightly fits within the maximum temperature range, this assumption must be revised.

With these assumptions made, the relation between spacecraft temperature and the heat balance equation (Equation 14.1) can be established. The temperature increase can be expressed as follows:

$$\Delta T = \frac{\Delta E}{C_p m} = \frac{Q_{net}\,(T)\,\Delta t}{C_p m} \tag{14.7}$$

With ΔE being the change in thermal energy, C_p the specific heat capacity, m the mass of the spacecraft, Δt an arbitrary time increment and Q_{net} the net heat power from Equation 14.1. Q_{net} is a function of the spacecraft's temperature as the radiated heat is proportional to the internal temperature:

$$Q_{rad} = \epsilon \sigma T^4 A \tag{14.8}$$

Where ϵ is the emissivity of the material, σ is the Stefan-Boltzmann constant:$5.67 \times 10^{-8}\,\mathrm{W/(m^2\,K^4)}$, T is the spacecraft temperature and A the radiation area (in this case 5 times the absorption area).

The internally generated heat, Q_{int}, is a hard parameter to predict. SERUM has a large number of mission phases, all with their respective power consumption and duration (see Figure 13.1). For the hot case, the highest continuously consumed power for a longer period of time is evaluated: $28.13\,\mathrm{W}$ during the 10 hour docking phase (Table 13.1). This power excludes the communications subsystem, which uses a peak power of $102\,\mathrm{W}$ for 10 minutes per orbit (of which $2.6\,\mathrm{W}$ is transmitted). It translates to an average internal power generation of $16\,\mathrm{W}$ for communications during docking. For the hot case, the total thus becomes $44.13\,\mathrm{W}$. The

cold case will be during the 21 years of sleep phase, when only standby communication and minor CDH loads are active, resulting in a constant generated power of 10 W.

With these numbers, a numerical relation can be established as follows:

$$T_{i+1} = \frac{\Delta t (Q_{net})_i}{C_p m} = \left(\frac{\Delta t}{C_p m}\right)\left[\alpha\left(Q_{inc} + Q_{alb}\right) + Q_{int} + \epsilon\left(Q_{IR} - \sigma A (T_i)^4\right)\right] \tag{14.9}$$

Table 14.1 provides the absorptivity and emissivity values for several typical surface finishes used in the simulation. An orbital period of 98 min was taken, with a maximum eclipse time of 35 min for both the hot and cold case.

Table 14.1: Absorptivity and emissivity of typical spacecraft finishes [71]

Surface Finish	α (beginning of life)	ϵ
Optical Solar Reflectors		
8 mil Quartz Mirrors	0.05 to 0.08	0.8
2 mil Silvered Teflon	0.05 to 0.09	0.66
5 mil Silvered Teflon	0.05 to 0.09	0.78
2 mil Aluminized Teflon	0.1 to 0.16	0.68
5 mil Aluminized Teflon	0.1 to 0.16	0.78
White paints		
S13G-LO	0.2 to 0.25	0.85
Z93	0.17 to 0.2	0.92
Z0T	0.18 to 0.2	0.91
Chemglaze A276	0.22 to 0.28	0.88
Black paints		
Chemglaze Z306	0.92 to 0.98	0.89
3M black Velvet	0.97	0.84
Aluminized Kapton		
1/2 mil	0.34	0.55
1 mil	0.38	0.67
2 mil	0.41	0.75
5 mil	0.46	0.86
Metallic		
Vapor Deposited Aluminum (VDA)	0.08 to 0.17	0.04
Bare Aluminum	0.09 to 0.17	0.03 to 0.1
Vaporized Deposited Gold	0.19 to 0.3	0.03
Anodized Aluminum	0.25 to 0.86	0.04 to 0.88
Misc		
Beta Cloth	0.32	0.86
Astro Quartz	0.22	0.8
MAXORB	0.9	0.1

The coatings were inputted into the numerical cycle in Equation 14.9. One coating resulted in a possible passive control surface finish: Anodized Aluminum with an α of 0.25 and ϵ of 0.17.[1] Running the model for 60 orbits, starting from a mean temperature of the temperature range ($T_{start} \approx 30\,°C$), gives the following cycles:

All figures are purposefully plotting a very high number of orbits to clearly showcase the steady-state response for thermal critical phases. It is visible that the model slowly converges to an equilibrium temperature and oscillates no more than $\pm 3\,°C$

[1] Aluminum can be anodized and treated to achieve certain desirable optical properties [71].

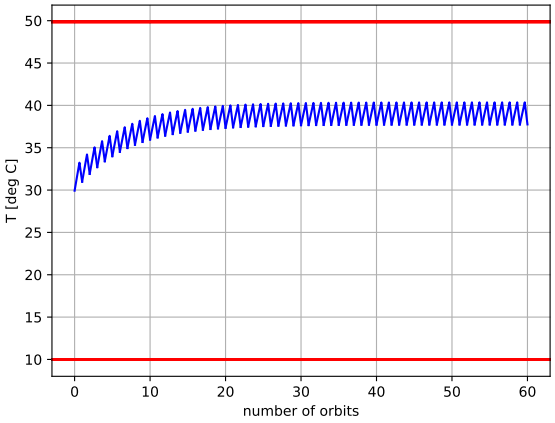

Figure 14.2: 60 thermal cycles during docking in hot case with anodized aluminum surface ($\alpha = 0.25$ and $\epsilon = 0.17$), horizontal red lines being T_{max} and T_{min}

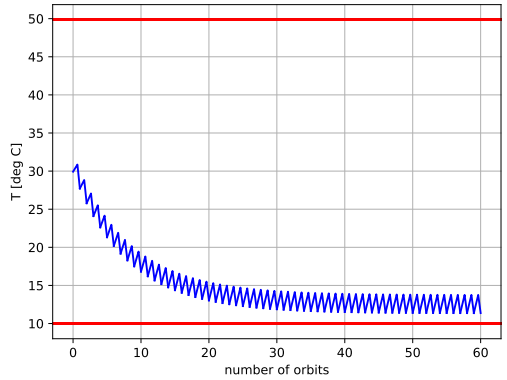

(a) 60 thermal cycles in cold case during sleep mode

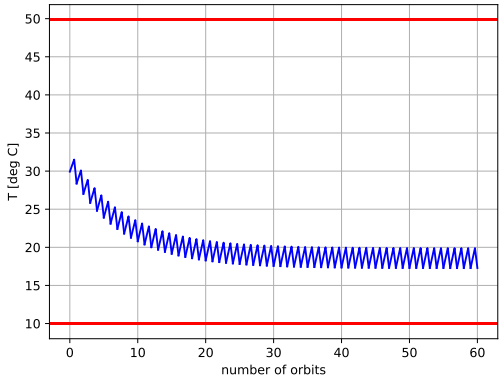

(b) 60 thermal cycles in hot case during sleep mode

Figure 14.3: Sleep mode Thermal cycles for hot and cold case with anodized aluminum, horizontal red lines being T_{max} and T_{min}

Figure 14.2 shows a thermal cycles in the absolute hot case, during maximum continuous internal heat generation (docking sequence), when SERUM is coated with anodized aluminum. Note that the actual duration of the docking sequence will take around 6 orbits, thus, in reality the spacecraft will likely not reach the visualized peak temperature. The maximum steady-state internal heat of the spacecraft fluctuates around ± 39 °C. This means that the spacecraft, in its most heat absorbent mode, is well below the maximum operational temperature. This implies that an underestimation of the heat generation of the communications subsystem could possibly be handled in this margin during high communication loads.

Figure 14.3 shows two thermal cycles during the 21 year hibernation ”sleep” of SERUM (least internal power), when coated with anodized aluminum. Figure 14.3a shows the thermal fluctuations in this absolute cold case. It can be seen that a slight margin of -1 °C is present. This margin might be too risky considering the broad assumptions made previously. As a mitigation, it might be wise to include heaters near the propellant tank in case of unforeseen heat emissions. Figure 14.3b Shows the spacecraft temperature during hibernation in the hot case. This case stays well within range and does not need mitigation measures.

It should also be noted that aluminum degrades heavily in space, increasing the absorptivity while keeping a relatively constant emissivity [71].[2] It was analyzed that a maximum increase in absorptivity of 0.14 could be handled without the addition of an emissive thermal component. A detailed analysis is necessary on how much the absorptivity would increase during this phase, but this is beyond the scope of this report. Thus, the requirement for the ability to keep the spacecraft within the thermal range can not be verified (SYS-006-TCS-014).

[2] http://esmat.esa.int/materials_news/isme09/pdf/10-In-flight/Remaury%20Paper.pdf

To have SERUM designed conservatively in this report, a louver would be a sound addition to the thermal control system preliminary design, so that SERUM is kept from overheating during the long end-of-life mission phase. The louver could remain closed during initial mission operations and be very gradually opened passively with well-calibrated thermal springs when an excessive increase in temperature is reached.

A detailed sizing of the heaters and the emissive components is not feasible within the time and scope of this project, as these require more detailed simulations like inclusion of solar panels, detailed internal and external power generation from subsystem components, spacecraft time dependent attitude w.r.t. the sun, shadow from the drag-sail, heat absorption from the drag-sail and detailed internal heat distributions. However, an estimation can be made, even though it should be noted that the entire thermal design and its components will likely vary in later iterations of the design of SERUM.

Looking at some specification sheets of louvers, it is deduced that the closed and fully opened configuration have an ϵ of 0.14 and 0.73 respectively.[3] Assuming that the absorptivity of the louver equals that of the anodized aluminum and considering new radiation and infrared heat absorptivity areas and emissivity factors, the required louver area becomes $0.18\,\mathrm{m}^2$.

14.3. Components Selection & budgets

As stated in the previous section, heaters will be added as a risk mitigation measure and louvers can be attached to the outer surface in a way to compensate for surface optical degradation.

Using some limited extrapolation from louver datasheets, it was determined that one $0.18\,\mathrm{m}^2$ louver would weigh about $1.6\,\mathrm{kg}$.[3] Kapton - silicon flexible heater elements have a near negligible mass and will thus not be counted.[4] The anodized aluminum surface material will not add additional mass to the thermal subsystem as it can be regarded as part of the structural subsystem.

As mentioned before, the spacecraft's thermal regulation is very sensitive to detailed spacecraft attitude and internal components. More thermal components will surely be included in further detailed design phases like: heat conducting tapes or heat pipes and small radiators on components with a short heat peak (like communication transmitters). To facilitate later iterations, a margin of $25\,\%$ is applied, bringing the mass budget to $2\,\mathrm{kg}$. Note that the inclusion of a louver on the outer surface of the spacecraft structure reduces the overall structure mass, as part of the structure is replaced by a thermal component.

No quotation from louver or heater manufacturers was able to be obtained and considering the uncertainty of detailed thermal components, it is decided to keep the estimated cost of the thermal subsystem from the midterm report. This results in an estimated cost of 462 kEUR

14.4. Conclusion

Passive thermal control will be used by using anodized aluminum as outer structure with absorptivity of 0.25 and emissivity of 0.17. This will keep the spacecraft within minimum and maximum thermal ranges for the duration of the repair mission. It is however not sufficient when considering the 21 year long end-of-life de-orbiting sequence which will degrade the optical surface properties to such extend that the spacecraft will most certainly overheat. To survive this phase, an emissive component shall need be added to ensure survival. Unfortunately, the determination of the increase in absorptivity during 21 years is not known, thus the ability to thermally control the spacecraft for the duration of the operational lifetime cannot be verified.

To still provide an approximate component sizing as a starting point for future iterations, a doubling in absorptivity at end-of-life is assumed which results in a $0.18\,\mathrm{m}^2$, $1.6\,\mathrm{kg}$ louver on the outside surface of the spacecraft. Flexible heaters could also be attached to critical components in order to mitigate the risk of cooling down too much (they will use excess battery power). Later stages of detailed design is expected to result in additional thermal control components, thus the approximate mass is assumed to become $2\,\mathrm{kg}$ and cost 462 kEUR

[3] https://satsearch.co/products/sierra-space-passive-thermal-louvers

[4] https://www.nph-processheaters.com/assets/uploads/pdfs/flexible-heaters/Kapton_Insulated_and_Silicone_Rubber_Flexible__Heaters.pdf

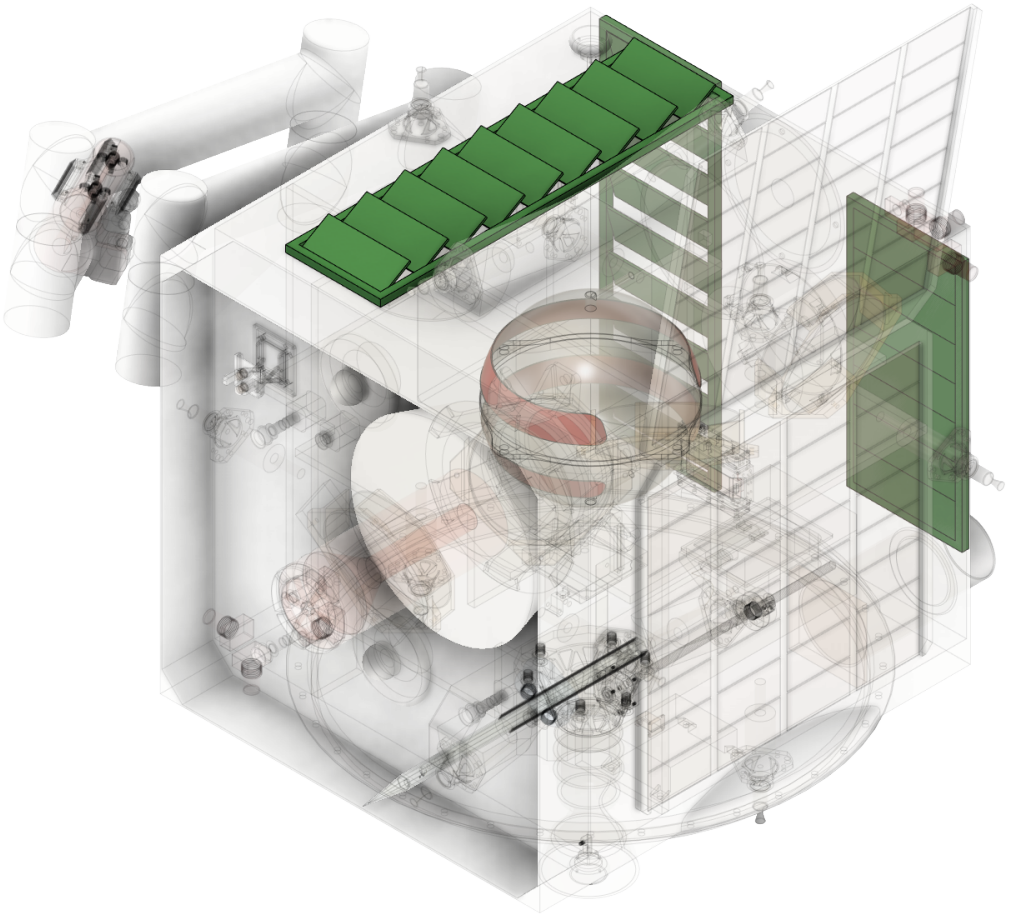

(a) The thermal control subsystem integrated in SERUM

(b) Propellant tank heaters

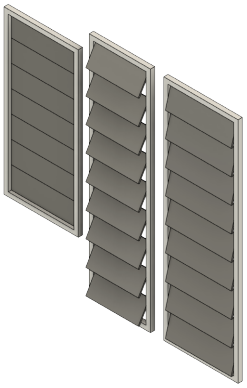

(c) Louvers

Figure 14.4: Components of the thermal control subsystem

15 Structures

A collection of parts in a pile does not constitute a spacecraft. The role of the structures subsystem is to support all components of other subsystem to allow them to function as designed. The driving factors in the design of the structural subsystem is the positioning of components and surviving the launch loads to be compatible with the launch vehicle (SYS-001). As the design is in a very early stage of development no detailed structural analysis was performed. The overall design of the structural subsystem is discussed in Section 15.1, budgets are provided in Section 15.2 and the final design is shown in Section 15.3.

15.1. Sizing

To obtain a initial design of the structure, a CAD model was made of all subsystem components. These were arranged with their respective pointing and position needs. They were arranged to fit in a roughly cube like shape. Internal panels were added based on the SSETI Express spacecraft. The internal structure can be seen in Figure 15.1b. The internal structure is made from sandwich panels. The external sheets consist of thin monolithic panels, around 1 mm thick.

In addition to the main structural components to hold all components, the structural system has to accommodate a docked SSETI Express and the payload operations related to it. For this, thin plates extend from the outer shell on the docking side of SERUM. These plates can be seen on the left side in Figure 15.1a. These plates have to support the force that the Zond produces. As these forces are relatively low, approximately 500 N, these plates can be thinner than the external side panels. In addition the edges of the panels are made of a deformable material to prevent damaging SSETI Express.

15.1.1. Material Choice

The material of the outer panels is driven by the thermal subsystem (Chapter 14). This limits the material choices to anodized aluminum. The material of the sandwich panel and all other structural elements, the bulk material, is not limited by the thermal subsystem.

To determine the bulk material for SERUM, the environmental impact of aluminum alloys and carbon fiber composites (CFRP) was analyzed. The energy cost (i_e) in MJ/kg, CO2 footprint (i_c) in kg/kg and mechanical properties were taken from a level 1 material database [44]. Due to the vastly different specific strength ($\frac{\rho}{\sigma_{yield}}$) of these materials, 10 kg MN/m and 37.3 kg MN/m, Equation 15.1 was used to correct for this. From the results of this analysis, shown in Table 15.1, it is clear that there is no significant difference in CO2 footprint. Additionally the energy cost for both materials differs by only 7 %.

$$i_{corrected} = i \cdot \frac{\rho}{\sigma_{yield}} \tag{15.1}$$

Material	**Energy cost** [MJ MN/m]	**CO2 footprint** [kg MN/m]
Aluminium alloys	14.38	480
CFRP	15.38	485
Difference	7 %	1 %

Table 15.1: Results of environmental impact analysis for the production of aluminum alloys and CFRPs normalized to strength.

The study does not take into account the different weight of the satellite. Since a satellite made of CFRP will most likely be lighter than one made of aluminum alloys, CFRP is more environmentally friendly in the launch and transport phases. As this may be enough to off-set the lower energy cost, it is concluded that CFRP and aluminum alloys perform equally in terms of sustainability. In particular when considering that the material used in the spacecraft cannot be recycled after it burn up in the atmosphere. Therefore both CFRP and aluminum alloys should be considered in a more detailed design iteration.

15.2. Other Budgets

As no detailed design was performed for the structure, the cost and mass budgets where taken from the midterm report. In the midterm report a cost and mass estimation was made based on [3, Table 14-18].

Table 15.2: Mass budget contribution of example subsystem

Sub-components	**Cost [**kEUR**]**	**Mass** [kg]
Structure	2724	22
	2724	**22**

15.3. Conclusion

The design of the structure is shown in Figure 15.1. Figure 15.1a shows the external panels and the docking support. Figure 15.1b shows the internal sandwich panels.

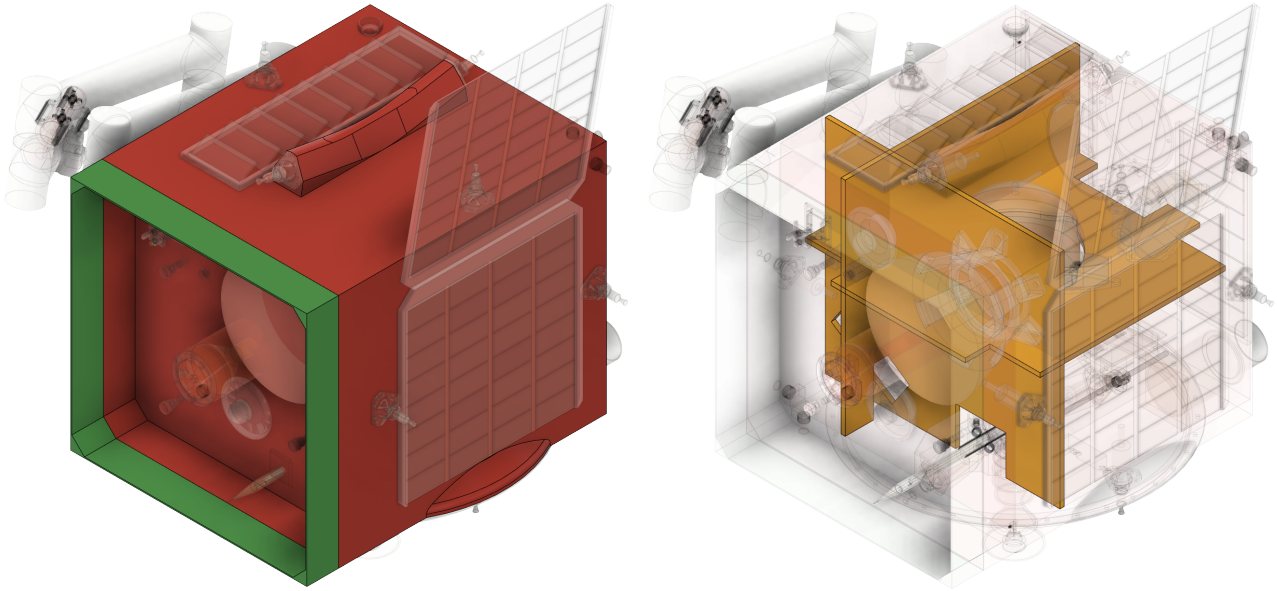

(a) External structure

(b) Internal structure

Figure 15.1: The structure subsystem as integrated in SERUM

16 Launch Vehicle

The launch vehicle (LV) to be used for this mission was already decided on in the midterm report. Section 16.1 describes why the SpaceX Falcon 9 24" full plate rideshare slot was chosen and Section 16.2 goes over its characteristics.

16.1. Launcher

There are several launchers that can bring SERUM to a 500 km Sun-Synchronous LEO (MIS-004) within the project budget of 20 MEUR (MIS-003) and without using solid propellant. Solid propellant cannot be used since it has a high chance of expelling particulates, thus creating space debris (which does not comply to MIS-008). The SpaceX Falcon 9 24" full plate rideshare slot was chosen as the best option for this project, since it is the cheapest one and it has the highest reliability. The launcher is partly reusable (good for sustainability reasons), has a big enough payload volume according to the first estimations of SERUM, and is flight proven.

16.2. Characteristics

The launch vehicle implies several constrains on SERUM. The chosen launch has a rideshare with a 24 inch diameter mechanical interface variant of the dispenser ring (the adapter and ring can be seen in Figure 16.1a and Figure 16.1b respectively). It allows the volume shown in Figure 16.2, with a base of 1219 mm by 1494.5 mm and a 90 deg cone extending 1416 mm. The maximum mass is 200 kg and it will cost 910 000 €[1].

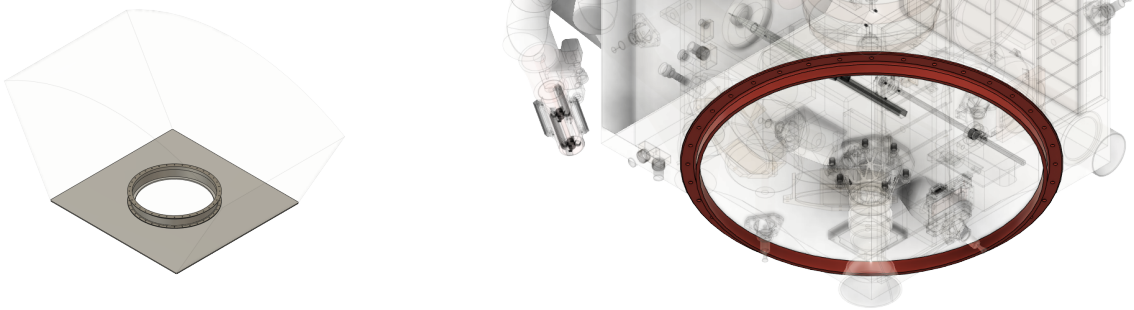

(a) The adapter

(b) The ring

Figure 16.1: The interface between SERUM and the launcher

As the volumetric limitations of Falcon 9 are very important for the design of the mission, the team must ensure that SERUM fits. Therefore, a CAD model of SERUM was placed inside a CAD model of the Falcon 9 rideshare volume. It was confirmed that the preliminary design of SERUM fits the launch volume as seen in Figure 16.3.

During the design of SERUM, the launch loads experienced in this specific launcher [74] have been taken into account in the choice of off-the-shelf components, as well as in the design of the structure (in order to meet SYS-001).

[1] https://rideshare.spacex.com/book/

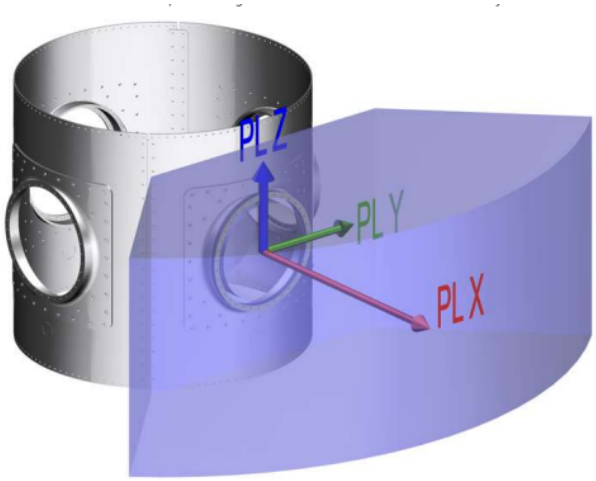

Figure 16.2: Falcon 9 Rideshare Volume [74]

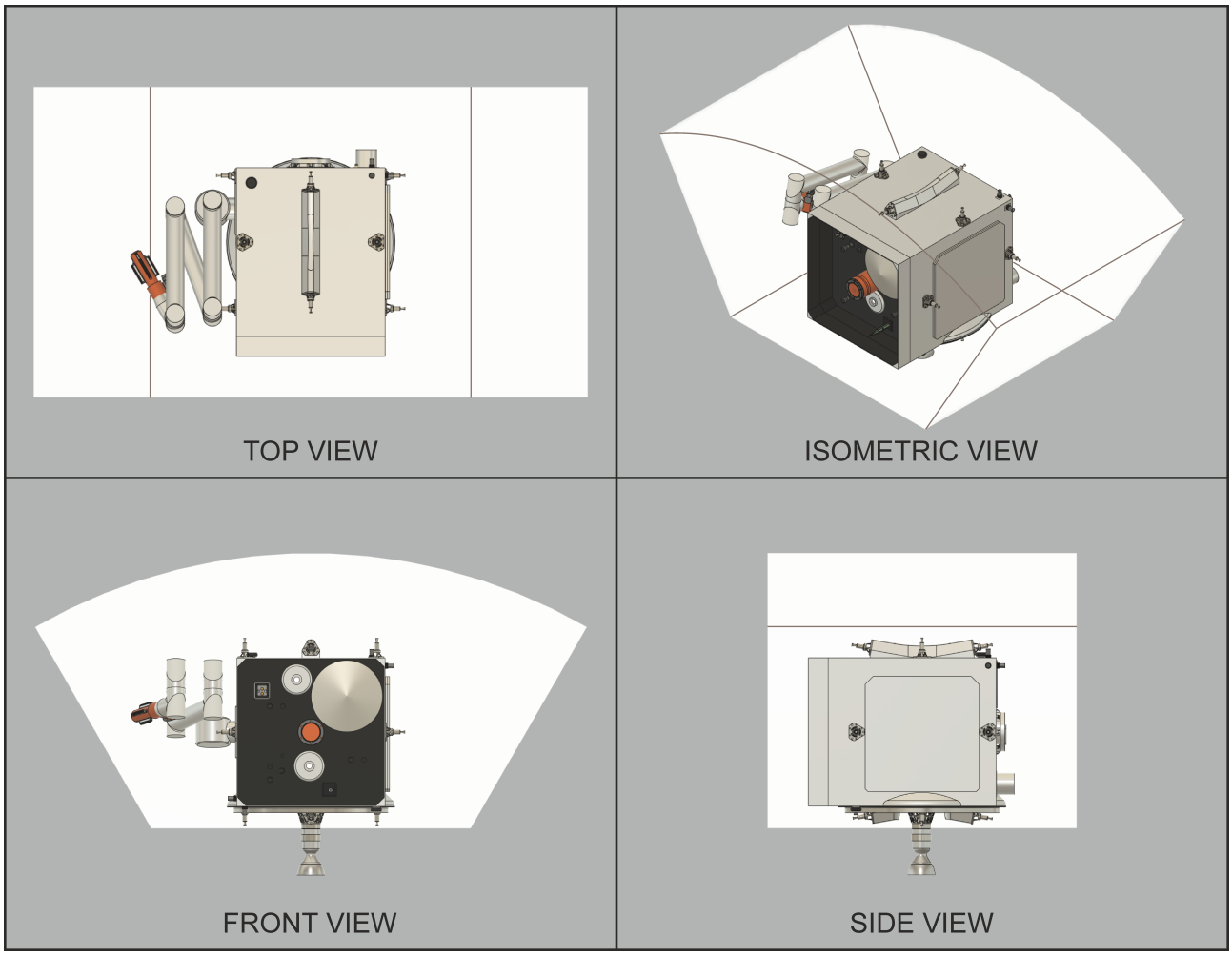

Figure 16.3: SERUM placed inside the launch volume

17 Astrodynamic Characteristics

In order to determine how SERUM needs to maneuver through space, an astrodynamic analysis is performed. This analysis aims at obtaining an efficient maneuvering plan for the mission. The propulsive transfer to SSETI Express as well as debris avoidance and end-of-life are considered.

In order to do an astrodynamical analysis, the order of maneuvers needs to be determined. Therefore, in Section 17.1, the astrodynamic maneuvering planning will be discussed. Afterwards, in Section 17.2, the method for determination of the orbits is discussed. Lastly, in Section 17.3, the observation orbit is presented and simulations are done for debris avoidance. The simulations also present how much propellant is needed, which allows for setting up a ΔV budget.

17.1. Maneuver Planning

SERUM will be released in a circular 500 km orbit by the launcher (sketched in Figure 17.1a). As SERUM will observe SSETI Express[1] before proceeding to docking (see Chapter 4), it will transfer from this circular orbit to an observation orbit first, as sketched in Figure 17.1b. This transfer will be achieved a Hohmann transfer, and thus two finite burns: first, the apogee will be raised, followed by raising the perigee of the transfer orbit.

The observation orbit is a relative elliptical orbit (as seen from SSETI Express' perspective) around SSETI Express with a semi-minor axis of 10 m and a semi-major axis of 20 m. The observation orbit will be maintained as long as required to observe SSETI Express, which is defined to be 1 month (Chapter 13).

If docking to SSETI Express is found to be safe, SERUM will approach SSETI Express to allow the docking mechanism to dock (Chapter 5), visible in Figure 17.2. In the budgets, this maneuver will be planned for multiple times, to account for failed docking attempts.

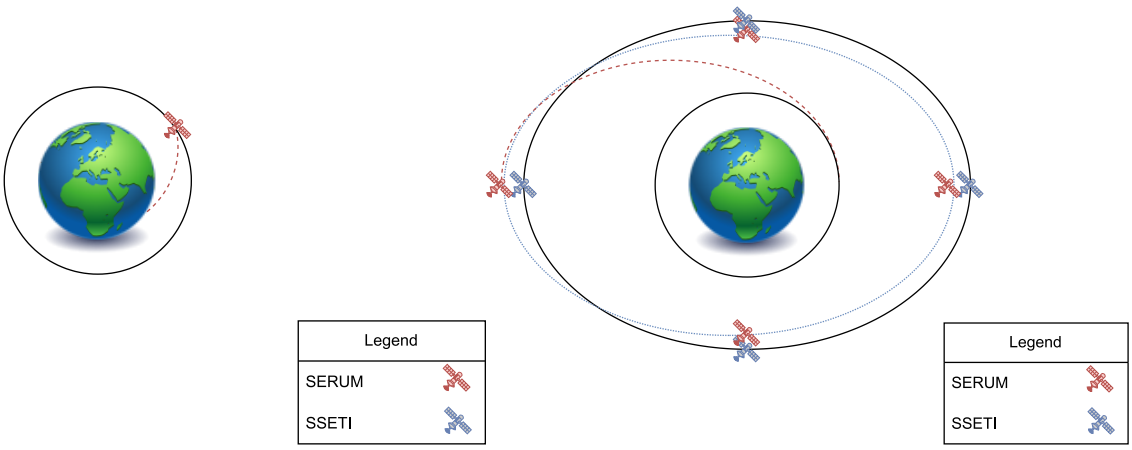

(a) Circular 500 km orbit

(b) Transfer to observation orbit

[1] Its perigee and apogee are retrieved from Space-Track, 681.1 km and 703.8 km respectively.

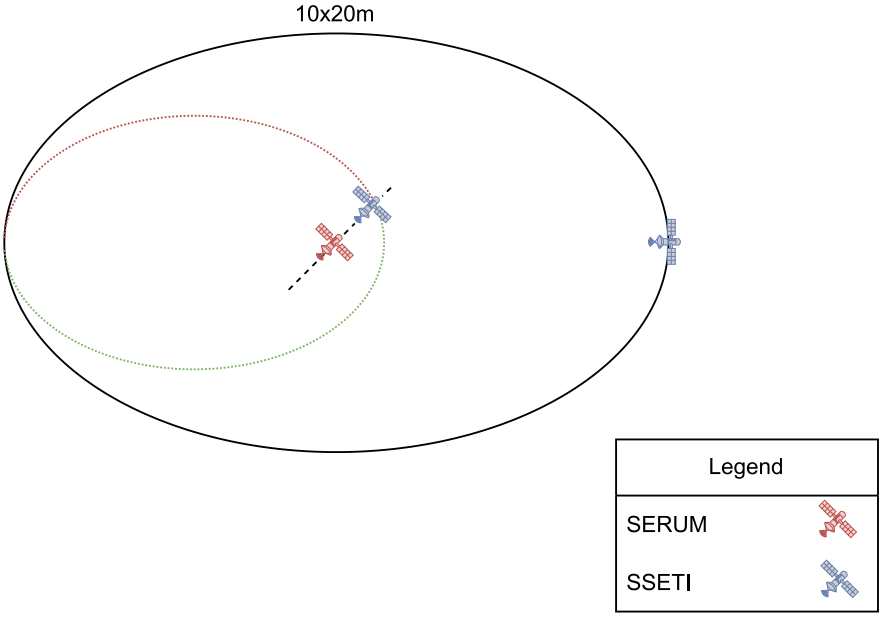

Figure 17.2: Relative observation orbit and approach maneuver

After SSETI Express has performed its mission or a de-orbit is initiated earlier in the mission (Chapter 4), a drag sail is deployed to increase orbit decay (Section 8.2). However, as found by a DRAMA simulation, some parts of the spacecraft will survive the re-entry burn. In order to control their landing positions, a controlled re-entry is required. For this, the thrusters present on the spacecraft will be used.

17.2. Relative Orbit Determination

SSETI Express will be observed from an observation orbit. This orbit will be designed relative to SSETI Express, based on relative orbits derived from [75] and work done by Dr. Gehly (Steve Gehly, interpersonal communication, June, 2023). It has been concluded that a semi-minor axis of 10 m and a semi-major axis of 20 m for this relative orbit is preferred.

The inertial position and velocity vectors of SERUM are:

$$\vec{d} = \vec{r_c} + [ON]^T \cdot \vec{\rho} \qquad (17.1)$$

$$\cdot\vec{r_d} = \vec{r_c} + [ON]^T \cdot (\frac{d\vec{\rho}}{dt} + n \cdot O_h x \vec{\rho}) \qquad (17.2)$$

The relative position and velocity vector of SERUM with respect to SSETI Express are:

$$\vec{\rho} = \begin{bmatrix} A_0 \cdot cos(n \cdot t + \alpha) \\ -2 \cdot A_0 \cdot sin(n \cdot t + \alpha) \\ 2 \cdot A_0 \cdot cos(n \cdot t + \beta) \end{bmatrix} \qquad (17.3)$$

$$\frac{d\vec{\rho}}{dt} = A_0 \cdot \begin{bmatrix} -n \cdot sin(n \cdot t + \alpha) \\ -2 \cdot n \cdot cos(n \cdot t + \alpha) \\ -2 \cdot \cdot sin(n \cdot t + \beta) \end{bmatrix} \qquad (17.4)$$

With these vectors, it is possible to determine the inertial orbital characteristics of the defined observation orbit. For this, the vectors were plugged into code obtained from Dr. Gehly to solve the unit vector matrix [ON]. From this, SERUM's position and velocity vector in the inertial reference frame can be calculated. The obtained vectors were propagated in GMAT in order to obtain SERUM's orbital parameters. α and β were taken as zero for simplicity. The semi-major axis of the observation orbit is then found to be $7063.449\,98$ km with an eccentricity of $0.001\,600\,244$.

17.3. Simulations & Final Results

With the orbital parameters known, the required propellant and burn times for the different maneuvers are evaluated. Therefore, in Subsection 17.3.1, the ΔV required to avoid debris to an acceptable collision probability level is calculated. In Subsection 17.3.2 and Subsection 17.3.3, the same thing will be done for the transfer

from the initial orbit to the observation orbit and the controlled de-orbit respectively. The final ΔV budget is then stated in Subsection 17.3.4. DRAMA and GMAT are simulation programs that can be considered reliable as they were made by ESA and NASA, respectively and are still used as professional tools for astrodynamics.

17.3.1. Lifetime ΔV Required for Debris Avoidance

As defined by SYS-005, SERUM is required to avoid debris during its mission. As avoidance maneuvers will be performed by the thrusters, an understanding of the amount of ΔV required for this is necessary. An estimation of this ΔV is based on DRAMA's program ARES, using an acceptable collision probability level of 1×10^{-6} Figure 17.3. When using one orbit around Earth to avoid the debris, the required ΔV for debris avoidance is $0.1\,\mathrm{m/s}$. Assuming one of these maneuvers per year, this equated to $0.8\,\mathrm{m/s}$ for the entire mission, implying a required propellant mass of $0.031\,\mathrm{kg}$ and a margin of $0.006\,\mathrm{kg}$.

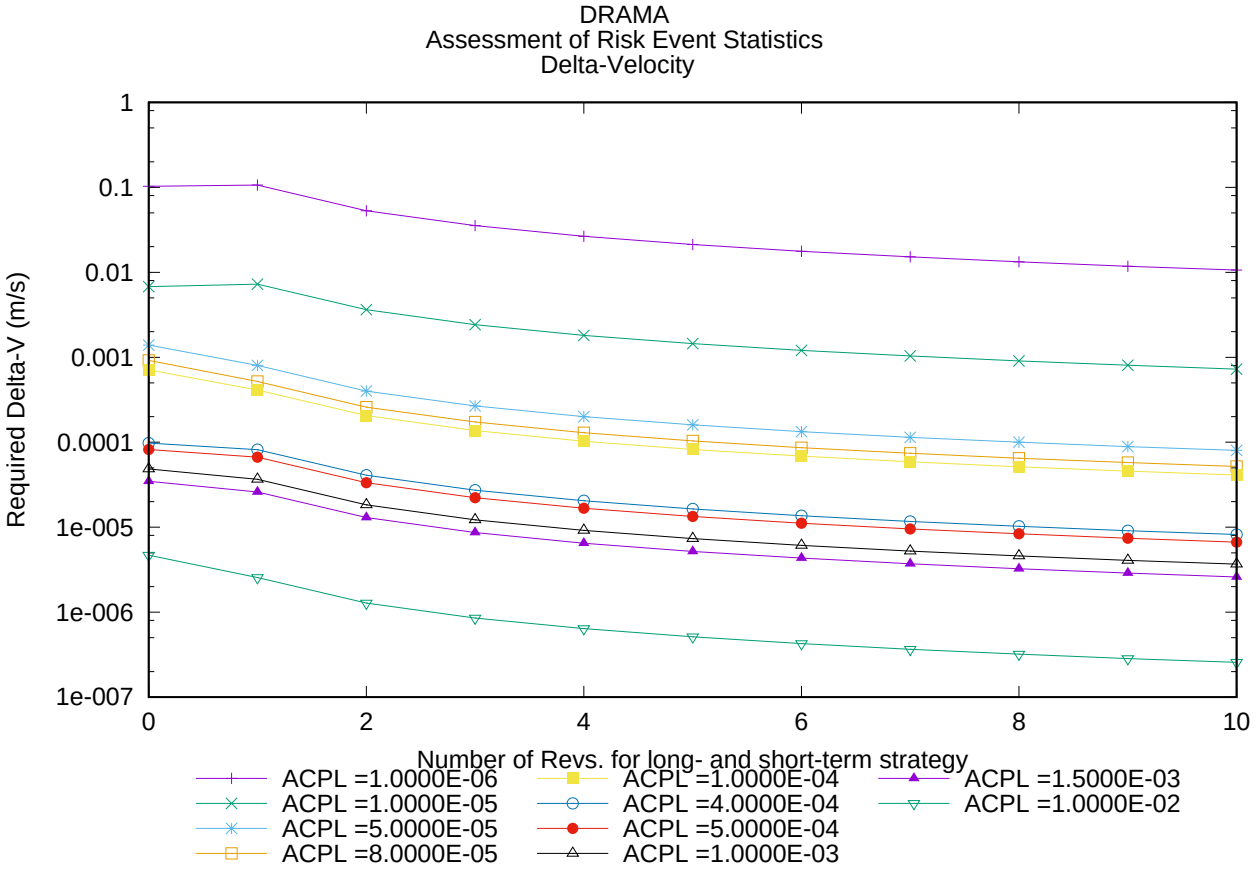

Figure 17.3: DRAMA Debris Avoidance Simulation

17.3.2. Transfer Maneuver Calculations

The ΔV required for the transfer is determined using GMAT. The simulation is constructed by defining SSETI Express with its mass and orbit, SERUM with its thruster, mass and initial orbit and the desired observation orbit. Applying the maneuvers described in Section 17.2, the simulation gave a required ΔV of $101.13\,\mathrm{m/sec}$ and a required propellant mass of $4.12\,\mathrm{kg}$ from Table 17.1 and Table 17.2. The two burns combined have a burn time of $445\,\mathrm{s}$.

Table 17.1: Data Summary for Apogee Change

Burn Time	228.88 s
Difference Achieved to Targeted	0.000 194 km
Propellant Needed	2.112 kg

Table 17.2: Data Summary for Perigee Change

Burn Time	217.12 s
Difference Achieved to Targeted	0.000 455 km
Propellant Needed	2.004 kg

For this phase of the design, a 20% margin was added to the propellant mass. This margin accounts for the approach, docking and other manoeuvres not taken into account yet. Therefore, an extra 0.824 kg of propellant will be budgeted.

17.3.3. End of Life Controllable Re-Entry

For the controlled de-orbit, a DRAMA simulation was performed, where the thrusters turn on at 140km altitude and make a targeted de-orbit to ground level. The simulation returned a required propellant mass of 2.06 km, as can be seen in the output data in Table 17.3.

Table 17.3: DRAMA Results for Propulsive De-Orbit

Title	General Output
Perigee altitude required to achieve direct de-orbit	0 km
Delta-V required	37.28 m/s
Propellant mass required	2.06 kg

17.3.4. ΔV Budget

With the data obtained, a ΔV and propellant mass budget can be set up. In the propellant mass budget, a margin of 20% is added to mitigate RI-PROP-1 , RI-PROP-3 and RI-PROP-4 (Chapter 19). The final budgets are listed in Table 17.4.

Table 17.4: Propellant & ΔV Budget

Maneuvers	**Propellant [kg]**	**ΔV [m/s]**
Transfer to Observation	4.12	104.54
Debris Avoidance	0.031	0.80
Controllable De-Orbit	2.06	54.06
Margin (20% Propellant)	1.242	30.64
	7.453	**190.04**

17.4. Conclusion

In conclusion, SERUM starts at a circular orbit of 500 km and transfers to an observation orbit with semi-major axes of 7063.449 98 km and an eccentricity of 0.001 600 244. The transfer will require 4.12 kg of propellant. From this observation orbit, SSETI Express will be approached prior to docking. 4.43 kg of propellant is reserved for debris avoidance during the mission and 2.06 kg of propellant will be required for a controlled de-orbit. As this is phase 0 of the design process, a margin of 20 % was put on the propellant mass. This will also account for approach, docking and unforeseen maneuvers not budgeted. SERUM will need 7.788 kg of propellant. For the next design phase, the propellant mass required for one docking attempt should be calculated. This will translate to a propellant mass. Depending on the mass, the spacecraft will cost more, which then translates to a customer decision on how many attempts can be done.

18 Development Strategy

The development of SERUM will be very specific and dedicated to this mission. However, as SERUM aims at demonstrating a concept, a general production of in-orbit servicing can be deduced from it. By producing such spacecraft on a larger scale, it is even more important to consider the sustainability of the design and mission, which is discussed in Section 18.1. Section 18.2 discusses the plan for manufacturing the satellite. Sourcing the components, as well as making a very preliminary plan for production will be showcased. Section 18.3 will then evaluate what parts of the production can potentially be scaled for servicing satellites.

18.1. Sustainability

As the world is more and more aware of the impact greenhouse gasses have on the environment, the consequences plastic has on ocean life and the difficulties space debris brings to novel missions, this project can not hide from its responsibilities in the field of sustainability. Sustainability in this project is implemented in two main ways, those being the sustainability of the physical satellite itself, and the sustainability of the mission concept overall, which are treated in Subsection 18.1.1 and Subsection 18.1.2 respectively.

18.1.1. Product sustainability

Sustainability played a big role in the development of the spacecraft itself. It was implemented top down, from the requirements.MIS-008 states that no toxic fuel can be used to propel the spacecraft. Hydrazine, the conventional spacecraft propellant, is a highly toxic substance and a known carcinogen, to which millions of workers in Europe are exposed each year [1]. For this reason, only 'green' propellants have been considered for propulsion, which are safer to handle and pose less of a risk in case of incidents. Another consideration was the impact of the launch vehicle. During its trade-off, sustainability was considered both in terms of propellant cleanliness but also re-usability, where re-usability has the benefit of both requiring less material and creating less waste. Furthermore, the design of the repair-payload is such that creation of chips, flakes or other forms of potential space-debris is completely avoided, thereby not polluting low earth orbit.

18.1.2. Mission sustainability

Also to consider, are the sustainability aspects of the mission concept as a whole. Firstly, the aspect of in-orbit repair: spacecraft service missions have the potential to reduce the amount of rocket launches by repairing aging spacecraft instead of replacing them. A single spacecraft can repair or service multiple satellites which would otherwise have had to be replaced, leading to a reduction in both launches but also overall material and development costs.

Additionally, there is the sustainability of debris-removal. With low earth orbit becoming more and more populated with satellites in the lower mass ranges, the possibility of catastrophic collisions increases. Due to its uncontrolled nature, large size and relatively stable orbit, SSETI Express poses a significant risk for orbital collisions with other uncontrolled objects. The prospects of actively removing uncooperative debris can be of great use in the fight against space-pollution, and this mission will demonstrate removal of the heaviest piece of space-debris to date.

18.2. Manufacturing, Assembly and Integration Plan

SERUM is a satellite that will be designed for the repair of SSETI Express specifically. As the spacecraft will be designed for this mission specifically (as seen in the design of for example the capturing mechanism Chapter 5), the manufacturing will not be standardized. However, as this mission aims at demonstrating in orbit servicing, one can think about scaling of the manufacturing of very similar spacecraft. This will be discussed in more detail in Section 18.3.

18.2.1. Development of Custom Components

The majority of the custom components are used by the payload. The bus subsystems can all be sourced from commercial components or TRL6 components as defined by requirement MIS-011 (the exact components can be found in their respective chapters). The expansion mechanism and the zond will be manufactured for SERUM specifically. They can be made in a workshop which allows for machining, extrusion, metal 3D-printing and post-processing. Also, rubber will need to be cut to specific dimensions for the expansion mechanism.

[1] https://roadmaponcarcinogens.eu/hydrazine

The piercing mechanism is a custom built hex tube with hardened tip and an electrically driven rack and pinion system. No new technological development is required, simply manufacturing the appropriate components. The tube itself can be extruded, while the tip CNC machined. The gear racks can then be welded onto the sided of the tube, although this will be challenging as they are fairly thin.

While the endoscope is a custom component, its development has already been mostly carried out by [14]. Only the tip of the tool, the wiretap, would be fully custom and developed in house. This is a very small and detailed component that would be best suited for 3D printing in high strength resin. The ceramic blade can milled from a larger block of material in the pre-sintered state, and the wire tapping blades should be made using EDM or a high precision CNC mill.

The other auxilliary components of the piercing and wiretapping system, such as the mounting sled and enclosure, can be machined conventionally as they are not complex parts. Many other components are off the shelf, such as the ball screw, motors and camera.

The bypass connector is a custom designed assembly and will be for the majority CNC-machined out of aluminium, with the compliant flexures machined from metal using EDM. For actuation it will use a commercial space-rated servo-motor.

Lastly, the majority of the software will also be developed for the mission specifically.

18.2.2. Manufacturing, Assembly and Integration

The big lines of the manufacturing process are outlined in Figure 18.1.

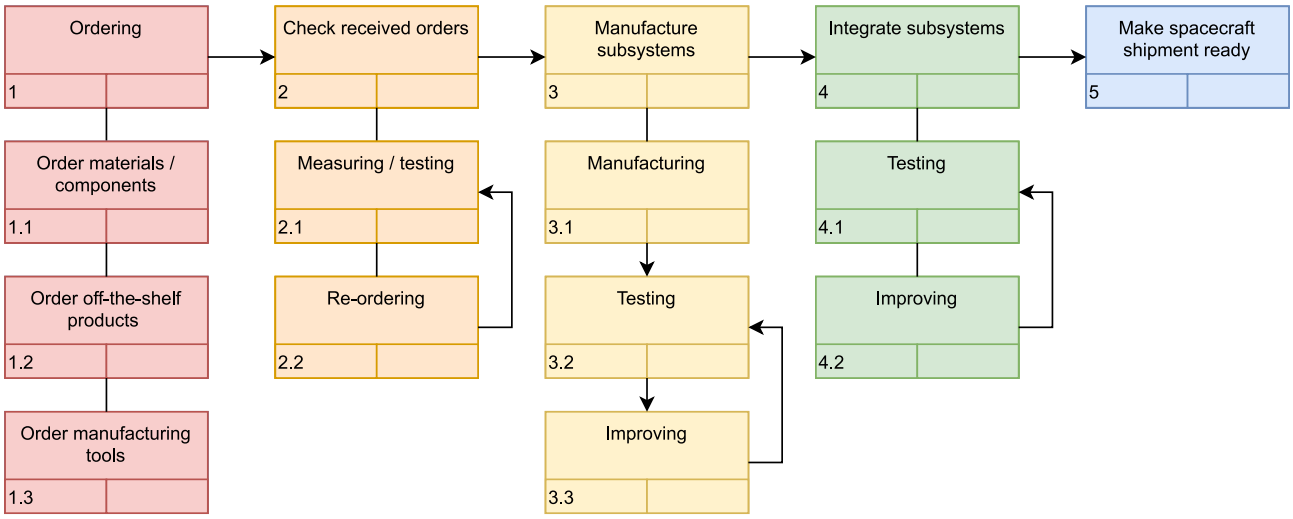

Figure 18.1: Manufacturing flow diagram

18.3. Potential for Production

Major parts of SERUM will be useful for other servicing satellites as well. If the endoscopic method will prove to be successful, this tool can be copied for other satellites. Its capabilities can be extended by making it compatible with more tool tips such as pliers and screw drivers. As done for medical endoscope, its production can be scaled up.

The bus can be standardized, similar to how this is done for CubeSats. The propellant tank can be scaled according to the mission, the tools onboard can be interchanged and the container can be discharded as no debris was created by the piercing. If there indeed is a market for the service this spacecraft can provide, the line production can even be considered, similar to how SpaceX manufactures its Starlink constellation [2].

[2] https://www.cnbc.com/2020/08/10/spacex-starlink-satellte-production-now-120-per-month.html

19 Risk Analysis

In order to ensure the successful completion of the mission, it is crucial to identify, assess, and mitigate potential risks that may arise during the execution of the mission. Therefore, this chapter contains a risk analysis. In Table 19.1, the technical risks are identified. Each risk is provided with a unique ID and name. The cause and consequence are described and a score for probability and impact is assigned. The scoring system is described below. Finally, a mitigation strategy is provided with the new probability and impact scores. This comprehensive assessment allows the team to be prepared for potential challenges and develop strategies to address them effectively.

19.1. Risk Assessment

The scale used for the probability is:

1. **Very unexpected:** The cause rarely occurs.
2. **Unexpected:** The cause has a low chance of happening during the mission.
3. **Medium probability:** The cause is expected to occur at least once during the mission.
4. **High probability:** The cause is expected to occur multiple times during the mission.
5. **Very high probability:** The cause is expected to occur on a regular basis.

And the scale used for the impact is:

1. **Negligible:** The consequence has negligible consequences on the mission objectives, schedule, or resources. The mission can continue as planned with little or no adjustments.
2. **Mild:** The consequence may result in minor disruptions, slight cost increases, or small adjustments to resources. The mission can still proceed with minimal modifications or additional efforts.
3. **Moderate:** The consequence has the potential to cause notable disruptions to the mission objectives, schedule, or resources. It may require considerable adjustments or reallocation of resources to keep the mission on track.
4. **Severe:** The consequence poses a significant threat to the mission's success. The mission objectives might still be met but in a less optimal way.
5. **Inhibiting:** The consequence has a critical impact on the mission. The mission objectives will not be (fully) met anymore.

Table 19.1: Risk identification

Risk code	Name of risk	Cause	Consequence	Probability	Impact	Mitigation	New Probability	New Impact
RI-0	Radiation	The presence of more radiation than accounted for in the spacecraft design.	Damage spacecraft and reduced structural performance.	2	3	Assess the radiation tolerance of components and shield the vulnerable ones.	1	3
RI-1	Solar flares	The presence of more solar flares than was designed for.	Damage spacecraft, reduced structural performance and potential shutdown of both spacecraft.	3	5	Implement hard reboot capability through an external watchdog.	2	4

Table 19.1 (continued)

Risk code	Name of risk	Cause	Consequence	Probability	Impact	Mitigation	New Probability	New Impact
RI-2	Micro-meteorites and space debris	Being hit by objects bigger or with more momentum than designed for.	Damage spacecraft with potential failure of systems.	2	5	Accept non-detectable ones, have contact with Earth for avoiding detectable ones. Shield such that small particles do not penetrate the skin.	2	3
RI-3	Human error	Human error during design, testing or operation.	Incorrect configuration, programming errors, equipment failure which can affect the systems performance.	3	2	Rehearse operations.	3	2
RI-4	Launch failure	Technical difficulties during launch.	Catastrophic failure such as explosion or malfunction that prevents spacecraft from reaching or being inserted in the wrong LEO.	2	5	Use a reliable launcher.	1	5
RI-5	System malfunction	Mechanical, electrical, or software errors.	Impact on spacecraft's ability to operate effectively.	2	4	Functional tests.	2	4
RI-6	Power failure	Problems with solar panels, batteries, or other power systems.	Loss of critical functions.	2	4	Power margin	2	3
RI-7	Running out of budget	Design can turn out more expensive, unexpected extra costs may appear or due to inflation parts become more expensive, geopolitics.	Need for more money or design simplification and adjustment.	4	2	Avoid dependence on one single component suppliers and apply budget margin.	3	2
RI-8	Failed startup sequence.	Once the spacecraft is outside the launcher initiates its mission, it fails to initiate.	System will remain inactive	1	5	Accept unavoidable risk.	1	5
RI-9	Not meeting set deadlines	Delays due to any problems.	Postponing launch, extra cost due to overtime.	4	2	Continuous tracking of progress and risk management	3	2
RI-COM-0	Signal Interference	The higher the frequency, the more prone a signal is to interference by atmospheric attenuation and rain.	Affect reliability and quality of communication.	2	4	Rain attenuation can be mitigation by either power restoral or signal modification restoral [76].	2	3

Table 19.1 (continued)

Risk code	Name of risk	Cause	Consequence	Probability	Impact	Mitigation	New Probability	New Impact
RI-COM-1	Limited Resources	Power, bandwidth and data storage capacity limited resources.	Limit systems performance or capabilities.	4	2	Requesting use of more bandwidth.	3	2
RI-COM-2	Cyber-security	System is vulnerable to cyberattacks such as hacking, malware and other forms of cyber threats.	Compromised integrity and confidentiality of communication system.	2	4	Coding and security.	1	4
RI-COM-3	Software Errors	Bugs or software errors in the communication subsystem.	Incorrect data transmission or reception, that can affect accuracy and reliability of the system.	4	4	Software verification.	2	4
RI-COM-4	Ground station (infrastructure) failure	Power outages, equipment failure, network congestion.	Affect subsystems performance.	1	3	Being able to pause manual control at every moment.	1	2
RI-COM-5	Incorrect antenna pointing for video stream	Spacecraft and ground station antenna are not properly aligned at moment of docking and repair.	Video stream can't be send down, compromising docking and repair.	2	5	Use of (multiple) omnidirectional antennas	1	5
RI-THE-0	Insufficient heat dissipation	Blocked radiator or general thermal system failure.	The spacecraft gets too hot causing some subsystems to malfunction.	2	5	Shut down components, increase dissipation surfaces.	1	5
RI-THE-1	Excessive heat dissipation	Errors or failure thermal design.	The spacecraft gets too cold causing some subsystems to malfunction.	2	5	Create heat source, redirect heat to parts that need it.	1	5
RI-THE-2	Active thermal control component failure	An active component of the thermal control system fails.	The temperature will not be raised or lowered as designed anymore causing subsystem malfunctioning.	3	5	Including redundant components.	1	5
RI-THE-3	Heat from SSETI Express	Activated SSETI Express generates unforeseen heat.	The spacecraft heats up and the heat dissipation might not be enough causing subsystem malfunctioning.	1	3	Connect in a way that heat from SSETI Express doesn't affect satellite.	1	2
RI-GNC-0	More power needed	The GNC system can at a certain moment require more power than is available.	The spacecraft will not have the desired attitude or other subsystems have less power available to them.	3	2	Include safety margin on power budget.	2	2

Table 19.1 (continued)

Risk code	Name of risk	Cause	Consequence	Probability	Impact	Mitigation	New Probability	New Impact
RI-GNC-1	Influence from SSETI Express	During docking the system and SSETI Express are close to each other.	The GNC performance can be influenced by both the system and SSETI Express.	2	3	Safety margins on power budget, delay until power is available.	2	2
RI-GNC-2	Component failure	A component of the GNC might fail.	Reduced performance in attitude control or no control at all.	2	4	Have redundancy.	2	2
RI-GNC-3	No control over SSETI Express	If the spin rates of SSETI Express are more than anticipated the GNC might not be strong enough to manage attitude when connected to SSETI Express.	Communication and power systems can function less as well as the payload of SSETI Express.	2	5	Safety margins on required torque.	1	5
RI-GNC-4	Counteracted by SSETI Express	The GNC of SSETI Express might counteract the movements of the systems GNC more than anticipated.	Reduced performance communication system, power system and payload of SSETI Express.	1	4	Don't perform GNC maneuvers when docked to SSETI Express, until communication with SSETI Express is restored.	1	2
RI-GNC-5	Sloshing instability	Propellant sloshing in the tanks causes tumbling or instability.	Reduced capability of fine maneuvers, structural failure.	3	5	Sloshing dynamics characterizations and anti-slosh tanks.	2	4
RI-GNC-6	Insufficient RCS propellant	Insufficient propellant budgetted for the GNC system.	Possible mission failure, decreased fuctionality, shortened lifetime.	2	4	Add safety margin to propellant budget.	1	4
RI-GNC-7	SSETI Express exhaust damage	Using RCS thrusters whilst in the vicinity of SSETI Express.	Possible failure of SSETI Express structure/components.	2	4	Don't use corrosive propellants.	1	4
RI-PAY-1	Inside of SSETI Express exposed to space environment	Holes created or components removed during operations.	SSETI Express can experience thermal and other damage inside.	2	3	Holes created or parts disassembled during repair will be covered during and after repair.	1	3

Table 19.1 (continued)

Risk code	Name of risk	Cause	Consequence	Probability	Impact	Mitigation	New Probability	New Impact
RI-PAY-2	Novel use in space	Use of technology that is not tested and proven to work in space.	Increased chance of failure.	3	4	For components, buy them at companies that did already make other components that were tested in space. Also build in redundancy.	2	3
RI-PAY-3	Missing a docking opportunity	Too slow or not prepared spacecraft.	Having to wait till next opportunity, increasing time and cost.	3	2	Schedule resources for missed opportunities.	3	1
RI-PAY-4	Damage during docking	Damaging SSETI Express to an extent that it loses function during docking.	SSETI Express broken and possible debris.	2	5	Dock only after ground station confirms successful capture.	1	5
RI-PAY-5	Technology not working	Docking mechanism does not work as expected.	Docking impossible.	2	5	Perform more extensive V&V for the payload.	1	5
RI-PAY-6	Docking breaking	Docking mechanism breaks due to contact with SSETI Express.	Broken docking system and possible debris generation.	2	5	Conservative capture and docking plan.	1	5
RI-PAY-7	Docking releasing	Docking mechanism realising in unplanned manner.	Docking needs to be re-attempted.	1	4	Accept unavoidable risk.	1	4
RI-PAY-8	High energy radiation	Single event effects such as bit-flip or single event transient [43].	OBC (On Board Computer) functioning not as intended.	4	5	Self error correcting memory, radiation hardened chips.	2	5
RI-PAY-9	System crash	System overloaded.	Computer permanently broken.	2	5	Implement external system watchdog.	2	5
RI-PAY-10	Hacking	Onboard computer is hacked.	System not functioning.	3	5	Security.	1	5
RI-PAY-11	Critical coding errors	Errors in the code.	System malfunction.	4	5	Code verification.	2	5
RI-PAY-12	Not working equipment	Repair system not working as intended.	SSETI Express cannot be repaired.	2	5	Extensive testing.	1	5
RI-PAY-13	Duration procedure	Gaining access to inside of SSETI Express takes too long.	Damaged or overheated equipment.	1	4	Take into account during equipment design.	1	3
RI-PAY-14	Shift in SSETI Express	Insides of SSETI Express have shifted around.	Repair site inaccessible.	1	5	Make repair mechanism more universal & flexible.	1	5

Table 19.1 (continued)

Risk code	Name of risk	Cause	Consequence	Probability	Impact	Mitigation	New Probability	New Impact
RI-PAY-15	Stuck repair	Cramped working environment.	Repair mechanism gets stuck inside before repair.	1	5	Accept unavoidable risk.	1	5
RI-PAY-16	Functionality not repaired	Planned repair does not restore functionality of SSETI Express.	SSETI Express cannot be fixed.	1	5	Accept unavoidable risk.	1	5
RI-PAY-17	Net fails to deploy	The net fails to deploy.	Catching impossible.	2	5	Have redundant components in the net system.	1	5
RI-PAY-18	Net misses the target	The net fails to hit SSETI.	SSETI is not caught making it impossible to de-orbit it.	1	5	Accept risk of failure of conditional back-up system.	1	5
RI-PAY-19	Net fails to close	The net fails to envelop and close around SSETI.	The net fails to secure SSETI.	1	5	Have redundant components in the net system.	1	5
RI-PAY-20	The net creates debris	The net during deployment and contact with SSETI causes the release of debris.	The creation of debris.	2	5	Test the net to know its deployment behaviour to determine better how, when and with how much force to deploy it.	1	5
RI-PAY-21	Net rips	The net when making contact with SSETI rips.	Failure to catch SSETI and creation of debris.	2	5	Have a margin on the strength of the lines of the net.	1	5
RI-PAY-22	Failed drag sail deploy	Mechanism stuck, commands not arriving, no power arriving, etc.	Mission not de-orbited in time.	2	5	Test the deploy of the drag sail and improve it based on found risks.	1	5
RI-PAY-23	Partly deploy drag sail	Mechanism getting stuck or sail getting tangled.	Slower de-orbiting.	2	4	Have a margin, so that with a not fully deployed sail it is still able to de-orbit in time.	2	2
RI-PAY-24	Drag sail creates debris	Component (of the sail or of the spacecraft) breaking off whilst unfolding or during operation.	Debris created.	2	5	Make sure it is positioned away from other system to prevent entangling.	1	5
RI-PAY-25	SERUM does not 'wake-up'	SERUM does not get out of its sleep mode at the end of the de-orbiting phase	No controlled de-orbot possible	2	5	Send a signal to SERUM from Earth initiating a reboot of the system	1	5
RI-PAY-26	Propulsion systgem failure EOL	The propulsion system does not work during the final EOL maneuver.	No controlled de-orbot possible	1	5	Accept risk.	1	5

Table 19.1 (continued)

Risk code	Name of risk	Cause	Consequence	Probability	Impact	Mitigation	New Probability	New Impact
RI-STR-0	Material imperfections	Inconsistent manufacturing conditions, age and wear, design flaws.	Decreased performance.	2	2	Include safety factors.	2	2
RI-STR-1	Damaged oxidation layer	Damage to material.	Possible cold welding.	2	2	Care-full assembly.	2	2
RI-POW-0	Static discharges	Higher voltage than designed for discharge.	Damage power system.	2	5	Providing paths for the safe discharge of static electricity.	2	2
RI-POW-1	SSETI Express power	SSETI Express draws more power than expected.	Drain batteries of spacecraft or overload electronics.	2	3	Putting an upper limit on the amount of power that can go to SSETI Express.	2	1
RI-POW-2	Entering SSETI Express	Getting access into SSETI Express takes longer than expected.	Drain batteries of spacecraft if energy intensive method and not in sunlight.	3	3	Allowing a pause in operations and do operations mostly in sunlight.	1	3
RI-PROP-0	Valve malfunction	Valve could stick open or closed.	Loss of some or all propulsive power.	2	5	Stress testing.	1	5
RI-PROP-1	Poor orbit injection	More ΔV required than expected.	Fuel shortage for mission.	3	4	Include a margin on fuel.	3	2
RI-PROP-2	Fuel Leak	Fuel leaking out of the spacecraft.	Loss in control ability and ΔV.	1	4	Choosing a non-conductive, non-corrosive fuel.	1	4
RI-PROP-3	Faulty fuel consumption estimation	The fuel used in estimated wrongly, changing the ΔV provided.	The empirical mass models are not accurate.	1	4	Put a margin on fuel.	1	2
RI-PROP-4	Not enough ΔV	Faulty ΔV budget due to inaccurate astronomical models.	Not enough ΔV to perform maneuvers.	2	4	Put a margin on the ΔV budget.	1	1
RI-PROP-5	Structural defects	Wrong load cycle/intensity estimation.	Failure.	2	4	Use load factors.	1	4
RI-PROP-6	Material Defects	Errors in the production of the material.	Critical Failure of the Component.	3	5	Non-Destructive Testing.	1	5
RI-PROP-7	Part manufacturing defects	Errors in the part manufacturing and assembly.	Possible mission failure caused by launch loads	2	5	Inspection and Testing.	1	5
RI-PROP-8	Part failure	Part has an unexpected early failure.	Inoperable Part.	2	5	Designing with part redundancy.	2	2

19.2. Risk Map

The identified risks are plotted in Table 19.3. In this map, areas of concern can be easily identified, focusing on the lower right corner. In Table 19.4 the risks after implementing the mitigation strategies are plotted. All of the risks with probability 4 and 5 have been mitigated to a lower probability. There are still some high impact risks, with the most important ones being in the cell with a probability of 2 and an impact of 5. These will be the risks that are monitored most closely.

Table 19.3: Risk map of the risks stated in Table 19.1, green cells indicate a low probability · impact and red a high probability · impact

Probability \ Impact	1	2	3	4	5
1			RI-COM-4, RI-THE-3	RI-GNC-4, RI-PAY-7, RI-PAY-13, RI-PROP-2, RI-PROP-3, RI-PROP-5	RI-PAY-14, RI-PAY-15, RI-PAY-16, RI-PAY-18, RI-PAY-19
2			RI-0, RI-GNC-1, RI-PAY-1, RI-STR-0, RI-STR-1, RI-POW-1	RI-5, RI-6, RI-COM-0, RI-COM-2, RI-PAY-23, RI-GNC-2, RI-GNC-6, RI-GNC-7, RI-PROP-4	RI-2, RI-4, RI-8, RI-10, RI-COM-5, RI-THE-1, RI-THE-2, RI-GNC-3, RI-PAY-4, RI-PAY-5, RI-PAY-6, RI-PAY-9, RI-PAY-12, RI-PAY-17, RI-PAY-20, RI-PAY-21, RI-PAY-22, RI-PAY-24, RI-PAY-25, RI-PAY-26, RI-POW-0, RI-PROP-0, RI-PROP-7, RI-PROP-8
3		RI-3, RI-GNC-0, RI-PAY-3	RI-POW-2	RI-PAY-2, RI-PAY-24, RI-PROP-1	RI-1, RI-THE-2, RI-GNC-5, RI-PAY-10, RI-PROP-6
4		RI-7, RI-9, RI-COM-1		RI-COM-3	RI-PAY-8, RI-PAY-11
5					

Table 19.4: Risk map of the risks after implementing the mitigation strategies stated in Table 19.1, green cells indicate a low probability · impact and red a high probability · impact

Probability \ Impact	1	2	3	4	5
1	RI-PRC 4	RI-COM-4, RI-THE-3, RI-GNC-4, RI-PROP-3	RI-0, RI-PAY-1, RI-PAY-13, RI-POW-2	RI-COM-2, RI-GNC-6, RI-GNC-7, RI-PAY-7, RI-PROP-2, RI-PROP-5	RI-4, RI-10, RI-COM-5, RI-THE-0, RI-THE-1, RI-THE-2, RI-GNC-3, RI-PAY-5, RI-PAY-10, RI-PAY-12, RI-PAY-14, RI-PAY-15, RI-PAY-16, RI-PAY-17, RI-PAY-18, RI-PAY-19, RI-PAY20, RI-PAY-21, RI-PAY-22, RI-PAY-24, RI-PAY-25, RI-PAY-26, RI-PROP-0, RI-PROP-6, RI-PROP-7
2	RI-POW 1	RI-GNC-0, RI-GNC-1, RI-GNC-2, RI-PAY-23, RI-STR-0, RI-STR-1, RI-POW-0, RI-PROP-8	RI-2, RI-6, RI-COM-0, RI-PAY-2	RI-1, RI-5, RI-8, RI-COM-3, RI-GNC-5, RI-PAY-24	RI-PAY-5, RI-PAY-6, RI-PAY-8, RI-PAY-9, RI-PAY-11
3	RI-PAY-3	RI-3, RI-7, RI-9, RI-COM-1, RI-PROP-1			
4					
5					

20 Budgets

Besides the link budget (Table 9.3), power budget (Table 13.1) and delta-v budget (Table 13.3), a mass and cost breakdown is done. These contain the mass and cost of all subsystems combined. Additionally, a margin of 20% is added. It is assumed that some subsystems might need a bit more margin and other might need less, but that in general 20% can be added to the total cost or mass. The final cost or mass with margin is then compared with the maximum cost and mass defined in the requirements, to determine if it is compliant. The cost and mass budgets for SERUM can be seen in Table 22.1 and Table 22.2, respectively.

Table 20.1: Spacecraft cost budget, based on the current design

Subsystem	**Cost Estimate [kEUR]**
Payload docking	5209
Payload repair	1910
Payload EOL	223
Structural	2724 [3]
Thermal	462 [3]
EPS	175
TT&C	536
GNC	411
Propulsion	799
Fuel	3.1 [77][78]
CDH	44
Launch	890
Integration, assembly and test	1987 [3]
Program level	3273 [3]
Ground support equipment	943 [3]
Total Cost	19589
Final cost + 20% margin	23507
Requirement	20000
	Compliant: No

Table 20.2: Spacecraft mass budget, based on the current design

Subsystem	**Mass Estimate [kg]**
Payload docking	16.4
Payload repair	2.4
Payload EOL	7.6
Structural	22
Thermal	2
EPS	3.3
TT&C	1.2
GNC	5.9
Propulsion	10.1
CDH	1.0
Other (balance + launch)	2.5 [3]
Total Dry Mass	74.3
Total Dry Mass + 20% margin	89.16
Main Propellant + 20% margin	7.5
Total wet mass + 20% margin	96.7
Requirement	200
	Compliant: Yes

For the mass budget, again SMAD is used for the other cost, as this is unknown in this phase of the design. The propellant mass is simulated in DRAMA. As can be seen, the total wet mass with margin is significantly under the budget stemming from the maximum mass allowed in the launcher. For the cost budget, no exact cost is known for the structural and thermal subsystem. The value chosen is therefore from SMAD. The same holds for integration, assembly and test, program level and ground support equipment. After the propellant mass is simulated in drama, its cost is calculated with the found cost per kg for LMP-103S. Furthermore, the cost budget is not compliant with the requirement, imposing a maximum of 20 kEUR. However, as this is a first phase of the design and, as mentioned above, some costs are a rough estimate, this is not considered a problem for now. Also, as discussed in Chapter 18, the design of SERUM could be extended to a larger scale production or possibly a series production. The standardization of the design will bring down the cost, making it possible to stay within budget. This simplification of a design and following series production was demonstrated by Apex[1].

[1] https://www.apexspace.com

21 Verification & Validation

A total of 245 requirements were established in the beginning and during the project. These were structured in such a way to allow people to work on their consecutive subsystems in parallel. In theory, once all subsystem requirements are verified, it becomes very straightforward to verify the higher level general system, mission, and eventually stakeholder requirements. For clarity reasons, not all requirements are included in this report; many subsystems have standard requirements which are repeated many times (for example: specific aspects in surviving LEO environment). In this chapter, a compliance matrix is shown in Section 21.1. Then some design observations with respect to the design requirements will be mentioned in Section 21.2, in Section 21.3 the verification methods will be reported and finally, the future validation of the design will be proposed in Section 21.4.

21.1. Compliance Matrix

The following tables show the compliance matrix for relevant requirements and where their verification is justified in the report.

Table 21.1: Stakeholder requirement compliance matrix

ID	Requirement	Verified	Compliance	Location
STH-001	The system shall comply with the EU space law regulations.	NO	Non-Compliant	N/A
STH-002	The system shall adhere to the communication protocols specified by the International Telecommunication Union (ITU) for space communication.	YES	Compliant	Section 9.3
STH-003	The system shall be compatible with the launcher.	YES	Compliant	Chapter 16
STH-004	The system shall be designed to prevent any damage which leads to loss of functionality of SSETI Express during operation.	YES	Compliant	Chapter 5
STH-005	The total mission cost shall not exceed 20 million euros.	NO	Compliant	Chapter 20
STH-006	The mission shall aim to restore SSETI Express' functionality.	YES	Compliant	Chapter 23
STH-007	The mission shall be completed within 8.00year.	YES	Compliant	Section 4.5
STH-008	No orbital debris shall be released.	YES	Compliant	Section 7.4
STH-009	The mission shall adhere to the agreements set in the outer space treaty.	NO	Non-Compliant	N/A

Table 21.2: Mission requirement compliance matrix

ID	Requirement	Verified	Compliance	Location
MIS-001	The mission shall enable SSETI Express to perform its mission objectives.	YES	Compliant	Chapter 23
MIS-002	The mission shall not generate any debris during any mission phase.	YES	Compliant	Section 7.4
MIS-003	The total mission cost (including launch and ground segment) shall be less than 20.00MEUR.	NO	Compliant	Chapter 20

Table 21.2: (continued)

ID	Requirement	Verified	Non- Compliant	Location
MIS-004	The mission shall be able to reach the target satellite orbit starting from a 500.00km Sun-Synchronous orbit.	YES	Compliant	Chapter 11
MIS-005	The mission shall be able to de-orbit SSETI Express within 25 years from the end of its operational lifetime.	NO	Compliant	Chapter 8
MIS-006	The mission shall adhere to the Dutch and UN space treaties and agreements.	NO	Non-Compliant	N/A
MIS-006-LEG-002	The system shall comply with radiation rules as stated in Council Directive 2013/59/Euratom.	YES	Compliant	Chapter 13
MIS-007	The mission shall de-orbit in case of mission failure.	YES	Compliant	Chapter 13
MIS-008	Non-toxic propellants shall be used.	YES	Compliant	Chapter 11
MIS-009	The mission shall be able to fix SSETI Express.	YES	Compliant	Chapter 23
MIS-010	The mission shall be executed in 8.00year.	YES	Compliant	Section 4.5
MIS-011	The system shall use a technology readiness level of at least TRL-6 for all non payload components.	YES	Compliant	Chapter 18

Table 21.3: System requirement compliance matrix

ID	Requirement	Verified	Compliance	Location
SYS-001	The system shall be compatible with the launch vehicle.	YES	Compliant	Chapter 16
SYS-002	The system shall survive launch.	YES	Compliant	Chapter 16
SYS-003	The system shall be able to dock to an uncollaborative satellite tumbling at a rate of 1.00rpm on one arbitrary axis.	YES	Compliant	Section 5.7
SYS-004	The system shall be able to de-orbit SSETI Express.	NO	Compliant	Section 21.2
SYS-005	The system shall include an automatic escape sequence to avoid impact with SSETI Express.	YES	Compliant	Section 10.2
SYS-006	The system shall survive the low Earth orbit environment.	NO	Compliant	Section 21.2
SYS-007	The system shall be able to keep functioning when docked to SSETI Express.	YES	Compliant	Chapter 23
SYS-009	The system shall survive at least 8.00year in orbit.	YES	Compliant	Section 4.5
SYS-010	The system shall be able to gain access to the inside of SSETI Express.	YES	Compliant	Subsection 6.3.2
SYS-011	The system shall dock to SSETI Express without impairing the functionality of the satellite.	YES	Compliant	Section 5.1
SYS-012	Accessing SSETI Express shall not happen later than 1 year into the mission lifetime.	YES	Compliant	Section 4.5

Table 21.4: Subsystem requirement compliance matrix

ID	Requirement	Verified	Compliance	Location
SYS-006-CDH-000	The CDH subsystem shall survive the low Earth orbit environment.	NO	Compliant	Chapter 10
MIS-004-CDH-001	The CDH subsystem shall be able to navigate to SSETI Express after being released from the launcher.	YES	Compliant	Section 10.2
SYS-004-CDH-001	The CDH subsystem shall support a controlled end-of-life phase of the mission.	NO	Compliant	Section 10.5
DOCK-001-COMM-001	The communication subsystem shall be able to acquire 2 way communication with Earth ground stations.	YES	Compliant	Section 9.6
DOCK-001-COMM-002	The communication subsystem shall have an uplink data rate of at least 10000.00bps	YES	Compliant	Section 9.3
DOCK-001-COMM-003	The communication subsystem shall have one downlink system with a data rate of at least 5.00Mbps.	YES	Compliant	Section 9.3
DOCK-001-COMM-007	The communication subsystem shall account for losses.	YES	Compliant	Section 9.3
DOCK-001-COMM-010	The communication subsystem shall have one downlink system with a data rate of at least 30.00kbps.	YES	Compliant	Section 9.3
DOCK-001-COMM-006	The communication subsystem shall account for noise.	YES	Compliant	Section 9.3
SYS-003-DOCK-002	The docking system shall dissipate static discharge between the system and SSETI Express with a voltage of at most 400.00V.	YES	Compliant	Chapter 5
MIS-005-DOCK-001	The docking subsystem shall be able to remain docked to SSETI Express for the entire duration of deorbiting.	YES	Compliant	Section 5.3
SYS-010-DOCK-001	The docking subsystem shall not obstruct access to the inside of SSETI Express.	YES	Compliant	Section 5.5
MIS-010-DOCK-001	The docking subsystem shall perform the capture procedure in 2 minutes from when the spacecraft have a distance of at least 0.5m with no relative velocity.	YES	Compliant	Chapter 5
SYS-011-DOCK-001	The docking subsystem shall not impair the functionality of SSETI Express.	YES	Compliant	Section 5.1
SYS-007-DOCK-001	The docking subsystem shall maintain a rigid connection when docked to SSETI Express.	YES	Compliant	Section 5.3
SYS-003-DOCK-001	The docking subsystem shall be able to dock to an un-collaborative satellite tumbling at a rate of 1.00rpm on one arbitrary axis.	YES	Compliant	Chapter 5
MIS-002-DOCK-001	The docking subsystem shall not generate any debris while docking to SSETI Express.	YES	Compliant	Section 5.1
DOCK-001-OBS-001	The docking subsystem shall be able to determine the range and bearing of SSETI Express during the observation phase from a distance of 1.00km.	YES	Compliant	Subsection 5.4.1

Table 21.4: (continued)

ID	Requirement	Verified	Non- Compliant	Location
DOCK-001-OBS-002	The docking subsystem shall be able to determine the 6DOF pose of SSETI Express during the observation phase from a distance of 10.00m between the center of gravities of both spacecraft.	YES	Compliant	Subsection 5.4.2
DOCK-001-OBS-003	The docking subsystem shall be able to determine the 6DOF pose of SSETI Express during the docking phase from a distance of less than 10m and more than 1.5m between the centre of gravities of both spacecraft.	YES	Compliant	Subsection 5.4.2
DOCK-001-OBS-004	The docking subsystem shall be able to track the T-POD of SSETI Express during the docking phase from a distance of less than 2m and more than 0.2m from the T-POD.	YES	Compliant	Subsection 5.4.3
MIS-007-EOL-001	The end-of-life system shall de-orbit the spacecraft in case of mission failure.	YES	Compliant	Chapter 8
SYS-004-EOL-001	The end-of-life system shall deorbit SSETI Express in case of unsuccesful docking.	YES	Compliant	Chapter 8
MIS-005-EOL-001	The end-of-life system shall deorbit SSETI Express within 25 years.	YES	Compliant	Chapter 8
SYS-004-EOL-002	The end-of-life system shall deorbit SSETI Express in case of succesful docking.	YES	Compliant	Chapter 8
SYS-007-GNC-001	The GNC system shall be able to function while docked to SSETI Express.	YES	Compliant	Section 12.5
MIS-008-GNC-001	The GNC system shall not make use of toxic propellants.	YES	Compliant	Section 11.2
SYS-005-GNC-001	The GNC system shall be able to perform a SSETI Express avoidance manoeuvre in a timeframe of 10s.	YES	Compliant	Section 12.7
SYS-011-EPS-001	The EPS shall be able to replace any electrical functionality loss incurred by SSETI Express as a result of docking.	YES	Compliant	Section 13.5
MIS-009-EPS-001	The EPS shall be able to provide 20W of power to SSETI Express.	YES	Compliant	Section 13.5
MIS-008-PROP-001	The propulsion subsystem shall use non-toxic propellants.	YES	Compliant	Section 11.2
MIS-004-PROP-002	The propulsion subsystem shall provide a delta-V of 101.00m/s.	YES	Compliant	Subsection 17.3.4
SYS-004-PROP-001	The propulsion system shall provide a final end of life burn with a Delta V of 37.53 m/s.	YES	Compliant	Chapter 11
MIS-001-REP-001	The repair system shall be able to return SSETI Express to nominal functionality.	YES	Compliant	Section 6.7
MIS-002-REP-001	The repair subsystem shall not generate any debris while repairing SSETI Express.	YES	Compliant	Section 7.4
SYS-010-REP-001	The repair system shall be capable of gaining access to the inside of SSETI Express.	YES	Compliant	Subsection 6.3.2
MIS-009-REP-001	The repair system shall be able to reach the EPS of SSETI Express.	YES	Compliant	Subsection 6.3.3
MIS-009-REP-002	The repair system shall be able to determine if SSETI Express was successfully fixed.	YES	Compliant	Section 6.5

Table 21.4: (continued)

ID	Requirement	Verified	Non- Compliant	Location
SYS-002-STR-001	The structure shall survive launch loads.	YES	Compliant	Chapter 15
SYS-001-STR-001	The structure shall fit within its slot in the (rideshare) vehicle.	YES	Compliant	Chapter 16
SYS-001-STR-002	The structure shall be able to interface with the launch vehicle (rideshare) slot.	YES	Compliant	Chapter 16
SYS-006-TCS-014	The thermal control subsystem shall keep the internal spacecraft temperature between 49.85degC and 10.00degC during the operational mission lifetime.	NO	Compliant	Section 14.2

It is visible that requirements STH-001, STH-005, STH-009, MIS-003, MIS-005, MIS-006, SYS-004, SYS-006, SYS-006-CDH-000, SYS-004-CDH-001, and SYS-006-TCS-014 are not verified. The next section will delve deeper into why this is the case.

21.2. Design Observations

First, we shall investigate STH-001, STH-009, and MIS-006 (the latter two are essentially the same). These are all requirements related to the legality of SERUM. During design, the team put in effort making sure that chosen components and operations are legal; verification of the legality of every aspect of the mission is unfeasible within the scope of the project and with the expertise of the team. However, up until this point in the design, no international treaties are violated, as far as the team knows. In further detailed iterations, it is advised to consult people with legal competence. The requirements are also non-compliant as they are not mentioned in detail in the report.

The next non-verified requirements is the requirement to stay within financial budget (STH-005 and MIS-003), as can be seen in Chapter 20, the whole mission cost will probably not stay below 20 MEUR .

Then a bigger issue is revealed in the following requirements: MIS-005 and SYS-004. These relate to the ability of the system to de-orbit SSETI Express within 25 years. As was mentioned in Section 8.2 the system shall need to de-orbit SSETI Express in a controlled manner. This stems from the non-verified SYS-006 requirement. The command and data handling subsystem cannot reasonably survive 21 years in orbit to give control commands (SYS-006-CDH-000 and SYS-004-CDH-001) while the thermal control system's ability to control the internal temperature for this long period is unverifiable (SYS-006-TCS-014). The collection of these unfeasible requirements causes the current design to be inadequate to perform the full mission and thus, it is necessary to perform a first iteration on the design (see Chapter 22).

21.3. Verification

This section will describe the verification methods used to verify the requirements. The following methods were used:

- **Review**: requirement is verified by reviewing research papers or spec sheets, or there is high confidence that the system can be designed to comply with the requirement.
- **Analysis**: requirement is verified by performing mathematical analysis or numerical models.
- **Inspection**: requirement is verified by inspecting the CAD model.
- **Test**: requirement is verified by performing a test.
- **Child requirement verification**: requirement is verified if all child requirements are verified.

The final method is a custom verification method for high level stakeholder, mission and system requirements. All subsystem requirements are either linked to these higher level requirements, or other subsystem requirements. They are called "child requirements". for example: SYS-006 (the system shall survive LEO environment) is connected to all subsystems with the identifier SYS-006-SUBSYS-XXX (like SYS-006-CDH-000 and SYS-006-TCS-014), once all subsystems are verified to be able to survive LEO, this means the system itself shall survive LEO.

Table 21.5: Verification methods for subsystem requirements in Table 21.4

Verification method	Requirement
Review	MIS-004-CDH-001, DOCK-001-COMM-001, DOCK-001-COMM-002, DOCK-001-COMM-003, DOCK-001-COMM-007, DOCK-001-COMM-010, DOCK-001-COMM-006, SYS-003-DOCK-002, MIS-005-DOCK-001, SYS-007-DOCK-001, MIS-002-DOCK-001, SYS-004-EOL-001, SYS-004-EOL-002, SYS-007-GNC-001, MIS-008-GNC-001, SYS-005-GNC-001, SYS-011-EPS-001, MIS-008-PROP-001, MIS-004-PROP-002, SYS-004-PROP-001, MIS-009-REP-001, MIS-009-REP-002, SYS-002-STR-001, SYS-001-STR-002
Analysis	MIS-007-EOL-001, MIS-005-EOL-001, MIS-010-DOCK-001, SYS-010-REP-001, MIS-009-EPS-001, SYS-003-DOCK-001, DOCK-001-OBS-001
Inspection	SYS-010-DOCK-001, SYS-011-DOCK-001, SYS-001-STR-001
Child verification	DOCK-001-OBS-002, DOCK-001-OBS-003, DOCK-001-OBS-004, MIS-001-REP-001
Test	MIS-002-REP-001

21.4. Validation

Models can be validated in three ways. The first is by experience, with application of similar models in similar circumstances. Secondly, analysis can be done to show that elements of the model are correct and are correctly integrated. Finally, the model can be compared with test cases in the form of independent models of proven validity or actual test data [79]. This is done by letting the model run multiple simulations with the same experimental data to produce compatible data sets.

Once a model is created, an analysis can be conducted on the assumptions made for creating the model. By showing that the effects are small, the assumptions themselves can be validated. Once large deviations arise, this may indicate a bad assumption resulting into a lower accuracy for the model.

Several technologies and techniques proposed for this mission are novel and will need to be validated before being put into use, these technologies are identified as the following:

- Docking maneuver to a tumbling object
- Docking arm expander mechanism
- Zond mechanism
- Bypass system
- Piercing method
- Endoscope technology
- General spacecraft characteristics

For each of these points, a validation strategy will be discussed.

Docking manuever to a tumbling object Docking to a tumbling, uncooperative object in orbit is a challenging task and the procedure will have to be validated before it is performed. A proposed validation method is simulating variations of the docking scenario in a Monte Carlo type simulation, thereby validating the image processing systems, control algorithms and general docking procedure.

Docking arm expander mechanism The docking arm expander mechanism is a custom component that will grab into the T-POD to dock. To validate this system, it is proposed to make a test-setup to test the correct application of forces applied and friction experienced, by rehearsing the grabbing action with a replica T-POD on earth.

Zond mechanism Similarly, the zond mechanism is a custom part as well, which will grab into the hole in the lower honeycomb panel of SSETI Express. Again, it is proposed to test the full setup on earth with a replicated part of SSETI Express, measuring the clamping forces induced by the mechanism.

Bypass system The bypass system will charge SSETI Express' battery directly by accessing the battery charge stud. This system can be tested beforehand on a mock-up of the battery circuit of SSETI Express, thereby proving it can be successfully used to charge the battery.

Piercing method It has been demonstrated by the team in Chapter 7, that aluminium honeycomb panels can be pierced without generating debris of any kind. This is deemed as validation of the piercing method as it has shown correct functioning of this method according to the system requirements. Further tests could be performed with the piercing mechanism in the setup as it is expected to be in the final satellite.

Endoscope technology The endoscope is custom developed for this mission and its function will also need to be validated before deployment. A proposed validation method is to test it in a mock-up of the internals of SSETI Express, testing if it can perform its function and if any issues arise.

General spacecraft characteristics The general functioning of the spacecraft will also need to be validated before launch. Typical methods can be applied here, such as: FEM analysis, vibration testing, vacuum chamber testing of thrusters and simulating space conditions. These tests will ensure that the spacecraft will be able to function in the environment of low earth orbit.

Overall, these validation processes involve a combination of simulations, tests on Earth using replicated components, and specific validation methods tailored to each technology or component. This validation approach helps ensure the reliability and functionality of the systems and technologies proposed for this mission.

21.5. Conclusion

In this chapter, verification and validation of the design was discussed. First, a compliance matrix containing some of the 245 requirements was set up. It shows the requirement and whether it is verified, compliant and if so, where in the report the compliance can be found. After that, the requirements that are not verified (yet) were elaborated on. All the requirements are kept in Valispace., where they are connected through so called parents-children links. This allows for the parents to be verified if the children are all verified. Parent-child verification is one of five methods to verify the requirements in the compliance matrix, others are: review, analysis, inspection and test. Finally, validation of the design was discussed. For the novel technologies discussed in this report, a validation method was proposed.

22 First iteration

This chapter will present an iteration on the design presented. The change will be explained in Section 22.1. Section 22.2 till Section 22.7 will elaborate on the effects of this change on the affected subsystems. Lastly, the budgets will be updated in Section 22.8.

22.1. Mission Change

During the design phase treated in this report, it was discovered that a controlled de-orbit indeed is necessary, since not all components will burn-up in the atmosphere. It also was decided that this would not be done using a controllable drag sail, since the state of development of controllable drag sails is not far enough to be able to be developed further during this project, also because for the docking and repair phase there is already a lot of development needed. Moreover, since not creating debris is an important requirement (MIS-002), a de-orbit method with a high TRL is preferred. Therefore, the only viable option was to use the propulsive system for de-orbiting. Either for the final burn after lowering the orbit using a drag sail, or for a fully propulsive de-orbit. Initially, the choice was made for a final propulsive burn, since that would make the mass of the de-orbiting system three times lower than in the case of a fully propulsive de-orbit. A fully propulsive de-orbit would also mean that more than twice the amount of propellant would be used for de-orbiting than for getting to SSETI Express. This was not deemed logical, since the EOL subsystem is only a part of the total mission.

However, once the mass budget estimated in this design phase was finished, it turned out that SERUM is still lighter than the upper boundary on the mass given by the maximum mass that can be carried by the current chosen ride share launch (as explained in Chapter 16). Meaning mass is not that much of a limiting factor anymore. Along the way, it was also discovered that the 21 years of being in sleeping mode, was a complex requirement to be met by a lot of subsystems. Also keeping in mind that currently the regulations are going towards a desired de-orbit time of five years [1], it now seems way more efficient to design for a fully propulsive de-orbit. Increasing the size of the drag sail would also lower the de-orbit time, but it would still be in terms of years and not be as quick as a fully propulsive de-orbit. This chapter will go over the subsystems that are affected by this choice and mention the changes. The dry mass estimation that will be used for describing the subsystem changes will be the dry mass resulting from the mass budget described in Chapter 20.

22.2. Simulations & Astrodynamics

DRAMA and GMAT were used to resimulate the required fuel needed for maneuvers till the de-orbit phase, which resulted in 12.912 kg fuel needed, with 20% margin. For the propulsive de-orbiting 5.316 kg propellant is needed, with 20% margin. Leading to a total propellant mass of 18.228 kg.

22.3. Payload - End of Life

Now that is chosen for a fully propulsive de-orbiting method, the propulsion tank will be made bigger since a fully propulsive de-orbit will need more fuel than just a final burn. The drag sail will still be included, to mitigate the risk of the propulsion system failing and not being able to do the de-orbiting. In that case, it will not be a controlled de-orbit anymore, however, the requirement of de-orbiting within 25 years (MIS-005) will still be met. The net system will stay the same. Section 22.8 shows the updated subsystem budgets, for the EOL subsystem the drag sail and net values stay the same and the updated values for the propulsion system will be included in the propulsion budget.

22.4. Electrical Power System

The 21 years of de-orbit affected the EPS considerably. Doing a propulsive de-orbit will therefore change the design. First of all, the probability of the components surviving rises. Next to that, the weight of the system will go down, as there is no need for a super-capacitor anymore. As the propulsive de-orbit burn takes longer than the transfer orbit, it will not be done in one go. Rather, it will be done in a staged manner, where in every orbit, the solar panels will charge the battery while heating the 1N thrusters (which leaves 51.92 W for charging the battery). When the battery is fully charged, the reaction wheels will orient SERUM and SSETI Express and a burn will be performed.

[1] https://spacenews.com/fcc-approves-new-orbital-debris-rule/#:~:text=Under%20the%20new%20rule%2C%20spacecraft,the%20end%20of%20their%20mission.

22.5. Command & Data Handling

Due to the propulsive de-orbit the CDH computer's required lifetime reduces from 21 years to 8 years and potentially even less. 8 years stems from the user requirements (STH-007), but it is expected that the mission nominally will survive 2 years. The designing for 8 years thus makes the design more reliable and adds redundancy. This is within the operational life of some off-the-shelf CDH computers. For example, the Eddie OBC could be used [2]. It is thus no longer needed to have a special, radiation hardened computer, which lowers the cost.

22.6. Propulsion

To perform a fully propulsive burn, additional fuel is required. Using the information from Section 11.6, the propellant tank would need to have 8.7 L more volume to be able to store the additional 10.76 kg of fuel. Since the spherical fuel tank does not have a big enough volume, a cylindrical extension section is required. Given a propellant density of 1.24 g/cm, the length of the extended section can be calculated using Equation 22.1.

$$l_{extention} = \frac{V_{req} - \frac{4}{3}\pi r^3}{\pi r^2} \tag{22.1}$$

This results in a height increase of 20 cm, just fitting in the current architecture of SERUM as shown in Figure 22.1. The tank mass will increase by 401 g. Other than the increase in mass and volume, the power and cost will also increase.

22.7. Thermal Control System

Not having the 21 year sleeping period, in which the aluminum side panels degrade, will make the design of the thermal control subsystem a lot easier. The louvers can be removed and fully passive control is now possible. However, the active thermal components like the heaters will be kept as a risk mitigation strategy. Because of this iteration, the thermal control system will be more reliable and verifiable. The requirement of keeping the necessary temperate range during SERUM's operational lifetime (SYS-006-TCS-014) can now be met. Also the mass and cost will be reduced (it is assumed that the cost is halved as fewer extra components are needed for heat transfer and the louver mass is removed).

22.8. Cost and mass budget

With the changed design, also the cost and mass budget are set up again. In **bold**, the values that are changed can be seen. For the payload EOL, the drag sail and net mass are included, the propellant and tank mass for EOL are included in the propulsion budget. The thermal subsystem mass and cost also changes. This leads to a new dry mass and thus new fuel mass. This then leads to a new fuel cost as well, also changing the total budget.

Table 22.3 shows the change in mass and cost before and after the second iteration. As can be seen, the cost goes down with the second iteration. Now, the cost is still over budget, but less than for the first iteration. The mass went up, but this is not a problem as it is still well below the requirement of 200 kg.

Table 22.3: Comparison of cost and mass before and after the second iteration

	Cost	**Mass**
Before iteration	23507	96.7
After iteration	23235.6	105.9

[2] https://satsearch.co/products/spacemanic-eddie-the-on-board-computer

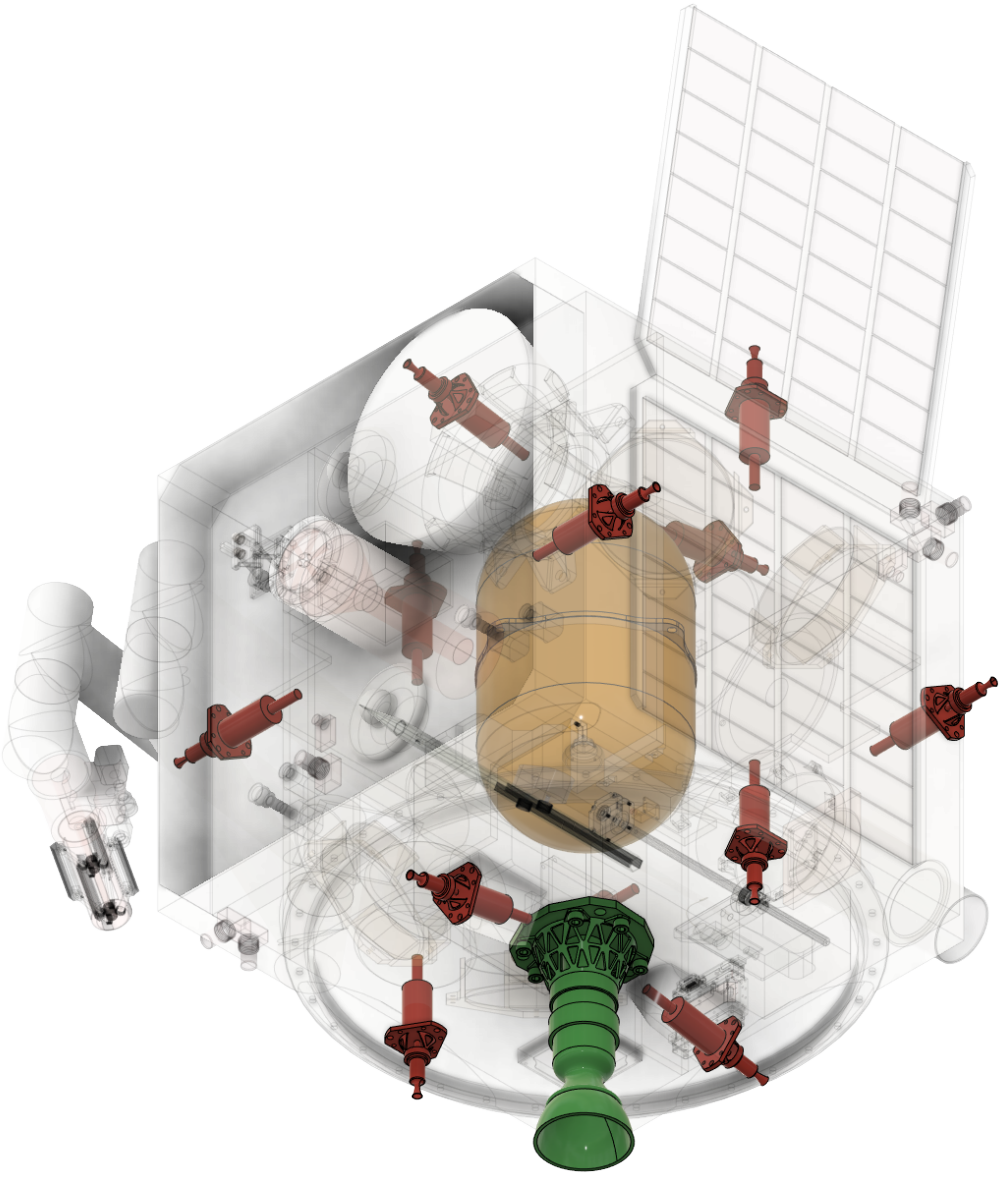

Figure 22.1: The extended fuel tank integrated in SERUM

Table 22.1: Spacecraft cost budget after second iteration

Subsystem	**Cost Estimate [**kEUR**]**
Payload docking	5209
Payload repair	1910
Payload EOL	223
Structural	2724 [3]
Thermal	**231**
EPS	175
TT&C	536
GNC	411
Propulsion	799
Fuel	**7.6** [77] [78]
CDH	44
Launch	890
Integration, assembly and test	1987 [3]
Program level	3273 [3]
Ground support equipment	943 [3]
Total Cost	**19363**
Final cost + 20% margin	**23235.6**
Requirement	20000
	Compliant: No

Table 22.2: Spacecraft mass budget after second iteration

Subsystem	**Mass Estimate [kg]**
Payload docking	16.4
Payload repair	2.4
Payload EOL	**7.6**
Structural	22
Thermal	**0.4**
EPS	3.3
TT&C	1.2
GNC	5.9
Propulsion	10.1
CDH	1.0
Other (balance + launch)	2.5 [3]
Total Dry Mass	**73**
Total Dry Mass + 20% margin	**87.6**
Main Propellant + 20% margin	**18.3**
Total wet mass + 20% margin	**105.9**
Requirement	200
	Compliant: Yes

23 Conclusion

In conclusion, this report presents the detailed design process for SERUM aimed at repairing and de-orbiting SSETI Express. Based on the findings of the SSETI Express failure report, two potential solutions were identified: connecting an external charging circuit to the satellite to bypass the fault, or intercepting an electrical wire within SSETI Express to redirect power. Implementing either or both of these fixes is expected to restore the spacecraft's full functionality.

After being deployed at a 500 km orbit by the launch provider, SERUM will use its main thruster to inject into SSETI Express' 700 km sun-synchronous polar orbit, observing it from a relative orbit. The GNC system will maneuver SERUM into a docking position where it will use a docking arm and clamping mechanism for attaching itself to the broken satellite. Attempts at repair will be made, and it is expected that after 2 years the spacecraft will both de-orbit using propulsive methods. If docking is considered unsafe, an alternative approach using a net launcher will be attempted to capture SSETI Express for propulsive de-orbit as well.

After performing trade-offs and sensitivity analyses in the midterm report, the design of each subsystem was further detailed. This involved selecting components, determining their sizes, and establishing mass, cost, and power budgets. A subsequent iteration simplified the system and improved its reliability. The final components chosen for SERUM are summarized in Table 23.1. Furthermore, the design requirements have been verified, and the major risks identified and mitigated to reduce their impact.

Moving forward, the next steps in this project include the full detailed design, manufacturing, assembly, and integration of the spacecraft. The future verification and validation processes will ensure compliance with the design specifications. Once successfully completed, the satellite will be operated, leading to the eventual mission closure. The launch is planned for 2028, with the mission expected to conclude in 2035, representing a significant achievement in the restoration and utilization of SSETI Express and demonstrating novel methods in the fight against space-debris.

Table 23.1: Components summary table

Component		Chosen design
Payload		
	Docking	Robotic arm with expansion mechanisms into T-POD, followed by docking 'zond' into bottom
	Accessing	Piercing
	Fixing	Bypass with stud connector and extender and/or intercepting wiretap with endoscopic arm
	Catching	Net
	De-orbiting	Extended propulsion burn
GNC		
	Attitude control	1 N m reaction wheel
	Attitude determination	Cubestar Star Tracker, Cubesense Sun sensor
	Angular rate & acceleration sensing	STIM380H IMU
	Absolute position tracking	Celeste GNSS Receiver
CDH		
	Payload computer	SE-2 computer with FPGA module
	CDH computer	No particular one chosen
Communication		
	Telecommunication & data	S-band (uplink) and X-band (downlink)
	Video	Ka-band (downlink)
	Groundstation	KSAT Svalbard
Power		
	Power source	Deployable solar panels
	Power storage	Lithium-ion battery and super-capacitor
Propulsion		
	Propellant	LMP-103S
	Thruster	22 N HPGP thruster and 12 1 N HPGP thrusters
	Propellant tank	PEPT-230 propellant tank
Launch vehicle		SpaceX' Falcon 9 24" full plate rideshare slot
Thermal Control		
	Passive control	Anodized aluminum surface
	Heating	Kapton flexibe heaters

Bibliography

[1] L. A. Fernández, C. Wiedemann, and V. Braun, “Analysis of space launch vehicle failures and post-mission disposal statistics,” *Aerotecnica Missili Spazio*, vol. 101, no. 3, pp. 243–256, 2022, ISSN: 0365-7442 2524-6968. DOI: 10.1007/s42496-022-00118-5.

[2] B. T. C. Zandbergen, *Ae1222-ii - part spacecraft (bus) design and sizing*, Electronic Book, 2017.

[3] J. Wertz, W. Larson, and J. Puschell, *Space Mission Engineering: The New SMAD*. Microcosm Press, 2011.

[4] C. o. t. P. U. o. O. S. United Nations Secretariat, *Information furnished in conformity with the convention on registration of objects launched into outer space*, Pamphlet, 2006.

[5] L. Alminde, “Sseti express failure analysis report,” Report, 2005.

[6] N. Melville, “Sseti ex press phase d – integration logbook,” Report, 2004.

[7] M. J. Strube, R. Henry, E. Skelton, J. V. Eepoel, N. Gill, and R. Mckenna, “Aas 15-111 raven: An on-orbit relative navigation demonstration using international space station,” 2015.

[8] D. G. Delphine Ly Romain Lucken, “Correcting tles at epoch: Application to the gps constellation,” Report, 2019. [Online]. Available: https://www.hou.usra.edu/meetings/orbitaldebris2019/orbital2019paper/pdf/6132.pdf.

[9] JenaOptronik, *Rvs 3000 - ready for the next rendezvous*, Datasheet, 2022.

[10] B. Forrai, T. Miki, D. Gehrig, M. Hutter, and D. Scaramuzza, “Event-based agile object catching with a quadrupedal robot,” 2023. DOI: 10.48550/arXiv.2303.17479.

[11] Dragonfly Aerospace, *Chameleon imager*, Datasheet, 2022.

[12] N. Messikommer, C. Fang, M. Gehrig, and D. Scaramuzza, “Data-driven feature tracking for event cameras,” in *IEEE/CVF Conference on Computer Vision and Pattern Recognition (CVPR)*, pp. 5642–5651. DOI: https://doi.org/10.48550/arXiv.2211.12826.

[13] IniVation, *Specifications – current models*, Specification Sheet, 2021.

[14] M. B. Hong and Y.-H. Jo, “Design of a novel 4-dof wrist-type surgical instrument with enhanced rigidity and dexterity,” *IEEE/ASME Transactions on Mechatronics*, vol. 19, no. 2, pp. 500–511, 2014, ISSN: 1083-4435-1941-014X. DOI: 10.1109/tmech.2013.2245143.

[15] B. T. Guglelmo S. Aglietti, “The active space debris removal mission removedebris. part 2: In orbit operations,” 28/08/2019 2020. [Online]. Available: https://www.sciencedirect.com/science/article/pii/S0094576519312500.

[16] E. S. D. O. (OPS-SD), “Drama-software-user-manual,” Report, 2022.

[17] F. Hogervorst, “Optimization of semi-controlled low-thrust de-orbit strategies to reduce human casualty risk,” Thesis, 2018.

[18] J. L. Forshaw, G. S. Aglietti, N. Navarathinam, *et al.*, “Removedebris: An in-orbit active debris removal demonstration mission,” *Acta Astronautica*, vol. 127, pp. 448–463, 2016, ISSN: 00945765. DOI: 10.1016/j.actaastro.2016.06.018.

[19] R. Axthelm, B. Klotz, D. I. Retat, U. Schlossstein, W. Tritsch, and S. Vahsen, “Net capture mechanism for debris removal demonstration mission,” 2017.

[20] A. Black and D. A. Spencer, “Dragsail systems for satellite deorbit and targeted reentry,” *Journal of Space Safety Engineering*, vol. 7, no. 3, pp. 397–403, 2020, ISSN: 24688967. DOI: 10.1016/j.jsse.2020.07.030.

[21] N. E. Works, Catalog, 2023.

[22] G. S. Aglietti, B. Taylor, S. Fellowes, *et al.*, “The active space debris removal mission removedebris. part 2: In orbit operations,” *Acta Astronautica*, vol. 168, pp. 310–322, 2020, ISSN: 00945765. DOI: 10.1016/j.actaastro.2019.09.001.

[23] A. Hall, J. M. Phil Allen, M. Trichas, and J. Wickham-Eade, “Airbus active debris removal projects,” Report STO-MP-AVT-336, 2021.

[24] C. Redding, *Overview of leo satellite systems*, Audiovisual Material, 1999.

[25] N. T. J. Downey M. Evans, “Dvb-s2 experiment over nasa’s space network,” 2017. DOI: 10.13140/RG.2.1.2715.0327.

[26] S. C.-L. J. Pelton S. Madry, *Handbook of Satellite Applications*. New York: Springer Science+Business Media, 2013.

[27] S. C.-L. J. Pelton S. Madry, *Handbook of Satellite Applications*. New York: Springer Science+Business Media, 2013, p. 1281, ISBN: 978-1-4419-7672-7. DOI: 10.1007/978-1-4419-7671-0.

[28] A. N. K. Singh, “Overview of modulation schemes selection in satellite based communication,” *ICTACT Journal on Communication Technology*, vol. 11, no. 03, 2020, ISSN: 2229-6948. DOI: 10.21917/ijct.2020.0326.

[29] O. K. T. Bilten, “Comparison of advanced modulation schemes for leo satellite downlink communications,” 2003.

[30] NASA, *Near earth network (nen) user’s guide*, Standard, 2019.

[31] S.Speretta, *Spacecraft telecommunications*, Audiovisual Material, 2021.

[32] D. Systems, *Modular satellite demodulators*, Pamphlet.

[33] S.Speretta, *Spacecraft: Recap, practical examples and exercises*, Audiovisual Material, 2021.

[34] I. T. Unit, “Specific attenuation model for rain for use in prediction methods,” 2005.

[35] D. D. Crombie, “Electromagnetic wave propagation,”

[36] A. Cervone and A. Elham, *Ae2111-ii aerospace design and systems engineering elements ii*, Audiovisual Material, 2021.

[37] T. Unlimited, *Swift-ktx*, Pamphlet.

[38] Endurosat, *Datasheet x band transmitter*, Pamphlet.

[39] S. Millimeter, *Sao-2734030345-kf-r1*, Pamphlet, 2018.

[40] MI-WAVE, *267x/smaf test data sheet*, Pamphlet, 2020.

[41] Spiral Blue, *Space edge computer*, Datasheet, Apr. 2023.

[42] NVIDIA, *The world’s first ray tracing gpu - nvidia quadro rtx 8000*, Datasheet, Mar. 2019.

[43] European Cooperation for Space Standardization (ECSS), *Space product assurance - techniques for radiation effects mitigation in asics and fpgas handbook*, Handbook, Sep. 2016.

[44] Granta Design Limited, *Ces edupack 2019*, Database, 2019.

[45] A. E. S. Nosseir, A. Cervone, and A. Pasini, “Review of state-of-the-art green monopropellants: For propulsion systems analysts and designers,” *Aerospace*, vol. 8, no. 1, p. 20, Jan. 2021, ISSN: 2226-4310. DOI: 10.3390/aerospace8010020. [Online]. Available: http://dx.doi.org/10.3390/aerospace8010020.

[46] A. Mayer and W. Wieling, “Green propulsion research at tno the netherlands,” *Transactions on Aerospace Research*, vol. 2018, no. 4, pp. 1–24, 2018. DOI: doi:10.2478/tar-2018-0026. [Online]. Available: https://doi.org/10.2478/tar-2018-0026.

[47] ECHA, *Substance infocard hydrazine*, 2023. [Online]. Available: https://echa.europa.eu/nl/substance-information/-/substanceinfo/100.005.560.

[48] R. K. Masse, M. Allen, E. Driscoll, *et al.*, “Af-m315e propulsion system advances & improvements,” *AIAASAEASEE Joint Propulsion Conference.*, vol. 52, 2016.

[49] K. Hori, T. Katsumi, S. Sawai, N. Azuma, K. Hatai, and J. Nakatsuka, “Han-based green propellant, shp163 – its r&d and test in space,” *Propellants, Explosives, Pyrotechnics*, vol. 44, no. 9, pp. 1080–1083, 2019. DOI: https://doi.org/10.1002/prep.201900237. eprint: https://onlinelibrary.wiley.com/doi/pdf/10.1002/prep.201900237. [Online]. Available: https://onlinelibrary.wiley.com/doi/abs/10.1002/prep.201900237.

[50] K. Hori, T. Katsumi, S. Sawai, N. Azuma, K. Hatai, and J. Nakatsuka, “Han□based green propellant, shp163 – its r&d and test in space –,” *Propellants, Explosives, Pyrotechnics*, vol. 44, Aug. 2019. DOI: 10.1002/prep.201900237.

[51] A. E. S. Nosseir, A. Cervone, and A. Pasini, “Modular impulsive green monopropellant propulsion system (mimps-g): For cubesats in leo and to the moon,” *Aerospace*, vol. 8, p. 169, 2021. DOI: https://doi.org/10.3390/aerospace8060169.

[52] N. Wingborg, M. Johansson, and L. Bodin, “Initial developemnt of a laboratory rocket thruster for ADN-based liquid monopropellants,” Swedish defense research agency, Tech. Rep., 2006.

[53] K. Anflo and N. Wingborg, *Ammonium dinitrimide based liquid monopropelants exhibiting improved combustion stability and storage life*, Jul. 2011.

[54] A. Larsson and N. Wingborg, “Green propellants based on ammonium dinitramide (adn),” in *Advances in Spacecraft Technologies*, J. Hall, Ed., Rijeka: IntechOpen, 2011, ch. 7. DOI: 10.5772/13640. [Online]. Available: https://doi.org/10.5772/13640.

[55] B. R. Greene, D. L. Baker, and W. Frazier, “Hydrogen peroxide accidents and incidents: What we can learn from history,” NASA Johnson Space Center White Sands Test Facility, 2005.

[56] T. Finke, “Non-catalytic microwave ignition of green hydrazine replacements,” in ch. 7, p. 7. [Online]. Available: https://apps.dtic.mil/sti/trecms/pdf/AD1151714.pdf.

[57] R. A. Spores, “Gpim af-m315e propulsion system,” in *51st AIAA/SAE/ASEE Joint Propulsion Conference*. DOI: 10.2514/6.2015-3753. eprint: https://arc.aiaa.org/doi/pdf/10.2514/6.2015-3753. [Online]. Available: https://arc.aiaa.org/doi/abs/10.2514/6.2015-3753.

[58] M. Wilhelm, M. Negri, H. Ciezki, and S. Schlechtriem, “Preliminary tests on thermal ignition of adn-based liquid monopropellants,” *Acta Astronautica*, vol. 158, pp. 388–396, 2019, ISSN: 0094-5765. DOI: https://doi.org/10.1016/j.actaastro.2018.05.057. [Online]. Available: https://www.sciencedirect.com/science/article/pii/S0094576518301152.

[59] G. Mungas, M. Vozoff, and B. Rishikof, “Nofbx™: A new non-toxic, ” green ” propulsion technology with high performance and low cost,” Oct. 2012. DOI: 10.2514/6.2012-5235.

[60] L. K. Werling, T. Hörger, K. Manassis, *et al.*, “Nitrous oxide fuels blends: Research on premixed monopropellants at the german aerospace center (dlr) since 2014,” in *AIAA Propulsion and Energy 2020 Forum*. DOI: 10.2514/6.2020-3807. [Online]. Available: https://arc.aiaa.org/doi/abs/10.2514/6.2020-3807.

[61] O. Romantsova and V. Ulybin, “Safety issues of high-concentrated hydrogen peroxide production used as rocket propellant,” *Acta Astronautica*, vol. 109, pp. 231–234, 2015, ISSN: 0094-5765. DOI: https://doi.org/10.1016/j.actaastro.2014.10.022. [Online]. Available: https://www.sciencedirect.com/science/article/pii/S0094576514004007.

[62] M. Ventura, “Long term storability of hydrogen peroxide,” in *41st AIAA/ASME/SAE/ASEE Joint Propulsion Conference & Exhibit*. DOI: 10.2514/6.2005-4551. [Online]. Available: https://arc.aiaa.org/doi/abs/10.2514/6.2005-4551.

[63] C. Maleix, P. Chabernaud, R. Brahmi, *et al.*, “Development of catalytic materials for decomposition of adn-based monopropellants,” *Acta Astronautica*, vol. 158, pp. 407–415, 2019, ISSN: 0094-5765. DOI: https://doi.org/10.1016/j.actaastro.2019.03.033. [Online]. Available: https://www.sciencedirect.com/science/article/pii/S0094576519304783.

[64] D. Hasan, N. Naveh, E. Ore, *et al.*, “The pept-230 micro-satellite propellant tank design,” 2000.

[65] J. J. Sellers, M. Paul, M. Meerman, and R. Wood, “Investigation into low-cost propulsion systems for small satellite missions,” 1995.

[66] A. R. d. O. S. S. Melro, “Análise estrutural e estudo de configuração de um micro-satélite,” Universidade do porto, Report, 2004.

[67] V. Knap, L. K. Vestergaard, and D.-I. Stroe, “A review of battery technology in cubesats and small satellite solutions,” *Energies*, vol. 13, no. 16, 2020, ISSN: 1996-1073. DOI: 10.3390/en13164097.

[68] M. Qadrdan, N. Jenkins, and J. Wu, “Chapter ii-3-d - smart grid and energy storage,” in *McEvoy’s Handbook of Photovoltaics (Third Edition)*, S. A. Kalogirou, Ed., Third Edition, Academic Press, 2018, pp. 915–928, ISBN: 978-0-12-809921-6. DOI: https://doi.org/10.1016/B978-0-12-809921-6.00025-2. [Online]. Available: https://www.sciencedirect.com/science/article/pii/B9780128099216000252.

[69] U. Bhattacharjee, S. Ghosh, M. Bhar, and S. K. Martha, “6 - electrochemical energy storage part i: Development, basic principle and conventional systems,” in *Emerging Trends in Energy Storage Systems and Industrial Applications*, Prabhansu and N. Kumar, Eds., Academic Press, 2023, pp. 151–188, ISBN: 978-0-323-90521-3. DOI: https://doi.org/10.1016/B978-0-323-90521-3.00001-6. [Online]. Available: https://www.sciencedirect.com/science/article/pii/B9780323905213000016.

[70] P. Fortescue, G. Swinerd, and J. Stark, *Spacecraft Systems Engineering*. Wiley, 2011.

[71] J. Wertz and W. Larson, *Space Mission Analysis and Design*. Springer, 1999, ISBN: 9780792359012. [Online]. Available: https://books.google.nl/books?id=veyGEAKFbiYC.

[72] L. Kauder, “Spacecraft thermal control coatings references,” *NASA*, 2005.

[73] R. Á. d. Luis, “Standardized thermal control, solutions for pocketqubes,” *TU Delft*, 2019.

[74] SpaceX, “Spacex rideshare payload users guide,” Report, 2021.

[75] J. L. J. Hanspeter Schaub, *Analytical Mechanics of Space Systems, Fourth Edition (AIAA Education Series)*, 4th. AIAA American Institute of Aeronautics & Astodynamics, 2018.

[76] L. J. Ippolito, “Rain fade mitigation,” in *Satellite Communications Systems Engineering: Atmospheric Effects, Satellite Link Design and System Performance*. 2017, pp. 205–234. DOI: 10.1002/9781119259411.ch8.

[77] M. Negri, M. Wilhelm, and H. K. Ciezki, “Thermal ignition of adn□based propellants,” *Propellants, Explosives, Pyrotechnics*, vol. 44, no. 9, pp. 1096–1106, 2019, ISSN: 0721-3115 1521-4087. DOI: 10.1002/prep.201900154.

[78] Y. Vasconcelos, “Green propulsion,” *International issue*, 2017.

[79] E. Gill, *Verification and validation for the attitude and orbit control system*, Audiovisual Material, 2023.